

RILEM State-of-the-Art Reports

Nicolas Roussel  
Dirk Lowke *Editors*

# Digital Fabrication with Cement-Based Materials

State-of-the-Art Report of the RILEM TC  
276-DFC



 Springer

The Springer logo features a stylized white chess knight (horse) facing left, positioned above the word "Springer" in a white, serif font.

# **RILEM State-of-the-Art Reports**

# RILEM STATE-OF-THE-ART REPORTS

## Volume 36

---

RILEM, The International Union of Laboratories and Experts in Construction Materials, Systems and Structures, founded in 1947, is a non-governmental scientific association whose goal is to contribute to progress in the construction sciences, techniques and industries, essentially by means of the communication it fosters between research and practice. RILEM's focus is on construction materials and their use in building and civil engineering structures, covering all phases of the building process from manufacture to use and recycling of materials. More information on RILEM and its previous publications can be found on [www.RILEM.net](http://www.RILEM.net).

The RILEM State-of-the-Art Reports (STAR) are produced by the Technical Committees. They represent one of the most important outputs that RILEM generates – high level scientific and engineering reports that provide cutting edge knowledge in a given field. The work of the TCs is one of RILEM's key functions.

Members of a TC are experts in their field and give their time freely to share their expertise. As a result, the broader scientific community benefits greatly from RILEM's activities.

RILEM's stated objective is to disseminate this information as widely as possible to the scientific community. RILEM therefore considers the STAR reports of its TCs as of highest importance, and encourages their publication whenever possible.

The information in this and similar reports is mostly pre-normative in the sense that it provides the underlying scientific fundamentals on which standards and codes of practice are based. Without such a solid scientific basis, construction practice will be less than efficient or economical.

It is RILEM's hope that this information will be of wide use to the scientific community.

Indexed in SCOPUS, Google Scholar and SpringerLink.



More information about this series at <https://link.springer.com/bookseries/8780>

Nicolas Roussel · Dirk Lowke  
Editors

# Digital Fabrication with Cement-Based Materials

State-of-the-Art Report of the RILEM TC  
276-DFC




 Springer

The Springer logo consists of a stylized chess knight piece above the word "Springer" in a serif font.

*Editors*

Nicolas Roussel   
Navier Laboratory  
Université Gustave Eiffel  
Champs sur Marne, France

Dirk Lowke   
Department of Building Materials  
Technische Universität Braunschweig  
Braunschweig, Germany

ISSN 2213-204X

ISSN 2213-2031 (electronic)

RILEM State-of-the-Art Reports

ISBN 978-3-030-90534-7

ISBN 978-3-030-90535-4 (eBook)

<https://doi.org/10.1007/978-3-030-90535-4>

© RILEM 2022

No part of this work may be reproduced, stored in a retrieval system, or transmitted in any form or by any means, electronic, mechanical, photocopying, microfilming, recording or otherwise, without written permission from the Publisher, with the exception of any material supplied specifically for the purpose of being entered and executed on a computer system, for exclusive use by the purchaser of the work. Permission for use must always be obtained from the owner of the copyright: RILEM.

The use of general descriptive names, registered names, trademarks, service marks, etc. in this publication does not imply, even in the absence of a specific statement, that such names are exempt from the relevant protective laws and regulations and therefore free for general use.

The publisher, the authors and the editors are safe to assume that the advice and information in this book are believed to be true and accurate at the date of publication. Neither the publisher nor the authors or the editors give a warranty, expressed or implied, with respect to the material contained herein or for any errors or omissions that may have been made. The publisher remains neutral with regard to jurisdictional claims in published maps and institutional affiliations.

This Springer imprint is published by the registered company Springer Nature Switzerland AG  
The registered company address is: Gewerbestrasse 11, 6330 Cham, Switzerland

# Committee

The present work results from discussions that were carried out between the years 2016 and 2021. These discussions involved the following RILEM experts.

## TC 276-DFC Members

Nicolas Roussel, Gustave Eiffel University, France  
Dirk Lowke, Technische Universität Braunschweig, Germany  
Robert Flatt, ETHZ, Switzerland  
Viktor Mechtcherine, Dresden University, Germany  
Timothy Wangler, ETHZ, Switzerland  
Alexandre Pierre, Cergy University, France  
Geert De Schutter, Ghent University, Belgium  
Arnaud Perrot, Université de Bretagne Sud, France  
Venkatesh Naidu Nerella, Dresden University, Germany  
Fabrice Toussaint, Lafarge-Holcim, France  
Giovanni Volpatti, CEMEX Innovation Holding AG, Switzerland  
Mohammed Sonebi, Queen's University Belfast, UK  
Ksenija Vasilic, German Society for Concrete and Construction Technology, Germany  
Richard Buswell, Loughborough University, UK  
Wilson Ricardo Leal da Silva, Danish Technical Institute, Denmark  
Liberato Ferrara, Politecnico Di Milano, Italy  
Norman Hack, Technische Universität Braunschweig, Germany  
Steffen Grünewald, Delft University of Technology, The Netherlands  
Karel Lesage, Ghent University, Belgium  
Asko Fromm, Hochschule Wismar, Germany  
Roel Schipper, Delft University of Technology, The Netherlands  
Dietmar Stephan, Technische Universität Berlin, Germany  
Ena Lloret-Fritschl, ETHZ, Switzerland

Shirin Fataei, Dresden University, Germany  
Lex Reiter, ETHZ, Switzerland  
Domenico Asprone, Università degli Studi di Napoli Federico II, Italy  
Costantino Menna, Università degli Studi di Napoli Federico II, Italy  
Aurélie Papon, Institut National des Sciences Appliquées Toulouse, France  
Harald Kloft, Technische Universität Braunschweig, Germany  
Sandro Moro, Master Builders Solutions Italia Spa, Italy  
Kim Van Tittelboom, Ghent University, Belgium  
Jolien Van Der Putten, Ghent University, Belgium  
Jaime Mata Falcón, ETHZ, Switzerland  
Hela Bessaies-Bey, Gustave Eiffel University, France  
Vítor Cunha, University of Minho, Portugal  
Daniel Weger, Technical University of Munich, Germany  
Freek Bos, Technical University Eindhoven, The Netherlands  
Tilo Salet, Technical University Eindhoven, The Netherlands  
Zhendi Wang, Institute of Concrete Science and Engineering, China  
Christoph Gehlen, Technical University of Munich, Germany  
Chalermwut Snguanyat, Siam Research and Innovation Co Ltd., Thailand  
Mahzad Azima, Ghent University, Belgium  
Hélène Lombois-Burger, Lafarge-Holcim, France  
Melody D'Hondt, Centre Scientifique et Technique du Bâtiment, France  
Rob Wolfs, Technical University Eindhoven, The Netherlands  
Irina Ivanova, Dresden University, Germany

# RILEM Publications

The following list is presenting the global offer of RILEM Publications, sorted by series. Each publication is available in printed version and/or in online version.

## RILEM Proceedings (PRO)

**PRO 1:** Durability of High Performance Concrete (ISBN: 2-912143-03-9; e-ISBN: 2-351580-12-5; e-ISBN: 2351580125); *Ed. H. Sommer*

**PRO 2:** Chloride Penetration into Concrete (ISBN: 2-912143-00-04; e-ISBN: 2912143454); *Eds. L.-O. Nilsson and J.-P. Ollivier*

**PRO 3:** Evaluation and Strengthening of Existing Masonry Structures (ISBN: 2-912143-02-0; e-ISBN: 2351580141); *Eds. L. Binda and C. Modena*

**PRO 4:** Concrete: From Material to Structure (ISBN: 2-912143-04-7; e-ISBN: 2351580206); *Eds. J.-P. Bournazel and Y. Malier*

**PRO 5:** The Role of Admixtures in High Performance Concrete (ISBN: 2-912143-05-5; e-ISBN: 2351580214); *Eds. J. G. Cabrera and R. Rivera-Villarreal*

**PRO 6:** High Performance Fiber Reinforced Cement Composites—HPFRCC 3 (ISBN: 2-912143-06-3; e-ISBN: 2351580222); *Eds. H. W. Reinhardt and A. E. Naaman*

**PRO 7:** 1st International RILEM Symposium on Self-Compacting Concrete (ISBN: 2-912143-09-8; e-ISBN: 2912143721); *Eds. Å. Skarendahl and Ö. Petersson*

**PRO 8:** International RILEM Symposium on Timber Engineering (ISBN: 2-912143-10-1; e-ISBN: 2351580230); *Ed. L. Boström*

**PRO 9:** 2nd International RILEM Symposium on Adhesion between Polymers and Concrete ISAP '99 (ISBN: 2-912143-11-X; e-ISBN: 2351580249); *Eds. Y. Ohama and M. Puterman*



**PRO 10:** 3rd International RILEM Symposium on Durability of Building and Construction Sealants (ISBN: 2-912143-13-6; e-ISBN: 2351580257); *Ed. A. T. Wolf*

**PRO 11:** 4th International RILEM Conference on Reflective Cracking in Pavements (ISBN: 2-912143-14-4; e-ISBN: 2351580265); *Eds. A. O. Abd El Halim, D. A. Taylor and El H. H. Mohamed*

**PRO 12:** International RILEM Workshop on Historic Mortars: Characteristics and Tests (ISBN: 2-912143-15-2; e-ISBN: 2351580273); *Eds. P. Bartos, C. Groot and J. J. Hughes*

**PRO 13:** 2nd International RILEM Symposium on Hydration and Setting (ISBN: 2-912143-16-0; e-ISBN: 2351580281); *Ed. A. Nonat*

**PRO 14:** Integrated Life-Cycle Design of Materials and Structures—ILCDES 2000 (ISBN: 951-758-408-3; e-ISBN: 235158029X); (ISSN: 0356-9403); *Ed. S. Sarja*

**PRO 15:** Fifth RILEM Symposium on Fibre-Reinforced Concretes (FRC)—BEFIB'2000 (ISBN: 2-912143-18-7; e-ISBN: 291214373X); *Eds. P. Rossi and G. Chanvillard*

**PRO 16:** Life Prediction and Management of Concrete Structures (ISBN: 2-912143-19-5; e-ISBN: 2351580303); *Ed. D. Naus*

**PRO 17:** Shrinkage of Concrete—Shrinkage 2000 (ISBN: 2-912143-20-9; e-ISBN: 2351580311); *Eds. V. Baroghel-Bouny and P.-C. Aïtcin*

**PRO 18:** Measurement and Interpretation of the On-Site Corrosion Rate (ISBN: 2-912143-21-7; e-ISBN: 235158032X); *Eds. C. Andrade, C. Alonso, J. Fullea, J. Polimon and J. Rodriguez*

**PRO 19:** Testing and Modelling the Chloride Ingress into Concrete (ISBN: 2-912143-22-5; e-ISBN: 2351580338); *Eds. C. Andrade and J. Kropp*

**PRO 20:** 1st International RILEM Workshop on Microbial Impacts on Building Materials (CD 02) (e-ISBN 978-2-35158-013-4); *Ed. M. Ribas Silva*

**PRO 21:** International RILEM Symposium on Connections between Steel and Concrete (ISBN: 2-912143-25-X; e-ISBN: 2351580346); *Ed. R. Eligehausen*

**PRO 22:** International RILEM Symposium on Joints in Timber Structures (ISBN: 2-912143-28-4; e-ISBN: 2351580354); *Eds. S. Aicher and H.-W. Reinhardt*

**PRO 23:** International RILEM Conference on Early Age Cracking in Cementitious Systems (ISBN: 2-912143-29-2; e-ISBN: 2351580362); *Eds. K. Kovler and A. Bentur*

**PRO 24:** 2nd International RILEM Workshop on Frost Resistance of Concrete (ISBN: 2-912143-30-6; e-ISBN: 2351580370); *Eds. M. J. Setzer, R. Auberg and H.-J. Keck*

**PRO 25:** International RILEM Workshop on Frost Damage in Concrete (ISBN: 2-912143-31-4; e-ISBN: 2351580389); *Eds. D. J. Janssen, M. J. Setzer and M. B. Snyder*

**PRO 26:** International RILEM Workshop on On-Site Control and Evaluation of Masonry Structures (ISBN: 2-912143-34-9; e-ISBN: 2351580141); *Eds. L. Binda and R. C. de Vekey*

**PRO 27:** International RILEM Symposium on Building Joint Sealants (CD03; e-ISBN: 235158015X); *Ed. A. T. Wolf*

**PRO 28:** 6th International RILEM Symposium on Performance Testing and Evaluation of Bituminous Materials—PTEBM'03 (ISBN: 2-912143-35-7; e-ISBN: 978-2-912143-77-8); *Ed. M. N. Partl*

**PRO 29:** 2nd International RILEM Workshop on Life Prediction and Ageing Management of Concrete Structures (ISBN: 2-912143-36-5; e-ISBN: 2912143780); *Ed. D. J. Naus*

**PRO 30:** 4th International RILEM Workshop on High Performance Fiber Reinforced Cement Composites—HPFRCC 4 (ISBN: 2-912143-37-3; e-ISBN: 2912143799); *Eds. A. E. Naaman and H. W. Reinhardt*

**PRO 31:** International RILEM Workshop on Test and Design Methods for Steel Fibre Reinforced Concrete: Background and Experiences (ISBN: 2-912143-38-1; e-ISBN: 2351580168); *Eds. B. Schnütgen and L. Vandewalle*

**PRO 32:** International Conference on Advances in Concrete and Structures 2 vol. (ISBN (set): 2-912143-41-1; e-ISBN: 2351580176); *Eds. Ying-shu Yuan, Surendra P. Shah and Heng-lin Lü*

**PRO 33:** 3rd International Symposium on Self-Compacting Concrete (ISBN: 2-912143-42-X; e-ISBN: 2912143713); *Eds. Ó. Wallevik and I. Nilsson*

**PRO 34:** International RILEM Conference on Microbial Impact on Building Materials (ISBN: 2-912143-43-8; e-ISBN: 2351580184); *Ed. M. Ribas Silva*

**PRO 35:** International RILEM TC 186-ISA on Internal Sulfate Attack and Delayed Ettringite Formation (ISBN: 2-912143-44-6; e-ISBN: 2912143802); *Eds. K. Scrivener and J. Skalny*

**PRO 36:** International RILEM Symposium on Concrete Science and Engineering—A Tribute to Arnon Bentur (ISBN: 2-912143-46-2; e-ISBN: 2912143586); *Eds. K. Kovler, J. Marchand, S. Mindess and J. Weiss*

**PRO 37:** 5th International RILEM Conference on Cracking in Pavements—Mitigation, Risk Assessment and Prevention (ISBN: 2-912143-47-0; e-ISBN: 2912143764); *Eds. C. Petit, I. Al-Qadi and A. Millien*

**PRO 38:** 3rd International RILEM Workshop on Testing and Modelling the Chloride Ingress into Concrete (ISBN: 2-912143-48-9; e-ISBN: 2912143578); *Eds. C. Andrade and J. Kropp*

**PRO 39:** 6th International RILEM Symposium on Fibre-Reinforced Concretes—BEFIB 2004 (ISBN: 2-912143-51-9; e-ISBN: 2912143748); *Eds. M. Di Prisco, R. Felicetti and G. A. Plizzari*

**PRO 40:** International RILEM Conference on the Use of Recycled Materials in Buildings and Structures (ISBN: 2-912143-52-7; e-ISBN: 2912143756); *Eds. E. Vázquez, Ch. F. Hendriks and G. M. T. Janssen*

**PRO 41:** RILEM International Symposium on Environment-Conscious Materials and Systems for Sustainable Development (ISBN: 2-912143-55-1; e-ISBN: 2912143640); *Eds. N. Kashino and Y. Ohama*

**PRO 42:** SCC'2005—China: 1st International Symposium on Design, Performance and Use of Self-Consolidating Concrete (ISBN: 2-912143-61-6; e-ISBN: 2912143624); *Eds. Zhiwu Yu, Caijun Shi, Kamal Henri Khayat and Youjun Xie*

**PRO 43:** International RILEM Workshop on Bonded Concrete Overlays (e-ISBN: 2-912143-83-7); *Eds. J. L. Granju and J. Silfwerbrand*

**PRO 44:** 2nd International RILEM Workshop on Microbial Impacts on Building Materials (CD11) (e-ISBN: 2-912143-84-5); *Ed. M. Ribas Silva*

**PRO 45:** 2nd International Symposium on Nanotechnology in Construction, Bilbao (ISBN: 2-912143-87-X; e-ISBN: 2912143888); *Eds. Peter J. M. Bartos, Yolanda de Miguel and Antonio Porro*

**PRO 46:** Concrete Life'06—International RILEM-JCI Seminar on Concrete Durability and Service Life Planning: Curing, Crack Control, Performance in Harsh Environments (ISBN: 2-912143-89-6; e-ISBN: 291214390X); *Ed. K. Kovler*

**PRO 47:** International RILEM Workshop on Performance Based Evaluation and Indicators for Concrete Durability (ISBN: 978-2-912143-95-2; e-ISBN: 9782912143969); *Eds. V. Baroghel-Bouny, C. Andrade, R. Torrent and K. Scrivener*

**PRO 48:** 1st International RILEM Symposium on Advances in Concrete through Science and Engineering (e-ISBN: 2-912143-92-6); *Eds. J. Weiss, K. Kovler, J. Marchand, and S. Mindess*

**PRO 49:** International RILEM Workshop on High Performance Fiber Reinforced Cementitious Composites in Structural Applications (ISBN: 2-912143-93-4; e-ISBN: 2912143942); *Eds. G. Fischer and V. C. Li*

**PRO 50:** 1st International RILEM Symposium on Textile Reinforced Concrete (ISBN: 2-912143-97-7; e-ISBN: 2351580087); *Eds. Josef Hegger, Wolfgang Brameshuber and Norbert Will*

**PRO 51:** 2nd International Symposium on Advances in Concrete through Science and Engineering (ISBN: 2-35158-003-6; e-ISBN: 2-35158-002-8); *Eds. J. Marchand, B. Bissonnette, R. Gagné, M. Jolin and F. Paradis*

**PRO 52:** Volume Changes of Hardening Concrete: Testing and Mitigation (ISBN: 2-35158-004-4; e-ISBN: 2-35158-005-2); *Eds. O. M. Jensen, P. Lura and K. Kovler*

**PRO 53:** High Performance Fiber Reinforced Cement Composites—HPFRCC5 (ISBN: 978-2-35158-046-2; e-ISBN: 978-2-35158-089-9); *Eds. H. W. Reinhardt and A. E. Naaman*

**PRO 54:** 5th International RILEM Symposium on Self-Compacting Concrete (ISBN: 978-2-35158-047-9; e-ISBN: 978-2-35158-088-2); *Eds. G. De Schutter and V. Boel*

**PRO 55:** International RILEM Symposium Photocatalysis, Environment and Construction Materials (ISBN: 978-2-35158-056-1; e-ISBN: 978-2-35158-057-8); *Eds. P. Baglioni and L. Cassar*

**PRO 56:** International RILEM Workshop on Integral Service Life Modelling of Concrete Structures (ISBN 978-2-35158-058-5; e-ISBN: 978-2-35158-090-5); *Eds. R. M. Ferreira, J. Gulikers and C. Andrade*

**PRO 57:** RILEM Workshop on Performance of cement-based materials in aggressive aqueous environments (e-ISBN: 978-2-35158-059-2); *Ed. N. De Belie*

**PRO 58:** International RILEM Symposium on Concrete Modelling—CONMOD'08 (ISBN: 978-2-35158-060-8; e-ISBN: 978-2-35158-076-9); *Eds. E. Schlangen and G. De Schutter*

**PRO 59:** International RILEM Conference on On Site Assessment of Concrete, Masonry and Timber Structures—SACoMaTiS 2008 (ISBN set: 978-2-35158-061-5; e-ISBN: 978-2-35158-075-2); *Eds. L. Binda, M. di Prisco and R. Felicetti*

**PRO 60:** Seventh RILEM International Symposium on Fibre Reinforced Concrete: Design and Applications—BEFIB 2008 (ISBN: 978-2-35158-064-6; e-ISBN: 978-2-35158-086-8); *Ed. R. Gettu*

**PRO 61:** 1st International Conference on Microstructure Related Durability of Cementitious Composites 2 vol., (ISBN: 978-2-35158-065-3; e-ISBN: 978-2-35158-084-4); *Eds. W. Sun, K. van Breugel, C. Miao, G. Ye and H. Chen*

**PRO 62:** NSF/ RILEM Workshop: In-situ Evaluation of Historic Wood and Masonry Structures (e-ISBN: 978-2-35158-068-4); *Eds. B. Kasal, R. Anthony and M. Drdácý*

**PRO 63:** Concrete in Aggressive Aqueous Environments: Performance, Testing and Modelling, 2 vol., (ISBN: 978-2-35158-071-4; e-ISBN: 978-2-35158-082-0); *Eds. M. G. Alexander and A. Bertron*

**PRO 64:** Long Term Performance of Cementitious Barriers and Reinforced Concrete in Nuclear Power Plants and Waste Management—NUCPERF 2009 (ISBN: 978-2-35158-072-1; e-ISBN: 978-2-35158-087-5); *Eds. V. L'Hostis, R. Gens and C. Gallé*

**PRO 65:** Design Performance and Use of Self-consolidating Concrete—SCC'2009 (ISBN: 978-2-35158-073-8; e-ISBN: 978-2-35158-093-6); *Eds. C. Shi, Z. Yu, K. H. Khayat and P. Yan*

**PRO 66:** 2nd International RILEM Workshop on Concrete Durability and Service Life Planning—ConcreteLife'09 (ISBN: 978-2-35158-074-5; ISBN: 978-2-35158-074-5); *Ed. K. Kovler*

**PRO 67:** Repairs Mortars for Historic Masonry (e-ISBN: 978-2-35158-083-7); *Ed. C. Groot*

**PRO 68:** Proceedings of the 3rd International RILEM Symposium on ‘Rheology of Cement Suspensions such as Fresh Concrete (ISBN 978-2-35158-091-2; e-ISBN: 978-2-35158-092-9); *Eds. O. H. Wallevik, S. Kubens and S. Oesterheld*

**PRO 69:** 3rd International PhD Student Workshop on ‘Modelling the Durability of Reinforced Concrete (ISBN: 978-2-35158-095-0); *Eds. R. M. Ferreira, J. Gulikers and C. Andrade*

**PRO 70:** 2nd International Conference on ‘Service Life Design for Infrastructure’ (ISBN set: 978-2-35158-096-7, e-ISBN: 978-2-35158-097-4); *Eds. K. van Breugel, G. Ye and Y. Yuan*

**PRO 71:** Advances in Civil Engineering Materials—The 50-year Teaching Anniversary of Prof. Sun Wei’ (ISBN: 978-2-35158-098-1; e-ISBN: 978-2-35158-099-8); *Eds. C. Miao, G. Ye and H. Chen*

**PRO 72:** First International Conference on ‘Advances in Chemically-Activated Materials—CAM’2010’ (2010), 264 pp., ISBN: 978-2-35158-101-8; e-ISBN: 978-2-35158-115-5; *Eds. Caijun Shi and Xiaodong Shen*

**PRO 73:** 2nd International Conference on ‘Waste Engineering and Management—ICWEM 2010’ (2010), 894 pp., ISBN: 978-2-35158-102-5; e-ISBN: 978-2-35158-103-2, *Eds. J. Zh. Xiao, Y. Zhang, M. S. Cheung and R. Chu*

**PRO 74:** International RILEM Conference on ‘Use of Superabsorbent Polymers and Other New Additives in Concrete’ (2010) 374 pp., ISBN: 978-2-35158-104-9; e-ISBN: 978-2-35158-105-6; *Eds. O.M. Jensen, M.T. Hasholt, and S. Laustsen*

**PRO 75:** International Conference on ‘Material Science—2nd ICTRC—Textile Reinforced Concrete—Theme 1’ (2010) 436 pp., ISBN: 978-2-35158-106-3; e-ISBN: 978-2-35158-107-0; *Ed. W. Brameshuber*

**PRO 76:** International Conference on ‘Material Science—HetMat—Modelling of Heterogeneous Materials—Theme 2’ (2010) 255 pp., ISBN: 978-2-35158-108-7; e-ISBN: 978-2-35158-109-4; *Ed. W. Brameshuber*

**PRO 77:** International Conference on ‘Material Science—AdIPoC—Additions Improving Properties of Concrete—Theme 3’ (2010) 459 pp., ISBN: 978-2-35158-110-0; e-ISBN: 978-2-35158-111-7; *Ed. W. Brameshuber*

**PRO 78:** 2nd Historic Mortars Conference and RILEM TC 203-RHM Final Workshop—HMC2010 (2010) 1416 pp., e-ISBN: 978-2-35158-112-4; *Eds. J. Válek, C. Groot and J. J. Hughes*

**PRO 79:** International RILEM Conference on Advances in Construction Materials Through Science and Engineering (2011) 213 pp., ISBN: 978-2-35158-116-2, e-ISBN: 978-2-35158-117-9; *Eds. Christopher Leung and K.T. Wan*

**PRO 80:** 2nd International RILEM Conference on Concrete Spalling due to Fire Exposure (2011) 453 pp., ISBN: 978-2-35158-118-6; e-ISBN: 978-2-35158-119-3; *Eds. E.A.B. Koenders and F. Dehn*

**PRO 81:** 2nd International RILEM Conference on Strain Hardening Cementitious Composites (SHCC2-Rio) (2011) 451 pp., ISBN: 978-2-35158-120-9; e-ISBN: 978-2-35158-121-6; *Eds. R.D. Toledo Filho, F.A. Silva, E.A.B. Koenders and E.M.R. Fairbairn*

**PRO 82:** 2nd International RILEM Conference on Progress of Recycling in the Built Environment (2011) 507 pp., e-ISBN: 978-2-35158-122-3; *Eds. V.M. John, E. Vazquez, S.C. Angulo and C. Ulsen*

**PRO 83:** 2nd International Conference on Microstructural-related Durability of Cementitious Composites (2012) 250 pp., ISBN: 978-2-35158-129-2; e-ISBN: 978-2-35158-123-0; *Eds. G. Ye, K. van Breugel, W. Sun and C. Miao*

**PRO 84:** CONSEC13—Seventh International Conference on Concrete under Severe Conditions—Environment and Loading (2013) 1930 pp., ISBN: 978-2-35158-124-7; e-ISBN: 978-2-35158-134-6; *Eds. Z.J. Li, W. Sun, C.W. Miao, K. Sakai, O.E. Gjorv and N. Banthia*

**PRO 85:** RILEM-JCI International Workshop on Crack Control of Mass Concrete and Related issues concerning Early-Age of Concrete Structures—ConCrack 3—Control of Cracking in Concrete Structures 3 (2012) 237 pp., ISBN: 978-2-35158-125-4; e-ISBN: 978-2-35158-126-1; *Eds. F. Toutlemonde and J.-M. Torrenti*

**PRO 86:** International Symposium on Life Cycle Assessment and Construction (2012) 414 pp., ISBN: 978-2-35158-127-8, e-ISBN: 978-2-35158-128-5; *Eds. A. Ventura and C. de la Roche*

**PRO 87:** UHPFRC 2013—RILEM-fib-AFGC International Symposium on Ultra-High Performance Fibre-Reinforced Concrete (2013), ISBN: 978-2-35158-130-8, e-ISBN: 978-2-35158-131-5; *Eds. F. Toutlemonde*

**PRO 88:** 8th RILEM International Symposium on Fibre Reinforced Concrete (2012) 344 pp., ISBN: 978-2-35158-132-2; e-ISBN: 978-2-35158-133-9; *Eds. Joaquim A.O. Barros*

**PRO 89:** RILEM International workshop on performance-based specification and control of concrete durability (2014) 678 pp., ISBN: 978-2-35158-135-3; e-ISBN: 978-2-35158-136-0; *Eds. D. Bjegović, H. Beushausen and M. Serdar*

**PRO 90:** 7th RILEM International Conference on Self-Compacting Concrete and of the 1st RILEM International Conference on Rheology and Processing of Construction Materials (2013) 396 pp., ISBN: 978-2-35158-137-7; e-ISBN: 978-2-35158-138-4; *Eds. Nicolas Roussel and Hela Bessaies-Bey*

**PRO 91:** CONMOD 2014—RILEM International Symposium on Concrete Modelling (2014), ISBN: 978-2-35158-139-1; e-ISBN: 978-2-35158-140-7; *Eds. Kefei Li, Peiyu Yan and Rongwei Yang*

**PRO 92:** CAM 2014—2nd International Conference on advances in chemically-activated materials (2014) 392 pp., ISBN: 978-2-35158-141-4; e-ISBN: 978-2-35158-142-1; *Eds. Caijun Shi and Xiadong Shen*

**PRO 93:** SCC 2014—3rd International Symposium on Design, Performance and Use of Self-Consolidating Concrete (2014) 438 pp., ISBN: 978-2-35158-143-8; e-ISBN: 978-2-35158-144-5; *Eds. Caijun Shi, Zhihua Ou and Kamal H. Khayat*

**PRO 94 (online version):** HPRCC-7—7th RILEM conference on High performance fiber reinforced cement composites (2015), e-ISBN: 978-2-35158-146-9; *Eds. H.W. Reinhardt, G.J. Parra-Montesinos and H. Garrecht*

**PRO 95:** International RILEM Conference on Application of superabsorbent polymers and other new admixtures in concrete construction (2014), ISBN: 978-2-35158-147-6; e-ISBN: 978-2-35158-148-3; *Eds. Viktor Mechtcherine and Christof Schroefl*

**PRO 96 (online version):** XIII DBMC: XIII International Conference on Durability of Building Materials and Components (2015), e-ISBN: 978-2-35158-149-0; *Eds. M. Quattrone and V.M. John*

**PRO 97:** SHCC3—3rd International RILEM Conference on Strain Hardening Cementitious Composites (2014), ISBN: 978-2-35158-150-6; e-ISBN: 978-2-35158-151-3; *Eds. E. Schlangen, M.G. Sierra Beltran, M. Lukovic and G. Ye*

**PRO 98:** FERRO-11—11th International Symposium on Ferrocement and 3rd ICTRC—International Conference on Textile Reinforced Concrete (2015), ISBN: 978-2-35158-152-0; e-ISBN: 978-2-35158-153-7; *Ed. W. Bramshuber*

**PRO 99 (online version):** ICBBM 2015—1st International Conference on Bio-Based Building Materials (2015), e-ISBN: 978-2-35158-154-4; *Eds. S. Amziane and M. Sonebi*

**PRO 100:** SCC16—RILEM Self-Consolidating Concrete Conference (2016), ISBN: 978-2-35158-156-8; e-ISBN: 978-2-35158-157-5; *Ed. Kamal H. Kayat*

**PRO 101 (online version):** III Progress of Recycling in the Built Environment (2015), e-ISBN: 978-2-35158-158-2; *Eds I. Martins, C. Ulsen and S. C. Angulo*

**PRO 102 (online version):** RILEM Conference on Microorganisms-Cementitious Materials Interactions (2016), e-ISBN: 978-2-35158-160-5; *Eds. Alexandra Bertron, Henk Jonkers and Virginie Wiktor*

**PRO 103 (online version):** ACESC'16—Advances in Civil Engineering and Sustainable Construction (2016), e-ISBN: 978-2-35158-161-2; *Eds. T.Ch. Madhavi, G. Prabhakar, Santhosh Ram and P.M. Rameshwaran*

**PRO 104 (online version):** SSCS'2015—Numerical Modeling—Strategies for Sustainable Concrete Structures (2015), e-ISBN: 978-2-35158-162-9

**PRO 105:** 1st International Conference on UHPC Materials and Structures (2016), ISBN: 978-2-35158-164-3; e-ISBN: 978-2-35158-165-0

**PRO 106:** AFGC-ACI-fib-RILEM International Conference on Ultra-High-Performance Fibre-Reinforced Concrete—UHPFRC 2017 (2017), ISBN: 978-2-35158-166-7; e-ISBN: 978-2-35158-167-4; *Eds. François Toutlemonde and Jacques Resplendino*

**PRO 107 (online version):** XIV DBMC—14th International Conference on Durability of Building Materials and Components (2017), e-ISBN: 978-2-35158-159-9; *Eds. Geert De Schutter, Nele De Belie, Arnold Janssens and Nathan Van Den Bossche*

**PRO 108:** MSSCE 2016—Innovation of Teaching in Materials and Structures (2016), ISBN: 978-2-35158-178-0; e-ISBN: 978-2-35158-179-7; *Ed. Per Goltermann*

**PRO 109 (2 volumes):** MSSCE 2016—Service Life of Cement-Based Materials and Structures (2016), ISBN Vol. 1: 978-2-35158-170-4; Vol. 2: 978-2-35158-171-4; Set Vol. 1&2: 978-2-35158-172-8; e-ISBN : 978-2-35158-173-5; *Eds. Miguel Azenha, Ivan Gabrijel, Dirk Schlicke, Terje Kanstad and Ole Mejlhede Jensen*

**PRO 110:** MSSCE 2016—Historical Masonry (2016), ISBN: 978-2-35158-178-0; e-ISBN: 978-2-35158-179-7; *Eds. Inge Rörig-Dalgaard and Ioannis Ioannou*

**PRO 111:** MSSCE 2016—Electrochemistry in Civil Engineering (2016); ISBN: 978-2-35158-176-6; e-ISBN: 978-2-35158-177-3; *Ed. Lisbeth M. Ottosen*

**PRO 112:** MSSCE 2016—Moisture in Materials and Structures (2016), ISBN: 978-2-35158-178-0; e-ISBN: 978-2-35158-179-7; *Eds. Kurt Kielsgaard Hansen, Carsten Rode and Lars-Olof Nilsson*

**PRO 113:** MSSCE 2016—Concrete with Supplementary Cementitious Materials (2016), ISBN: 978-2-35158-178-0; e-ISBN: 978-2-35158-179-7; *Eds. Ole Mejlhede Jensen, Konstantin Kovler and Nele De Belie*

**PRO 114:** MSSCE 2016—Frost Action in Concrete (2016), ISBN: 978-2-35158-182-7; e-ISBN: 978-2-35158-183-4; *Eds. Marianne Tange Hasholt, Katja Fridh and R. Doug Hooton*

**PRO 115:** MSSCE 2016—Fresh Concrete (2016), ISBN: 978-2-35158-184-1; e-ISBN: 978-2-35158-185-8; *Eds. Lars N. Thrane, Claus Pade, Oldrich Svec and Nicolas Roussel*

**PRO 116:** BEFIB 2016—9th RILEM International Symposium on Fiber Reinforced Concrete (2016), ISBN: 978-2-35158-187-2; e-ISBN: 978-2-35158-186-5; *Eds. N. Banthia, M. di Prisco and S. Soleimani-Dashtaki*

**PRO 117:** 3rd International RILEM Conference on Microstructure Related Durability of Cementitious Composites (2016), ISBN: 978-2-35158-188-9; e-ISBN: 978-2-35158-189-6; *Eds. Changwen Miao, Wei Sun, Jiaping Liu, Huisu Chen, Guang Ye and Klaas van Breugel*



**PRO 118 (4 volumes):** International Conference on Advances in Construction Materials and Systems (2017), ISBN Set: 978-2-35158-190-2; Vol. 1: 978-2-35158-193-3; Vol. 2: 978-2-35158-194-0; Vol. 3: ISBN:978-2-35158-195-7; Vol. 4: ISBN:978-2-35158-196-4; e-ISBN: 978-2-35158-191-9; *Ed. Manu Santhanam*

**PRO 119 (online version):** ICBBM 2017—Second International RILEM Conference on Bio-based Building Materials, (2017), e-ISBN: 978-2-35158-192-6; *Ed. Sofiane Amziane*

**PRO 120 (2 volumes):** EAC-02—2nd International RILEM/COST Conference on Early Age Cracking and Serviceability in Cement-based Materials and Structures, (2017), Vol. 1: 978-2-35158-199-5, Vol. 2: 978-2-35158-200-8, Set: 978-2-35158-197-1, e-ISBN: 978-2-35158-198-8; *Eds. Stéphanie Staquet and Dimitrios Aggelis*

**PRO 121 (2 volumes):** SynerCrete18: Interdisciplinary Approaches for Cement-based Materials and Structural Concrete: Synergizing Expertise and Bridging Scales of Space and Time, (2018), Set: 978-2-35158-202-2, Vol.1: 978-2-35158-211-4, Vol.2: 978-2-35158-212-1, e-ISBN: 978-2-35158-203-9; *Eds. Miguel Azenha, Dirk Schlicke, Farid Benboudjema, Agnieszka Knoppik*

**PRO 122:** SCC'2018 China—Fourth International Symposium on Design, Performance and Use of Self-Consolidating Concrete, (2018), ISBN: 978-2-35158-204-6, e-ISBN: 978-2-35158-205-3; *Eds. C. Shi, Z. Zhang, K. H. Khayat*

**PRO 123:** Final Conference of RILEM TC 253-MCI: Microorganisms-Cementitious Materials Interactions (2018), Set: 978-2-35158-207-7, Vol.1: 978-2-35158-209-1, Vol.2: 978-2-35158-210-7, e-ISBN: 978-2-35158-206-0; *Ed. Alexandra Bertron*

**PRO 124 (online version):** Fourth International Conference Progress of Recycling in the Built Environment (2018), e-ISBN: 978-2-35158-208-4; *Eds. Isabel M. Martins, Carina Ulsen, Yury Villagran*

**PRO 125 (online version):** SLD4—4th International Conference on Service Life Design for Infrastructures (2018), e-ISBN: 978-2-35158-213-8; *Eds. Guang Ye, Yong Yuan, Claudia Romero Rodriguez, Hongzhi Zhang, Branko Savija*

**PRO 126:** Workshop on Concrete Modelling and Material Behaviour in honor of Professor Klaas van Breugel (2018), ISBN: 978-2-35158-214-5, e-ISBN: 978-2-35158-215-2; *Ed. Guang Ye*

**PRO 127 (online version):** CONMOD2018—Symposium on Concrete Modelling (2018), e-ISBN: 978-2-35158-216-9; *Eds. Erik Schlanger, Geert de Schutter, Branko Savija, Hongzhi Zhang, Claudia Romero Rodriguez*

**PRO 128:** SMSS2019—International Conference on Sustainable Materials, Systems and Structures (2019), ISBN: 978-2-35158-217-6, e-ISBN: 978-2-35158-218-3

**PRO 129:** 2nd International Conference on UHPC Materials and Structures (UHPC2018-China), ISBN: 978-2-35158-219-0, e-ISBN: 978-2-35158-220-6

**PRO 130:** 5th Historic Mortars Conference (2019), ISBN: 978-2-35158-221-3, e-ISBN: 978-2-35158-222-0; *Eds. José Ignacio Álvarez, José María Fernández, Íñigo Navarro, Adrián Durán, Rafael Sirera*

**PRO 131 (online version):** 3rd International Conference on Bio-Based Building Materials (ICBBM2019), e-ISBN: 978-2-35158-229-9; *Eds. Mohammed Sonebi, Sofiane Amziane, Jonathan Page*

**PRO 132:** IRWRMC'18—International RILEM Workshop on Rheological Measurements of Cement-based Materials (2018), ISBN: 978-2-35158-230-5, e-ISBN: 978-2-35158-231-2; *Eds. Chafika Djelal, Yannick Vanhove*

**PRO 133 (online version):** CO2STO2019—International Workshop CO2 Storage in Concrete (2019), e-ISBN: 978-2-35158-232-9; *Eds. Assia Djerbi, Othman Omikrine-Metalssi, Teddy Fen-Chong*

**PRO 134:** 3rd ACF/HNU International Conference on UHPC Materials and Structures—UHPC'2020, ISBN: 978-2-35158-233-6, e-ISBN: 978-2-35158-234-3; *Eds. Caijun Shi and Jiaping Liu*

## **RILEM Reports (REP)**

**Report 19:** Considerations for Use in Managing the Aging of Nuclear Power Plant Concrete Structures (ISBN: 2-912143-07-1); *Ed. D. J. Naus*

**Report 20:** Engineering and Transport Properties of the Interfacial Transition Zone in Cementitious Composites (ISBN: 2-912143-08-X); *Eds. M. G. Alexander, G. Arliguie, G. Ballivy, A. Bentur and J. Marchand*

**Report 21:** Durability of Building Sealants (ISBN: 2-912143-12-8); *Ed. A. T. Wolf*

**Report 22:** Sustainable Raw Materials—Construction and Demolition Waste (ISBN: 2-912143-17-9); *Eds. C. F. Hendriks and H. S. Pietersen*

**Report 23:** Self-Compacting Concrete state-of-the-art report (ISBN: 2-912143-23-3); *Eds. Å. Skarendahl and Ö. Petersson*

**Report 24:** Workability and Rheology of Fresh Concrete: Compendium of Tests (ISBN: 2-912143-32-2); *Eds. P. J. M. Bartos, M. Sonebi and A. K. Tamimi*

**Report 25:** Early Age Cracking in Cementitious Systems (ISBN: 2-912143-33-0); *Ed. A. Bentur*

**Report 26:** Towards Sustainable Roofing (Joint Committee CIB/RILEM) (CD 07) (e-ISBN 978-2-912143-65-5); *Eds. Thomas W. Hutchinson and Keith Roberts*

**Report 27:** Condition Assessment of Roofs (Joint Committee CIB/RILEM) (CD 08) (e-ISBN 978-2-912143-66-2); *Ed. CIB W 83/RILEM TC166-RMS*

**Report 28:** Final report of RILEM TC 167-COM ‘Characterisation of Old Mortars with Respect to Their Repair (ISBN: 978-2-912143-56-3); *Eds. C. Groot, G. Ashall and J. Hughes*

**Report 29:** Pavement Performance Prediction and Evaluation (PPPE): Interlaboratory Tests (e-ISBN: 2-912143-68-3); *Eds. M. Partl and H. Piber*

**Report 30:** Final Report of RILEM TC 198-URM ‘Use of Recycled Materials’ (ISBN: 2-912143-82-9; e-ISBN: 2-912143-69-1); *Eds. Ch. F. Hendriks, G. M. T. Janssen and E. Vázquez*

**Report 31:** Final Report of RILEM TC 185-ATC ‘Advanced testing of cement-based materials during setting and hardening’ (ISBN: 2-912143-81-0; e-ISBN: 2-912143-70-5); *Eds. H. W. Reinhardt and C. U. Grosse*

**Report 32:** Probabilistic Assessment of Existing Structures. A JCSS publication (ISBN 2-912143-24-1); *Ed. D. Diamantidis*

**Report 33:** State-of-the-Art Report of RILEM Technical Committee TC 184-IFE ‘Industrial Floors’ (ISBN 2-35158-006-0); *Ed. P. Seidler*

**Report 34:** Report of RILEM Technical Committee TC 147-FMB ‘Fracture mechanics applications to anchorage and bond’ Tension of Reinforced Concrete Prisms—Round Robin Analysis and Tests on Bond (e-ISBN 2-912143-91-8); *Eds. L. Elfgrén and K. Noghabai*

**Report 35:** Final Report of RILEM Technical Committee TC 188-CSC ‘Casting of Self Compacting Concrete’ (ISBN 2-35158-001-X; e-ISBN: 2-912143-98-5); *Eds. Å. Skarendahl and P. Billberg*

**Report 36:** State-of-the-Art Report of RILEM Technical Committee TC 201-TRC ‘Textile Reinforced Concrete’ (ISBN 2-912143-99-3); *Ed. W. Bramehuber*

**Report 37:** State-of-the-Art Report of RILEM Technical Committee TC 192-ECM ‘Environment-conscious construction materials and systems’ (ISBN: 978-2-35158-053-0); *Eds. N. Kashino, D. Van Gemert and K. Imamoto*

**Report 38:** State-of-the-Art Report of RILEM Technical Committee TC 205-DSC ‘Durability of Self-Compacting Concrete’ (ISBN: 978-2-35158-048-6); *Eds. G. De Schutter and K. Audenaert*

**Report 39:** Final Report of RILEM Technical Committee TC 187-SOC ‘Experimental determination of the stress-crack opening curve for concrete in tension’ (ISBN 978-2-35158-049-3); *Ed. J. Planas*

**Report 40:** State-of-the-Art Report of RILEM Technical Committee TC 189-NEC ‘Non-Destructive Evaluation of the Penetrability and Thickness of the Concrete Cover’ (ISBN 978-2-35158-054-7); *Eds. R. Torrent and L. Fernández Luco*

**Report 41:** State-of-the-Art Report of RILEM Technical Committee TC 196-ICC ‘Internal Curing of Concrete’ (ISBN 978-2-35158-009-7); *Eds. K. Kovler and O. M. Jensen*

**Report 42:** ‘Acoustic Emission and Related Non-destructive Evaluation Techniques for Crack Detection and Damage Evaluation in Concrete’—Final Report of RILEM Technical Committee 212-ACD (e-ISBN: 978-2-35158-100-1); *Ed. M. Ohtsu*

**Report 45:** Repair Mortars for Historic Masonry—State-of-the-Art Report of RILEM Technical Committee TC 203-RHM (e-ISBN: 978-2-35158-163-6); *Eds. Paul Maurenbrecher and Caspar Groot*

**Report 46:** Surface delamination of concrete industrial floors and other durability related aspects guide—Report of RILEM Technical Committee TC 268-SIF (e-ISBN: 978-2-35158-201-5); *Ed. Valerie Pollet*

# Contents

<b>1 Digital Fabrication with Cement-Based Materials—The Rilem D.F.C. Technical Committee History, Strategy and Achievements</b> .....	1
Nicolas Roussel, Dirk Lowke, and Richard Buswel	
<b>2 Digital Fabrication with Cement-Based Materials: Process Classification and Case Studies</b> .....	11
R. A. Buswell, F. P. Bos, Wilson Ricardo Leal da Silva, N. Hack, Harald Kloft, Dirk Lowke, Niklas Freund, Asko Fromm, E. Dini, Timothy Wangler, E. Lloret-Fritschi, Roel Schipper, Viktor Mechtcherine, Arnaud Perrot, K. Vasilic, and Nicolas Roussel	
<b>3 Digital Fabrication with Cement-Based Materials: Underlying Physics</b> .....	49
Viktor Mechtcherine, S. Fataei, F. P. Bos, R. A. Buswell, Wilson Ricardo Leal da Silva, E. Keita, H. W. Krauss, Dirk Lowke, Arnaud Perrot, Venkatesh Naidu Nerella, Nicolas Roussel, Mohammed Sonebi, Timothy Wangler, Daniel Weger, and Rob Wolfs	
<b>4 Printable Cement-Based Materials: Fresh Properties Measurements and Control</b> .....	99
Timothy Wangler, Robert J. Flatt, Nicolas Roussel, Arnaud Perrot, Mohammed Sonebi, Rob Wolfs, Freek Bos, Dirk Lowke, Niklas Freund, Dietmar Stephan, Ursula Pott, Lex Reiter, Steffen Grünewald, Wilson Ricardo Leal da Silva, and Geert De Schutter	

**5 Properties and Testing of Printed Cement-Based Materials in Hardened State** ..... 137  
Jolien Van Der Putten, Venkatesh Naidu Nerella,  
Viktor Mechtcherine, Mélody D’Hondt, Mohammed Sonebi,  
Daniel Weger, Zhendi Wang, Constantino Menna, Nicolas Roussel,  
Dirk Lowke, Kim Van Tittelboom, and Geert De Schutter

**6 Structural Design and Testing of Digitally Manufactured Concrete Structures** ..... 187  
Domenico Asprone, Costantino Menna, Freek Bos,  
Jaime Mata-Falcón, Liberato Ferrara, Ferdinando Auricchio,  
Ezio Cadoni, Vítor M. C. F. Cunha, Laura Esposito, Asko Fromm,  
Steffen Grünewald, Harald Kloft, Viktor Mechtcherine,  
Venkatesh Naidu Nerella, and Roel Schipper

# Chapter 1

## Digital Fabrication with Cement-Based Materials—The Rilem D.F.C. Technical Committee History, Strategy and Achievements



Nicolas Roussel, Dirk Lowke, and Richard Buswel

### 1.1 Background

In the last decade, the potential of 3D printing (and more generally of digital manufacturing) in the construction industry has been widely reported in the media. In 2017, CNN website posed the question “Will the world next megacity drip out of a 3D printer?”. This question is indeed timely as many groups world-wide engaged in research and enterprise while large organisations are investing in the technology. Academic and industrial R&D partnerships have been established and there has been a proliferation of approaches stemming from the early work in the mid-late 2000’s (Lim et al. 2012) to the richer variety found in the contemporary field (Labonnote et al. 2016; Buswell et al. 2018; Wangler et al. 2019).

There is a strong sense of anticipation in the construction industry, fuelled by the international recognition of the need for the wider automation of construction (Siemens 2017a; HM Government 2017). Several specialist companies, such as XtreeE or Apis Cor, have emerged and start-up initiatives are proliferating. At the start of 2013, there were 20 start-ups in the field. 5 years later, there were more than 65 offering services, tools, building components or even entire buildings and the numbers continue to grow (The Boston Consulting Group 2018). In parallel, several large established companies in Europe, such as Vinci, have taken the decision to be early adopters of this technology and have made strategic moves and start acquiring

---

N. Roussel (✉)

Laboratoire Navier, Gustave Eiffel University, Champs sur Marne, France  
e-mail: [nicolas.roussel@ifsttar.fr](mailto:nicolas.roussel@ifsttar.fr)

D. Lowke

Institute of Building Materials, Concrete Construction and Fire Safety, Technische Universität Braunschweig, Braunschweig, Germany

R. Buswel

School of Architecture, Building and Civil Engineering, Loughborough University, Loughborough, UK

© RILEM 2022

N. Roussel and D. Lowke (eds.), *Digital Fabrication with Cement-Based Materials*, RILEM State-of-the-Art Reports 36, [https://doi.org/10.1007/978-3-030-90535-4\\_1](https://doi.org/10.1007/978-3-030-90535-4_1)

specialized skills and capabilities in robotics (Buswell et al. 2018). Finally, regulation and numerous public policy measures are encouraging the adoption of 3D printing in many parts of the world such as the Middle East, the United Kingdom, China (with a draft for a national standard for 3D-concrete-printing) and the US. The Boston Consulting Group concluded in its 2018 report that “As this evolution proceeds, the construction industry as a whole will be transformed. Companies and governments would do well to prepare for this transformation and to influence it as far as possible to their own advantage” (Buswell et al. 2018).

## 1.2 The Expected Benefits of Digital Fabrication with Concrete

The reasons behind this exploding trend are many but these digital manufacturing technologies are described as being able to provide a means to simultaneously tackle issues around productivity, cost, health, safety and quality.<sup>1</sup>

First, their adoption is driven by the need to adopt digital processes and automation in the sector to deliver the anticipated renovation of infrastructure and housing. Hence, for most actors, the timing synchronises perfectly with commercial needs. This has not happened over night, the construction sector has been digitising its design methods and developing new tools allowing for a better management of the different construction stages over the last decade, *e.g.* Building Information Modelling (BIM). Digital manufacturing therefore pushes the construction sector beyond the digitalisation of design, data management and planning into the digital control and actuation of its manufacturing processes: a significant step towards Industry 4.0.

Second, construction manufacturing is traditionally labour intensive and the implementation of automation is expected to compensate for the urgent skill shortage in the sector,<sup>2,3,4</sup> enhance health & safety<sup>5</sup> and enable savings of up to 40% in the way projects are delivered and maintained.<sup>6</sup> Large-scale additive manufacturing, commonly referred to as 3D Concrete Printing (3DCP) have, alongside many other novel digital fabrication methods, emerged worldwide in response to the global call to modernise construction manufacturing (HMGov 2017; Siemens 2017b; Barbosa et al. 2017). The advanced involvement of robots in the construction site of the future is moreover expected to improve working conditions for the labour force.

---

<sup>1</sup> McKinsey&Company. Available From: <https://www.mckinsey.com//media/McKinsey/Industries/Capital>.

<sup>2</sup> <https://www.gov.uk/government/topical-events/the-uks-industrial-strategy>.

<sup>3</sup> [https://www.arcadis.com/media/4/B/9/%7B4B999107-2F44-42E2-94D7-43FDD0963378%7D9784\\_Talent%20Scale%20FINAL%20WEB\\_2102.pdf](https://www.arcadis.com/media/4/B/9/%7B4B999107-2F44-42E2-94D7-43FDD0963378%7D9784_Talent%20Scale%20FINAL%20WEB_2102.pdf).

<sup>4</sup> [https://www.engineeringuk.com/media/1356/enguk\\_report\\_2017\\_synopsis.pdf](https://www.engineeringuk.com/media/1356/enguk_report_2017_synopsis.pdf).

<sup>5</sup> <http://www.iaarc.org/publications/fulltext/ISARC2016-Paper036.pdf>.

<sup>6</sup> <https://www.mckinsey.com/industries/capital-projects-and-infrastructure/our-insights/infrastructure-productivity>.



The increase in productivity through 3DCP in construction does not necessarily mean the replacement of all hand operations by automation, but the reduction of intermediate stages required in fabrication, such as the need for a mould (Gibson et al. 2015). Because of this, 3DCP offers value-added because it enables a significant amount of customisation in design with little if any increase of fabrication costs (Hague et al. 2003).

Finally, digital manufacturing offers a great and inexpensive freedom of design, which answers the need for tailor-made and customized solutions. This technology allows for the production of complex systems as special functions such as thermal or acoustic insulations can be integrated directly into the printouts. By doing so, it reduces environmental impacts as freedom of design and multi-functionality allow for the consumption of lower amounts of raw materials.

### 1.3 Obstacles

The outlook is therefore very promising. It is anticipated that 3D printing will become competitive with conventional in-situ and off-site construction if the existing technological obstacles can be overcome and the integration of these processes within the sector is supported by both standards and relevant human resources. The degree of importance of these obstacles varies significantly depending on the application and its technology readiness level, which we illustrate here using the most common class of cement-based, additive manufacturing, material extrusion (Buswell et al. 2020).

Extrusion-based additive manufacturing uses digital models of the desired geometries to drive the manufacturing process by digitally slicing the 3D object into a number of layers, spaced at an equivalent distance to the deposition layer thickness the machine uses. The cement mortar is initially a dry blended powder mix with a number of constituent ingredients which typically might be aggregates (sand), cement, fillers, often industrial by-products such as silica fume and water (Le et al. 2012a).

The materials vary in characteristics because they are natural products or by-products of other industrial processes. Even the manufacture of cement produces significant variations in the reactive compounds from batch to batch. The shape, size and grading of these constituents along with environmental conditions all affect how the fresh material behaves when pumped and extruded (Roussel 2011) and how the material hardens. This process is strongly time-dependent and the specific conditions, under which a layer of fresh material is placed on an older one, have consequences for the strength of the joint formed (Le et al. 2012b).

In a typical configuration of a 3D printing system, the dry material is mixed in a batch, where admixture might be added to fine-tune fresh properties (Aïtcin and Flatt 2016). This mixing might also be carried out continuously. The material is placed in the hopper of a pump and conveyed, often by a positive displacement pump, down a supply line to a nozzle where it is extruded and deposited. The extrusion rate and nozzle diameter might be varied, and the robotic arm provides a means of positioning

the extruded filament. A mixing chamber might also be placed in the nozzle so that other admixtures might be added that can help to tune the stiffening of the material (Chen et al. 2019; Dorn et al. 2020) and its kinetics.

The geometric quality of manufactured parts is not only affected by the precision of the printing but also by the deformation under self-weight during manufacture (Wolfs et al. 2018; Perrot et al. 2016; Reiter et al. 2018; Jie et al. 2020). The time dependent characteristics of cement hydration and hardening plays a significant role in the performance of the resultant material and printed element. Fresh material must initially remain fluid enough to facilitate extrusion and inter-layer bonding during manufacture (Buswell et al. 2020; Le et al. 2012a; Roussel 2018), but materials that are too fluid can lead to buckling and collapse of structures under the increasing weight of the successive layers (Roussel 2018; Alexandridis and Gardner 1981; Lu and Wang 2010). The importance of these mechanisms has driven significant efforts in recent works: determining the rheological requirements of the fresh material (Roussel 2018); quantifying buildability (Kruger et al. 2019, 2020); and predicting structural failure (Suiker 2018; Wolfs and Suiker 2019) for controlling deformation behaviours. Undesirable effects can be exacerbated by poor control of material delivery, filament placement and toolpath planning. Being able to measure, assess and benchmark process and material performance using standardised and internationally accepted approaches is therefore essential for the industrial future of the technology.

The international community has demonstrated a wide range of applications for many various manufacturing technologies, but the field needs now to move from *one off production* to *routine production at volume*. There needs to be a greater uptake by industry to realize these benefits in the sector but the lack of standardisation and formal certification of 3DCP products and processes remains a significant barrier to adoption: for example, the ambitions for printing the 25% of buildings in Dubai by 2025 in 2016<sup>7</sup> has almost ceased due to a lack of regulation compliance.

Standardised methods and principles for evaluating the performance of 3DCP materials, processes and products do not exist. Achieving this is challenging, requiring many manufacturing platforms, products and materials to generate robust standards and assessment methods. This requires a collective work and the existence of strong scientific community around the topic.

## 1.4 RILEM Technical Committee Creation and Scientific Strategy

On the 15th of May 2016, in Washington DC, during the SCC 2016 conference, a couple tens of researchers from all around the world met for the first time to discuss the need for some collective action with regard to Digital Fabrication with Concrete (DFC).

---

<sup>7</sup> <https://www.weforum.org/agenda/2018/05/25-of-dubai-s-buildings-will-be-3d-printed-by-2025/>.

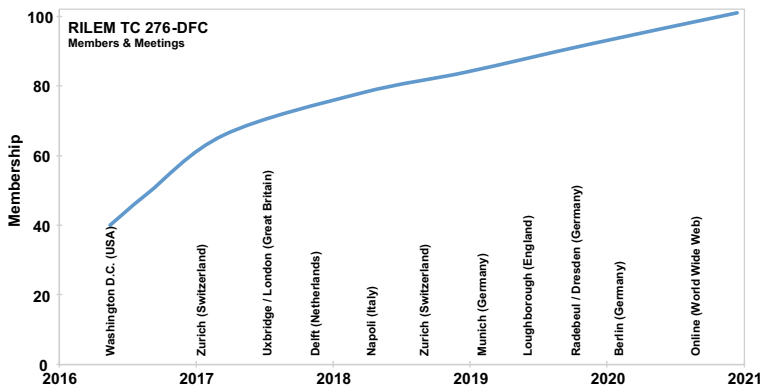


**Fig. 1.1** RILEM TC 276-DFC—membership and meetings

This group of RILEM experts took the first internationally collaborative steps in pre-standardisation by bringing together world-leading research facilities with the key industrial actors of a future market for DFC, which included material suppliers, technology providers, designers, end-user manufacturers and regulating authorities.

The most important outcomes of the technical committee are:

- a unified process classification for digital fabrication with concrete
- a state of the art of the testing methods (both at a material and structural level) that could form the foundation of some quality control procedure for fresh properties along with hardened and service life performance.

With 101 members from 21 nations, TC 276-DFC “Digital fabrication with cement-based materials” was one of the largest RILEM TCs of its time. The interest in the work of the TC kept on increasing steadily over the years, Fig. 1.1. In addition to the kick-off meeting in Washington D.C., a total of ten working meetings were held, which were organised by the universities in Zurich, London, Delft, Napoli, Munich, Loughborough and Dresden as well as by the German Concrete and Construction Society. Due to the COVID-19 pandemic, the last meeting was held as an online meeting. In conjunction with the working meetings, six workshops and mini-symposia were organised in Zurich, Uxbridge, Delft, Napoli and Loughborough on which the latest state of research and development was presented and discussed.

In the first meetings, initial experiences with digital technologies in concrete construction, which at that time was still a new field of research and development addressed by only a few universities and companies, were exchanged and the working methodology and objectives of the TC were discussed.

The majority of the members voted for preparing a state-of-the-art-report in order to provide a first impulse towards a future standardisation in the field of digital manufacturing in construction. In the course of the discussion, the need for a classification of the various technologies at the core of the STAR became apparent, in order to

provide a systematisation of the so far hardly organised diversity of processes and applications. Its purpose was also to serve as an important basis for a collective technical communication and form the basis of the semantics of the field. This classification was intensively discussed and developed in a series of working meetings. In addition, further topics that are essential for digital fabrication with cement-based materials, such as the underlying physics, fresh properties measurements and control, properties and testing in hardened state as well as structural design and testing were addressed in the discussions of the TC DFC, and the corresponding state of research and development was consolidated in the STAR that is now available. In addition, numerous joint scientific publications were initiated by the members of the TC DFC, which are, amongst others, published in the Cement and Concrete Research Special Issues “Digital concrete 2018” and “Digital Concrete 2020”.

## 1.5 Achievements and Today’s Status

Today, there are more than 35 commercial organisations of various sizes and states of maturity offering 3DCP services and products. About 50% of those print buildings walls in-situ and about 50% manufacture off-site. Most are based on material extrusion controlled digitally via robot arm, gantry or crane system. The processes found in DFC are similar to conventional Additive Manufacturing processes in many respects, except the multiphase material combined with the large scale of manufacture generate unique challenges and questions which largely revolve around the handling, preparation and control of the material. The ever-advancing state of the commercial environment surrounding the technology will increase the need for continued improvement of material and process control and greater understanding of durability, design and production logistics.

Following the first international RILEM conference on Digital Fabrication with Concrete in Zurich in September 2018<sup>8</sup> and the second international RILEM conference organized online by TU Eindhoven (Freek Bos et al. 2020), we have now established the foundations of a collaborative international community that includes both academic and industrial actors working together to advance the technology from a collective understanding of the current start of the art.

The present report gathers the fruits of our meetings, conferences and publications over the last years. It is defining the basis of this new field while listing the opened questions along with research needs. The book is divided into 5 chapters in addition to this introduction.

Chapter 2, *Digital Fabrication with Cement-Based Materials: Process classification and case studies*, contains the process classification resulting from our collective discussions along with a show case of various applications.

Chapter 3, *Digital fabrication with cement-based materials: underlying physics*, presents an overview of the underlying physics relevant to an understanding of the

---

<sup>8</sup> digitalconcrete2018.ethz.ch.

processing of cement-based materials during various production steps of digital fabrication.

Chapter 4, *Printable Cement-based Materials: Fresh Properties Measurements & Control*, focuses on the fresh key properties identified in Chap. 3. It giving a focus to yield stress and structural build-up. The traditional measurements for properties of interest are then described, followed by a more detailed description of the newest measurement techniques that have been developed so far specifically for digital fabrication.

Chapter 5, *Properties and testing of printed cement-based materials in hardened state*, focus on the consequences of such a drastic change in processing on material properties (strength and durability). It highlights the role of interfaces and the resulting on mechanical performance, transport properties and durability behaviour.

Chapter 6, *Structural design and testing of digitally manufactured concrete structures*, focuses on the specifics of structural design and engineering of Digital fabrication. It introduces the specific challenges of structural design and engineering by providing an overview of the structural typologies that have been developed so far and by comparing the underlying structural principles with the standard codified approaches used in conventional reinforced concrete.

This book was written over a period of five years from the initial concept to the final editing. All members of the RILEM technical committee TC 276-DFC “Digital fabrication with cement-based materials”, the co-authors of this book and the chairs of the committee hope you will find in the above chapters some answers to any questions you could have on these ground breaking technologies.

*Nicolas Roussel, chair of RILEM TC-DFC.*

*Dirk Lowke, co-chair of RILEM TC-DFC.*

*Richard Buswell, Chap. 2 convener and leader of the unified process classification task group.*

## References

- Aïtcin, P., and Flatt, R. (2016). *Science and technology of concrete admixtures*. Woodhead Press, Cambridge.
- Alexandridis, A., and Gardner, N. J. (1981). Mechanical behaviour of fresh concrete. *Cement and Concrete Research*, 11(3), 323–339. [https://doi.org/10.1016/0008-8846\(81\)90105-8](https://doi.org/10.1016/0008-8846(81)90105-8).
- Barbosa, F., Woetzel, J., Mischke, J., Ribeirinho, M. J., Sridhar, M., Parsons, M., Bertram, N., and Brown, S. (2017, February). Reinventing construction: a route to higher productivity.
- Buswell, R. A., Leal da Silva, W. R., Bos, F. P., Schipper, H. R., Lowke, D., Hack, N., Kloft, H., Mechtcherine, V., Wangler, T., Roussel, N. (2020). A process classification framework for defining and describing Digital Fabrication with Concrete, Vol. 134, pp. 106068. <https://doi.org/10.1016/j.cemconres.2020.106068>.
- Buswell, R., de Silva, W. L., Jones, S., and Dirrenberger, J. (2018). 3d printing using concrete extrusion: a roadmap for research. *Cement and Concrete Research* 112, 37–49. SI: Digital concrete 2018.

- Chen, Y., Chaves Figueiredo, S., Yalcinkaya, C., Copuroglu, O., Veer, F., and Schlangen, E. (2019). The effect of viscosity-modifying admixture on the extrudability of limestone and calcined clay-based cementitious material for extrusion-based 3d concrete printing. *Materials* 12 (9).
- Dorn, T., T. Hirsch, and D. Stephan (2020). Study on the influence of accelerators on the hydration of portland cement and their applicability in 3d printing. In V. Mechtcherine, K. Khayat, and E. Secieru (Eds.), *Rheology and Processing of Construction Materials*, Cham, pp. 382–390. Springer International Publishing.
- Freek Bos, Rob Wolfs, Theo Salet, CCR Digital Concrete 2020 SI: Editorial, Cement and Concrete Research Volume 135, September 2020, 106157.
- Gibson, I., Rosen, D., and Stucker, B. (2015). *Additive manufacturing technologies: 3D printing, Rapid Prototyping, and Direct Digital Manufacturing*. Springer, New York.
- Hague, R., Campbell, I., and Dickens, P. (2003). Implications on design of rapid manufacturing. *Journal of Mechanical Engineering Science* 1(1), 25–30.
- HM Government (2017). *Industrial Strategy Report*.
- HMGov. (2017, November). *Industrial strategy: building a Brittan fit for the future*.
- Jie Xu, Richard A. Buswell, Peter Kinnell, Istvan Biro, John Hodgson, Nikolaos Konstantinidis, Liyun Ding. (2020). Inspecting manufacturing precision of 3D printed concrete parts based on geometric dimensioning and tolerancing. *Automation in Construction*, 117, 103233, <https://doi.org/10.1016/j.autcon.2020.103233>.
- Kruger, J., Zeranka, S., and van Zijl, G. (2019). 3D concrete printing: a lower bound analytical model for buildability performance quantification. *Automation in Construction*, 106, 102904. <https://doi.org/10.1016/j.autcon.2019.102904>.
- Kruger, J., Zeranka, S., and van Zijl, G. (2020). Quantifying constructability performance of 3D concrete printing via rheology-based analytical models. In: Mechtcherine, V., Khayat, K., Secieru, E. (Eds.) *Rheology and Processing of Construction Materials*. RheoCon 2019, SCC 2019. RILEM Bookseries, vol 23. Springer, Cham. [https://doi.org/10.1007/978-3-030-22566-7\\_46](https://doi.org/10.1007/978-3-030-22566-7_46).
- Labonnote, N., Rønquist, A., Manum, B., and Ruther, P. (2016). Additive construction: State-of-the-art, challenges and opportunities. *Automation in Construction* 72(Part 3), 347–366.
- Le, T. T., Austin, S. A., Lim, S., Buswell, R. A., Gibb, A. G., and Thorpe, T. (2012). Mix design and fresh properties for high-performance printing concrete. *Materials and Structures*, 45(8), 1221–1232. <https://doi.org/10.1617/s11527-012-9828-z>.
- Le, T., Austin, S., Lim, S., Buswell, R., Law, R., Gibb, A., and Thorpe, T. (2012). Hardened properties of high-performance printing concrete. *Cement and Concrete Research* 42(3), 558–566.
- Lim, S., Buswell, R., Le, T., Austin, S., Gibb, A., and Thorpe, T. (2012). Developments in construction- scale additive manufacturing processes. *Automat Constr* 21, 262–268.
- Lu, G., and Wang, K. (2010). Investigation into yield behavior of fresh cement paste: model and experiment. *ACI Materials Journal*, 107(1), 12.
- Perrot, A., Rangeard, D., and Pierre, A. (2016). Structural built-up of cement-based materials used for 3D-printing extrusion techniques. *Materials and Structures*, 49(4), 1213–1220. <https://doi.org/10.1617/s11527-015-0571-0>.
- Reiter, L., Wangler, T., Roussel, N., and Flatt, R. J. (2018). The role of early age structural build-up in digital fabrication with concrete. *Cement and Concrete Research*, 112, 86–95. <https://doi.org/10.1016/j.cemconres.2018.05.011>.
- Roussel, N. (2011). *Understanding the Rheology of Fresh Concrete*. Woodhead Publishing.
- Roussel, N. (2018). Rheological requirements for printable concretes. *Cement and Concrete Research*, 112, 76–85. <https://doi.org/10.1016/j.cemconres.2018.04.005>.
- Siemens. (2017a). *Made Smarter Report*.
- Siemens. (2017b, October). *Made smarter review*.
- Suiker, A. S. J. (2018). Mechanical performance of wall structures in 3D printing processes: theory, design tools and experiments. *International Journal of Mechanical Sciences*, 137, 145–170. <https://doi.org/10.1016/j.ijmecsci.2018.01.010>
- The Boston Consulting Group. (2018). *Will 3D Printing remodel the construction industry?*

- Wangler, T., Roussel, N., Bos, F., Salet, T., and Flatt, R. (2019). Digital concrete: a review. *Cement and Concrete Research*, 123.
- Wolfs, R. J. M., and Suiker, A. S. J. (2019). Structural failure during extrusion-based 3D printing processes. *The International Journal of Advanced Manufacturing Technology*, 1–20. <https://doi.org/10.1007/s00170-019-03844-6>.
- Wolfs, R. J. M., Bos, F. P., and Salet, T. A. M. (2018). Early age mechanical behaviour of 3D printed concrete: Numerical modelling and experimental testing. *Cement and Concrete Research*, 106, 103–116. <https://doi.org/10.1016/j.cemconres.2018.02.001>.

# Chapter 2

## Digital Fabrication with Cement-Based Materials: Process Classification and Case Studies



**R. A. Buswell, F. P. Bos, Wilson Ricardo Leal da Silva, N. Hack, Harald Kloft, Dirk Lowke, Niklas Freund, Asko Fromm, E. Dini, Timothy Wangler, E. Lloret-Fritschi, Roel Schipper, Viktor Mechtcherine, Arnaud Perrot, K. Vasilic, and Nicolas Roussel**

**Abstract** The need for methods for forming concrete has existed for as long as concrete has been used in constructing the built environment. Creating flat, rectilinear formers have traditionally been the cost and time efficient default for the majority of applications. The desire for greater design freedom and the drive to automate construction manufacturing is providing a platform for the continued development of a family of processes called Digital Fabrication with Concrete

---

R. A. Buswell (✉)

School of Architecture, Building and Civil Engineering, Loughborough University,  
Loughborough, UK

e-mail: [r.a.buswell@lboro.ac.uk](mailto:r.a.buswell@lboro.ac.uk)

F. P. Bos

Department of the Built Environment, Eindhoven University of Technology, Eindhoven,  
Netherlands

W. R. L. da Silva

Danish Technological Institute, Taastrup, Denmark

N. Hack · H. Kloft

Institute of Structural Design, Technische Universität Braunschweig, Braunschweig, Germany

D. Lowke · N. Freund

Institute of Building Materials, Concrete Construction and Fire Safety, Technische Universität Braunschweig, Braunschweig, Germany

A. Fromm

Hochschule Wismar. University of Applied Sciences, Technology, Business and Design—structural design, Wismar, Germany

E. Dini

Monolite Ltd, 101 Wardour Street, London W10UN, UK

T. Wangler · E. Lloret-Fritschi

Institute for Building Materials, Physical Chemistry of Building Materials, ETH Zurich, Zurich,  
Switzerland

R. Schipper

Department Materials, Mechanics, Management & Design, Delft University of Technology, Delft,  
Netherlands

© RILEM 2022

N. Roussel and D. Lowke (eds.), *Digital Fabrication with Cement-Based Materials*,  
RILEM State-of-the-Art Reports 36, [https://doi.org/10.1007/978-3-030-90535-4\\_2](https://doi.org/10.1007/978-3-030-90535-4_2)



(DFC) technologies. DFC technologies are many and varied. Much of the material science theory is common, but the process steps vary significantly between methods, creating challenges as we look towards performance comparison and standardisation. Presented here is a framework to help identify and describe process differences and a showcase of DFC application case studies that explain the processes behind a sub-set of the technologies available.

## 2.1 Introduction

Productivity, cost overruns and quality in the construction sector has for many years been a recognised problem (Latham 1994; Egan 1998). Productivity in particular has stagnated over the last 25 years, compared to almost doubling in other sectors (Changali et al. 2015). Automation and the digitisation of information exchange, communication and control are expected to play a key role in helping to mitigate these issues (Barbosa et al. 2017; Siemens 2017; HMGovernment 2017). While innovation in construction machines is not new (Urshel 1941), automation presents a significant departure from conventional construction methods. Historically, the application of robotics has been of significant interest (Kuntse et al. 1995; Yamazaki and Maeda 1998; Gambao et al. 2000).

Digital Fabrication with Concrete (DFC) methods are a family of technologies that offer digital control over the design and manufacturing process (Buchi et al. 2018; Buswell et al. 2020). They promise the manufacture of both architectural and structural components (Hack et al. 2013; Labonnote et al. 2016; Buswell et al. 2018; Aspone et al. 2018; Mechtcherine et al. 2019) and have been the focal point for significant development in the field of cement-based mortars, particularly with respect to the hardened properties (Le et al. 2012a; Nerella et al. 2019; Tay et al. 2019); control and understanding of rheology (Le et al. 2012b; Roussel 2018); control of structural build-up and on-demand setting (Reiter et al. 2018; Marchon et al. 2018); and the mechanics of the building up layers of wet material without formwork (Wolfs 2018a, 2019a).

DFC methods have been around for some time with its roots in Computer Numeric Control (CNC), which took hold in the 1960s. CNC developed through the 1970 and 1980s where the computer revolution initiated the development of computer-aided

---

V. Mechtcherine

Institute of Construction Materials, Technische Universitat Dresden, Dresden, Germany

A. Perrot

Univ. Bretagne Sud, UMR CNRS 6027, IRDL, 56100 Lorient, France

K. Vasilic

German Society for Concrete and Construction Technology, Berlin, Germany

N. Roussel

Laboratoire Navier, Gustave Eiffel University, Eiffel, France

design software that allows for ‘parametric’ design (Howe 2000; Schodek et al. 2005; Menges 2006). These tools have driven architectural design for many years and the construction of Frank Gehry’s Zollhoff Towers in Dusseldorf (2000) which was modelled in CATIA, and used CNC cutting and milling to generate foam moulds used to cast the structure of the building, is just one example (Kolarevic 2005).

In the product design field, the computer-aided design (CAD) environment allowed for the digital design of products; however, a prototype model for aesthetic and/or functional testing needed to be carried out by hand. In the 1980s, the first layer-based manufacturing process emerged that made it possible for a physical model to be created directly from CAD data. This significantly reduced the cycle time for evaluating product prototypes, and Rapid Prototyping was established (Lipson and Kurman 2013).

Over the last 25 years, there have been considerable developments in materials. The use of these *Rapid Prototyping* machines for the production of end-use parts has developed into *Additive Manufacturing* (Gibson et al. 2015). The flexibility in the geometries that could be produced led to early actors exploring similar principles to create large architectural components (Lim et al. 2012). However, additive approaches are just one process type in the DFC family and moulding systems such as TailorCrete (Andersen et al. 2016) and Smart Dynamic Casting (Lloret-Fritschi 2020) are just two examples of alternative methods.

The contemporary field is becoming populated with many actors internationally, both commercial and academic, and there is a terrific variety in the materials and processes used. Indeed, there is a significant variation in system maturity and in the manufacturing applications under investigation. The configuration of mixing and pumping, the use of admixtures, the mortar/concrete composition and the design of what is being manufactured all affect the process design and the criticality of operational parameters. The comparison of the performance of two systems as well as the quality of the material produced by them is, therefore, challenging.

Recognising the need to clearly understand and articulate the differences between DFC processes, and thus allow performance comparison and the initiation of standardisation, the RILEM TC-276 undertook to develop a classification framework for DFC. This has been recently published and provides an overview of classification methods, developing the state of the art into a set of principles and an approach to allow the unambiguous definition and description of a DFC process (Buswell et al. 2020). The work is published under an open access agreement. This chapter describes the above classification framework and is followed by a series of DFC application case studies that illustrate the differences in practice.

## 2.2 Assembly and Material Forming Processes

Buildings, like cars, are complex assemblies comprising of parts (windscreen in a car/window in a building) and sub-assemblies (the engine in a car/an air-conditioning chiller in a building). These require the design and manufacture of many components, using different shaping processes, dictated by the material characteristics and the

form required. The complexity of the form will limit what is achievable in a single component, compare a plastic spoon to the bodywork on a car, or the façade of a building. Individual parts, therefore, need to be assembled to produce the whole product, and that assembly requires the joining of adjacent parts.

Permanent *joining* can be achieved using methods such as *welding/brazing* and *soldering/adhesives*, or through the application of permanent fasteners (snap-fits is one example, (Troughton 2009)). Welding uses energy to melt the material, typically metals and thermoplastics, to create a pool of material which then cools joining parts through fusion. There are many sub-classes of welding, of which two are Gas Metal Arc (MIG) and Electron Beam. Brazing and soldering use a second material that is melted to join two parts, rather than melting the part material: the temperature, at which the filler material melts, determines which name is used. Adhesives use a chemical bonding process. There are many examples of these methods in all industries and to pick two within DFC: MeshMould utilises welding to permanently assemble a reinforcement cage (Hack et al. 2020), the Fastbrick (Bonwetsch 2015) utilises adhesive bonding to join bricks. When components need to be removed for maintenance, replacement, or disassembly at the end of life, temporary fastenings may be deployed where screws, nuts and bolts are examples of *threaded fasteners*.

Parts can require *surface treatment, coating*, or other deposition processes to achieve a particular function, often to increase durability or provide an aesthetic finish. Examples in metals are case-hardening, through diffusion or heat treatments and in concrete, include hydrophobic impregnation. Painting is a common coating throughout manufacturing and construction that provides protection of the material from the environment in addition to providing aesthetic options.

The production of the individual parts themselves requires the shaping of material, which can be achieved using either *formative, additive* or *subtractive* processes. Formative methods shape a finite volume of material using a preformed mould, die or surface. Approaches that rely on the *solidification* of material use a mould into which the fluid material is poured, or injected. The forces required to take on the shape of the form depend on the material properties: being driven by gravity in the conventional casting of concrete, or under high-pressure in injection moulding, for example. *Deformation* approaches rely on the plastic state of the material and include methods such as stamping, rolling and pressing. DFC processes such as Smart Dynamic Casting (SDC, Sect. 2.4.6) and Adapta (Sect. 2.4.7) rely on the plastic state of concrete/cement-based mortar.

Subtractive methods shape the desired geometry from a larger volume of material, that is cut, drilled, milled and ground away until the form is realised. Examples include stone masonry, sculpture or turning items on a lathe or other CNC tool. In DFC, milling or hot wire cutting is commonly used to create bespoke moulds (Garcia 2010). Additive Manufacturing, however, is the inverse where material is progressively placed until the final form has been created. ISO 17296 2015, 2016 recognise seven additive process classes, of which the three that are commonly found in manufacturing and DFC are: *material extrusion* (Fuse Deposition Modelling, 3D concrete printing, i.e. Sects. 2.4.1, 2.4.2, 2.4.3, and 2.4.8); *material jetting* (Thermojet, Shotcrete 3D concrete printing, Sect. 2.4.4); and Binder Jetting (3D

Systems ZPrinter) which is often referred to as *Particle-bed Binding* in construction applications (Sect. 2.4.5). Further details on Additive Manufacturing can be found in Gibson et al. (2015).

### 2.3 Classification of DFC Processes

The full details of the classification framework are presented in Buswell et al. (2020), which is an open access publication. In principle, it should:

- encompass the broad spectrum of processes found in DFC;
- maintain differentiation between on-site, in-situ processes and processes for the production of parts in a factory;
- be based on pre-existing definitions and commonly understood frameworks of material forming and assembly processes; and,
- seek to build on (or adopt) existing standards where practicable.

Within the board DFC family, the material used is similar in so far as the binding agent belongs to the family of cements with related properties, and these are often combined with aggregates to form a mortar or concrete material. DFC process are typically designed and tested to manufacture a family of cement based products: such as panels, or walls, or columns. These applications tend to inform the selection of critical process and material parameters (Buswell et al. 2018).

Once these requirements are identified, additional processes are employed to affect particular operations, which could be surface smoothing, in the case of Contour Crafting (Khoshnevis 2006), hydration control when the objects under manufacture need to be rapidly built in the vertical direction (Gosselin 2016), or the assembly of the reinforcement mesh prior to casting in the MeshMould application (Hack and Lauer 2014). A closer inspection of the technology, reveals yet more sub-processes that could incorporate automated measurement such as that used to control deposition height through real-time feedback control (Wolfs et al. 2018b) or the mixing and pumping of mortars (in almost all processes) for example.

These sub-processes are often required to enable the main material forming process to take place, and so with the intent to create a meaningful classification method, we find that we can distinguish the processes based on the primary material forming process, for which frameworks exist. However, we must take care to clearly identify sub-process to either differentiate methods or identify those that are effectively equivalent.

It can also be helpful to consider the operations involved in manufacture against a notional time scale where processes may be found to operate in series (one after the other in relative isolation, where a formwork might be printed and subsequently used for forming cast material), simultaneously (where they happen at the same time, wire reinforcement for example (Asprone et al. 2018), or contiguously where processes alternate at repeated stages in a process, such as the addition of a support material

in an additive manufacturing process). An approach to visualising these interactions using ‘process sketches’ is given in Buswell et al. (2020).

In addition to defining the nature of the process boundaries, implementation and sequencing, it is useful to identify the *Material*, and, with concrete and mortars, we are referring to the mix design as these vary significantly. The (intended) *Application* environment is also important, and this is principally whether it is for off-site or on-site use, since environmental factors play a significant role in the process operation and success. Next, the *Product* under manufacture also affects the *Process* as does size and mass: for example, the requirements for the set control for the production of vertical walls is significantly different from a thin horizontal panel, as is using DFC to manufacture a formwork for casting or to create solid end-use components with additive processes directly (Buswell et al. 2018). These form the so-called *MAPP (Material-Application-Product-Process)* definitions that delimit the suggested classification allowing the clear communication of a specific implementation of DFC technology.

Figure 2.1 presents the classification framework, which largely follows a conventional manufacturing view of assembly and shaping processes (adapted from Grover 2012) and includes surface treatments. As long as the boundaries of the process are well defined, most DFC processes will fall into this classification. Care needs to be taken in order that the object and purpose of the process is not conflated. For example: milling of a foam former is a subtractive DFC method, applied to form polystyrene—the product being a mould, which is part of a two-step process, in which a second step is to cast the actual part.

Additive Manufacturing processes fall outside conventional manufacturing and have a second tier of classification as part on (ISO 17296: 2015 and 2016) and these are reflected here with the exception that ‘binder jetting’ has been replaced with the term ‘particle-bed binding’. The approach is readily extensible if/when other process types emerge. In the following section, eight case study applications with different processes are presented that cover a significant proportion of the classes presented.

## 2.4 Case Studies

Eight case studies are presented here. They represent different application environments, materials, products and processes, covering a good proportion of the classification framework pictured in Fig. 2.1. These case studies illustrate the key differences between the processes used, thus providing a context for Chaps. 3 to 6 in this book. Table 2.1 provides an overview of the MAPP definition (Buswell et al. 2020) for each of the case studies. Although some technologies are used to manufacture the same products, or hold the same process classification, note that the combination of main forming process (on which the classification is based) and essential sub-processes is different in every case.

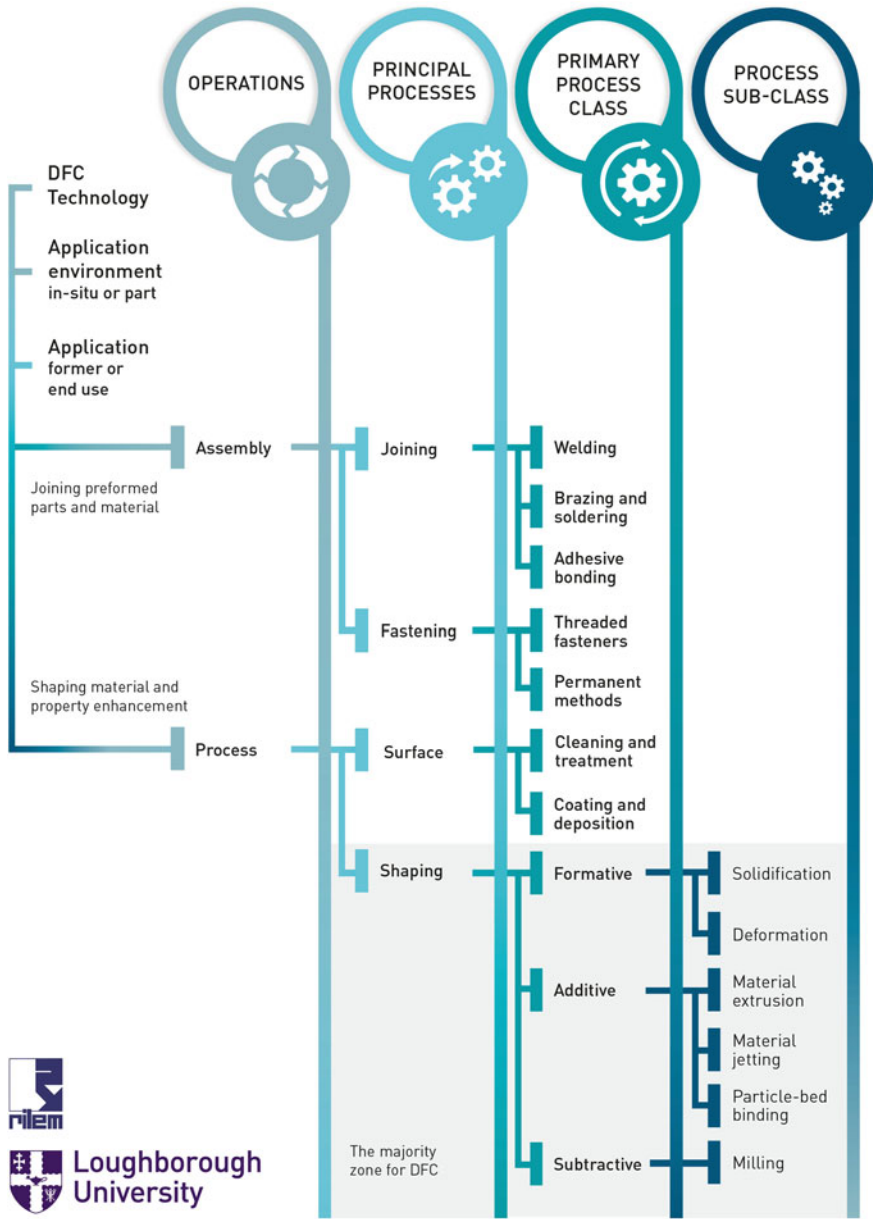


Fig. 2.1 A process classification framework for Digital Fabrication with Concrete, indicating the majority zone in which most DFC processes reside (Buswell et al. 2020)

**Table 2.1** The MAPP definition for each case study

Case Study	Material	Application	Product	Process (Classification)	Sub-processes	Organisation	Country
1	Wet mix, cement mortar <1 mm	Off-site production	Printing and assembling a 6.5 m Bicycle Bridge	Additive manufacturing: Material Extrusion	Insertion of wire reinforcement in the extruded filament	TU Eindhoven	Netherlands
2	Wet mix, cement mortar <2 mm	Off-site production	Manufacturing double-curved panels with conformal voids	Additive manufacturing: Material Extrusion	Use of a second temporary support material	Loughborough University	UK
3	Wet mix, cement mortar <10 mm	On-site and in-situ	The 'BOD': a 49m2 office building	Additive manufacturing: Material Extrusion	None	COBOD	Denmark
4	Wet mix, Cement mortar <4 mm	Off-site production	Shotcrete printing a reinforced double-curved concrete wall	Additive manufacturing: Particle-bed binding	Accelerating the setting, placement of reinforcement	TU Braunschweig	Germany
5	Cement paste bound sand <1 mm	Off-site production	Enabling weight reduction a 12 m footbridge	Additive manufacturing: Particle-bed binding	None	Dshape	Spain
6	Cement mortar <4 mm	Off-site production	Column and beam manufacture	Formative: Deforming	Accelerating the setting, placement of reinforcement	Ethz	Switzerland
7	Self compacting concrete <8 mm	Off-site production	Commercial panel manufacture using flexible moulds	Formative: Either Deforming, or Solidification	Casting, or material jetting	TU Delft	Netherlands

(continued)

**Table 2.1** (continued)

Case Study	Material	Application	Product	Process (Classification)	Sub-processes	Organisation	Country
8	Conventional concrete <20 mm	On-site and in-situ	Full scale, reinforced concrete wall production in-situ	Additive manufacturing: Material Extrusion	Vibrating nozzle and placement of reinforcement	huaShang Tenda	China



### 2.4.1 Printing and Assembling a 6.5 m Bicycle Bridge

This case study describes the manufacture of the bicycle bridge installed in Gemert in the Netherlands in 2017, pictured in Fig. 2.2. It was made at Eindhoven University of Technology with an additive manufacturing process based on material extrusion (Salet et al. 2018).

#### Process & facility details

The material was supplied via a continuous mixing and pumping process. The position of print head is controlled via a g-code operated, large scale gantry robot with four degrees of freedom: the fourth degree required to keep the rectangular nozzle perpendicular to the direction of movement. A rectangular extrusion nozzle is used, programmed to remain tangential to the print path, Fig. 2.3 (Bos et al. 2016). The deposition quantity is adjustable, with a default setting of approximately 2.4 l/min. The print head can optionally be equipped with a cable reinforcement device capable of simultaneously applying flexible reinforcement cables into the print filament (Bos et al. 2017).

#### Material details

The material used was Weber 3D 115–1, a single-phase, shape stable, thixotropic, cementitious print mortar, comprised of CEM I Portland cement, aggregate (1 mm maximum particle size), filler and additives, rheology modifiers and a small amount of PP-fibres (Wolfs et al. 2018a, c). Although some experiments were performed, studies on hardened properties of Weber 3D 115–1 have not been published because



Fig. 2.2 Completed bridge at the opening. *Photo Kuppens fotografie*



Fig. 2.3 Printing of a bicycle bridge element

an improved version of the mortar was developed, Weber 3D 145–2, where details are given in (Wolfs et al. 2019b).

### Application details

The bridge consists of six identical horizontally printed elements that were rotated 90° after production, adhesively bonded with epoxy and prestressed with unbonded post-tensioned tendons, Fig. 2.4. The tendons are anchored in conventional cast concrete blocks at both ends of the bridge. Full prestress is applied, i.e. the full concrete section of the bridge remains in compression at all times. In each element, approximately the bottom 10% of layers are provided with a high strength steel reinforcement cable, entrained with the cable reinforcement device. The cable acts

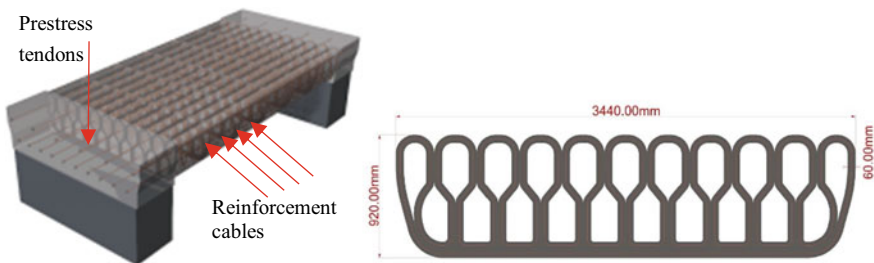


Fig. 2.4 Schematic 3D image showing prestress tendons and reinforcement cable zones (left) and print element section geometry (right)



**Fig. 2.5** In-situ testing of the bridge with water-filled containers

as passive reinforcement in the transverse direction, while the prestress tendons provide active reinforcement in the longitudinal direction of the bridge. Figure 2.5 depicts the bridge under test in-situ (Bos et al. 2018).

The uniformly distributed design load was  $q_{Ed} = 5.0 \text{ kN/m}^2$ . Prior to the project, the available data on the structural properties of the available print material (Weber 3D 115–1 mortar) was limited. Furthermore, the use of printed concrete or mortar was not covered by the structural engineering codes prevailing in the Netherlands. Therefore, extensive attention was paid to the structural safety, by adopting a ‘fail-safe’ design, i.e. a design that relied on a tried-and-true principle of a print concrete section entirely in compression (full prestress scenario), rather than on more uncertain properties such as tensile strength or the performance of innovative reinforcement technologies. The design was analysed through a full 3D Finite Element Analysis, to ensure that no unexpected local stress situations would cause structural damage. In addition, construction approval was obtained by applying the ‘Design by Testing’ option available in Annex D of the EN (1990). In addition to extensive material testing, there was also a 1:2 scale destructive mock-up test, Fig. 2.6, as well as an in-situ test to the serviceability limit state load, Fig. 2.5.

The print path followed the outer contour of the bridge and a bottle-shaped inner pattern, coming to 25.1 m length per layer (Fig. 2.4). Each element took approximately eight hours to print. The open internal structure allows room for the prestressing tendons.

As the prestress in the tendons results from their (forced) elongation, its level is directly dependent on any shortening of the concrete, which may be due to elastic deformations, creep and shrinkage. As printing mortars generally contain a relatively high cement content, they are more sensitive to these phenomena than ordinary concretes. Besides creep and shrinkage tests that have been performed preceding the



**Fig. 2.6** Scale model in 4-point bending test set-up

project, the bridge is therefore subjected to a long-term monitoring program, and the prestress system has been designed to allow future restressing.

### ***2.4.2 Manufacturing Double-Curved Panels with Conformal Voids***

This case study describes the manufacture of double-curved panels with conformal voids manufactured as concept parts at Loughborough University in 2011, pictured in Fig. 2.7. The panels were made using an additive manufacturing process based on material extrusion in combination with a printed secondary support material (Lim et al. 2016).

#### **Process & facility details**

The extrusion-based printing process used a batch mixing approach supplying the cementitious mortar to storage and feed hopper and pumping process combined with a second extrusion head for printing the support material (Austin et al. 2011). Both printing heads were adjacently mounted in parallel on a large-scale gantry with three degrees of freedom, controlled through g-code. The materials were extruded through circular, 9 mm diameter, nozzles with a layer height of 6 mm less than the diameter, such that the top layer was flattened during printing, Fig. 2.8. The nozzle velocity was in the order of 30 mm/s (Lim et al. 2012).



Fig. 2.7 Double-curved panels printed with conformal voids

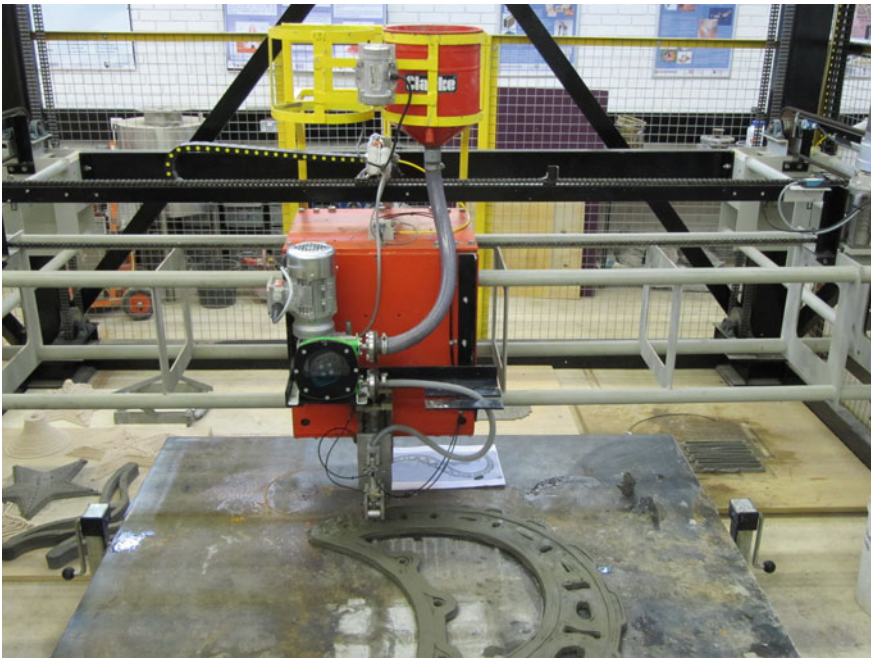
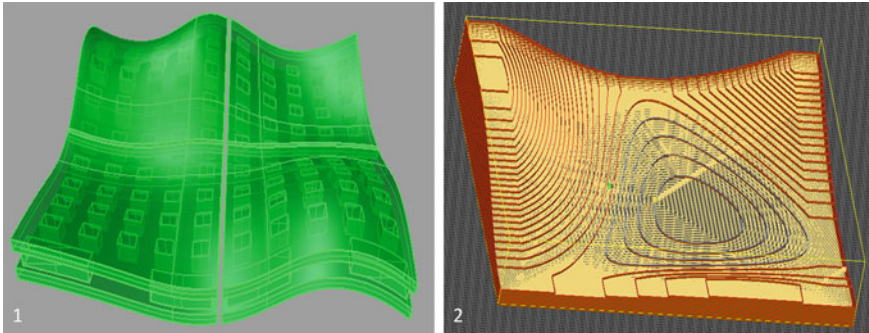


Fig. 2.8 The mortar extrusion hopper and pump mounted on the gantry system

### Material details

The build material was a shape stable, thixotropic, cementitious print mortar, which comprised of CEM I Portland cement, fly ash and undensified silica fume, aggregate (2 mm maximum particle size), superplasticiser, retarder and some polypropylene microfibres (hardened properties: Le et al. 2012a and fresh properties: Le et al.



**Fig. 2.9** The 3D CAD model of the panels on the left and the right-hand image is of the model of the base component of sand support for the top right panel

2012b). The support material comprised of sand and a water-soluble binding agent that can be added in variable quantities to stiffen the printed material so that it could support the load of the wet build material.

### Application details

The four panels demonstrated the manufacture of the first fully three-dimensional geometry to be printed in mortar with conformal voids with the aid of a removable, temporary support material. The demonstrator comprised of four unique panels approximately  $800 \times 800$  mm that formed a single, double-curved surface once assembled on a mounting frame (Fig. 2.7).

Similarly to conventional Additive Manufacturing processes, the generation of the machine instructions is derived from a 3D CAD model shown on the left-hand side of Fig. 2.9. Printing in flat layers for (relatively) thin curved panels can be cumbersome to achieve in practice and so a non-conventional approach was used. Tool paths that printed conformally to the surface were developed using Grasshopper and proved effective at improving efficiency, performance and surface quality (Lim et al. 2016).

The processing of the CAD model is more complicated with the support material: two models are required, one to base the generation of the tool path of the build material (cement-based mortar) (Fig. 2.9–1) and one for the creation of the support structure (Fig. 2.9–2).

Figure 2.10 depicts six stages of manufacture. Figure 2.10–1, shows the printing of the sand support to create the bottom curved working surface. Once the support was completed, the layers of the bottom shell are printed conformally on the base using the extruded mortar (Fig. 2.10–1). The internal voids and interconnecting ‘pillars’ are then formed, ensuring a good bond between the shell and pillar (Fig. 2.10–3).

The base support material of each part was relatively easy to define in CAD and was actually printed using a conventional flat layer approach, making the generation of the tool paths straightforward. As previously mentioned, generating conformal printing paths was more demanding and some considerable time invested in developing a Grasshopper tool to do this (Lim et al. 2016).



**Fig. 2.10** Six stages of manufacturing one of the panels and the CAD model compared to the finished parts

The support was dispensed via a specially designed tool that allowed the sand to be ‘extruded’ with very similar dimensions to the mortar, hence making the creation of the tool paths in the centre of the component (layers that were 50% solid and 50% void) easier to compute. However, the actual manufacture was challenging in practice and required some intervention to ensure the build was completed correctly.

Once the pillars and supporting material were in place, the top shell was printed, and the part left to cure, before being separated from the support and washed clean (Fig. 2.10–4, 5 and 6). Figure 2.10–7 and 8 depict the CAD model and the finished component.

The CAD model for each panel was extracted from the whole surface and was printed over-sized by 25–50 mm so that the precise joints between each panel can be located and cut using a conventional diamond saw. This was done by hand in this test application, but it could be automated.

The addition of the second support material enables far more freedom in the components that can be designed and manufactured, although this needs to be

traded off in the greater processing burden and the more complex interaction of two deposition systems.

### **2.4.3 The ‘BOD’: A 49 m<sup>2</sup> Office Building**

This case study describes an extrusion-based additive approach that utilises a mix design containing recycled aggregates to print the walls of a building in-situ rather than in the factory (as the approaches from Sects. 3.1 and 3.2). The project was completed by COBOD International (former 3DPrintHuset) in Nordhavn, Denmark in 2017, Fig. 2.11–8.

#### **Process & facility details**

The extrusion-based print process was carried out in-situ using batch mixing and a continuous pumping system to deliver material to a hopper mounted on a large gantry system having four degrees of freedom. A rectangular extrusion nozzle (50 × 10 mm) was used for most of the construction, and the nozzle orientation is set to remain tangential to the print path. The average volume flow rate for the extrusion was 0.36 m<sup>3</sup>/h, although this was adjusted several times during the process. The maximum travel velocity of the printing head reached 100 mm/s, while the practical travel speed was found to be about 60% of this.

#### **Material details**

A custom-design concrete mix based on CEM II was used. This mix included fine aggregates with a maximum particle size of 4.0 mm. In addition, crushed-red roofing tiles and bricks were used. The fine and recycled aggregates were pre-mixed prior to delivery. Immediately before printing, the pre-mixed aggregates were placed into a concrete mixer (100 L drum mixer) in which cement, water, polypropylene fibres and superplasticizer were added. The pre-mixed material was then transported to a progressive cavity pump, which conveyed the material to an extrusion nozzle (Fig. 2.11–3) that works under a screw system principle. The mix design is listed in Table 2.2 and yielded a compressive strength of 52.0 MPa.

It is worth mentioning that during the initial phase of the printing process, it was observed that the pre-mixed aggregates (especially the recycled fraction) were out of specification in relation to the maximum particle size, which was problematic for pumping. It turned out that more than 10% of the aggregates were above not only 4 mm but up to 20 mm. This resulted in clogging the hose when pumping and the subsequent pressure build-up ruptured the supply hose in one printing sessions. Subsequently, the premixed materials were sieved using a 10 mm sieve. Hence, the final mix comprised aggregate particles with size up to 10 mm.

#### **Application details**

The project was the first 3DCP building project to receive an approval/permit by a municipality in Europe. The printing process was intended to be applied to the





**Fig. 2.11** Main phases in the construction of the BOD: 1. 3DCP of the foundation slab contour; 2. Concrete casting of the foundation slab; 3. 3DCP of the building walls and printing nozzle; 4. Detail of the insulation material; 5. Detail of the manually added rebar; 6. The BOD walls right after printing; 7. Application of roof, doors and windows; 8. The BOD after its completion

**Table 2.2** Mix design of the concrete used in ‘The BOD’

Materials	Composition [kg/m <sup>3</sup> ]	Mass Fraction [kg/kg]	Total mass [ton]	Total Cost [Euro]
CEM II	735.4	1.00	6.12	1,392
Sand N.1: 0–2 mm	420.6	0.57	3.50	79
Sand N.2: 0–4 mm	420.6	0.57	3.50	86
Recycled agg.: 0–4 mm <sup>a</sup>	526.3	0.72	4.38	70
Superplasticizer	4.8	0.007	0.04	26
Polypropylene fibres	2.4	0.003	0.02	139
Water	199.5	0.27	1.66	8
<b>Total</b>	–	–	19.22	1,800

<sup>a</sup>Specification provided by the producer, thought the maximum particle size was up to 10 mm

building of the walls and structural columns that carry the roof. However, the subcontractor in charge of executing the foundation slab faced challenges to produce a formwork that matched the shape of the building and, hence, 3DCP was also used to print the external perimeter of the foundation (total height of 600 mm, Fig. 2.11–1). Traditional casting method was then used to form the foundation (Fig. 2.11–2).

This allowed for the placement of reinforcement using standard practices; thus, the structural elements were produced to existing codes—leaving the printed parts as a permanent formwork. The installation of the roof, windows, doors and surface finishes was carried out using standard building practices. Similar to the foundation, the printed walls (Fig. 2.11–3 to 5) were not considered as load-bearing elements. For the load-bearing elements such as columns, a similar formwork approach was applied to produce 11 columns that were also reinforced and then cast to carry the imposed loads.

The 3DCP of the foundation perimeter, walls and columns were finalised in about two months; six weeks of which were spent adjusting the process to cope with the problems with the pre-mixed materials. The project was complete in eight months, mainly due to the availability of labour. Without interruption, the total printing time was approximately 55 h.

#### 2.4.4 Shotcrete Printing a Reinforced Double-Curved Concrete Wall

In this study, the manufacture of a double-curved wall is carried out (Fig. 2.12–6) with an additive manufacturing process based on material jetting (Neudecker et al.



**Fig. 2.12** Fabrication process; 1. Shotcrete 3D Printing of the wall; 2. manual placement of the pre-bent horizontal reinforcement; 3. precise cutting of the surface, while the concrete is still in the plastic state; 4. threading in the vertical reinforcement; 5. embedding the reinforcement by vertically spraying onto the printed structure; 6. final trowelling with a rotating plastic disc

2016), as opposed to material extrusion, discussed in Sects. 3.1, 3.2 and 3.3. The incorporation of reinforcement is demonstrated using a dual application approach and was realised at Technical University of Braunschweig.

### Material details

In shotcrete 3D Printing (SC3DP), the layers are built up by a spray deposition (or jetting) process using compressed air to carry the materials to the working plane. It is an evolution of the traditional shotcrete processes. The jetting velocity results in very good bonding behaviour between layers (Nolte et al. 2018) and the ability to encase reinforcement. A pre-mixed cement-based mortar is mixed in a conventional batch mixing approach and is subsequently conveyed to the printing nozzle using standard pumping equipment. An accelerator is added at the nozzle to enable faster building rates.

### Process details

The print head is mounted on a large gantry system with two vertical axes of which one is equipped with a six-axes robot and the other with a three-axes milling device. The overall cooperative build volume is  $10.5 \times 5.25 \times 2.5$  m high.

The nozzle velocity was set to 0.25 m/s, resulting in a layer height of 1 cm. This enables a material deposition rate of  $1\text{m}^3$  per hour. For this specific case-study, the total printing path length was added up to be 675 m, resulting in a (calculated) printing time of 45 min. After every 40 layers, the printing process was paused, and pre-fabricated 10 mm horizontal steel reinforcement elements were manually placed lengthening the actual manufacturing time to 80 min.

### Application details

To demonstrate both the structural and design potential of shotcrete printing, a concept part was designed: a double-curved, reinforced concrete wall with high surface quality. The wall has a length of 2.5 m, a thickness of 18 cm and a height of 2.3 m. The manufacture of the wall integrated the shaping and the placement of structural reinforcement. In addition, the surface finish of the sprayed component has a rather coarse resolution and so to address this, subtractive processing for surfaces and edges were applied.

The modelling process included a structural analysis of the geometry using, Rhino 3D ([www.rhino3d.com](http://www.rhino3d.com)) and Karamba ([www.karamba3d.com](http://www.karamba3d.com)) for Grasshopper ([www.grasshopper3d.com](http://www.grasshopper3d.com)) to test that the wall would be stable during manufacture. The wall was realised using two spraying processes. The first spraying operation used flat layers in an additive manufacture fashion to form the core of the wall (Fig. 2.12–1), pausing to hand place pre-bent horizontal reinforcement (Fig. 2.12–2). While the concrete was still plastic, a subtractive process was applied to improve the potential jointing surfaces (Fig. 2.12–3). Vertical reinforcement was then added (Fig. 2.12–4), utilising the undulating profile of the core print. The reinforcement was encapsulated with the second sprayed layer application in the vertical direction (Fig. 2.12–5) and then trowelled smooth, again while the concrete was plastic (Fig. 2.12–6).

Currently, the fabrication process requires a team of at least five people. Three people are needed for handling the concrete supply chain, one to control the machine and one to supervise the process and to intervene should problems arise.

### 2.4.5 Enabling Weight Reduction of a 12 m Footbridge

This case study describes a 12 m long footbridge, installed in Madrid, Spain by Acciona in 2017 (Fig. 2.13). The D-Shape<sup>®</sup> process was used to realise weight reduction in an assembly of eight pieces that form the bridge. This additive manufacturing process uses a particle-bed and binder approach, rather than the



**Fig. 2.13** The footpath bridge in Madrid by Acciona (© Enrico Dini)

deposition of a pre-mixed wet mortar used in extrusion and jetting methods mentioned in previous case studies (Valencia 2017).

### **Material Details**

The material is a compacted, dry sand (maximum particle size of 0.2 mm) spread and cement that is locally activated by spraying or jetting water or a water-admixture solution into the packed particles thus forming a cement paste matrix around the aggregate particles. Capillary effects draw the water into the matrix, and the water spreads out to the size of the nominal voxel. Careful compaction of the matrix material is critical to control the dispersion of water in the voxel and ensure that full layer penetration is achieved as these factors affect the resultant mechanical properties (Lowke et al. 2018).

### **Process Details**

In general, the printing process consists of two repetitive work steps. In the first step, a layer of dry particles is spread over the printing area with a uniform thickness of about 5 to 10 mm. The second step is the selective deposition of a fluid onto the particle bed by means of a print head in order to bind the particles. This process is repeated in series until the component is complete. Once cured, the non-bonded particles are removed in a post-processing step of de-powdering, Fig. 2.14 (Lowke et al. 2018).

There are two methods of binding the particles: either by selective paste intrusion, where a cement paste is deposited on the surface to the packed bed and is drawn into the dry material under gravity (Pierre et al. 2018), or where the cement component is added in its dry state to the particle-bed, before it is selectively activated by adding water to the surface. In this case study, the footbridge was manufactured using selective cement activation.



**Fig. 2.14** D Shape<sup>®</sup> 3D-printer (left) and print head (right) (Lowke et al. 2018)

The D Shape<sup>®</sup> printer used in manufacture consists of a horizontal aluminium frame lifted by four columns giving a print area of  $2 \times 2 \times 2 \text{ m}^3$ . The horizontal frame contains a print head with 100 nozzles at 20 mm intervals and a blade to spread the sand. To fill the gaps within the array of nozzles and to ensure that the whole cross-section would be uniformly reached by the fluid, each layer is produced in multiple passes with a 5 mm offset of the print head, Fig. 2.14. The average printing speed of the printhead is around 15–20 cm/sec.

### Application details

A D Shape<sup>®</sup> particle-bed binding printer was used to build a footpath bridge shown in Fig. 2.13. The bridge has a total length of 12 m, a width of 1.5 m and a bridge railing height of 1.3 m (IAAC 2019). The supporting structure of the bridge consists of two lateral Vierendeel metal structures and eight printed concrete elements. The metal structure has a variable height of about 1.3 m at the supports and 1.1 m in the middle of the bridge. The forces introduced into the structure are transmitted through the metal structure to the supports located on the two banks. During the building process, the metal structures were installed first followed by the modular installation of the printed concrete elements. Figure 2.15 gives a schematic overview of the installation process.

### 2.4.6 Column and Beam Manufacture

Here, Smart Dynamic Casting is applied to manufacture the façade mullions installed in the DFAB house at the NEST building on the Empa campus in Dübendorf, Switzerland (Fig. 2.16). The process is based on the principles of slip-forming and is a formative process that deploys extrusion vertically to shape the cross-sectional area of beams and columns. The cross-sectional area can be either rigid, or adjusted to provide customisation (Lloret et al. 2019).

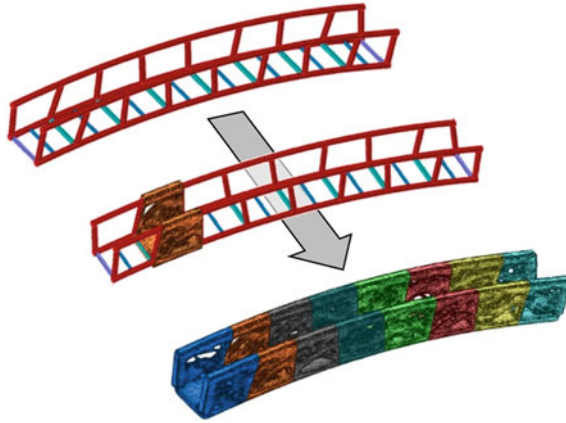


**Fig. 2.15** Substructure and building process of the footpath bridge (Acciona 2019)



**Fig. 2.16** Final installation of façade mullions in the DFAB House, on the left-hand side of the image

## Material details

The approach used a cement mortar with a maximum aggregate size of 4 mm, which is batch mixed conventionally. The method relies on shaping concrete in the moments when it is still plastic but has adequate strength to support its own weight as well as the weight of some additional concrete within the formwork (Lloret et al. 2015, 2016). To achieve this, the measurement of the material to determine its plastic state, and the control of setting through the addition of admixtures just before deposition into the formwork are critical aspects to the process (Mettler et al. 2016; Lloret et al. 2017). Controlling when this moment occurs and timing it correctly with the vertical slipping speed, is crucial. Slipping too fast will cause plastic collapse of the material lacking enough strength. Too slow slipping will result in high friction within the formwork and brittle failure from a material that has almost set.

## Process details

SDC is a scaled-down version of slip-forming, or vertical extrusion, in which a vertically moving and reconfigurable formwork shapes gravity-fed material either within the formwork, or at the moment it exits. The material is a batch mixed, cement-based mortar which is then deposited into the formwork either manually or via a pump.

The formwork is about 40 cm in height, and 80–800 cm<sup>2</sup> in cross-sectional area depending on the specific implementation. It moves at a vertical slipping speed of 10–20 mm/min via either a 6-axis robotic arm or a linear axis. The columns can be deformed by rotation of the formwork on the robotic arm, or via a rotating table at the base of the linear axis (Fig. 2.17–1); by linear actuators placed at the bottom of the

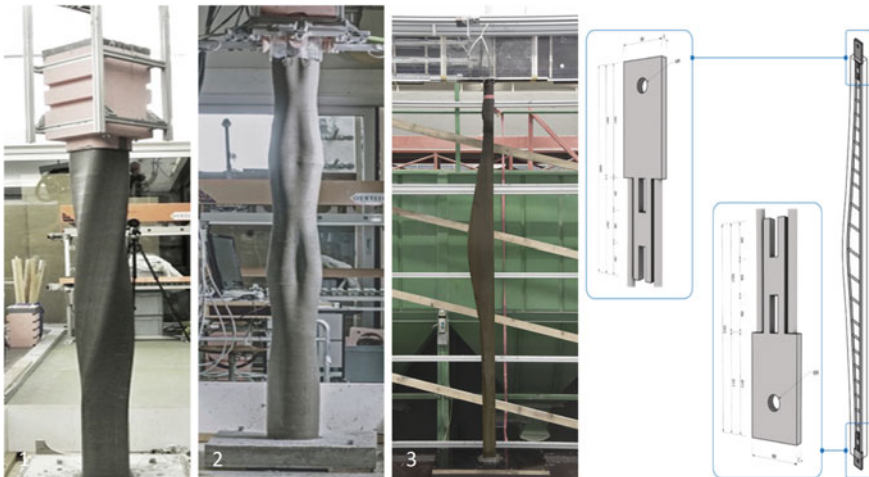


**Fig. 2.17** 1. rigid formwork, rotational deformation; 2. rigid formwork, linear actuator deformation at exit; 3. single sided deformation, reinforced column demonstrator; 4. schematic of top and bottom couplers used in tensioning reinforcement for production



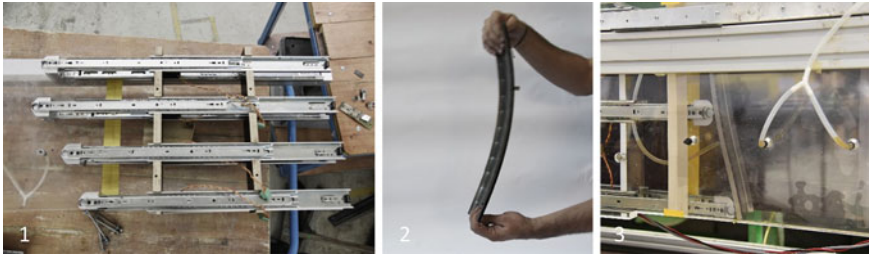


**Fig. 2.18** Process details for application 3 in Fig. 2.17: 1. linear actuators for deformation within formwork; 2. scaled metallic strip for deformation; 3. capillary oiling system in constructed formwork

rigid formwork, requiring the placement of a void space in the centre of the column to allow the incompressible material a place to flow (Fig. 2.17–2); or by the use of linear actuators, on one or two sides, is moved vertically to change the rectangular in cross-sectional area (Fig. 2.17–3).

Formwork friction is minimised through the use of low-friction synthetic material inside the formwork as well as the installation of capillary oiling systems. In the latter application, a forming strip (Fig. 2.18–2) is coupled magnetically to the actuators (Fig. 2.18–1), and is ‘scaled’ to allow flexible deformation and entry of oil via a capillary oiling system (Fig. 2.18–3). Formwork friction was monitored with process feedback using load cells mounted on the formwork. Strength build-up was monitored by measuring formwork pressure at a sensor positioned just before material exit (Lloret et al. 2017, 2019).

### Application details

The reinforced façade mullions in the DFAB house in Dübendorf, Switzerland, were manufactured using the flexible formwork approach depicted in Fig. 2.17–3. This method has been demonstrated to be more versatile than the fixed formwork methods depicted in Fig. 2.17–1 and 2.

In total 15 mullions were manufactured for the DFAB house, each with a different form to match required material amounts in the centre of the mullion with calculated façade wind loads and variable tributary lengths. The mullions were approximately 3 m high, and each took approximately 3 h to slip-form, and approximately 8 h in total production time per mullion.

During the manufacturing set-up, the reinforcement sections (Fig. 2.17–4) were cut, bent and welded prior to slip forming. Coupling plates were fitted to each end such that the reinforcement could be held vertically and tensioned during manufacture, and the same plates were used for on-site installation. For production, the mould system was then installed around the reinforcement, and the slip forming then carried out to completion of the mullion (Lloret et al. 2019).

One complicating factor for the application of these methods is the precision in the control of the curing required. In addition, the loss of the formwork leads to a

higher risk of drying shrinkage cracks and deformation. In the DFAB house, these issues are being treated by through life monitoring.

### 2.4.7 Commercial Panel Manufacture Using Flexible Moulds

Flexible moulding is a DFC technology that has been used on various commercial projects including the Arnhem OV Hub in the Netherlands (architect UNStudio, concrete product manufacturer mbX), the interior cladding of two Crossrail underground stations in London (architect Grimshaw, panels by mbX) and Kuwait International Airport terminal vaulted roof (architect Foster + partners, panels by Limak / Adapa). The method can be deployed as a deformation process, where the panels are shaped after casting (used in the former two examples) or as a solidification process, where the moulds are deformed before material placement (in the latter example), Fig. 2.19.

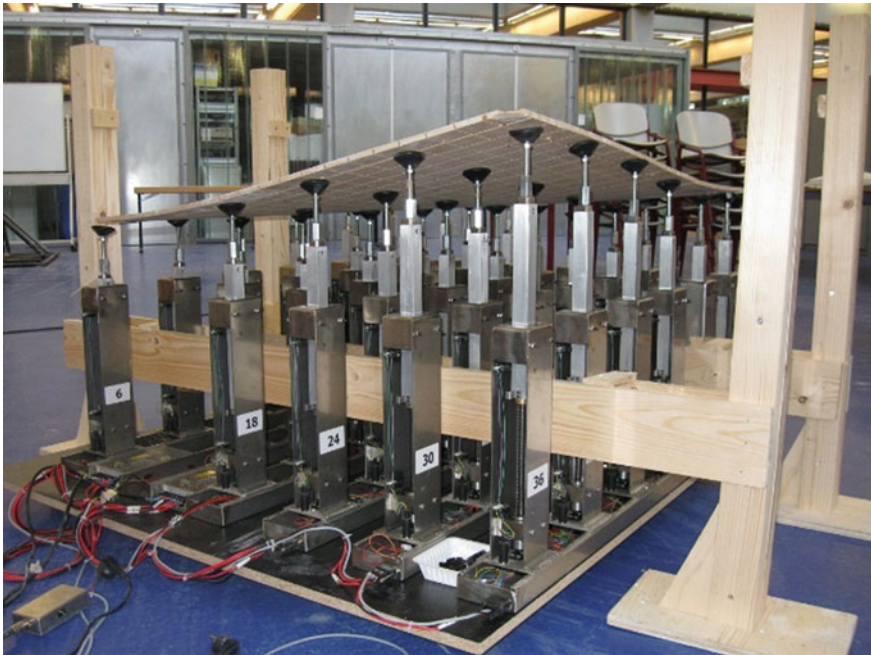


**Fig. 2.19** Prototype mould of Vollers and Rietbergen at TU Delft (2010) (patent described in Vollers et al. 2010)



**Fig. 2.20** Prototype of the flexible mould as developed in a Dutch R&D project operating in mode 1, deformation: Setting out formwork (Schipper et al. 2015b)

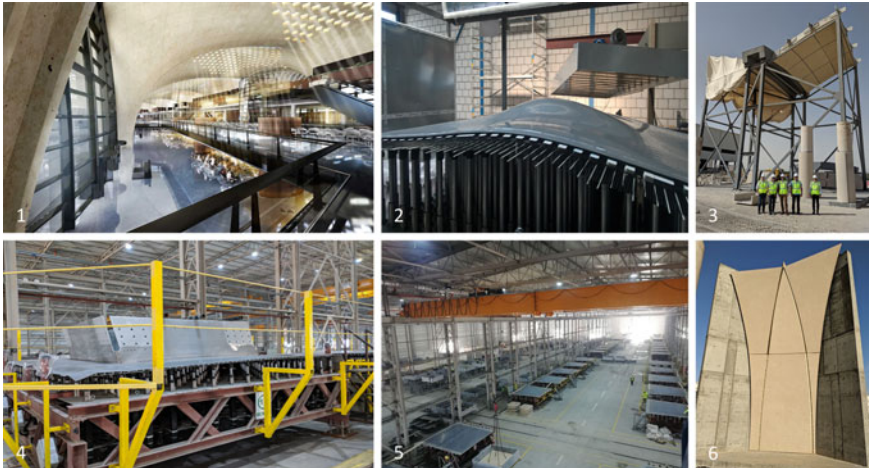


**Fig. 2.21** Images from the realisation of Kuwait International Airport using flexible moulds from Adapa: 1. artists impression of the finished building; 2. the pin bead and mould surface; 3. and 6. an on-site mock-up of the panels; 4. and 5. production facilities required for the industrial-scale manufacture of the roof

## Material details

Typically, self-compacting concretes or zero-slump concretes for spray applications are used, depending on system configuration, see Table 2.3. In mode 1 (deformation), the control of the thixotropy is critical. A fast, initial setting of the fluid concrete is needed, to allow for deformation without spilling. At the same time, the material should still be sufficiently plastic/compliant to prevent cracking during this deformation (Schipper et al. 2015a).

In mode 2 (solidification), once the mould is deformed first, the concrete is applied on a sloping mould surface, requiring that the yield strength of the mixture is high enough to resist gravity. Often spraying is used. If a zero-slump concrete is applied, the process is comparable to plastering or rendering.

Mode 1 only allows for compliant reinforcement, such as very thin steel nets, short or long chopped fibres in steel, PVA or glass, or alkali-resistant textiles in glass-fibre. Mode 2, due to the application method of the concrete, is mostly served



**Fig. 2.22** The completed two-story villa

**Table 2.3** Typical concrete mix for a self-compacting HPC with an average cube compressive strength (28 days, cubes with 150 mm ribs) of 76 MPa and an average prism flexural strength (28 days, prisms 40 × 40 × 160 mm<sup>3</sup>) of 13 MPa

Concrete component	KG/1000 L
Cement CEM I 52.% R white	600
White limestone powder (Betoflow D, O)	180
White pigment	6
PVA Fibers L = 8 mm (Kuraray)	5.2
Superplasticizer Glenium 51 (BASF)	3.2
Water	228
Sand 0.125–0.25 mm	229
Sand 0.125–0.25 mm	408
Sand 0.5–1 mm	637

by short fibres that can be mixed and sprayed together with the concrete, but can also be applied in combination with regular steel reinforcement, like in the Kuwait airport case.

**Process details**

The process is based on reconfigurable pin bed is deployed in one of two ways: either as part of a deformation process, where the material is cast flat and the

pin bed deformed while the material is compliant (mode 1, Fig. 2.20); or as a solidification process where the mould shape is determined prior to the addition of the material (mode 2). The method is typically used for creating non-structural panels of 10 to 50 mm thickness used for non-structural applications, such as façade or roof cladding in free-form architecture that has limited repetition of standard elements. It is also used to produce panels that are used in structural applications as permanent formwork of volumetric curved concrete structures (e.g. curved bridge decks or curved structural concrete roofs of which the thin shell is topped with in-situ traditionally reinforced concrete).

The flexible mould consists of an elastic, rubber-like surface containing steel rods in two directions to guide and smoothen the deformation of the rubber mat (Fig. 2.20–2). On this rubber mat, it is possible to cast or deposit any mouldable and solidifying material. The shape of the rubber mat can be controlled with CNC-controlled actuators directly from the 3D-file from flat into any doubly curved surface (Fig. 2.20–3). The contours of the elements are placed manually on the surface after conventional laser projection on the exact location (Fig. 2.20–1), which is non-trivial in a doubly-curved geometry (Schipper and Eigenraam 2016).

### **Application details**

Among the first companies to really deploy the adaptive mould at full industrial scale and within a digitally driven process is Adapa, holding various patents in the field (Kristensen and Raun 201; Raun and Henriksen 2014). At the time of writing (2019–2020), Adapa is involved in the construction of Kuwait International Airport, an immense 1.2 km length terminal designed by Foster + Partners and ARUP, comprising vaulted, parametrically shaped roofs with very limited repetition of panels.

The sheer size, number of panels, and lack of repetition forced the designers to prescribe the use of a digitally controlled flexible mould in the brief, to make the project feasible. Figure 2.21–1 shows an artist impression of one of the terminal areas. The smooth rubber surface and the digitally controlled actuators of an Adapa mould are visible in 2.21–2. For the Kuwait project, a steel edge profile was used as a delimiter for the concrete, whereas the adaptable mould surface forms the basis of each cast, each panel having a slightly different curvature. Traditional reinforcement is placed before casting. Figure 2.21–5 gives an impression of the production line needed for this immense project. Figure 2.21–3 and 6 are on-site mock-ups of the produced vault and cladding panels.

An advantage of the process is the architectural surface quality of the parts; however, as concrete is alkaline, it shortens the life of the rubber used as the flexible casting surface.

### 2.4.8 *In-Situ Production of Full Scale, Reinforced Concrete Walls*

This final case study presents the production of a residential villa, in Tongzhou, Beijing, China in 2016 by HuaShang Tenda, Fig. 2.22. The case study illustrates construction automation enabled by material extrusion using conventional concrete in such a way as to encase preplaced reinforcement mesh.

#### **Material details**

The material used is ordinary vibrated concrete comprised of Portland cement, sand (0–5 mm), coarse aggregates (5–20 mm) and water. No additives were used. The average compressive strength of hardened concrete was between 30 and 40 MPa. Concrete is produced in a conventional gravity mixer with a capacity of 1 m<sup>3</sup> and placed batch by batch into the hopper. When filled, the printhead can accommodate approximately 0.3 m<sup>3</sup> concrete.

#### **Process details**

The material is conveyed vertically in the large printhead under gravity, assisted by vibration. The vibration is generated by an unbalanced mass and propagates along the length of the nozzle. The nozzle is forked and held by the print head mounted on a large-scale gantry robot with four degrees of freedom, including rotation (Fig. 2.23–1).

The outer dimensions of the application reported here are 15 × 15 × 9 m. The gantry system carrying the printhead is 20 m wide and moves on rails (Fig. 2.23–1). The vertical steel mesh reinforcement is fixed by hand prior to printing. The concrete is then deposited layer-by-layer, gradually enclosing the reinforcing bars from all sides, see Fig. 2.23–3 and –1 to 3.

A given machine configuration is designed to operate at a constant volume flow rate, and the velocity of the printhead horizontal movement during the construction of the villa was approximately 0.3 m/min while printing the 100 mm thick walls. The average thickness of each layer was 50 mm.

#### **Application details**

This project realised a two-storey, 400 m<sup>2</sup> villa on the grounds of the company in Tongzhou Beijing, China. The design was performed according to the Chinese code (incl. earthquake load case). The layout planning was carried out with AutoCAD. The foundation slab with connective reinforcement was produced in a conventional manner, see Fig. 2.23–3. The vertical steel mesh reinforcement and plastic installation tubes were placed manually. The vertical walls, both straight and curved, were then manufactured additively by deposition of concrete layers which encapsulated the reinforcement and tubes. At openings (doors, windows) the concrete conveying was interrupted, and some manual help was provided to ensure the desired geometrical accuracy. Provisory wooden supports were utilised to deposit concrete over the openings. The ceilings and the roof were made of composite slabs (manually placed

profiled steel sheets served as permanent formwork and concrete was deposited automatically upon them).

Although the vibration is applied at a considerable distance from the nozzle orifices, they propagate towards the orifices, resulting in quasi-compaction of concrete, improving the quality of both concrete and bond between concrete and reinforcement. It should be noted that reinforcement mats provide kind of stabilising support to the freshly deposited concrete layers; however, the extent of such effect still needs to be investigated.

The concrete works were carried out between mid of October and end of November 2015 on the firm's compound using the printer built the same year. The entire building process took 45 days, according to HuaShang Tengda Ltd.

The approach is promising; however, at this stage, it exhibits some limitations. First, the height of individual mesh sheets is limited to the size of the forked nozzle, which is quite large: here the mesh sheet height was approximately 1.7 m while the height of the entire printhead was approximately 3.5 m. The second limitation is that only one or two reinforcement layers can be easily integrated into the middle of the wall cross-section. However, not only reinforcement but also some simple installations such as cable tubes and even thermal insulation can be accommodated, see Fig. 2.23–4. Furthermore, only vertical walls (no inclination) and only rounded transitions (no sharp corners) can be produced, while the walls' surfaces exhibit a rough texture, see Fig. 2.24. Finally, since the gantry system must be very massive



**Fig. 2.23** On-site 3D-printing by HuaShang Tengda: 1. gantry-based printer with a hopper on the top of the printhead; 2. raw materials and mixer; 3. foundation and connective steel bars; 4. deposition of the first layer



**Fig. 2.24** Construction of the two-storey villa: 1. forked nozzle lays concrete on both sides of the rebars, 2. printing a bow; 3. manual help at the opening, when the material flow is interrupted; 4. forming a vertical element

and stiff to enable a robust control of a heavy and vibrating printhead, the transport and mounting of such printer limit its mobility and flexibility.

## 2.5 Summary and Outlook

This chapter provided a brief background of contemporary DFC and demonstrated the diversity in existing technologies. These differences are more than skin deep and are often driven by the product that the process is designed (or optimised) to produce. In one case study (Sect. 3.7), the actual implementation of the technology determined its classification.

By acknowledging the type of *Material* used, the *Application* environment, the *Product* and the *Process* it is possible to clearly delimit the scope of a technology and so identify differences and similarities that would otherwise not be obvious. The MAPP definitions should also identify the enabling sub-processes that are necessary during fabrication as these are often where important differences are found. Nonetheless, the method classification should be based on the main assembly, or material forming process, following convention.



Eight representative case studies which fit within the classification framework were used to illustrate the similarities and the differences between materials, applications, products and processes, Summarised in Table 2.1. The process descriptions have never been brought together in this way before, and we hope that readers find the case studies informative in their own right, but also a useful resource on which to reflect when understanding how to more appropriately compare and contrast difference DFC technologies.

**Acknowledgements** The work was supported by: the UK Industrial Strategy Challenge Fund: Transforming Construction initiative (EPSRC grant number EP/S031405/1) and EPSRC Grant number EP/P031420/1; the I-Site Future initiative, through the DiXite program at Gustave Eiffel University, Paris, France; the Swiss National Science Foundation, National Centre for Competence in Research: Digital Fabrication in Architecture; the Deutsche Forschungsgemeinschaft (DFG, German Research Foundation), Project Number 387152958 (GZ: ME 2938/20-1), within the priority program SPP 2005 OPUS FLUIDUM FUTURUM – Rheology of reactive, multiscale, multiphase construction materials; the Innovation Fund Denmark (Grant no. 8055-00030B: Next Generation of 3D-printed Concrete Structures); the Junior Professorship for Digital Building Fabrication is sponsored by the Gerhard and Karin Matthäi Foundation; the development of the Shotcrete 3D Printing technology (SC3DP) was funded by the Ministry for Science and Culture (MWK) of Lower Saxony and implemented with the DFG-funded Digital Building Fabrication Laboratory (DBFL). Mr. Wu from HuaShang Tenda provided information on the construction of the residential villa in Tongzhou, Beijing as well as Figs. 2.23-3 and 4 and 2.24.

## References

- Acciona. (2019). 3D Printing Skill Center. Personal communication, November 28th, 2019.
- Andersen, T. J., Leal da Silva, W. R. , and Thrane, L. N. (2016). Lessons from the TailorCrete Project. *Concrete International*, 38(3), 54–61.
- Asprone, D., Menna, C., Bos, F.P., Salet, T.A.M., Mata-Falcón, J., and Kaufmann, W. (2018). Rethinking reinforcement for digital fabrication with concrete. *Cement and Concrete Research*, 112(S.I.), 111–121. DOI: <https://doi.org/10.1016/j.cemconres.2018.05.020>.
- Austin S., Buswell, R. A., Lim, S., and Webster, J. (2011). *EP2886277A1*. Method and apparatus for delivery of cementitious material [PDF file]. Retrieved from: <https://patents.google.com/patent/EP2886277A1/en>.
- Barbosa, F., Woetzel, J., Mischke, J., Ribeirinho, M. J., Sridhar, M., Parsons, M. Bertram, N., and Brown, S. (2017). Reinventing construction: a route to higher productivity [PDF file]. Retrieved from: <https://www.mckinsey.com/~media/McKinsey/Industries/Capital%20Projects%20and%20Infrastructure/Our%20Insights/Reinventing%20construction%20through%20a%20productivity%20revolution/MGI-Reinventing-Construction-Executive-Summary.ashx>.
- Bonwetsch, T. (2015). Robotically assembled brickwork: Manipulating assembly processes of discrete elements. PhD Thesis, ETHZ. DOI: <https://doi.org/10.3929/ethz-a-010602028>.
- Bos, F., Wolfs, R., Ahmed, Z., and Salet, T. (2016). Additive manufacturing of concrete in construction: potentials and challenges of 3D concrete printing. *Virtual and Physical Prototyping*, 11(3), 209–225. DOI: <https://doi.org/10.1080/17452759.2016.1209867>.
- Bos, F., Ahmed, Z., Jutinov, E. R., and Salet, T. (2017). Experimental Exploration Metal Cable as Reinforcement in 3D Printed Concrete. *Materials (Basel)*, 10(11), E1314. DOI: <https://doi.org/10.3390/ma10111314>.

- Bos, F., Ahmed, Z., Wolfs, R., and Salet, T. (2018). 3D Printing Concrete with Reinforcement. In: D. A. Hordijk, M. Luković (Eds.), *High Tech Concrete: where Technology Engineering Meet*, Springer International Publishing, pp. 2484–2493. DOI: [https://doi.org/10.1007/978-3-319-59471-2\\_283](https://doi.org/10.1007/978-3-319-59471-2_283).
- Buchli, J., Gifftthaler, M., Kumar, N., Lussi, M., Sandy, T., Dörfler, K., and Hack, N. (2018). Digital in situ fabrication—Challenges and opportunities for robotic in situ fabrication in architecture, construction, and beyond. *Cement and Concrete Research*, 112(S.I.), 66–75. DOI: <https://doi.org/10.1016/j.cemconres.2018.05.013>.
- Buswell, R. A., Leal da Silva, W. R., Jones, S. Z., and Dirrenberger, J. (2018). 3D printing using concrete extrusion: A roadmap for research. *Cement and Concrete Research*, 112(S.I.), 37–49. DOI: <https://doi.org/10.1016/j.cemconres.2018.05.006>.
- Buswell, R. A., Leal da Silva, W. R., Bos, F. P., Schipper, R., Lowke, D., Hack, N., Kloft, H., Mechtcherine, V., Wangler, T., and Roussel, N. (2020). A process classification framework for defining and describing Digital Fabrication with Concrete. *Cement and Concrete Research*, 134(S.I.). DOI: <https://doi.org/10.1016/j.cemconres.2020.106068>.
- Changali, S., Mohammad, A., and van Nieuwland, M. (2015). The construction productivity imperative. McKinsey Productivity Sciences Center [PDF file]. Retrieved from: <https://www.mckinsey.com/~media/McKinsey/Industries/Capital%20Projects%20and%20Infrastructure/Our%20Insights/The%20construction%20productivity%20imperative/The%20construction%20productivity%20imperative.ashx>.
- Egan, J. (1998). Rethinking Construction, Department of the Environment, London [PDF file]. Retrieved from: [http://constructingexcellence.org.uk/wp-content/uploads/2014/10/rethinking\\_construction\\_report.pdf](http://constructingexcellence.org.uk/wp-content/uploads/2014/10/rethinking_construction_report.pdf).
- HMGov. (2017). Industrial strategy: building a Britain fit for the future [PDF file]. Retrieved from: [https://assets.publishing.service.gov.uk/government/uploads/system/uploads/attachment\\_data/file/664563/industrial-strategy-white-paper-web-ready-version.pdf](https://assets.publishing.service.gov.uk/government/uploads/system/uploads/attachment_data/file/664563/industrial-strategy-white-paper-web-ready-version.pdf).
- EN 1990:2002 (2002), Eurocode 0—Basis of structural design.
- Gambao, E., Balaguer, C., and Gebhart, F. (2000). Robot Assembly System for Computer-integrated Construction. *Automation in Construction*, 9(5-6), 479–487. DOI: [https://doi.org/10.1016/S0926-5805\(00\)00059-5](https://doi.org/10.1016/S0926-5805(00)00059-5).
- Gibson, D. Rosen, B., and Stucker. (2015). *Additive Manufacturing Technologies: 3D Printing, Rapid Prototyping, and Direct Digital Manufacturing*, Springer, New York, p. 498. DOI: <https://doi.org/10.1007/978-1-4939-2113-3>.
- Garcia, M. (2010). AD+ Practice Profile: Amanda Levet Architects (AL\_A). In *Architectural Design*, Published online 27th January 2010. Accessed 6/4/2020. DOI: <https://doi.org/10.1002/ad.1019>.
- Gosselin, C., Duballet, R., Roux, P., Gaudillière, N., Dirrenberger, J., and Morel, P. (2016). Large-scale 3d printing of ultra-high performance concrete—a new processing route for architects and builders. *Materials & Design*, 100(-), 102–109. DOI: <https://doi.org/10.1016/j.matdes.2016.03.097>.
- Groover, P. (2012). *Introduction to manufacturing processes*, John Wiley & Sons. p. 720. ISBN: 978-0470632284.
- Hack, N., Lauer, W., Langenberg, S., Gramazio, F., and Kohler, M. (2013). Overcoming Repetition: Robotic Fabrication Processes at a Large Scale. *International Journal of Architectural Computing*, 11(3), 285–299. DOI: <https://doi.org/10.1260/1478-0771.11.3.285>.
- Hack, N., and Lauer, W. V. (2014). Mesh-Mould: Robotically Fabricated Spatial Meshes as Reinforced Concrete Formwork. *Architectural Design*, 84(3), 44–53. DOI: <https://doi.org/10.1002/ad.1753>.
- Hack, N., Dörfler, K., Walzer, A. N., Wangler, T., Mata-Falcón, J., Kumar, N., Buchli, J., Kaufmann, W., Flatt, R. J., Gramazio, F., and Kohler, M. (2020). Structural Stay-In-Place Formwork For Robotic In Situ Fabrication Of Non-Standard Concrete Structures: A Real Scale Architectural Demonstrator. *Automation in Construction*, 115 (2020), 103197. <https://doi.org/10.1016/j.autcon.2020.103197>.

- Howe, A. S. (2000). Designing for automated construction. *Automation in Construction*, 9(3), 259–276. DOI: [https://doi.org/10.1016/S0926-5805\(99\)00041-2](https://doi.org/10.1016/S0926-5805(99)00041-2).
- Institute for Advanced Architecture of Catalonia, IAAC Barcelona. (2016). 3D printed bridge. Available online: [www.iaac.net/project/3d-printed-bridge/](http://www.iaac.net/project/3d-printed-bridge/) (accessed on May 8th, 2019).
- ISO 17296–2:2015, Additive manufacturing—General principles Part 2: Overview of process categories and feedstock (2016), Standard, International Organization for Standardization, Geneva, CH.
- ISO 17296–3:2016, Additive manufacturing—General principles Part 3: Main characteristics and corresponding test methods (2016), Standard, International Organization for Standardization, Geneva, CH.
- Khoshnevis, B., Hwang, D., Yao, K., and Yeh, Z., (2006). Mega-scale fabrication by contour crafting. *International Journal Industrial and Systems Engineering*, 1(3), 301–320. DOI: <https://doi.org/10.1504/IJISE.2006.009791>.
- Kolarevic, B. (2005). *Architecture in the Digital Age: Design and Manufacturing*, New York & London: Spon Press—Taylor & Francis Group, 308 p. ISBN: 978–0415381413.
- Kristensen, M. K., and Raun, C. (2011). Patent WO2012065614 (A1): A flexible mat for providing a dynamically reconfigurable double-curved moulding surface in a mould.
- Kuntse, H. B., Hirsch, U., Jacobasch, A., Eberle, F., and Goller, B. (1995). On the dynamic control of a hydraulic large range robot for construction applications. *Automation in Construction*, 4(1), 61–73. DOI: [https://doi.org/10.1016/0926-5805\(94\)00036-M](https://doi.org/10.1016/0926-5805(94)00036-M).
- Labonnote, N., Rønquist, A., Manum, B., and Rütther, P. (2016). Additive construction: State-of-the-art, challenges and opportunities. *Automation in Construction*, 72(3), 347–366. DOI: <https://doi.org/10.1016/j.autcon.2016.08.026>.
- Latham, M. (1994). *Constructing the Team*, HMSO, London [PDF file]. Retrieved from: <http://constructingexcellence.org.uk/wp-content/uploads/2014/10/Constructing-the-team-The-Latham-Report.pdf>.
- Le, T. T., Austin, S. A., Lim, S., Buswell, R. A., Law, R., Gibb, A. G. F., and Thorpe, T. (2012a). Hardened properties of high-performance printing concrete. *Cement and Concrete Research*, 42(3), 558–566. DOI: <https://doi.org/10.1016/j.cemconres.2011.12.003>.
- Le, T. T., Austin, S. A., Lim, S., Buswell, R. A., Gibb, A. G. F., and Thorpe, T. (2012b). Mix design and fresh properties for high-performance printing concrete. *Materials and Structures*, 45(-), 1221–1232. DOI: <https://doi.org/10.1617/s11527-012-9828-z>.
- Lim, S., Buswell, R. A., Le, T. T., Austin, S. A., Gibb, A. G. F., and Thorpe, T. (2012). Developments in construction-scale additive manufacturing processes. *Automation in Construction*, 21(-), 262–268. DOI: <https://doi.org/10.1016/j.autcon.2011.06.010>.
- Lim, S., Buswell, R. A., Valentine, P. J., Piker, D., Austin, S., and De Kestelier, X. (2016). Modelling curved-layered printing paths for fabricating large-scale construction components. *Additive Manufacturing*, 12(Part B), 216–230. DOI: <https://doi.org/10.1016/j.addma.2016.06.004>.
- Lipson, H., and Kurman, M., (2013). *Fabricated: the New World of 3D Printing*. John Wiley & Sons, Indianapolis, USA, 320 p. ISBN: 978–1–118–35063–8.
- Lloret, E., Shahab, A., Mettler, L., Flatt, R. J., Gramazio, F., Kohler, M., and Langenberg, S. (2015). Complex concrete structures: Merging existing casting techniques with digital fabrication. *Computer-Aided Design*, 60(-), 40–49. DOI: <https://doi.org/10.1016/j.cad.2014.02.011>.
- Lloret Fritschi, E. (2016). *Smart Dynamic Casting—A digital fabrication method for non-standard concrete structures*. (ETH Zurich) [PhD Thesis]. DOI: <https://doi.org/10.3929/ethz-a-010800371>.
- Lloret Fritschi, E., Reiter, L., Wangler, T., Gramazio, F., Kohler, M., and R.J. Flatt, (2017). Smart Dynamic Casting: Slipforming with Flexible Formwork – Inline Measurement and Control. In *HPC/CIC Tromsø 2017, Norway, March 6–8* (Norwegian Concrete Association). DOI: <https://doi.org/10.3929/ethz-b-000219663>.
- Lloret-Fritschi, E., Scotto, F., Gramazio, F., Kohler, M., Graser, K., Wangler, T., Reiter, L., Mata-Falcón, J., and Flatt, R. J. (2019) Challenges of Real-Scale Production with Smart Dynamic Casting. in *First RILEM International Conference on Concrete and Digital Fabrication – Digital*

- Concrete 2018 (eds. Wangler, T. & Flatt, R. J.) pp. 299–310. Springer International Publishing. DOI: [https://doi.org/10.1007/978-3-319-99519-9\\_28](https://doi.org/10.1007/978-3-319-99519-9_28).
- Lloret-Fritschil, E., Wangler, T., Gebhard, L., Mata-Falcón, J., Mantellato, S., Scotto, F., Burger, J., Szabo, A., Ruffray, N., Reiter, L., Boscaro, F., Kaufmann, W., Kohler, M., Gramazio, F., and Flatt, R. (2020). From Smart Dynamic Casting to a growing family of Digital Casting Systems. *Cement and Concrete Research*, 134(S.I.). DOI: <https://doi.org/10.1016/j.cemconres.2020.106078>.
- Lowke, D., Dini, E., Perrot, A., Weger, D., Gehlen, C., and Dillenburger, B. (2018). Particle-bed 3D printing in concrete construction—possibilities and challenges. *Cement and Concrete Research*, 112(S.I.), 50–65. DOI: <https://doi.org/10.1016/j.cemconres.2018.05.018>.
- Marchon, D., Kawashima, S., Bessaies-Bey, H., Mantellato, S., and Ng, S. (2018). Hydration and rheology control of concrete for digital fabrication: Potential admixtures and cement chemistry. *Cement and Concrete Research*, 112(S.I.), 96–110. DOI: <https://doi.org/10.1016/j.cemconres.2018.05.014>.
- Mechtcherine, V., Nerella, V. N., Will, F., Näther, M., Otto, J., and Krause, M. (2019). Large-scale digital concrete construction – CONPrint3D concept for on-site, monolithic 3D-printing. *Automation in Construction*, 107(-), 102933. DOI: <https://doi.org/10.1016/j.autcon.2019.102933>.
- Menges, A. (2006). Manufacturing diversity. *Architectural Design*, 76(2), 70–77. DOI: <https://doi.org/10.1002/ad.242>.
- Mettler, L. K., Wittel, F. K., Flatt, R. J., and Herrmann, H. J. (2016). Evolution of strength and failure of SCC during early hydration. *Cement and Concrete Research*, 89(-), 288–296. DOI: <https://doi.org/10.1016/j.cemconres.2016.09.004>.
- Nerella, V. N., Hempel, S., and Mechtcherine, V. (2019). Effects of layer-interface properties on mechanical performance of concrete elements produced by extrusion-based 3d-printing. *Construction and Building Materials*, 205(-), 586–601. DOI: <https://doi.org/10.1016/j.conbuildmat.2019.01.235>.
- Neudecker, S., Bruns, C., Gerbers, R., Heyn, J., Dietrich, F., Dröder, K., and Kloft, H. (2016). A New Robotic Spray Technology for Generative Manufacturing of Complex Concrete Structures Without Formwork. *Procedia CIRP*, 43(-), 333–338. DOI: <https://doi.org/10.1016/j.procir.2016.02.107>.
- Nolte, N., Heidmann-Ruhz, M., Krauss, H.-W., Varady, P., Budelmann, H., and Wolter, A. (2018). Development of shotcrete mixtures with controllable properties for the additive manufacturing of concrete structures. In: Prof. Wolfgang Kusterle (Ed.), *Spritzbeton-Tagung*. (pp. 1–13). Alpbach.
- Pierre, A., Weger, D., Perrot, A., and Lowke, D. (2018). Penetration of cement pastes into sand packings during 3D printing: analytical and experimental study. *Materials and Structures*, 51(1), 22. <https://doi.org/https://doi.org/10.1617/s11527-018-1148-5>.
- Raun, J. C., and Henriksen, Th. (2014). Patent 51403: Verfahren zur Herstellung eines flächenartigen Elements mit von einer ebenen Oberfläche abweichender Oberfläche, Formteil zur Herstellung eines derartigen flächenartigen Elements sowie flächenartiges Element.
- Reiter, L., Wangler, T., Roussel, N., and Flatt, R. J. (2018). The role of early age structural build-up in digital fabrication with concrete. *Cement and Concrete Research*, 112(S.I.), 86–95. DOI: <https://doi.org/10.1016/j.cemconres.2018.05.011>.
- Roussel, N. (2018). Rheological requirements for printable concretes. *Cement and Concrete Research*, 112(S.I.), 76–85. DOI: <https://doi.org/10.1016/j.cemconres.2018.04.005>.
- Salet, T., Ahmed, Z., Bos, F., and Laagland, H. L. M. (2018). Design of a 3D printed concrete bridge by testing. *Virtual and Physical Prototyping*, 13(3), 222–236. DOI: <https://doi.org/10.1080/17452759.2018.1476064>.
- Schipper, H. R., Grünewald, S., Eigenraam, P., Raghunath, P., and Kok, M. D. (2015a). Production of curved precast concrete elements for shell structures and free-form architecture using the flexible mould method. *New Building Materials & Construction World*, 20(8), 100–112.
- Schipper, H. R., Eigenraam, P., Grünewald, S., Soru, M., Nap, P., van Overveld, B., and Vermeulen, J. (2015b). Kine-mould: Manufacturing technology for curved architectural elements in concrete. In: Jeroen Coenders, Andrew Borgart, and Arno Pronk, editors, *Proceedings of the International Society Of Flexible Formwork (ISOFF) Symposium, Amsterdam*. KIVI.

- Schipper, H. R., and Eigenraam, P. (2016). Mapping double-curved surfaces for production as precast concrete shell elements. *HERON*, 61(3), 211–234 [PDF file]. Retrieved from: <http://heronjournal.nl/61-3/6.pdf>.
- Schodek, D., Bechthold, M., Griggs, K., Kao, and Steinberg, M. (2005). *Digital Design and manufacturing: CAD/CAM Applications in Architecture and Design*, First ed, Wiley and Sons, Hoboken, New Jersey, p. 384. ISBN: 978-0471456360.
- Siemens. (2017a). Made smarter review [PDF file]. Retrieved from: [https://assets.publishing.service.gov.uk/government/uploads/system/uploads/attachment\\_data/file/655570/20171027\\_MadeSmarter\\_FINAL\\_DIGITAL.pdf](https://assets.publishing.service.gov.uk/government/uploads/system/uploads/attachment_data/file/655570/20171027_MadeSmarter_FINAL_DIGITAL.pdf).
- Siemens. (2017b). Made smarter review. <https://www.gov.uk/government/publications/made-smarter-review>.
- Tay, Y. W. D., Ting, G. H. A., Qian, Y., Panda, B., He, L., and Tan, M. J. (2019). Time gap effect on bond strength of 3D-printed concrete. *Virtual and Physical Prototyping*, 14(1), 104–113. DOI: <https://doi.org/10.1080/17452759.2018.1500420>.
- Troughton, M. J. (2008). Mechanical fastening. In: *Handbook of Plastics Joining*, second edition, pp. 175–201. William Andrew Publishing (Chapter 8). ISBN 9780815515814, DOI: <https://doi.org/10.1016/B978-0-8155-1581-4.50020-2>.
- Urschel, W. E. (1941). US2339892A. Machine for building walls [PDF file]. Retrieved from: <https://patents.google.com/patent/US2339892>.
- Valencia, N. (2017). World's First 3D Printed Bridge Opens in Spain. Available online: [www.archdaily.com/804596/worlds-first-3d-printed-bridge-opens-in-spain](http://www.archdaily.com/804596/worlds-first-3d-printed-bridge-opens-in-spain) (Accessed on September 5th, 2019).
- Vollers, K.J., and Rietbergen, D. (2010). Patent NL 2001738 (C2): Curved panel producing method, involves depositing viscous-liquid material on horizontal plane of mold, hardening viscous-liquid material, providing flexible material in mold, forming edge profile, and cutting profile at regular intervals.
- Wolfs, R., Bos, F., and Salet, T. (2018a). Early age mechanical behaviour of 3D printed concrete: Numerical modelling and experimental testing. *Cement and Concrete Research*, 106, 103–116. <https://doi.org/10.1016/j.cemconres.2018.02.001>.
- Wolfs, R. J., Bos, F. P., van Strien, E. C., and Salet, T. A. (2018b). A real-time height measurement and feedback system for 3D concrete printing. In *High Tech Concrete: Where Technology and Engineering Meet*, pp. 2474–2483. Springer, Cham. DOI: [https://doi.org/10.1007/978-3-319-59471-2\\_282](https://doi.org/10.1007/978-3-319-59471-2_282).
- Wolfs, R., Bos, F., and Salet, T. (2018c). Correlation between destructive compression tests and non-destructive ultrasonic measurements on early age 3D printed concrete. *Construction and Building Materials*, 181(-), 447–454. DOI: <https://doi.org/10.1016/j.conbuildmat.2018.06.060>.
- Wolfs, R. J. M., and Suiker, A. S. J. (2019a). Structural failure during extrusion-based 3D printing processes. *International Journal of Advanced Manufacturing Technology*, 104(-), 565–584. DOI: <https://doi.org/10.1007/s00170-019-03844-6>.
- Wolfs, R., Bos, F., and Salet, T. (2019b). Hardened properties of 3D printed concrete: The influence of process parameters on interlayer adhesion. *Cement and Concrete Research*, 119(-), 132–140. DOI: <https://doi.org/10.1016/j.cemconres.2019.02.017>.
- Yamazaki, Y., and Maeda, J. (1998). The SMART system: an integrated application of automation and information technology in production process. *Computers in Industry*, 35(1), 87–99. DOI: [https://doi.org/10.1016/S0166-3615\(97\)00086-9](https://doi.org/10.1016/S0166-3615(97)00086-9).
- Yamazaki, Y., and Maeda, J. (1998). The SMART system: an integrated application of automation and information technology in production process. *Computers in Industry*, 35, 87–99.

# Chapter 3

## Digital Fabrication with Cement-Based Materials: Underlying Physics



**Viktor Mechtcherine, S. Fataei, F. P. Bos, R. A. Buswell,  
Wilson Ricardo Leal da Silva, E. Keita, H. W. Krauss, Dirk Lowke,  
Arnaud Perrot, Venkatesh Naidu Nerella, Nicolas Roussel,  
Mohammed Sonebi, Timothy Wangler, Daniel Weger, and Rob Wolfs**

**Abstract** The comprehending of the processes' physics is a prerequisite for the purposeful design and optimization of digital fabrication systems, as well as their efficient and robust process control. This chapter presents an overview of the underlying physics relevant to an understanding of the processing of cement-based materials during various production steps of digital fabrication. In this, the main focus was on various approaches of Additive Manufacturing, but selected aspects of formative

---

V. Mechtcherine (✉) · S. Fataei · V. N. Nerella  
Institute of Construction Materials, Technische Universität Dresden, Dresden, Germany  
e-mail: [viktor.mechtcherine@tu-dresden.de](mailto:viktor.mechtcherine@tu-dresden.de)

F. P. Bos · R. Wolfs  
Department of the Built Environment, Eindhoven University of Technology, P.O. Box 513,  
NL-5600 MB, Eindhoven, The Netherlands

R. A. Buswell  
School of Architecture, Building and Civil Engineering, Loughborough University,  
Loughborough, UK

W. R. L. da Silva  
Danish Technological Institute, Taastrup, Denmark

E. Keita · N. Roussel  
Laboratoire NAVIER, Gustave Eiffel University, 5 Boulevard Descartes, 77420  
Champs-sur-Marne, France

H. W. Krauss · D. Lowke  
Institute of Building Materials, Concrete Construction and Fire Safety, Technische Universität  
Braunschweig, Beethovenstr. 52, 38106 Braunschweig, Germany

A. Perrot  
University Bretagne-Sud, UMR CNRS 6027, IRDL, 56100, Lorient, France

M. Sonebi  
School of Natural and Built Environment, Queen's University Belfast, Belfast BT9 5AG, Northern  
Ireland, UK

T. Wangler  
Institute for Building Materials, ETH Zurich, Stefano-Francini-Platz 3, 8093 Zurich, Switzerland

D. Weger  
Centre for Building Materials (CBM), Technical University of Munich, 81245 Munich, Germany

processes were addressed as well. For some processes, analytical formulas based on the relevant physics have already enabled reasonable predictions with respect to material flow behaviour, buildability, and other relevant features. Nevertheless, further research efforts are required to develop reliable tools for the quantitative analysis of the entire process chains. To accomplish this, experimental efforts for the characterization of material properties need to be accompanied by comprehensive numerical simulation. The presented work results from collaborative research carried out by the authors in the framework of the RILEM Technical Committee 276 “Digital fabrication with cement-based materials”.

**Keywords** Concrete technology · Digital fabrication · Additive manufacturing · 3D concrete printing · Digital concrete · Underlying physics

### 3.1 Introduction

Digitalization and automation in construction bear great potential with respect to increases in productivity, in creating more attractive jobs, in compensating for shortages of skilled labour (Wangler et al. 2016; De Schutter et al. 2018). Digital fabrication with cement-based materials stands for a wide range of novel concrete technologies which enable to utilize digital data from the planning phase for actual automated production in factories and on construction sites (Buswell et al. 2007; Mechtcherine et al. 2019). This seamless data flow along with full automation can considerably rationalize and speed up production processes. Furthermore, the digital fabrication makes it technically and economically feasible to realize topologically optimized, geometrically complex structural elements designed according to the principle *form follows force*. Not only such topological optimization allows for elegant, material-minimized, and resource-saving structures (De Schutter et al. 2018; Lowke et al. 2018), but it also enables the integration of various functionalities.

Several approaches for Digital Fabrication with Concrete (DFC) have been developed over the last few years, and a number of full-scale applications have been successfully realized; see e.g. Salet et al. (2018), Valencia (2017). While the individual approaches vary considerably with respect to equipment, material concepts, and production steps, they all rely on sound interactions between material and machine along the entire processing chain. Thus, mastering material flow is a prerequisite for efficient and robust processes, let alone their optimization and control. Such mastering is only possible if the underlying physics of individual DFC processes are well understood and purposefully applied. In this light, the RILEM Technical Committee 276 “Digital fabrication with cement-based materials” dedicated considerable time and effort to the systematic analysis of the physical background of various DFC technologies and their individual processing steps. The main outcomes of this collaborative work is this chapter as well as an extra review paper focusing on Additive Manufacturing approaches based on material extrusion (Mechtcherine et al. 2020).

This contribution brings together the relevant knowledge in physics needed to understand and shape purposefully the relevant processes belonging to DFC. In doing so, first, in Sect. 3.2, the existing DFC approaches are briefly described, and relevant processing steps and related physics are given. This section also set the stage of the entire chapter by explaining which topics will be addressed comprehensively, and which only briefly or not at all. The following four sections deal with individual processing steps and corresponding physical mechanisms governing these processes:

- Section 3.3, Gravitational flow and capillary flow
- Section 3.4, Pumping and extrusion
- Section 3.5, Mixing after adding accelerator in the print-head/nozzle
- Section 3.6, Load bearing and deformation behaviour after deposition.

Section 3.7 discuss briefly the key physical properties relevant to the underlying physics described in the foregoing sections. In particular, rheological properties of fresh concrete, visco-elastic properties of fresh and hardening mixtures as well as surface tension and friction are addressed. Section 3.8 offers some deliberations on optimization of DFC technologies based on the understanding of underlying physics and illuminates that by two examples. Various processes relevant for some particular DFC approaches and not covered by previous sections are briefly described in Sect. 3.9. Section 3.10 summarizes the main conclusions of the review work. In this, special attention is paid to research needs, of which a great many remain.

## 3.2 Fabrication Approaches, Processing Steps and Related Physics

The fabrication approaches addressed in the chapter include material shaping processes within the additive and formative categories according to the classification framework from Chap. 2, see also (Buswell et al. 2020). The main focus is on Additive Manufacturing approaches, namely, the approaches based on material extrusion, on material jetting and on the particle-bed binding. As an example of a novel formative technology, adaptive formwork is illuminated in this section as well. A brief description of each fabrication approach, along with their classification and processing steps, is provided below. Note that the term “processing step” relates to how the material is handled prior/during production and the imposed loads during/after production.

The Additive Manufacturing technologies based on material extrusion, can be subdivided into three categories: (i) extrusion of stiff material, similar to conventional extrusion, (ii) extrusion of flowable material with or without adding admixture(s) in the print-head, and (iii) extrusion of material using additional energy input, e.g. vibration, which facilitates the delivery and deposition of stiff mixtures. The major processing steps include: transportation of build material to the print-head,



print-head process/extrusion by the print-head, deposition of build material, accompanied by its deformation, and depositions of further layers, accompanied by loading earlier deposited upper layer(s) by self-weight and process-induced forces, related deformation of build material after deposition followed by further deformation due early-age shrinkage, early-age creep, and thermal dilation.

Material jetting is an Additive Manufacturing approach which corresponds to a variation of conventional sprayed concrete, except that an automated positioning system (e.g. an industrial robotic arm) serves as mean to control the material spray onto the working surface. Hence, this fabrication approach requires a delivery system to convey the feedstock to the nozzle, which is then projected, deposited onto a surface and gradually loaded—at greater loads than that experienced in extrusion—as the process goes by.

As for particle-bed binding, this is an Additive Manufacturing fabrication approach that uses binder jetting. The process steps in particle-bed binding differ from all of the above approaches. Basically, the feedstock (dry material) is spread in sequential layers on the working surface by a nozzle; and a second nozzle selectively places the binding agent. The only similarity lies in that a binding agent is conveyed to the second nozzle using a pumping system. The final structure is only loaded post-process due to the de-powdering or removal of unbound material, which acts as support material as the processes progresses.

Finally, the adaptive formwork, this is a formative manufacturing fabrication approach that combines solidification and deformation processes. The process steps in adaptive formwork are similar to those in the extrusion approach. As the process progresses, the material is gradually loaded by a combination of forces exerted by the material's self-weight and the formwork movement.

Prior to discussing the commonality between the processing steps in the approaches covered in this chapter, the readers should bear in mind that a technical discussion on the processing step “mixing” (either in wet or dry form) is beyond the scope of this publication—and will only be presented in a succinct form for the sake of general information. Hence, we assume that the first step in each approach is “material delivery”.

By overlapping the processing steps from the discussed digital fabrication approaches, it is possible to derive the backbone of processing steps common to all cases. Specifically, Step 1 corresponds to material delivery to print-head (nozzle), Step 2 to any additional processing in the print-head, Step 3 to deposition and related loads/deformations, Step 4 to mechanical loading after deposition, and Step 5 to behaviour of material after deposition. Table 3.1 lists production steps, related processes and underlying physics relevant for given fabrication approaches. Note that mechanical loading after deposition as well as early-age shrinkage, early-age creep and thermal dilation of the material after deposition do not represent a production step as such, but still need to be considered for attaining products according to specification.

For the sake of clarity, one of the approaches is depicted in Fig. 3.1, which illustrates the processing steps belonging to the extrusion of concrete materials without the addition of admixture in the print-head.

**Table 3.1** Production steps, related processes and underlying physics relevant to selected fabrication approaches

Production step		Print-head process	Deformation of material during deposition	Mechanical loading after deposition	Behaviour of material after deposition
Fabrication approach	Transportation of material	Extrusion using primary motivation, ram extrusion, or screw extrusion; optionally dispersion of admixture by high-energy mixing	Gravitational flow, viscoelastic-plastic deformations	Layer self-weight, kinetic energy from deposition and/or print-head contact or vibration	Deformations due to self-weight and kinetic energy of deposition; additionally: early-age shrinkage, early-age creep, thermal dilation
	Pumping or gravitational flow with or without energy input	Screw extrusion or gravitational flow supported by vibration	Gravitational flow and compaction supported by vibration, elastic deformations		
Material extrusion	Pumping, pneumatic transport	Wet spraying, dry spraying	Impact compaction, gravitational flow	Spraying kinetic energy and layer self-weight	
Material extrusion by vibrating nozzle	Pumping, pneumatic transport gravitational flow	Gravitational flow, spraying	Gravitational flow in porous medium, wetting, capillary flow	Self-weight and kinetic energy after unbound material removal	
Material jetting	Pumping, gravitational flow	Compaction by self-weight and vibration	Elastic deformations	Self-weight, tensile force due to formwork sliding	
Particle-bed binding					
Adaptive formwork					

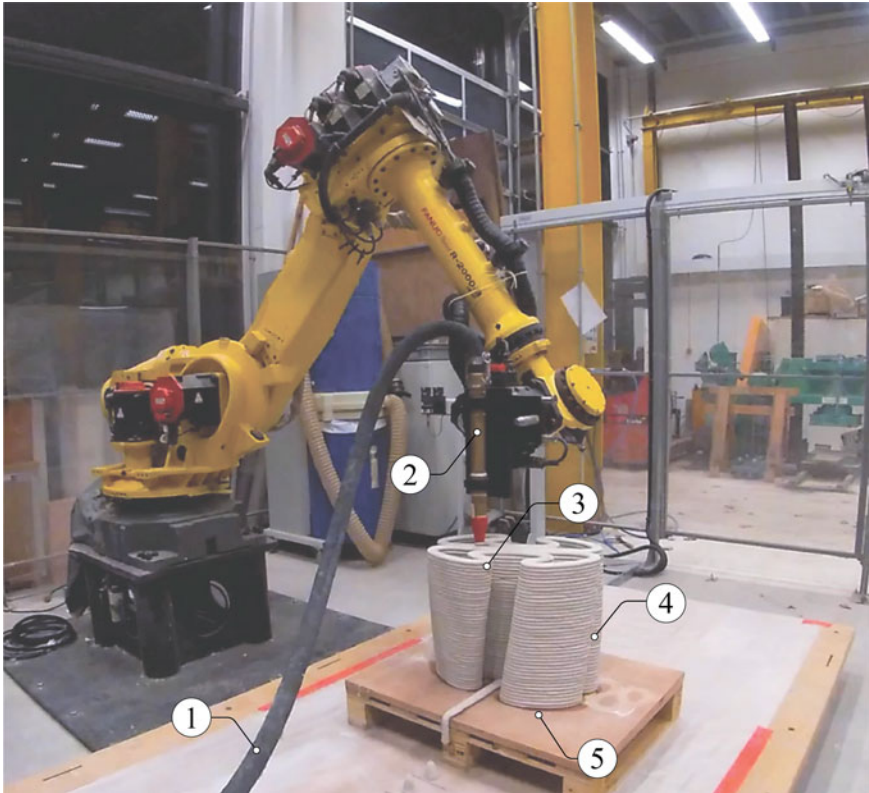


**Fig. 3.1** Processing steps in an extrusion-based additive manufacturing approach: (1) transportation of material, (2) print-head process, (3) deformation of material during deposition, (4) mechanical loading after deposition, (5) behaviour of material after deposition

The following sections will focus on underlying physics relevant to processes in various processing steps and fabrication approaches. Some related topics will not be addressed, since they are covered by the other chapters of the book:

- (1) Measurements of material properties of print concrete in the fresh state; this subject is covered by Chap. 4.
- (2) Properties of print cement-based materials in the hardened state; they are dealt with in Chap. 5. This also includes the bond between layers as such; however, the link between process parameter and the quality of layer-to-layer interface will be briefly addressed in this chapter.
- (3) Effect of reinforcement on process parameters and required physical properties. There is little information on that evaluable in the literature, but some information is provided in Chap. 6.

Some processes of secondary relevance with respect to the main focus of the chapter will be addressed only briefly or omitted completely for various reasons. Following topics belong to this group:

- mixing of slurry or mortar/concrete, since this is a process which is well established in concrete technology;
- pneumatic transport of dry mix, since this is a specific secondary process familiar in concrete construction from dry spraying;
- delivering dry material and spreading layers of it in selective binding, since this is a specific process well known from other industries and not specific to concrete;
- wet and dry spraying, since these processes are well established in concrete technology already;
- mould filling, since it is a standard process in formative approaches to shaping concrete; however, some aspects relevant to digital fabrication approaches such as filling 3D-printed mould, integrated formwork, or Mesh Mold are briefly addressed in Sect. 3.9.5;
- compaction under gravitational force, compaction by vibration, compaction through static forming element, impact compaction (spraying); these are highly interesting aspects relevant also to other concrete technologies and not really specific to digital fabrication; covering them goes beyond the scope and format of this contribution;
- kinetic energy from the upper layer deposition, spraying or print-head contact; these issues are of high relevance, but hardly covered by the existing literature; it is certainly an area in which more research is needed;
- tensile force due to the upward movement of formwork and friction or due to movement of temporary supports; highly relevant topic for adaptive formwork, and important for some extrusion-based approaches; again there is little information published as yet, thus, there is plenty of room for future research;
- kinetic energy by removal of unbound or support material; little knowledge is available on this issue as well; it is relevant for powder-bed binding in the first place, and with respect to support material to some other technologies too;
- early age shrinkage, early-age creep, and thermal dilation, since they are not considered to be principally different from conventional concrete construction from the physical point of view.

### 3.3 Gravitational Flow and Capillary Flow

#### 3.3.1 Gravitational Flow

Cementitious materials behave as visco-plastic materials when in their fresh state. Their behaviour can be roughly modelled using the Bingham model. Schematically,

they behave as elastic solid under a critical stress called yield stress,  $\tau_0$ , and critical shear strain,  $\gamma_0$ , and as viscous fluid when the stress and strain in the material are greater than the critical values; see Fig. 3.2. Depending on the production step, the material's elasto-plastic or visco-plastic properties have a specific contribution to the particular process. For example, in extrusion-based additive manufacturing/3D concrete printing, during transportation (pumping, extrusion) the visco-plastic behaviour dictates the flow profile, whereas during and after placement the elasto-plastic properties dictate the shape to the deposited layer (Roussel 2018).

When the material is at rest, i.e. after extrusion, gravity acts on the material, which flows if the gravitational forces overcome the material's yield stress at the bottom layer. For the case of pasty materials, such as printable cementitious mortar, the situation is close to the slump flow theory described by Roussel and Coussot (2005). Thus, the stress induced by the weight of the sample, i.e.  $\rho gh$  (where  $h$  is the layer height) have to be compared to the elongational yield stress of the material—which is equal to  $\sqrt{3} \cdot \tau_0$  for cementitious materials having a Von Mises' plasticity criterion (Ovarlez and Roussel 2006).

Thus, the final height of the deposited layer can be derived from the dimensionless ratio  $\rho gh / \alpha_{geom} \tau_0$ : if the ratio is lower than 1, the layer will maintain its initial shape provided by the nozzle and if the ratio is higher than one, the final layer height reads  $h = \alpha_{geom} \tau_0 / \rho g$  due to plastic settlement. The value of  $\alpha_{geom}$  ranges from 1 (thin layer, shear flow) to  $\sqrt{3}$  (elongational flow) depending on the shape of the deposited material. Note that when left at rest, the deposited cementitious material can also undergo elastic deformations, see Sect. 3.6.3 for more details.

Cementitious materials exhibit a viscous flow when the applied stress overcomes the yield stress. The example of the flow on a rough inclined plane is often used to illustrate the flow profile of a visco-plastic materials (Coussot and Boyer 1995). In this case, the stress linearly increases within the thickness of the layer and is equal to  $\rho gh \sin \theta$ , where  $\theta$  is the angle between the horizontal plane and the inclined plane,

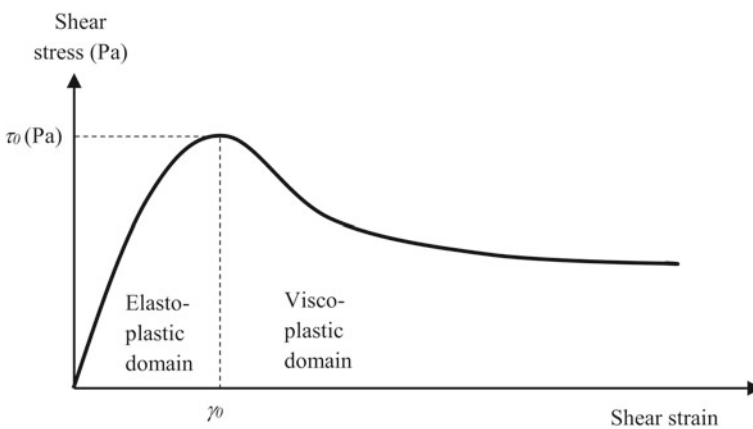


Fig. 3.2 Shear stress vs. shear strain for visco-plastic cementitious materials

at the cementitious material/mortar interface. The cementitious materials will be sheared on a layer of thickness  $\Delta h$  for which the stress is higher than the yield stress. At the interface between sheared and unsheared zones, the stress profile provides a stress value equal to the yield stress:  $\tau_0 = \rho g (h - \Delta h) \sin \theta$ . The unsheared part of the flow is known as the plug flow zone. The formation of the plug flow zone is also encountered in extrusion or pumping. However, it is worth noting that in real situation, flow-induced particles migration can lead to the formation of a lubrication layer that reduces the thickness of the shear zone. This will be discussed in this chapter, within the section dealing with extrusion and pumping.

Another important point is that fresh cementitious materials are time-dependent materials due to early cement hydration, i.e. their rheological properties evolve in time. Even more, the type of rheological behaviour can change during the early hydration from visco-plastic behaviour to frictional plastic behaviour after several hours of hydration (Mettler et al. 2016). This evolving rheological behaviour is a crucial point when dealing with the overall stability of the structures in time and will be discussed in details in Sect. 3.6.

### 3.3.2 *Gravitational Flow in Combination with Vibration*

It is well known that vibration affects the rheological behaviour of the concrete and makes it behave like a fluid, helping concrete to fill a formwork. In material extrusion fabrication approach, vibration helps ease the extrusion (Perrot et al. 2009).

A vibration solicitation can be described with its amplitude  $\alpha$  ( $m$ ) and frequency  $f$  ( $s^{-1}$ ). The vibration induces a shear rate at the vibrator/materials interface which is proportional to the following ratio  $\alpha \cdot f / D_{vib}$  where  $D_{vib}$  is the dimension of the vibrator (for example its radius for a vibration needle); see Banfill et al. (2011). This shear rate is sufficient to create a shear stress higher than the yield stress and locally makes the cementitious materials flow. Some authors have also shown that the rheology of the vibrated cementitious material is governed by the product  $\alpha \cdot f / D_{vib}$  (Perrot et al. 2009).

The zone of influence (i.e. where the concrete behaves like a fluid) is a crucial aspect for vibration. For example, it is often considered that for vibration needles, the area of action is about 10 times the diameter of the needle (Forsblad 1965). Some more precise prediction model of the impact zone can be found in the literature (Banfill et al. 2011; Grampeix 2013). However, for modern viscous concretes such as printable ones, the problem can be more complex, and the impact zone can be smaller than ten times the vibrator size (Grampeix 2013).

### 3.3.3 Gravitational Flow in a Porous Medium

Gravitational flow of cement paste through a porous medium consisting of sand assembly is the working mechanism involved in the particle-bed binding approach. In one of the variations of this Additive Manufacturing approach called selective paste intrusion, cement paste has to flow through the dry aggregates layer in order to fulfil the porosity of a layer made of sand particles of height  $h_{sand}$  (Perrot et al. 2014a).

In this method, the exact quantity of cement paste required to fill the porosity  $n_{sand}$  of the sand particles layer is deposited on top of this porous medium. The driving force that makes the cement paste penetrates within the porous medium is gravity. This driving force is initially equal to  $\rho gh_{paste}$  where  $h_{paste}$  is the initial height of cement paste. This driving force linearly increases with the friction depth as long as the penetration depth increases and finally reaches  $\rho gh_{layer}$ . The adverse force that opposes the flow is the friction forces acting at the cement paste/aggregates interface. At the flow stoppage, the shear rate tends to zero, and it can be assumed that yield stress  $\tau_0$  is reached at the interface between sand particles and cement pastes. Thus, the adverse friction force can be written as a function of the yield stress and of the specific area of the sand which is equal to  $6/D_p$  if we consider that sand particles (with diameter  $D_p$ ) are spherical, see Eq. 3.1:

$$F_{friction} = \frac{6}{D_p} \frac{n_{sand}}{1 - n_{sand}} \tau_0 \quad (3.1)$$

The computation of the friction force is close to the problem of modelling the pressure exerted by SCC on formwork which is reduced by the shearing of the concrete at the formwork and rebars surface (Ovarlez and Roussel 2006; Perrot et al. 2014a). By computing the ratio gravity/friction force, it is possible to have an idea of the balance between driving and adverse forces that influence the penetration of the cement paste.

The description and modelling of this problem can be done using an adaptation of the Darcy's law for visco-plastic materials (Chevalier and Talon 2015; Pierre et al. 2018). The work of Chevalier and Talon (Chevalier and Talon 2015) provides a general frame of applying Darcy's law for visco-plastic fluid. It allows to compute the flow rate under a given pressure gradient depending on the rheological characteristics of the visco-plastic fluids, see Eq. (3.2).

$$D\nabla P = \alpha\tau_0 + \beta k \left( \frac{v}{D_p} \right)^n \quad (3.2)$$

where  $\nabla P$  is the pressure drop per unit length ( $\text{Pa}\cdot\text{m}^{-1}$ ) and  $v$  is the liquid velocity ( $\text{m}\cdot\text{s}^{-1}$ ),  $k$  the consistency and  $n$  the power-law exponent of the Herschel-Bulkley law describing the fluid rheological behaviour. The coefficients  $\alpha$  and  $\beta$  are fitting parameters. For a Bingham material,  $k = \mu_p$  and  $n = 1$ . Pierre et al. have applied

this theoretical framework to the case of selective paste intrusion in order to predict the penetration depth (Pierre et al. 2018). However, their modelling remains one-dimensional, and some further works are required to predict 3D effects such as preferential flow path.

### 3.3.4 Wetting and Capillary Flow

Capillary flow within a porous medium is involved during the particle-bed binding with cement activation where water (with specific admixtures) has to flow through a layer composed of dry sand and cement (Lowke et al. 2018), see also Chap. 2, Sect. 4.5 and Sect. 9.1 in this chapter. The driving mechanism is capillary forces acting at the pore scale. It is responsible for porous medium imbibition, moisture-wicking or fluid intrusion in powders (Washburn 1921; Boyce et al. 2016).

Due to the fluid surface tension  $\gamma_l$ , the air–water interface forms a contact angle  $\theta$  at the solid surface. For example, this contact angle is equal to  $20^\circ$  for a dry cement–water interface (Feneuil et al. 2017). Using the Young–Laplace equation (see Eq. 3.3), it is possible to compute the magnitude of the capillary pressure  $\sigma_{cap}$  which is proportional to the surface tension and inversely proportional to the pore diameter  $D_{pore}$ . This pore diameter can be expressed in function of the particle diameter as shown by Roozbahani et al. (2017). In order to estimate the order of magnitude of capillary pressure, the pore size is considered to be equal to the particle diameter  $D_{pore} \approx D_p$ . It is important to note, however, that the use of geometric mean of the capillary, i.e.  $0.43 \cdot r$ , might be more appropriate to describe capillary pressure.

$$\sigma_{cap} = \frac{4\gamma_l \cos \theta}{D_p} \quad (3.3)$$

Then, it is possible to compare the magnitude of the gravitational force to the magnitude of the capillary forces. If we consider the problem of the intrusion of a droplet of diameter  $D_p$ , the level of pressure due to gravity is equal to  $\rho g D_p$  and it is possible to define a dimensionless number called Bond number  $B_o$  which defines the ratio of gravitational to capillary forces, see Eq. 3.4:

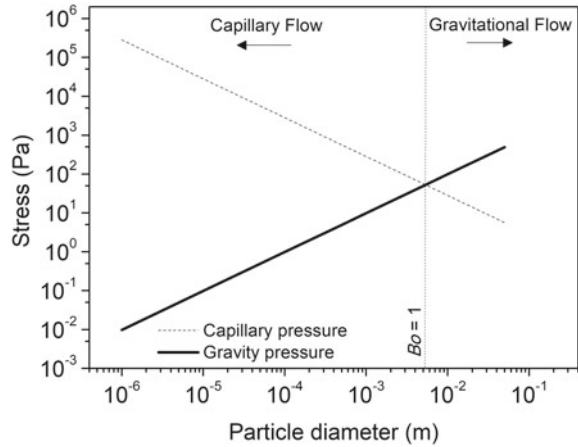
$$B_o = \frac{\rho g D_p^2}{4\gamma_l \cos \theta} \quad (3.4)$$

If  $B_o \gg 1$ , the capillary forces are negligible while if  $B_o \ll 1$ , the water flow is only driven by the capillary forces. It is worth to note that when  $B_o \ll 1$ , the flow cannot be considered as one dimensional because the porous network is a three-dimensional structure. In this case, further modelling works are required in order to predict the flow of fluid through the porous medium.

For water in the cement particles network, we can consider that the contact angle is  $20^\circ$  and the surface tension of water is  $0.075 \text{ N}\cdot\text{m}^{-1}$ . Then it is possible to predict



**Fig. 3.3** Magnitude of stress induced by capillary forces and gravity as a function of the particle diameter



the range of particle diameter for which the capillary or the gravitational force is the main driving force; see Fig. 3.3. The magnitude of stress induced by gravity and capillary forces in function of particle diameter are plotted on Fig. 3.3. It can be seen that for particles smaller than 1 mm, the main driving mechanism is capillary forces.

### 3.4 Pumping and Extrusion

The pumping (Processing Step 1) refers to transporting concrete/binder fluid from a reservoir/truck to the print-head (nozzle). Extrusion in DFC refers to the process of extruding concrete, in the print-head, from a reservoir to the nozzle outlet. Concretes' transient rheological properties and pumping specifications such as pipeline distance and geometry affect the pumping process. Numerous factors (cement particle dispersion, thixotropy of plug zone, water absorption by the aggregates, activation of superplasticizer and variation of air-content) govern whether the pumping process leads to a decrease or increase in the rheological parameters of fresh concrete (Jang et al. 2018; ACPA 2008; Guptill et al. 1996; Secrieru 2018). Such changes can have consequences to the successful execution of DFC. For example, in 3D printable concretes, a decrease in yield stress hinders the material deposition rate.

#### 3.4.1 Predicting Pumping Behaviour

There exist various models and test approaches for predicting pumping behaviour (Kaplan et al. 2005; Chapdelaine 2007; Feys 2009; Choi et al. 2013; Mechtcherine et al. 2014; Kwon et al. 2016; De Schutter and Feys 2016; Nerella and Mechtcherine 2018; Secrieru 2018). Traditionally pumping pressures are determined based on

empirical design charts. However, these empirical methods have many limitations and are unreliable for modern concretes like SCC and HPC (De Schutter and Feys 2016). The analytical approaches for predicting required pumping pressure for desired discharge for a pipeline were elaborated in Poiseuille (1844; Kaplan et al. 2005; Feys 2009; Kwon et al. 2016; De Schutter and Feys 2016; Secrieru 2018). For the laminar flow of a Newtonian fluid, the Poiseuille equation relates pressure  $P$  and discharge rate  $Q$  (Poiseuille 1844; De Schutter and Feys 2016). Pipe flow of a Bingham fluid can be described by the Buckingham-Reiner equation, which can result in over-estimation of pumping pressure up to 5 times (Jo et al. 2012; Mechtcherine et al. 2014; De Schutter and Feys 2016). Buckingham-Reiner equation does not consider the formation of lubrication layers and the flow profiles during pumping. The shear stress, shear rate and velocity profiles of concrete are presented in Fig. 3.4.

Due to shear-induced particle migration (SIPM) concrete flow during pumping is inhomogeneous; consisting of LL, shearing concrete and non-shearing concrete plug (Kaplan et al. 2005; De Schutter and Feys 2016; Jo et al. 2012; Mechtcherine et al. 2014; Secrieru 2018). The presence and properties of the LL have the most predominant influence on the discharge pressures. Kaplan introduced two analytical models using bulk and interface parameters ( $\tau_{oi}$  and  $\mu_i$ ) for the pipe flow (radius  $R$  and length  $L$ ) cases of (a) slip-plus-plug flow; Eq. 3.5 and (b) slip-plus-shear flow; Eq. 3.6 pipe using filling coefficient  $k$  and pipeline geometric specifications:

$$P = \frac{2L}{R} \left[ \frac{Q \cdot \mu_i}{\pi \cdot R^2 \cdot k} + \tau_{oi} \right] \tag{3.5}$$

$$P = \frac{2L}{R} \left[ \frac{\frac{Q}{\pi \cdot R^2 \cdot k} - \frac{R}{4\mu} \cdot \tau_{oi} + \frac{R}{s\mu} \tau_o}{1 + \frac{R}{4\mu} \mu_i} \cdot \mu_i + \tau_{oi} \right] \tag{3.6}$$

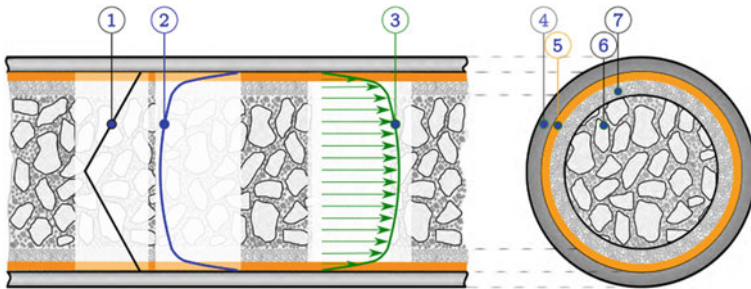


**Fig. 3.4** (1) Shear stress, (2) shear rate and (3) velocity profiles of a concrete flow inside a pumping pipeline (Nerella 2019). (4)-(7) indicate pipe, slip layer, plug zone and bulk-shear zone; adapted from Kwon et al. (2013), Choi et al. (2014)

where  $P$  is total pressure [Pa] and  $Q$  [m<sup>3</sup>/s] is the discharge rate. The shear stress, shear rate and velocity profiles of concrete are presented in Fig. 3.4. The interface rheological properties are typically measured using tribometers.

### 3.4.2 Ram Extrusion

In ram extrusion, the material in the extruder barrel is pushed by a ram that has the same section as the barrel towards a gradually reducing (in diameter) or abrupt die that gives its shape to the material.

Ram extrusion is not a conventional way to process materials at industrial scale, since it is not a continuous process; it requires a periodical refilling of the barrel. However, ram extrusion is often used at a laboratory scale to study the extrusion flow, describe the rheological behaviour and assess the extrudability of various materials (Zhou and Li 2005; Perrot et al. 2012; Alfani and Guerrini 2005; Kuder and Shah 2006). Ram extrusion is considered as the reference case given its simplicity and availability in the academic and industrial world. As described in Sect. 3.1, cementitious materials exhibit a visco-plastic behaviour. It can be described by Bingham or Herschel-Bulkley models with a high yield stress needed for shape stability; see also Chaves Figueiredo et al. (2019).

As proved by non-destructive or destructive testing, the ram extrusion flow of the cementitious materials can be divided into three parts (Perrot et al. 2007; Rabideau et al. 2010, 2012); see Fig. 3.5:

- plug flow in the extruder barrel;
- conical “dead” zone where the material remains immobile around the die entry (in an optimally designed progressive die the dead zone would not exist);

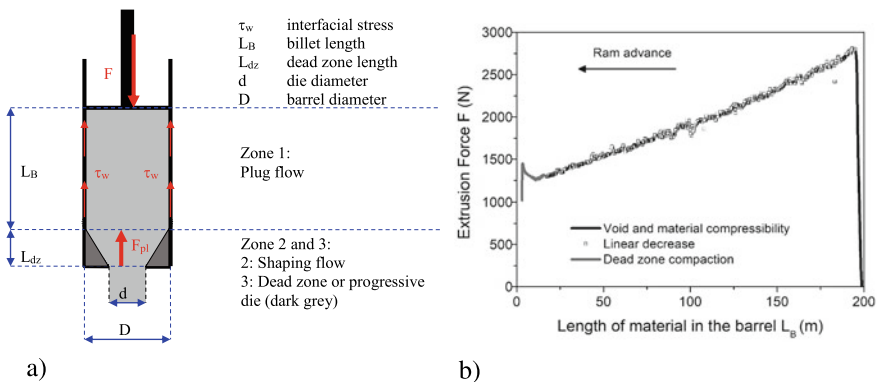


**Fig. 3.5** a Schematic view of an axisymmetric ram extrusion flow and b evolution of extrusion force  $F$  with length of material remaining in the plug flow zone

- “shaping” zone located inside the conical dead zone or inside the progressive die, where the material forming takes place and the billet diameter decreases to that of the orifice.

Each of them contributes to the total extrusion force according to Fig. 3.5 by the wall friction force  $F_{fr}$  along the extruder barrel, which linearly decreases with the reduction of the contact surface between material and barrel. Additionally, forming force  $F_{pi}$  is required for the plastic alteration of the material’s geometry and achieving its final shape in the die land.

In the shaping zone, the contraction induces an elongational flow that plastically deforms the cementitious visco-plastic material. Only a few studies have specifically focused on cement-based materials, but there are some numerical and experimental works aiming to describe the flow of visco-plastic materials in this zone; see Basterfield et al. (2005), Jay et al. (2001), Perrot et al. (2012), Rabideau et al. (2010, 2012). For high Bingham number fluids, the velocity increases as the material gets closer to the orifice as the barrel contracts. Just after flowing past the contraction, the material velocity becomes constant (Rabideau et al. 2010).

The model formulation for the forming force  $F_{pi}$  has been the subject of numerous studies. The reference work of Benbow and Bridgwater (1993), based on the computation of the energy needed to reduce the material section by plastic deformation, has been used successfully to describe the flow of cementitious materials (Zhou and Li 2005; Perrot et al. 2012; Zhou et al. 2013; Basterfield et al. 2005). Basterfield et al. (2005) and Perrot et al. (2012) have improved the modelling of the shear rate influence on the extrusion force by assuming a progressive contraction and by adding the contribution of shear on the tapered surface. This approach has been also applied in conjunction with extrusion-based 3D concrete printing; see Chen et al. (2019).

The cement-based material must remain homogeneous during extrusion. This can be studied from a soil mechanics perspective (Toutou et al. 2005). Khelifi et al. (2013; Perrot et al. 2014b) considered a competition between the velocity of the extrusion flow with the velocity of water drainage. Drainage criterion based on the Terzaghi consolidation coefficient has been used to predict if the material will retain its homogeneity (Perrot et al. 2014a; Martin et al. 2006); see Eq. 3.7:

$$\frac{t_{ext}}{H_{dr}^2/C_v} < 0.1 \quad (3.7)$$

With  $t_{ext}$  the extrusion time,  $H_{dr}$  the maximum drainage length and  $C_v$  the consolidation coefficient (function of materials permeability and compressibility). According to Terzaghi,  $H_{dr}/C_v$  is the characteristic consolidation time and therefore Eq. 3.7 means that the time of extrusion must be an order of magnitude shorter than the consolidation time. However, Perrot et al. (2014b) showed that two materials (a cement-based material and a clay-based material) with same  $H_{dr}/C_v$  can exhibit different behaviors during extrusion flow. The authors explained this discrepancy by the different impact of water filtration on the material’s rheological behaviour. Indeed, extrudable cement-based materials, on the contrary to clay-based systems,

present a closely packed granular network very sensitive to water content (Yammine et al. 2008). Eventually, the authors proposed a criterion that takes into account the sensitivity of the rheological behaviour to the liquid drainage:

$$Dc = \frac{1}{\tau_w} \left( \frac{d\tau}{de} \right)_{ini} \frac{t}{H^2/C_v} \quad (3.8)$$

where  $\tau_w$  is the shear stress along at the extruder wall,  $e$  is the material void ratio (liquid volume/solid volume) and  $\tau_{ini}$  is the initial shear stress before any drainage. Therefore,  $\left( \frac{d\tau}{de} \right)_{ini}$  is the variation of the shear stress at the material/extruder interface at the beginning of the flow.

### 3.4.3 Screw Extrusion

Screw extrusion is the most common extrusion technique, in which the material is continuously fed into the extruder barrel wherein an Archimedes screw is used to convey it toward the die (Burbidge and Bridgwater 1995), Fig. 3.6. When using an adequate feeding system, the screw extrusion enables high productivity at both industrial and semi-industrial scale (Händle 2007; Li and Zhou 2015). Screw extruders are also used at the lab scale to test the material extrudability as well as for mix design optimization; see Fig. 3.6 (Khelifi et al. 2015).

The inside surface of the extruder can exhibit a longitudinal groove in order to orient the material flow along the extruder screw and toward the die. A vacuum de-airing system is often added to reduce the entrapped air content and, therefore, increase the material density as well as its strength and durability. A particular model of the screw pumping system, namely, progressive cavity pumps (PCP), has been

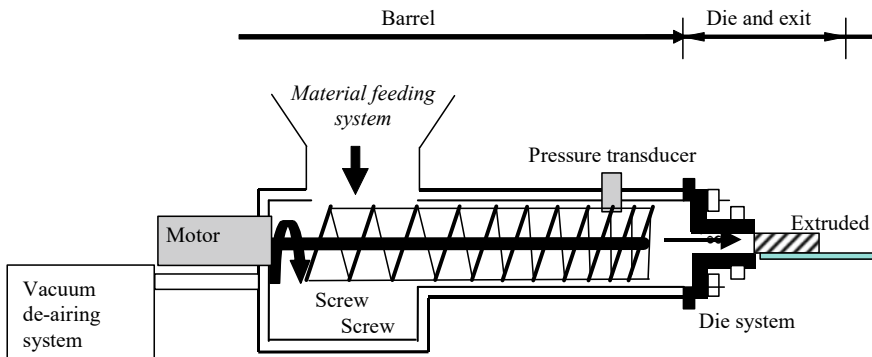


**Fig. 3.6** Schematic of a screw extrusion process

widely used in the context of concrete 3D-printing. Such a system is based on a rotor–stator set, i.e. a steel screw (the rotor) enclosed in a rubber case (the stator). The gap between the rotor and stator serves as the “conveying chambers” that drive the material forward, enabling good control of the flow rate given the positive displacement nature of the pumping system.

The modelling of the flow of visco-plastic materials through a screw extrusion system is difficult due to the complex geometry of the screw. Such flow has only been described in few studies for clay (Martin et al. 2006; Burbidge and Bridgwater 1995; Händle 2007) and cement-based materials (Mu et al. 1999; Perrot 2006). Perrot (2006) showed that the axial force acting on the screw is equal, as in the case of ram extrusion, to the sum of the shaping force and the frictional force acting on the extruder surface.

In the context of 3D printing, Nerella et al. have proposed a strategy in order to link the extrusion flow rate to the stator rotational velocity using a progressive cavity pump in the context of concrete 3D printing (Nerella et al. 2019a). Interestingly, the authors have shown that due to slippage at the elastomeric stator surface, the relationship between flow rate and rotational velocity is strongly non-linear. Also, the fact that the rotor and stator are made of different materials with different stiffness is likely to affect the relationship.

### 3.5 Mixing After Adding Accelerator in the Print-Head/nozzle

Many fabrication techniques involve a so-called acceleration of the material during or after deposition. Most of these techniques rely on the incorporation at the printing nozzle level of either a chemical accelerator able to modify the silicate/aluminate balance and accelerate one of these hydration reactions or an organic flocculant able to bridge the finest particles in the system. Both strategies lead to a faster and enhanced phase-change of the printed material, allowing for higher building rates and higher productivity for the same printed element geometry control. Such strategies moreover allow for the mixing, pumping and feeding of the robot with an extremely fluid material, which will then turn into a pseudo-solid once the accelerator is added.

However, the strategies require the dispersion of an active agent in the printing nozzle and raise several difficulties in terms of nozzle design. From a process point of view, as soon as a dispersion technology is involved as a sub-process, **residence (or retention) time** of the material in the dispersing zone becomes a key parameter. Considering that the nozzle cross-section is often close to the cross-section of the filament (except in the case of a strong contraction at the deposition level), this leads to the conclusion that the average material velocity in the nozzle is of the order of the nozzle velocity itself (typically from 1 to 10 cm/s (Buswell et al. 2018)). As most printing heads overall length is of the order of several tens of centimetres, this means that residence time shall vary between 1 and 100 s.

These accelerators are either mineral molecules of size of the order of less than a nanometer or organic macromolecules of the size of the order of 100 nm (Bessaies-Bey et al. 2016). Although the validity of the Stokes–Einstein fades when the size of the molecules gets closer to the size of the molecules of the solvent, we use it here to estimate the typical diffusion length from the natural diffusion coefficient of these accelerators; see Eq. 3.9.

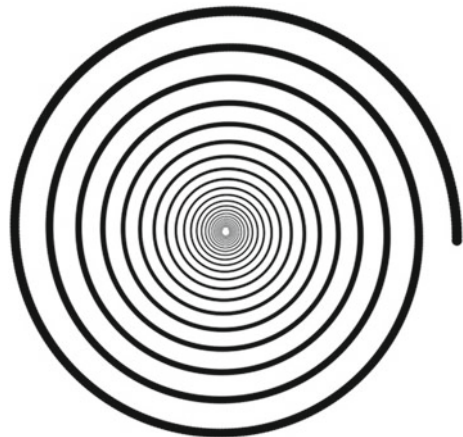
$$D = \frac{kT}{6\pi r\eta} \quad (3.9)$$

where  $k$  is the Boltzmann constant,  $T$  the temperature in Kelvin,  $r$  the size of the accelerator and  $\eta$  is the viscosity of the solvent. The typical diffusion length is of the order of  $\sqrt{Dt}$ , where  $t$  is the residence time. This leads to typical diffusion length between a few micrometres and few hundreds of micrometres. As a consequence, even for the smallest printing nozzles for pastes, full dispersion of accelerators in the nozzle cross-section requires some additional dispersion mechanism and cannot rely on natural diffusion alone. As the viscosity of cement-based materials is too high to allow for turbulent dispersion, it is in the field of convective mixing that solutions do exist.

The idea behind convective mixing is illustrated in Fig. 3.7. It relies on creating a secondary flow in the nozzle that allows for the distribution of the accelerator molecules. By shearing the material and therefore distributing the accelerator in layers, one can reach, after a sufficient residence time, the situation, in which the typical distance between two accelerator layers is of the order of the typical diffusion length estimated above.

From a technological point of view, this translates in nowadays existing technologies into either some so-called static mixers or some screw-mixing devices. The first ones are not moving as indicated by its name, and it is the overall flow of the material

**Fig. 3.7** Flow pattern for the accelerator molecules in a theoretical convective mixing system



around the surface of the static mixer that distributes the accelerator in layers. The second one is simply an additional mixing system with its own controls. Both are inserted into the print-head. The dispersion intensity of the static mixer is proportional to the flow rate in the nozzle while it is an independent tunable parameter in the case of the screw mixer.

The above features have however, never been studied in details for the specific conditions and requirements of cement-based materials printing. Print-heads and their mixing devices are therefore designed through trials and errors. Numerical simulations (Roussel et al. 2007; Roussel and Gram 2014) could in the future allow for a better understanding and the resulting progress in nozzle design.

### 3.6 Load Bearing and Deformation Behaviour After Deposition

A common denominator in digital fabrication processes of cementitious materials is the absence of (traditional) formwork. While this is clearly an advantage from a productivity and sustainability point of view, it introduces the possibility of object collapse during the manufacturing process—something that is practically impossible in conventional concrete casting due to the support provided by the formwork. This issue is not trivial, given the fact that the concrete only starts setting sometime after deposition and its resistance is thus initially low, in the same order of magnitude as the loads acting on the in-print object.

In the context of material extrusion, the resistance of a printable mortar to object collapse during printing is one of the primary concerns and globally indicated as “buildability” (Le et al. 2012; Lim et al. 2012). The majority of studies both in academic research and industrial practice is currently based on this type of DFC. Therefore, the main focus of this section is on extrusion-based additive manufacturing too. Nevertheless, object collapse during manufacturing is relevant for a number of other DFC technologies as well, such as adaptive formwork (Szabó et al. 2018) and material jetting (Kloft et al. 2019). On the other hand, it applies to a much lesser extent to particle-bed binding DFC technologies, as the unaffected powder supports the reacting parts. Thus, where appropriate, additional remarks outside the field of material extrusion, are occasionally made. Finally, it should be noted that this section is particularly concerned with the material and object behaviour *during* the manufacturing stage (i.e. from the start of deposition until the end of deposition), not the phase *after* manufacturing until use or beyond.



### 3.6.1 Acting Loads

Collapse during printing is induced by loads acting on the object. In the simplest assumption, which has been applied on all hitherto published analyses on this issue, this consists of the centred self-weight of a layer, and those stacked on top of it. Consequently, gravity-induced stresses grow as the height of the object increases. For relatively simple geometries and straightforward fabrication processes, the critical layer is the bottom one, as it is the first to be extruded and is therefore loaded by all subsequently deposited material.

However, several load types could also occur during manufacturing, as illustrated in Fig. 3.8. They depend on the process as well as the object design characteristics. For instance, eccentricities may be introduced by imperfections or oscillations in the process that result in a misalignment of subsequent layers. Additionally, considering the geometrical freedom that comes with the adoption of digital fabrication techniques, more extreme eccentricities may be introduced purposefully in cantilevering object designs. In some cases, granular filler materials such as sand are used (either permanently or as temporary support material for cantilevers), which induce additional, non-vertical pressures on the in-print object. Moreover, filaments are often not only confronted by subsequently stacked layers, but also by horizontally approaching

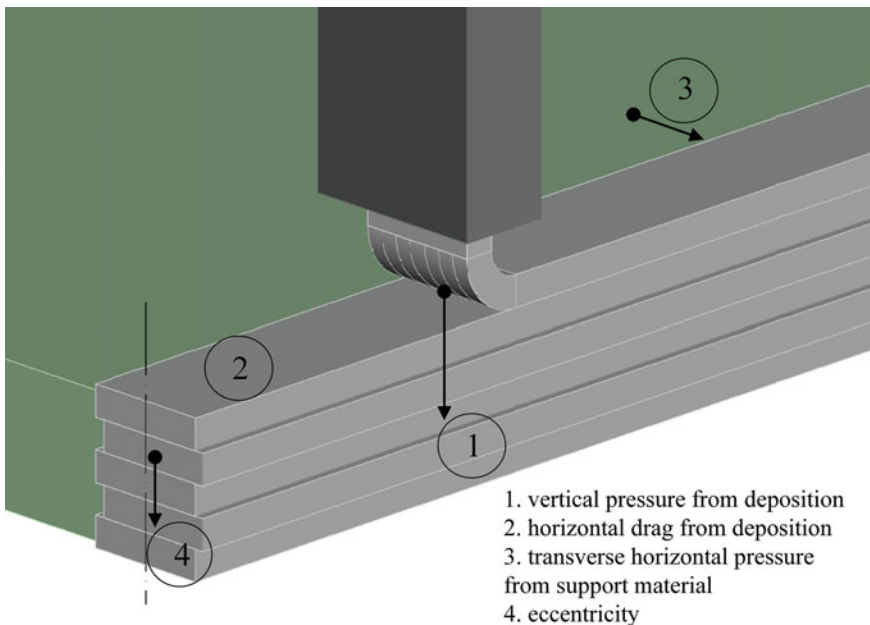


**Fig. 3.8** Besides the vertically acting self-weight of the material, several other loads may be acting on a print object during printing. Reprinted from Bos et al. (2021)

ones that also result in sideway pressures. Friction on the print bed may create support conditions that locally affect the stress field.

Furthermore, it should be noted that a print object may not only be subjected to static loads (as described above), but also to kinetic loads caused by the deposition of material. For extrusion-based technologies, no experimental data is currently available from the literature. However, the first numerical studies indicate that the magnitude of dynamic loading depends on process parameters such as the filament pressure, nozzle speed (including possible stops and restarts), filament dimensions, and layer height offset. Depending on the nozzle geometry and orientation, these loads would not necessarily act perpendicular to the print base. Reinold et al. (2019, 2020) investigated the intermediate stage of the extrusion and deposition processes in extrusion-based 3D concrete printing using a numerical model based on the Particle Finite Element Method (PFEM) and the Bingham constitutive model. Extensive parametric studies using this model enabled to delineate the influence of process and material parameters on the layer geometries, the dynamic surface forces generated under the extrusion nozzle and the inter-layer interactions. Among other insights, it was found that such forces are several times larger than those induced by the self-weight of one layer. Hence, lower layers would need to bear this load temporarily under the extrusion nozzle. Increasing the yield stress or the viscosity will increase the extrusion forces, due to higher forces that are necessary to print these materials. Smaller printing heights and higher printing speeds lead to larger forces (Reinold et al. 2020). Furthermore, the dynamic interactions between the printed layer and the substrate layer were analyzed. For certain combinations of process and material parameters, the lower layer might start yielding under the nozzle due to the additional forces from the extrusion process. As an indicator for measuring the influence of the extrusion process on the substrate layer, the volume of the yielded material was calculated. Relating the substrate yield stress to the volume yielded during the printing process, the minimum age-related yield stress necessary to carry the loads from the extrusion process was determined. The authors concluded that their findings might help in the design of printing materials and processes and possibly when transferred into a real-time steering software, may support adapting process parameters during printing (Reinold et al. 2020).

Kloft et al. reasoned that a shearing of the upper zone in the applied layer may occur in extrusion-based Additive Manufacturing, leading to a local compaction of this zone (Kloft et al. 2019), but an increase of adhesion between the layers due to topological interlocking should not be expected. In the realm of material jetting (or spraying), on the other hand, research is already available based on existing concrete spraying methods. The high velocity at which material is deposited for both dry- and wet-mix spraying, generally results in higher compaction compared to extrusion, as well as an increase in bond roughness and mechanical interlocking between the layers (Kloft et al. 2019). Rebound of aggregate particles will also occur (Armelin and Bantia 1998). Although it is clear that the kinetic loads caused by material jetting are likely to be much more dominant in the overall set of loads on a print object than for material extrusion, it remains largely uncharted territory what this means in quantitative terms for the buildability of objects through this technology.

Thus, the actual loading conditions on an object during manufacturing can result in stress distributions that are considerably more complex than a simple uniaxial compression, linearly decreasing with increasing height. The extent to which this can be relevant will need to be determined in future research. The important part in future research would also be on defining which of these loads plays the most relevant role which respects to the collapse of printed elements. After all, creating models that take into account all possible loads does not seem feasible from a practical point of view.

### 3.6.2 *Structural Failure*

Two fundamentally different mechanisms have been identified to cause collapse in DFC based on material extrusion, and thus to underlie the concept of buildability:

- material failure, i.e. when exceedance of the material strength results in fracture or uncontrolled deformation due to yielding or flow, and
- stability failure, i.e. when the object cannot retain equilibrium of forces.

These mechanisms often interact (extensive deformations due to material failure result in loss of stability, or loss of stability results in material failure due to (local) excessive stresses), but it is generally one or the other that initiates the collapse. Which mechanism is governing depends on a multitude of factors, including material and process characteristics, and, due to the transient nature of the material characteristics, also on the print strategy (e.g. speed) and object design (e.g. size). The prediction of material failure, furthermore, requires the adoption of a material failure criterion, indicating the onset of fracture, yielding, or flow; see Fig. 3.2. In the realm of continuum mechanics, many such criteria have been proposed (Irgens 2008). However, which one is appropriate is not directly obvious for DFC and therefore is the topic of ongoing research. The question is complicated by the fact that similar to the question of which failure mechanism governs, the issue of the appropriate material failure criterion is a function of the aforementioned parameters, and hence not only depends on the chosen material and print facility, but also on the part being manufactured.

It is obvious that in material extrusion-based techniques, the material develops over time from a (non-Newtonian) fluid into a solid from the moment of deposition, i.e. completely or partially during printing. Depending on the type of print mortar/concrete used, the filament either initially has a more or less fluid character—up to a behaviour that could be characterized as no-slump. For the modelling and prediction of material failure, this raises the question whether a material failure criterion should be adopted from fluid mechanics and rheology, based on the assumption of a (highly viscous) fluid, or from solid mechanics, considering the material as a very compliant visco-elastic or elasto-plastic solid. Which approach is taken determines the definition of relevant material properties and the experimental methods that should be applied to obtain them, but also determines the type of analysis that

may be performed. The solid mechanics approach allows recognition of anisotropic multi-axial stress states as well as a joint consideration of material and stability failure, whereas the latter is unusual in fluid mechanics, and only material failure in isotropic stress states is allowed for. On the other hand, this approach is more suitable to determine early flow displacements, see Sects. 3.1 and 3.6.3.

Considering this, it is unsurprising that in the literature, different approaches have been adopted to quantify buildability. Table 3.1 provides an overview and shows that even within a single approach to the material state (fluid or solid), many subsequent issues may still be addressed in different ways, including the material model, experimental procedure, geometrical model, and perhaps most notably, the inclusion of time dependency. The approaches are briefly discussed below. Chapter 4 elaborates on the associated experimental procedures.

The development of a fluid into a solid-state mortar/concrete (structural build-up), usually over the course of several hours (but sometimes minutes when fast-hardening cement or accelerators are used), implies the time dependency of several material properties, such as strength and deformability, that are relevant both to material and stability failure. This is discussed in Sects. 3.7.3 and 3.7.4, but can globally be divided into reversible physical processes (floculation induced thixotropy) and non-reversible chemical processes (hardening due to hydration/chemical reactions). This results in a (non-)linear increase in material strength. In rheology-based approaches, this is generally indicated as the structuration rate of the yield stress,  $A_{thix}$ . The rate of development of material properties is often of an order of magnitude that is relevant during the printing process, and should, thus, be accounted for when predicting failure. Likewise, the time dependency implies that buildability is not just a property of print material, but also of the object itself: a large object with long layer interval times will allow the print material to develop greater strength, enabling a higher build-up of the element before the collapse—though it should be noted that longer interval times may also negatively affect the interface strength, as discussed in Sect. 3.8.2.

A quantitative buildability approach was explored by Di Carlo et al. already in 2013 (Di Carlo et al. 2013). They used Finite Element Modelling (FEM) to recreate the unconfined uni-axial compression tests that were performed on specimens of different ages of fresh print mortar to obtain strength and rigidity properties. Although a Drucker-Prager failure criterion was applied in reference to (Famiglietti and Prevost 1994), the experimental procedure did not allow for the investigation of multi-axial stress states, and thus the approach was not generally applicable. Furthermore, the model did not include transient geometries and material properties, and modelling was hence limited to a (quasi-)static state.

Subsequent quantitative buildability approaches, presented by Perrot et al. (2016), Wangler et al. (2016) alternatively applied the rheological yield stress of the print mortar, which was assumed to behave as a non-Newtonian fluid (e.g. Bingham or Herschley-Buckley fluid), as the material failure criterion in time-dependent analytical models. That models considered the compressive stress in the bottom layer to be solely dependent on object height, which was assumed to increase linearly in

time. Effectively, these approaches are based on visco-plastic equilibrium considerations, as presented in Sect. 3.1. The buildable number of layers  $n_{layer} = \frac{h}{h_{layer}}$  is determined from the ratio  $h = \frac{\sqrt{3}\tau_{0s}}{\rho g}$ , so that  $n_{layer} = \frac{\sqrt{3}\tau_{0s}}{\rho g h_{layer}}$ . Note that  $\sqrt{3}$  corresponds here to geometry parameter  $\alpha_{geom}$  for elongational flow, see also Sect. 3.1. The (shear) yield stress  $\tau_{0s}$  can be obtained relatively easily from rotational rheometry. Both a linear and exponential development of yield stress, both based on  $A_{thix}$ , were proposed—where it should be noted that the exponential function is very close to the linear one over short time intervals, but allows more extended considerations into the time domain when hydration has become dominant (Table 3.2).

In 2018, Wolfs et al. (2018) presented a numerical FEM approach, which included the development of both the geometrical and the material properties as a function of time. Importantly, this method was the first to account for not only for material failure, but also for the prediction of stability induced collapse, which had been noticed to be the dominant failure mode in many print trials. Compared to the rheology-based approaches, the dual failure criteria of Mohr–Coulomb plastic yielding and elastic buckling requires significantly more experimental parameters to be determined, including the (apparent) Young’s modulus  $E(t)$ , Poisson’s ratio  $\nu(t)$ , the cohesion  $C(t)$ , angle of internal friction  $\varphi(t)$ , and dilatancy angle  $\psi(t)$ —all of which are time dependent. They were obtained through shear box tests with different vertical load ratios. These tests, contrary to the experimental campaign applied by Di Carlo et al. (2013), allowed to determine the full material failure envelope and thus enabled the analysis of multi-axial stress states (that could be induced by the various loads discussed in the previous subsection), and, in combination with unconfined uniaxial compression tests, to determine the deformation behaviour at various ages of the material. Note that load rate effects due to viscous behaviour (creep) were not included in the model. Whether creep would be relevant has not yet been established in the literature. Similar to the rheological approach, the authors established linear increases of both material strength and the (apparent) Young’s modulus over time. However, these increases were not correlated to  $A_{thix}$ .

In a subsequent paper (Wolfs et al. 2019), the authors attempted to improve the experimental approach by replacing the combined shear box and unconfined uniaxial compression tests by a single tri-axial compression test. Based on the same assumptions and experimental data, Suiker (2018) subsequently developed a parametric mechanistic model that allows for efficiently analyzing the strength and stability behaviour of wall-type structures printed under a wide range of process parameters.

In recognition of the relevance of stability failures, Roussel (2018) presented a mixed methodology that joined the rheological approach to material failure with the solid mechanics approach to stability. In a model proposed by Kruger et al. (2019), the material assumptions of Perrot et al. Wangler et al. and Roussel, were largely adopted, but for the material structuration in the first seconds after deposition. Rather than to apply a single structuration rate  $A_{thix}$ , they observed that the initial strength development in the first few minutes after deposition occurs much faster, which they attributed to re-flocculation and for which they introduced the parameter  $R_{thix}$ . In their experimental research  $R_{thix}$  appeared to be almost six times as high as  $A_{thix}$ .

**Table 3.2** Approaches to the quantification of “buildability” in literature

Publication	Failure mode(s)	Theory	Material failure criterion	Experimental procedure <sup>a</sup>	Time effect	Geometrical model	Validation
Di Carlo et al. (2013)	Material	Solid mechanics	Drucker-Prager	Unconfined uni-axial compression	Constant	2D in vertical section plan	Unconfined uni-axial compression
Perrot et al. (2016)	Material	Rheology	Yield stress of non-Newtonian fluid	Rotational rheometer	Linear & exponential	Vertical stack, 1D	Unconfined uni-axial compression
Wangler et al. (2016)	Material	Rheology	Yield stress of non-Newtonian fluid	n/a <sup>b</sup>	Linear	Vertical stack, 1D	n/a
Wolfs et al. (2018)	Material, stability	Solid mechanics	Mohr–Coulomb	Shear box + un-confined uni-axial compression	Linear	Vertical stack, 2D in vertical section plan	Cylindrical print trial
Suiker (2018)	Material, stability	Solid mechanics	Mohr–Coulomb	Shear box + un-confined uni-axial compression**	Linear & exponential decaying	Linear wall structures, 2D and 3D	Wall print trials
Roussel (2018)	Material, stability	Mixed	Yield stress of non-Newtonian fluid	Rotational rheometer <sup>b</sup>	linear & exponential	Vertical stack, 1D	n/a
Chaves Figueiredo et al. (2019)	Material	Rheology	Bulk yield stress from Benbow–Bridgewater model	Ram-extruder	Constant	Vertical stack, 1D	Cylindrical print trial
Jeong et al. (2019)	Material	Solid mechanics	Shear stress	n/a <sup>c</sup>	Linear	Vertical stack, 2D along print path length	n/a
Wolfs et al. (2019)	Material, stability	Solid mechanics	Mohr–Coulomb	Tri-axial compression	Linear	Vertical stack, 2D in vertical section plan	Wall print trials

(continued)

**Table 3.2** (continued)

Publication	Failure mode(s)	Theory	Material failure criterion	Experimental procedure <sup>a</sup>	Time effect	Geometrical model	Validation
Kruger et al. (2019)	Material	Rheology	Yield stress of non-Newtonian fluid	Rotational rheometer	Bi-linear	Vertical stack, 1D	Cylindrical print trial

<sup>a</sup>The experimental procedures to determine the properties of fresh mortar are extensively discussed in Chap. 4

<sup>b</sup>Theoretical, based on volume fraction and an average interparticle force

<sup>c</sup>Analytical paper, material failure properties based on data from other study

<sup>d</sup>Analytical paper, no direct relation to experimental work

Hence they based their buildability model on a bi-linear development of material strength over time.

Chaves Figueiredo et al. (2019) also based their buildability model for a study on printable Strain Hardening Cementitious Composite (SHCC) on a rheological material approach, but instead of assuming the material as a Bingham fluid, they applied the Benbow-Bridgwater model that is commonly used to analyze extrusion processes, and allows to distinguish between bulk material and sheared material. The material parameters were derived from ram-extrusion tests. Due to the considerable open time of over 12 h, no time dependency was assumed (properties constant during printing time).

Finally, Jeong et al. (2019) did not elaborate extensively on the appropriate material failure model, but assumed the (solid mechanics) shear strength to govern the failure, and went on to take the filament age along the print path length into account in a buildability model, rather than to assume an identical age throughout one filament layer.

Currently, it is yet unclear which approach provides the most accurate predictions—and which results in a fair balance between accuracy and (experimental and computational) effort. As indicated, this likely varies from one combination of material, process and product to another. Furthermore, it is conceivable that even other approaches will be explored in the future. It is clear, however, that due to their nature, no approach is capable of covering/simulating all types of failure analyses. But beyond that, there is very little experimental data available to compare them, which makes it impossible at this stage to draw solid conclusions on these matters.

### 3.6.3 *Deformation Behaviour*

The deformation behaviour (*before* failure) of cementitious mortar/concrete during material extrusion has received very little attention. Two principally different phenomena should be distinguished. In a number of DFC processes, the mortar/concrete still flows briefly after deposition. The use of viscosity modifying agents (VMAs) and/or accelerators ensures a rapid increase in yield stress which also effectively stops the visco-plastic flow in a matter of seconds. The flow and structuration characteristics along with the process parameters such as filament pressure, diameter, nozzle speed, etc. determine the stabilized filament shape that forms the basis on which the rest of the object is built. Hence these very early deformations are of paramount importance for the further performance of the object both during manufacturing and in later use. Numerical simulations might be very helpful to predict the resulting shapes of the deposited layers, without the need for an a priori time consuming trial-and-error testing, see e.g. Reinold et al. (2019). Furthermore, Reinold et al. (2020) demonstrated that using Particle Finite Element Method, also enables to analyze various “dynamic” scenarios such e.g. as when the printed cross-section is not supposed to be constant, but designed to change during the printing process to allow for a flexible control of the layer geometry. Conversely, the numerical



model can provide guidance on how to maintain a constant layer cross-section despite variations in material properties, by adapting the process parameters accordingly.

Early flow, as described in the previous paragraph, does not occur in extrusion-based processes that use stiff material deposited in an unsheared fashion, which keeps the shape of the nozzle orifice to a great extent. Such materials are in a visco-elastic state directly after deposition, whereas the more fluid mortars enter into this state after the early flow has stabilized. The visco-elastic state can last minutes to hours, depending on the chemical composition of the mortar/concrete. Deformations in this state can incur 2<sup>nd</sup>-order effects that may result in stability failures or affect geometrical conformity of the final product. Also, deformation behaviour affects the interaction between sideways touching layers and the (extent of the) bond that is formed between them.

To estimate the elastic deformations, the (apparent) Young's modulus  $E$  may be determined from unconfined compression experiments directly. It has been suggested that  $E$  could also be determined from the shear modulus  $G$  as they are linked by application of Poisson's ratio  $\nu$  through  $G = E/2(1 + \nu)$ . The shear modulus can be obtained from rheology tests as it is equal to the ratio of the shear yield stress to the critical shear rate  $G = \tau_{0s}/\dot{\gamma}_{0s}$ . However, Poisson's ratio cannot be determined from rheometry, and thus would need to be assumed. For one specific relatively stiff printable mortar, Wolfs et al. (2018), determined a Poisson's ratio of  $\nu = 0.3$  that was found to remain constant in the first 90 min after deposition, but for mortars/concretes in a more fluid state deformations may be assumed to occur without volume change, hence  $\nu = 0.5$  (De Schutter and Taerwe 1996).

No data are known in the literature with regard to load rate dependent (i.e. viscous creep) deformation behaviour in the time frame of manufacturing in material extrusion processes. Data from existing studies on early-age properties (further discussed in Sects. 3.7.3 and 3.7.4) are generally not applicable, as they start recording properties from 2 h after mixing at the earliest, but more often after 6, 12, or 24 h (Pane and Hansen 2008; Nehdi and Soliman 2011), while for DFC manufacturing the time frame between 0 and 2 h is crucial. Often hydration in the mortars/concretes has not yet accelerated (dormant state). Thus, it is likely that the material behaviour during manufacturing is decidedly different from what is commonly referred to as early age properties. Studying this phenomenon is further complicated by the fact that it is difficult to discern in this stage between instantaneous elastic deformations, creep, and shrinkage (which may also occur). Additionally, environmental conditions such as temperature, humidity, and ventilation, may influence creep as well as shrinkage. With regard to plastic and eventually drying shrinkage, similar observations hold true as for creep: no published information is available for the considered time frame, and it is difficult to separate one effect from the other.

As for the failure analysis, different modelling approaches can be adopted for deformation studies too. Again, the fundamental question regarding the assumption of the material state will dominate the subsequent approach and results. When supposing a visco-plastic material, as appropriate for some mortars during and directly after deposition, Computational Fluid Dynamics (CFD) may be used to predict displacements (Comminal et al. 2018). The supposition of a continuous

(visco-)elastic solid would result in the adoption of Finite Element Modelling (FEM) to analyze the deformation behaviour of static, extruded layers. A fully accurate deformation modelling approach covering the entire process may have to rely on a combination of both.

Alternatively, the application of the Discrete Element Method (DEM), which is suitable for granular materials and theoretically capable of modelling both flow and deformations, may also be explored (Hovad et al. 2016). The benefits of using DEM for purposeful configuration of print-head were recently demonstrated by Storch et al. (2020) who analyzed the flow process and forces in a print-head equipped with a progressive cavity pump. The assignment of appropriate model parameters remains however, a challenge. Matters are further complicated by the fact that some printable mortars are so stiff that their fracture strain may be exceeded during printing, e.g. due to non-constant material flow or when printing (sharp) corners, which results in non-continuous deformation behaviour.

All these issues, however, have hardly been touched upon in available research and are expected to be explored in the near future.

## 3.7 Physical Properties and Their Evolving in Time

### 3.7.1 Viscosity

The measure of the internal resistance of a fluid being deformed by shear stresses is called viscosity. In this context, the less viscous a fluid is, the easier it flows.

Due to the flocculation and stiffening of the cement-based materials, the apparent viscosity of the cement-based material increases with time at rest. However, as for the yield stress, this behaviour is reversible in time since the mixing power is sufficient to break down the links between particles.

It is important to note that the viscosity of the cement-based materials can evolve due to process-induced material variation during pumping or extrusion. Such variation can be associated, e.g. with particles migration under shear flow.

### 3.7.2 Yield Stress

The yield stress is the material property that denotes the transition between solid-like and fluid-like behaviour. Consequently, it is the minimum stress that makes the fluid flow like a viscous material. Inter-particle forces between the solids in a suspension result in a yield stress that must be overcome to start the flow, and an applied stress that is lower than the yield stress will result in a deformation like a solid instead of flowing. The existence of a yield stress has been questioned by some authors, e.g. Barnes and Walters (1985), due to the fact that, given accurate measurements at

very low shear rates, no yield stress exists. The historical concept of yield stress was summarized by Barnes (2000), and the argument on the existence of yield stress was concluded by the fact that it is acceptable to describe the material behaviour with a yield stress over a limited shear rate range; however, this is supported by limited data. The problem associated with the yield stress is the difficulty in determining it. Theoretically, at the yield stress, the apparent viscosity of the material changes from a finite value to infinity; therefore, an infinite duration of a test is required (Barnes 1997, 2000). Yield stress fluids show an elastic behaviour prior to reaching the yield stress. Prior to reaching the yield stress, the material behaviour changes to non-linearity from linearity and a residual stress is followed after the peak stress.

Static and dynamic yield stresses can be distinguished. The static yield stress is linked to the microstructural build-up and is defined as the stress required to make the material flowing and the dynamic yield stress can be defined as the yield stress measured in steady-state flow (unstructured cement paste).

### 3.7.3 *Thixotropy Parameter/Rate of Structural Build-Up/Structural Breakdown*

Any digital fabrication process takes advantage of the open time of concrete for placement, and generally requires some degree of structural build-up to ensure adequate strength for subsequent layer deposition.

Fresh cement-based materials undergo flocculation and cement hydration that impact their physical and rheological behaviour. It is this change in mechanical characteristics that allows the fresh material to build-up and be able to support the increasing load that is generated by the successive deposits of the layers of the printed structure. Therefore, it is necessary to consider the kinetics of the structural build-up of the material as they relate to the activity of cement in water (Perrot et al. 2016; Wangler et al. 2016). To illustrate and describe this phenomenon, the changes of the stiffness and the yield stress values are often reported by several researchers (Roussel 2005; Roussel 2006a; Roussel et al. 2012).

The increase of the progression of the yield stress over time is often considered to be linear and allows a structural build-up rate to be defined as  $A_{thix}$  in  $\text{Pa}\cdot\text{s}^{-1}$  (Roussel 2005; Roussel 2006b; Roussel et al. 2012). In this case, Eq. 3.10 is used:

$$\tau_0(t) = \tau_{0,t=0} + A_{thix}t. \quad (3.10)$$

With  $\tau_{0,t=0}$ , the shear yield stress of the material in a destructured state and  $t$  being the duration of the resting period of the material.

The linear modelling of the shear yield stress is generally valid during the first hour of the resting period of the cement-based material in materials unmodified by retarders or accelerators (Subramaniam and Wang 2010). Beyond that, the change accelerates and the kinetics of the structural build-up become exponential (Perrot

et al. 2014a; Lecompte and Perrot 2017). This change in rates can be explained by the beginning of the setting, the increase of the solid volume fraction with the possible interpenetration of the C-S-H crystals created. Perrot et al. (2014b) proposed a relationship for the exponential progression of the shear yield stress, tending towards the linear model for short time periods after material deposition. This model is given by Eq. 3.11:

$$\tau_0(t) = \tau_{0,t=0} + A_{thix} t_c (e^{\frac{t}{t_c}} - 1) \quad (3.11)$$

With  $t_c$  as a characteristic time over which the behaviour can be considered linear.

Equation 3.11 can be used to describe the progression of the shear threshold over longer periods. Other more sophisticated models have recently been reported in the literature (Mettler et al. 2016; Lecompte and Perrot 2017; Wolfs et al. 2018). Some authors have even shown that a Von Mises-type plasticity criterion may ultimately not be well-suited to account for the material failure. Effectively, at a certain stage in the development of the setting, the behaviour of the material displays a pressure-sensitive granular type of behaviour (probably related to the interconnection of the hydrates) and becomes sensitive to pressure. The mechanical behavior thus presents a progressive desymmetrization, with a resistance that is always higher in compression than in tension. The transition to hardened concrete behaviors starts at this time. The critical deformation decreases slightly with the hardening of the material (Mettler et al. 2016; Roussel 2018; Wolfs et al. 2018).

Additionally, the increase in stiffness over time is reflected in an increase in the elastic modulus. The increases in stiffness and strength allow the deposited material to withstand the increasing forces associated with the progressing printing of the structure. Under consideration of the development of material properties over time, it is possible to calculate and predict the optimal manufacturing speeds to guarantee the stability of the structure printed and to ensure the compensation for the elastic deformation.

To sum up: The strength build-up can be generally traced back to two physico-chemical phenomena: (1) thixotropy coming from flocculation processes, and (2) strength gain through irreversible chemical hydration. Thixotropy dominates during the open time, and even though Roussel et al. demonstrated that its roots are actually chemical in nature (Roussel et al. 2012), the maximum strength that can be reached via these processes is rather limited, and generally cannot support more than approximately 1.0 m in build height. Reiter et al. recently examined the phenomena and processing to control early age chemical hydration in detail (Reiter et al. 2018), and Marchon et al. reviewed the potential admixture solutions to control structural build-up for the purposes of digital fabrication with concrete (Marchon et al. 2018). In general, in these and other related works, it is seen that the initial yield stress is required for placement, but so-called buildability requires hydration control, thus possible two-step (or two admixture) solutions to control both initial yield stress and buildability are examined. More details on this topic are provided in Chap. 4.

### ***3.7.4 Visco-Elastic Behavior, Modulus of Elasticity and Creep Coefficient***

For digital fabrication approaches such as those based on material extrusion, the (visco-)elastic material behaviour is crucial with regard to early age load-bearing capacity, deformations and cracking. Therefore, controlling mechanical properties within the time span between placing (i.e., already before setting) and completion of print units (usually several hours) are of greatest interest. At present, very few results on the creep behaviour and modulus of elasticity of mortar/concrete for material extrusion can be found in the literature for that time span. In a recent study, Wolfs et al. (Wolfs et al. 2018) found that for typical 3D printing concrete elastic modulus and compressive strength increased linearly within the first 90 min of hydration. Values of 5 to 20 kPa for compressive strength and 0.08 to 0.20 MPa for the modulus of elasticity were reported for this time period. Similarly, a linear strength increase over time was found in Roussel et al. (2012) for small time scales below 90 min, whereas for longer time scales up to 7 h an exponential increase in strength over several orders of magnitude (from 2 to about 1000 kPa) was reported (Mettler et al. 2016).

Data from existing studies on early-age properties of cementitious mortars with comparable compositions (high binder content, small maximum aggregate size and low water-to-cement ratios, such as high strength concrete or spraying concrete) are generally not applicable to the manufacturing stage (see also Sect. 3.6.3), but can be of use for analyses and recommendations related to object performance during curing and use.

It is well-known that plastic shrinkage, autogeneous shrinkage and temperature changes due to hydration heat are the main sources of early age deformations and cracking of cementitious materials with mix compositions similar to printable mortars (Pane and Hansen 2008).

For both normal and high strength concrete, early age mechanical properties are largely related to the degree of hydration (Pane and Hansen 2008), which is consistent with the theory, that short-term creep deformations are due to redistribution of water in the microstructure (i.e., capillary pores) (Wittmann 1983). Different models describing early-age mechanical properties based on hydration degree were developed and validated, see for example (Gutsch 2000). Neuner et al. (2017) recently adopted models for the time-dependent (early-age) mechanical properties for modern spraying concrete mix compositions, which exhibit a distinctly stronger increase in stiffness and strength within the first 24 h of hydration than traditional spraying concretes. The differences may be attributed to the use of modern cements with higher fineness and/or modified chemical composition (aiming at a maximum early age strength), lower W/B and modern chemical admixtures (superplasticizers and accelerators).

Optimization strategies with regard to the modulus of elasticity or creep coefficient within the first 24 h of hydration can be adopted from literature (Nehdi and

Soliman 2011; Neville 2011; Thomas 2009). As creep deformations occur in the hardened cement paste phase only, with the aggregates acting as restraints, the aggregate volume influences creep directly. Furthermore, since early-age mechanical properties are largely controlled by the degree of hydration, all parameters that lead to an increase in early age hydration kinetics, i.e., lower W/C, higher temperature, higher cement fineness, or the addition of accelerating agents, at the same time affect an increase in stiffness and a decrease in creep coefficient. As creep deformations are significantly influenced by autogenous shrinkage, mix design parameters that refine the pore structure, i.e., the addition of silica fume, very fine fly ash and metakaolin, or low water content in combination with superplasticizers, may have an influence on creep (Nehdi and Soliman 2011). Moreover, the addition of shrinkage reducing admixtures or mineral additions with low reactivity can help mitigating autogenous shrinkage and hence may be favourable mix optimization strategies.

### 3.7.5 *Surface Tension and Friction*

Surface tension of the pore solution is involved in the particle-bed binding with selective cement activation method and it plays a major role in shrinkage of cement-based paste. During drying, water desaturation induced capillary pressure that depends on the surface tension of the pore fluid; see e.g. Ghourchian et al. (2018), Keita et al. (2019).

The surface tension of the pore solution remains in the order of magnitude of the that of water ( $0.075 \text{ N}\cdot\text{m}^{-1}$ ) but can vary with the concentration of ions in solution, with the presence of non-absorbed polymer (on the surface of the cement grains) and with the addition of a surfactant (Feneuil et al. 2017; Qian et al. 2018).

The evolution of friction of the fresh cement-based materials is described by the tribological behaviour of the material. This behaviour depends on both the aggregates content and the rheological behaviour of the fines' suspension. The evolution of the friction of cement-based materials has been studied in the context of the slip-form process (Fosså 2001; Craipeau et al. 2018). Till a critical time, the friction stress evolves in a similar way as the shear yield stress. Then, the increase in friction stress accelerates. The different authors attribute this phenomenon to two physical origins: underpressure caused by hydration and bonding of hydrates to the surface (Craipeau et al. 2018). As a consequence, forces between solid particles increase and the friction stress at the surface rises up.

During digital formative processes such as Smart Dynamic Casting (Lloret et al. 2017), friction occurs at the concrete-formwork interface, which has an impact on the success of the gravity-driven process. The friction was monitored for the purpose of feedback process control via load cells (Schultheiss et al. 2016), and a processing window characterized by monitoring structural build-up through the use of formwork pressure measurements (Lloret et al. 2017). Researchers at ETH Zurich developed a model relating the friction force to a hydrodynamic radius, demonstrating that as the surface area to volume ratio increases, processing windows increasingly narrow (Szabó et al. 2018).

### 3.8 Comments on Physically-Based Optimization Strategies

Independent of the choice of digital fabrication approach, the digitization of the entire process chain results in the following general, central requirement for the cement-based material used: In every process step, it should have precisely those properties that are predetermined by the digital execution data sets. As soon as the material properties do not correspond to the required features for each characteristic process step, the fabrication task cannot be completed properly. Such sensitivity results in a level of requirements with regard to quality and process monitoring that was previously unknown in concrete construction. The main challenge in this context is the fact that optimum properties are often very different for different process steps of the same fabrication technic. Thus, when trying to bring all the individual requirements along the process chain together, they often clearly contradict each other. An overall optimization is therefore difficult, which makes the understanding of underlying physics even more important. The following subsection provides two examples to illustrate this thought.

#### 3.8.1 *Example 1: Duality of (Balance Between) Easy Delivery to the Printhead and Shape Stability upon Deposition*

The delivery of concrete (e.g. pumping) requires low plastic viscosity and moderate dynamic yield stress. Upon deposition, high-and-growing static yield stress and viscosity are required. The optimum solution is to induce the phase change of the concrete shortly before the extrusion, closest to the nozzle outlet. This can be achieved by (a) pre-mixing an admixture that activates after a pre-defined delay time, (b) mixing a chemical admixture in the printhead and (c) by external activation of pre-mixed passive admixture (De Schutter and Lesage 2018). In case of low vertical construction rates, the required properties can be achieved by (d) adding plasticizer for maintaining open time and relying on high thixotropy for shape stability (Nerella 2019). If the pumping circuit is short and provided high capacity pump, (e) concretes with initial (before pumping) static yield stress high-enough to satisfy the shape stability requirements can be used (Wolfs et al. 2018).

Since the above solutions have individual limitations, the optimum strategy shall be chosen considering the target material properties (e.g. bond strength), vertical printing rate and process parameters (e.g. pumping circuit). The solutions “a”, “d” and “e” are time-bound and process interruptions can cause severe consequences due to uncontrolled growth of rheological properties at rest. For “b”, a second-stage mixer in the printhead is mandatory, which raises printhead weight, influences printing accuracy and limits the material flow rate. The solution “c” is still in early development and might not be suitable for large-scale DFC yet. Thixotropy of printable concretes is generally increased by the addition of supplementary cementitious

materials and (nano) clays. Chemical acceleration is achieved by the addition of set-and/or-hydration accelerators or combinations of retarders (e.g. sucrose) and activators e.g.  $\text{Ca}(\text{OH})_2$ . Theoretical background and details of rheological requirements, chemical admixtures and external activation are presented in Reiter et al. (2018; De Schutter and Lesage 2018; Marchon et al. 2018).

### 3.8.2 Example 2: Setting Material Deposition Intervals Depending on the Rate of Structural Build-Up

Following delivery to the printhead, it is essential that material has the proper rheology upon placement, which can be either self-supporting and stiff (for extrusion-based processes) or fluid and self-leveling (for slipforming or digital casting processes). Irrespective of the process, it is essential that material be strong enough to support its own weight and the weight of subsequent layers, whether that comes in the form of additional extruded layers (extrusion), or the removal of the temporary support (slipforming), or reaching the strength of a support (digital casting). This strength can come either in the form of a high initial yield stress, an increase in yield stress through thixotropy and flocculation processes, or an increase in yield stress through the formation of early hydration products. We consider in the following only the case of material extrusion.

A single extruded layer will have a static yield stress  $\tau_{0s}$ , which defines the maximum height  $h$  of a single layer according to Eq. 3.12:

$$\tau_{0s} = \frac{\rho g h}{\sqrt{3}} \quad (3.12)$$

If a process has a constant layer height and time interval between layers, then the minimum required time interval between successive layers writes as Eq. 3.13:

$$\Delta t = \frac{\rho g \Delta h}{\sqrt{3} A_{thix}} \quad (3.13)$$

where  $A_{thix}$  is the linear increase of yield stress with time (Roussel and Cussigh (2008)).

Typical values of  $\rho = 2300 \text{ kg/m}^3$ ,  $\Delta h = 0.01 \text{ m}$ , and  $A_{thix} = 0.5 \text{ Pa/s}$  for non-accelerated materials return a time interval between layers of approximately one minute. If one considers that the time between layers can be considered as the print path length  $L_{print}$  divided by the printhead velocity  $V_{print}$ , then one can control the layer time interval by modifying either of these two parameters. One should consider, however, that a maximum time between layers where a weak layer interface or “cold joint” can be formed can also be defined, but is not considered in this example—for this the reader is referred to Chap. 5.



The reader should note that this example does not take into account the initial yield stress, which can provide a “buffer” for an increased building rate until the building rate catches up to a slower structural build-up rate. Generally, processes operate with shorter time intervals between layers than this example demonstrates, and this is due to the usually quite high initial yield stresses.

### 3.9 Further Relevant Processes and Mechanisms

#### 3.9.1 *Weak Bond Strength Between Successive Layers in Extrusion-Based Additive Manufacturing: The Importance of Drying*

The layer interface strength is often considered to result from a proper mixing or remixing of two consecutive layers induced by the deposition process itself and therefore from the material thixotropic behaviour (Roussel and Cussigh 2008). Nerella et al. (2019b) investigated two 3D-printable cement-based compositions, namely C1 with Portland cement as a sole binder and C2 containing pozzolanic additives at testing ages of 1 day and 28 days and critically analyzed the influences of binder composition and the time interval between layers on layer-interface strength. The investigations revealed that Mixture C2 exhibited lower degrees of anisotropy and heterogeneity as well as superior mechanical performance in comparison to Mixture 1. In particular, Mixture C2 showed a less pronounced (below 25%) decrease in interface bond strength as observed in flexural tests for all time intervals under investigation. In contrast, the decrease in flexural strength measured for C1 specimens amounted to over 90% due to the higher porosity at the interfaces of the printed concrete layers.

Furthermore, Keita et al. (2019) recently demonstrated that, in the case of smooth interfaces, the drop in interface strength may find its origin in the water evaporation from the free surface occurring during the short time interval between two successive layers. It was suggested that the water loss is localized in a dry region at the free surface leading to incomplete cement hydration and high local porosity.

The results presented in Keita et al. (2019) showed that, when the first layer is protected from drying, interface strength remains constant with increasing resting time between layers up to 2 h; see Fig. 3.9. On the contrary, relative bond strength decreases for resting times as short as 10 min when the first layer is submitted to drying. Relative interface strength decreases then continuously during the first hour of rest and reaches a plateau afterwards at half its initial value.

Additionally, Keita et al. (2016) suggested that in material with low permeability, since the evaporative flux is higher than the maximal capillary flow, the porous material becomes unable to provide water to the free surface. A dry front is then expected to penetrate the material and water loss shall be localized close to the drying interface. Such a dry front was assessed using SEM experiments on hardened

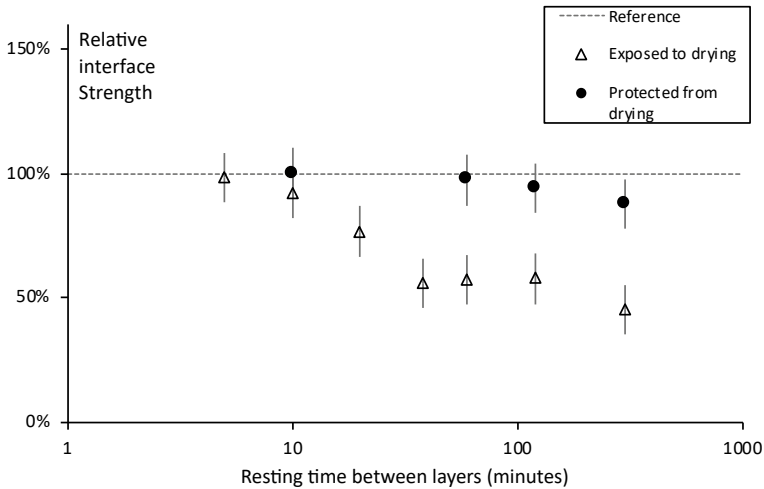


**Fig. 3.9** Relative interface strength as a function of resting time for sealed first layer and a first layer exposed to drying in the wind tunnel. The dashed line is the reference without any rest time between layers. W/C ratio is 0.2; see Keita et al. (2019) for more details

samples (Keita et al. 2019). Although this zone has a thickness of the order of a couple of hundred micrometers, the authors suggested that it is sufficient to induce a mechanical weakness of the layers' interface.

### 3.9.2 Powder Bed: Application of Dry Particle Layers in Particle-Bed Binding

For the direct production of concrete elements by particle-bed binding, two different techniques can be used: (a) selective cement activation and (b) selective paste intrusion (Lowke et al. 2018). The printing process of these techniques consists of two repetitive work steps: (1) application of a layer of dry particles and (2) selective deposition of a fluid phase onto the particle packing by means of a printhead or nozzle in order to bind the particles.

In the selective cement activation technique, the particle bed consists of a dry mixture of very fine aggregate (typically sand  $< 1$  mm) and cement. The cement is locally activated by spraying or jetting water or a water-admixture solution into the packed particles, thus forming a cement paste matrix around the aggregate particles. In order to achieve a high strength cementitious matrix, the particle bed must ensure high permeability for a homogenous distribution of the fluid over the height of the layer on the one hand (compare Sect. 3.4), and a high packing density to minimize the pore volume on the other hand. The application of the particle layers is commonly realized by dispensers or vibrating feeders, respectively. Afterwards, the particle bed

may be compacted by roller compaction (Budding and Vaneker 2013). The strength of the cementitious matrix increases with increasing packing density of the particle bed (Beitz et al. 2019). Alternatively, the packing density of the particle mixture can be increased by an optimization of the particle size distribution (De Larrard 1999).

In the cement paste intrusion technique, the particle bed consists of aggregate particles (typically with an average diameter  $\leq 5$  mm) without binder. The binder paste consists of cement, water and admixtures and is applied to the particle bed by means of nozzles. The cement paste must fill the voids between the particles to produce components with sufficient strength, compare (Pierre et al. 2018; Weger et al. 2018; Lowke et al. 2018). Therefore, for a homogenous and complete distribution of the cement paste, the voids between the particles must be large enough (typically  $\geq 1.0$  mm) to overcome the capillary forces and to ensure gravitational flow (compare Sects. 3.4 and 3.3). Thus, mostly monodisperse particles are used to create maximum void content. Caused by the good pourability of the aggregate particles and the direct contact points of the grains, further compaction of the layers is not necessary. The cement paste distribution has to be controlled by optimized rheology depending on the void structure of the aggregate layer.

### 3.9.3 *Pneumatic Transport of Dry Mix*

In construction pneumatic conveying of dry materials is utilized e.g. for delivering dry mortar or concrete to the nozzle in the dry spraying process (dilute phase conveying, see Sect. 3.9.4), but also for conveying sand or cement, e.g. at the production plant (dense phase conveying). In dilute-phase conveying, particles are fully suspended in the conveying air and transported at low pressure and high velocity (Novelli and Weyandt 2018). This system is typically used for conveying materials over short distances at low capacities. For proper pneumatic conveying of dry-mix mortar or concrete different material characteristics (maximum grain size, cohesion, fibre content, etc.) and process parameters (air pressure, feeding velocity, distance, etc.) have to be defined; for more details see e.g. Mills (2004; Klinzing et al. 2010; Novelli and Weyandt 2018).

### 3.9.4 *Wet and Dry Spraying*

Recently, concrete spraying has been established as an alternative 3D printing technique referred to as material jetting, see e.g. Kloft et al. (2019; Krauss et al. 2018). As rebound and dust formation is higher and quality control more difficult in case of the dry process, at present wet spraying is favoured for 3D printing (Kloft et al. 2019). In the wet process, the mixed material is fed into a pump and conveyed under pressure to the nozzle, where compressed air is injected to spray the material into

place (Austin et al. 2005). Accelerating admixtures can be added at the nozzle to specifically control setting and hardening of the placed material.

With regard to the proper material application process, “sprayability” of the material must be given in addition to “pumpability”, cf. Section 3.4.1. Sprayability can be defined as (1) the ability of the material to adhere to and build-up on vertical or overhead surfaces (adhesion), (2) the degree to which the material sticks to itself (cohesion) and (3) the rebound rate (Yun et al. 2015). Note, that optimizing sprayability and pumpability is somewhat contradicting because opposite material properties are required. Information on the influence of concrete constituents and processing parameters on “sprayability” and other concrete properties is given in Kusterle et al. (2014; Thomas 2009; Warner 1995; Wang et al. 2015).

### ***3.9.5 Mould Filling (3D-Printed Mould, Integrated Formwork, Etc.)***

While much attention has been focused on the printing of cement-based materials (generally via extrusion), due to the requirement of adding reinforcement, many technologies are rendered to that of printing concrete formworks, into which a structural concrete is placed with or without standard steel reinforcement. An early example of this includes the Contour Crafting process (Hwang and Khoshnevis 2004) as well as on the larger scale more recently by the company WinSun (Asprone et al. 2018). Even more recently, the French startup XTreeE 3d printed a truss-shaped hollow pillar as a hollow formwork which was subsequently infilled with UHPC (Gaudillière et al. 2018, 2019). 3D printed moulds need not be printed out of concrete as well, as demonstrated by recent examples of formworks printed from polymers such as PLA, PP or PET-G (Jipa et al. 2019; Burger et al. 2020), or polymer foams in the Batiprint process developed in Nantes (Furet et al. 2019).

The material challenges in filling a formwork, standard or not, have to do with (1) ensuring that the formwork is completely filled (no voids), (2) the concrete remains stable during and after the process (no segregation) and (3) the formwork does not burst or deform considerably under pressure induced by the concrete. Meeting these challenges has been the topic of considerable research for both conventionally vibrated concrete (Gardner and Ho 1979) and self-compacting concretes (Assaad and Khayat 2004); however, digitally fabricated (nonstandard) formworks offer unique challenges, as they often have very narrow geometries the concrete must infill, unconventional geometries such as cantilevering parts, and they generally lack the support structure and strong materials conventional formworks have used to resist formwork pressure. This has often led to alterations of the process; for example, in the above cited example of XTreeE, the pillar was printed in 4 parts, and a temporary (printed) support structure remained in place during UHPC casting, all to resist the expected formwork pressure. The Batiprint process fills the formwork in stages, allowing hydration to occur in layers to build strength. A PLA formwork concrete

canoe required counterpressure from simultaneously filled sand (Jipa et al. 2019), and the Eggshell process (Burger et al. 2020) uses a set on-demand process to build strength to resist formwork pressure. While formwork pressure evolution has been well investigated (Billberg et al. 2014), further investigation could be quite useful in terms of developing methods of casting in which formwork pressure can be well controlled to fill these newer, unconventional formworks.

### 3.9.6 *Filling of Mesh Mold*

The Mesh Mold process is a type of formwork printing, in which a robotic toolhead bends, cuts, and welds steel reinforcement bar into a shape that serves both as formwork, and as reinforcement after the concrete has been applied. The robotic toolhead is mounted either on a stationary robotic arm, or a mobile robot (Hack et al. 2017). The filling of this formwork requires one of two solutions: (1) filling with a high yield stress concrete that can be pumped or applied manually from the sides, or (2) utilizing jamming from granular interactions to hold the concrete in place, similar in physics to a previously analyzed filtration problem (Roussel et al. 2007; Gebhard et al. 2018). Both options also require the application of a cover layer, either applied manually or sprayed. The second option requires utilization of concrete that is highly flowable to fill the formwork with minimal vibration, but also with aggregate with dimensions on the order of the mesh spacing ( $\sim 1\text{--}2$  cm), creating a competition between aggregate stability and concrete flowability (Heller et al. 2018). Roussel (2006a) wrote that the stability of a particle of critical size  $d_c$  in a fluid is directly proportional to the yield stress of the fluid  $\tau_0$ , and inversely proportional to the difference in density between the particle and the fluid,  $\Delta\rho$ :

$$d_c \propto \frac{\tau_0}{\Delta\rho} \quad (3.14)$$

Generally, in very fluid concretes, the maximum particle size is limited, or the yield stress of the suspending fluid is adjusted to achieve stability. In this case, the maximum particle size was specified by the mesh, and the yield stress is required to be very low, thus researchers at ETH Zurich acted on the densities. They used density matched coarse aggregates (porous recycled brick aggregate), lightweight fine aggregates, and long stiff polymer fibres to fill. The aggregates added stability by matching densities between coarse aggregate and mortar, and the fibres acted to reduce the effective mesh spacing and enhance jamming. In a large scale demonstrator, researchers were forced to use option 1, as issues with fibre nest formation on mesh cross-ties could not be resolved.

### 3.10 Summary and Conclusions

Digital fabrication with cement-based materials (DFC) offers great potential to facilitate development towards sustainable Construction Industry 4.0, tackling existing problems such as low productivity and shortage of skilled labour in the process. To purposefully design and optimize digital fabrication systems, as well as to establish an efficient and robust process control, profound understanding of the processes' physics is required. This in mind, the authors performed a critical review of the physics behind the processing of cement-based materials during various production steps of digital fabrication. The provided explanations and statements are the result of collective research performed by them in the framework of the RILEM Technical Committee 276 "Digital fabrication with cement-based materials".

In summarizing the knowledge as presented, it can be concluded that underlying physics are already well understood for most relevant processes, especially for those in context of additive manufacturing by material extrusion, the most widespread DFC approach. This understanding can and should be utilized for a purposeful design of DFC systems rather than trying to shape the DFC processes following trial-and-error approach. The purposeful, systematic approaches based on the associated physics should facilitate the material design and mechanical engineering design as well as optimizing process regimes and process control.

For some processes, analytical scientifically-based formulas already offer reasonable predictions with respect to the material flow in the case of relatively simple geometries. Nevertheless, further research is needed in order to enable the development of reliable tools for quantitative process analysis and for predictions based on the underlying physics. The major challenges in analyzing DFC systems arise out of the complexity of flow regimes and patterns in various production steps as well as the time- and shear-history-dependent behaviour of cement-based materials, which are inherently complex multiscale, multiphase, densely-packed suspensions. Great effort needs to be invested in studying and describing specific flow behaviour and developing adequate testing technics to quantify key material parameters. Numerical simulation can contribute greatly to analyze flow processes under consideration of complex geometrical boundaries, and it has potential to be developed into a powerful design tool for shaping the DFC processes. The derivation of model parameters is the main issue here. Hence, appropriate experiments are required. This deliberation holds true as well for the estimation of material behaviour after deposition, including stability of print elements. For example, to estimate the buildability in context of the extrusion-based 3D concrete printing, material behaviour, the geometry of the printed element, particularities of printing process, and other aspects need to be considered collectively. While analytical formulas may deliver reasonable predictions for relatively simple cases, numerical simulation constitutes a promising approach for analysis of more complex cases.

## Appendix 1: Glossary of Basic Rheology

**Rheology** is the science of the deformation and flow of matter.

**Rheometric** refers to the measurement of rheological properties.

**Stress** represents the force per unit area.

**Shear** is the relative movement of parallel adjacent layers.

**Shear rate** ( $\dot{\gamma}$ ) or rate of shear strain, is the rate of change of shear strain with time.

**Shear stress** ( $\tau$ ) is the component of stress that causes successive parallel layers of a material to move relative to each other.

**Shear strain** ( $\gamma$ ) is the relative in-plane displacement of two parallel layers in a material body divided by the distance between them.

**Normal stress** ( $\sigma_n$ ) is the component of stress that acts in a direction normal to the plane of shear.

**Peclet number (Pe)** is a dimensional group used to compare the effect of applied shear with the effect of Brownian motion. For  $Pe \ll 1$ , the motion of particle is dominated by diffusional relaxation, but for  $Pe \gg 1$ , hydrodynamic effect is dominant.

**Poiseuille flow** represents the laminar flow in a pipe of circular cross section under a constant pressure gradient.

**Reynolds number** is a dimensional group that expresses the ratio of the inertial forces to the viscous forces.

**Newtonian** corresponds to a behavior where differential viscosity and coefficient of viscosity are constant with shear rate.

**Non-Newtonian** is any laminar flow characterized by a non-linear relationship between shear stress and shear rate.

Bingham plastic material obeys to the linear model between shear stress and shear rate (model). Above the apparent yield stress, the coefficient of viscosity decreases continuously.

**Shear thickening** is characterized by an increase in viscosity with increasing shear rate during steady shear flow. The term dilatant commonly used to indicate this behavior is incorrect.

**Shear thinning** is characterized by a decrease in viscosity with increasing shear rate during steady shear flow.

**Yield stress** is a critical shear stress value below which an ideal plastic or viscoelastic material will not flow (i.e. like a solid).

**Structural build-up rate** ( $A_{thix}$ ) rate of increase of yield stress over time at rest.

**Bingham number  $Bi$**  is a non-dimensional parameter defined as the ratio of yield stress to the viscous part of the stress (viscosity  $\times$  strain rate).

**Thixotropy** time-dependent shear thinning property linked to the state of microstructure that can be broken when the material is sheared.

## Appendix 2: List of Symbols and Abbreviations

$A_{thix}$	Structuration rate [Pa/s]	$h_{layer}$	Height of printed layer [m]
$Bo$	Bond number [-]	$h_{paste}$	Initial height of cement paste [m]
$C$	Cohesion [Pa]	$h_{sand}$	Height of sand particle [m]
$C_t$	Consolidation coefficient [m <sup>2</sup> /s]	$k$	Boltzmann constant [J/K]
$D$	Diffusion length [m]	$n$	Flow behavior index for Herschel-Bulkley [-]
$D$	Barrel diameter [m]	$n_{layer}$	Buildable number of layers [-]
$D_p$	Particle diameter [m]	$n_{sand}$	Sand porosity [-]
$D_{pore}$	Pore diameter [m]	$r$	Size of accelerator [m]
$D_{vib}$	Vibrator diameter [m]	$t$	Residence time [s]
$E$	Young modulus [Pa]	$t_c$	Characteristic time for linear region [s]
$F$	Extrusion force [N]	$t_{ext}$	Extrusion time [s]
$F_{fr}$	Wall friction force [N]	$\alpha_{geom}$	Geometrical factor [-]
$F_{pl}$	Plastic alteration forming force [N]	$\Gamma$	Shear strain or angle of deformation [-]
$G$	Shear modulus [Pa]	$\gamma_0$	Critical shear strain [-]
$H_{dr}$	Max. drainage length [m]	$\gamma_{0s}$	Shear strain at flow onset or static shear strain [-]
$K$	Flow consistency index for Herschel-Bulkley [Pa·s <sup>n</sup> ]	$\gamma_l$	Surface tension contact angle [-]
$L$	Length of pipeline [m]	$\dot{\gamma}$	Shear rate [1/s]
$L_B$	Length of billet [m]	$\epsilon$	Strain [-]
$L_{dz}$	Length of dead zone [m]	$\eta$	(Apparent) viscosity [Pa·s]
$L_{print}$	Length of print path [m]	$\theta$	Angle between horizontal and inclined planes [°]
$P$	Pumping pressure [Pa]	$\mu_i$	Interface viscosity [Pa·s/m]
$\Delta P$	Pressure drop per unit length [Pa/m]	$\mu_{pl}$	Plastic viscosity [Pa·s]
$R$	Radius of pipe [m]	$\nu$	Poisson's ratio [-]
$R_{thix}$	Re-flocculation rate [Pa/s]	$\rho$	Density [kg/m <sup>3</sup> ]
$Q$	Pumping flowrate [m <sup>3</sup> /s]	$\Sigma$	Axial stress [Pa]

(continued)



(continued)

$T$	Temperature [°C or K]	$\sigma_{cap}$	Capillary pressure [Pa]
$V$	Liquid velocity [m/s]	$T$	Shear stress [Pa]
$V_{print}$	Printhead velocity [m/s]	$\tau_{0d}$	Dynamic yield stress [Pa]
$A$	Vibration amplitude [m]	$\tau_{oi}$	Interface yield stress [Pa]
$d$	Die diameter [m]	$\tau_{0s}$	Static yield stress [Pa]
$d_c$	Particle critical size in mesh mold [m]	$\tau_{ini}$	Initial shear stress before any drainage [Pa]
$f$	Vibration frequency [1/s]	$\tau_w$	Shear stress along extruder wall or interfacial shear stress [Pa]
$g$	Gravitational acceleration [m/s <sup>2</sup> ]	$\varphi$	Angle of internal friction [-]
$h$	Total height [m]	$\psi$	Dilatancy angle [-]

## References

ACPA. (2008). *CONCRETE 101\_A guide to understanding the qualities of con-crete and how they affect pumping*. s.l.:s.n.

Alfani, R., and Guerrini, G. L. (2005). Rheological test methods for the characterization of extrudable cement-based materials—a review. *Materials and Structures*, 38(2), 239–247.

Armelin, H. S., and Banthia, N. (1998). Development of a general model of aggregate rebound for dry-mix shotcrete – Part II. *Materials and Structures*, 31(4), 195–202.

Asprone, D. et al. (2018). Rethinking reinforcement for digital fabrication with concrete. *Cement and Concrete Research*, 112, 111–121.

Assaad, J., and Khayat, K. H. (2004). Variations of Lateral and Pore Water Pressure of Self-Consolidating Concrete at Early Age. *ACI Materials Journal*, July, 101(4), 310–317.

Austin, S. A., Goodier, C. I., and Robins, P. J., 2005. Low-volume wet-process sprayed concrete: pumping and spraying. *Materials and Structures*, 38(3), 229–237.

Banfill, P., Teixeira, M., and Craik, R. (2011). Rheology and vibration of fresh concrete: predicting the radius of action of poker vibrators from wave propagation. *Cement and Concrete Research*, 41(9), 932–941.

Barnes, H. A. (1997). Thixotropy—a review. *Journal of Non-Newtonian Fluid Mechanics*, 70, 1–33.

Barnes, H. A. (2000). *A handbook of elementary rheology*. Aberystwyth, England: University of Wales, Institute of Non-Newtonian Fluid Mechanics.

Barnes, H. A., and Walters, K. (1985). The yield stress myth? *Rheologica Acta*, 24, 323–326.

Basterfield, R., Lawrence, C., and Adams, M. (2005). On the interpretation of orifice extrusion data for viscoplastic materials. *Chemical Engineering Science*, 60(10), 2599–2607.

Beitz, S. et al. (2019). Influence of Powder Deposition on Powder Bed and Specimen Properties. *Materials*, 12(2), 297.

Benbow, J., and Bridgwater, J. (1993). *Paste Flow and Extrusion*. s.l.:s.n.

Bessaies-Bey, H. et al. (2016). Organic admixtures and cement particles: Competitive adsorption and its mac-roscopic rheological consequences. *Cement and Concrete Research*, 80, 1–9.

Billberg, P. et al. (2014). Field validation of models for predicting lateral form pressure exerted by SCC. *Cement and Concrete Composites*, 54, 70–79.

- Bos, F., Kruger, P., Lucas, S., and van Zijl, G. (2021). Juxtaposing fresh material characterisation methods for printability assessment of 3D printable cementitious mortars. *Submitted to Cement and Concrete Composites*
- Boyce, C. M., Ozel, A., and Sundaresan, S. (2016). Intrusion of a Liquid Droplet into a Powder under Gravity. *Langmuir*, 32, 8631–8640.
- Budding, A., and Vaneker, T. (2013). New Strategies for Powder Compaction in Powder-based Rapid Prototyping Techniques. *Procedia CIRP*, 6, 527–532.
- Burbidge, A., and Bridgwater, J. (1995). The single screw extrusion of pastes. *Chemical Engineering Science*, 50(16), 2531–2543.
- Burger, J. et al. (2020). Eggshell: Ultra-Thin Three-Dimensional Printed Formwork for Concrete Structures. *3D Printing and Additive Manufacturing*, 7, 48–59.
- Buswell, R., Leal de Silva, W., Jones, S., and Dirrenberger, J. (2018). 3D printing using concrete extrusion: A roadmap for research. *Cement and Concrete Research*, 112, 37–49.
- Buswell, R. et al. (2020). The RILEM process classification framework for defining and describing Digital Fabrication with Concrete. *Cement and Concrete Research*, Volume (submitted for the Special Issue).
- Buswell, R., Soar, R., Gibb, A., and Thorpe, A. (2007). Freeform Construction: Mega-scale Rapid Manufacturing for construction. *Automation in Construction*, 16(2), 224–231.
- Chapdelaine, F. (2007). Fundamental and practical study on the pumping of concrete (Ph.D. Dissertation). Université Laval, Quebec: s.n.
- Chaves Figueiredo, S., Çopuroğlu, O., and Schlangen, E. (2019). Effect of viscosity modifier admixture on Portland cement paste hydration and microstructure. *Construction and Building Materials*, 212, 818–840.
- Chaves Figueiredo, S. et al. (2019). An approach to develop printable strain hardening cementitious composites. *Mater. Des.*, 169, 107651.
- Chen, Y. et al. (2019). The Effect of Viscosity-Modifying Admixture on the Extrudability of Limestone and Calcined Clay-Based Cementitious Material for Extrusion-Based 3D Concrete Printing. *Materials*, 12(9), 1374.
- Chevalier, T., and Talon, L. (2015). Generalization of Darcy's law for Bingham fluids in porous media: From flow-field statistics to the flow-rate regimes. *Physical Reviews E*, 91, 023011.
- Choi, M., Kim, Y., and Kwon, S. (2013). Prediction on pipe flow of pumped concrete based on shear-induced particle migration. *Cement and Concrete Research*, 52, 216–224.
- Choi, M. S., Young, J. K., and Jin, K. K. (2014). Prediction of Concrete Pumping Using Various Rheological Models. *International Journal of Concrete Structures and Materials*, 8(4), 269–278.
- Comminal, R., Serdeczny, M. P., Pedersen, D. B., and Spangenberg, J. (2018). Numerical Modeling of the Strand Deposition Flow in Extrusion-based Additive Manufacturing. *Additive Manufacturing*, 20, 68–76.
- Coussot, P., and Boyer, S. (1995). Determination of yield stress fluid behaviour from inclined plane test. *Rheologica Acta*, 34(6), 534–543.
- Craipeau, T., Lecompte, T., Toussaint, F., and Perrot, A. (2018). Evolution of Concrete/Formwork Interface in Slipforming Process. Zurich, Switzerland, s.n.
- De Larrard, F. (1999). *Concrete Mixture Proportioning, A Scientific Approach*. London: E&FN Spon.
- De Schutter, G., and Feys, D. (2016). Pumping of Fresh Concrete: Insights and Challenges. *RILEM Technical Letters*, 1, 76.
- De Schutter, G., and Lesage, K. (2018). Active control of properties of concrete: a (p)review. *Materials and Structures*, 51, 123.
- De Schutter, G. et al. (2018). Vision of 3D printing with concrete—Technical, economic and environmental potentials. *Cement and Concrete Research*, 112, 25–36.
- De Schutter, G., and Taerwe, L. (1996). Degree of hydration-based description of mechanical properties of early-age concrete. *Materials and Structures*, 29(6), 335–344.

- Di Carlo, T., Khoshnevis, B., and Carlson, A. (2013). Experimental and numerical techniques to characterize structural properties of fresh concrete. Proceedings of the ASME 2013 International Mechanical Engineering Congress & Exposition.
- Famiglietti, C. M., and Prevost, J. H. (1994). Solution Of The Slump Test Using A Fi-nite Deformation Elasto-Plastic Drucker-Prager Model. *International Journal For Numerical Methods In Engineering*, 37, 3869–3903.
- Feneuil, B., Pitois, O., and Roussel, N. (2017). Effect of surfactants on the yield stress of cement paste. *Cement and Concrete Research*, 100, 32–39.
- Feys, D. (2009). Interactions between Rheological Properties and Pumping of Self-Compacting Concrete. Ghent University, Belgium: s.n.
- Forsblad, L. (1965). Investigations of internal vibration of concrete. *Acta Pol Scan Civ Eng Bldg Constr/Swed/*.
- Fosså, K. T. (2001). Slipforming of Vertical Concrete Structures. Friction between Concrete and Slipform Panel. s.l.:Norwegian University of Science and Technology.
- Furet, B., Poullain, P., and Garnier, S. (2019). 3D printing for construction based on a complex wall of polymer-foam and concrete. *Additive Manufacturing*, 28, 58–64.
- Gardner, N., and Ho, P. (1979). Lateral Pressure of Fresh concrete. *ACI Journal*, 76–35, 809–820.
- Gaudillière, N. D. R. et al. (2018). Large-Scale Additive Manufacturing of Ultra-High-Performance Concrete of Integrated Formwork for Truss-Shaped Pillars. s.l., Springer, pp. 459–472.
- Gaudillière, N. et al. (2019). Building Applications Using Lost Formworks Obtained Through Large-Scale Additive Manufacturing of Ultra-High-Performance Concrete. Butterworth-Heinemann , s.n., pp. 37–58.
- Gebhard, L., Flatt, R. J., and Roussel, N. (2018). Spaghetti and meatball concrete or the art of engineered jamming. Zurich, s.n.
- Ghourchian, S., Wyrzykowski, M., and Lura, P. (2018). A poromechanics model for plastic shrinkage of fresh cementitious materials. *Cement and Concrete Research*, 109, 120–132.
- Grampeix, G. (2013). Vibration des bétons. Université Paris-Est: s.n.
- Guptill, N. et al. (1996). Placing Concrete by Pumping Methods-Report by ACI Committee 304. s.l.:s.n.
- Gutsch, A. W. (2000). Material properties of young concrete - experiments and models. DAFStb Heft, Volume 495.
- Hack, N. et al. (2017). Mesh Mould: An On Site, Robotically Fabricated, Functional Formwork. Tromsø, Norway, s.n.
- Händle, F. (2007). Extrusion in ceramics. s.l.:Springer Science & Business Media.
- Heller, H. et al. (2018). Challenges in Full Scale Filling of a Digitally Fabricated Leaky Formwork. Zurich, s.n.
- Hovad, E. et al. (2016). Simulating the DISAMATIC process using the Discrete Element Method—a dynamical study of granular flow. *Powder Technology*, 303, 228–240.
- Hwang, D., and Khoshnevis, B. (2004). Concrete Wall Fabrication by Contour Crafting. Jeju, South Korea, s.n.
- Irgens, F. (2008). Continuum Mechanics. Berlin, Germany: Springer.
- Jang, K. P. et al. (2018). Experimental Observation on Variation of Rheological Properties during Concrete Pumping. *International Journal of Concrete Structures and Materials*, 12, 79.
- Jay, P., Magnin, A., and Piau, J. M. (2001). Viscoplastic fluid flow through a sudden axisymmetric expansion. *AIChE Journal*, 47(10), 2155–2166.
- Jeong, H. et al. (2019). Rheological Property Criteria for Buildable 3D Printing Concrete. *Materials*, 12(4), 657.
- Jipa, A. et al. (2019). Formwork fabrication freedom for a concrete canoe. *Gestão & Tecnologia de Projetos*, 14, 25–44.
- Jo, S. et al. (2012). A Computational Approach to Estimating a Lubricating Layer in Concrete Pumping. *Computers, Materials and Continua*, 27, 189–210.
- Kaplan, D., De Larrard, F., and Sedran, T. (2005). Design of Concrete Pumping Circuit. *ACI Materials Journal*, 102, 110–117.

- Keita, E. et al. (2019). Weak bond strength between successive layers in extrusion-based additive manufacturing: measurement and physical origin. *Cement and Concrete Research*, 123, 105787.
- Keita, E. et al. (2016). Water retention against drying with soft-particle suspensions in porous media. *Phys. Rev. E*, 94, 033104.
- Keita, E., Rifaai, Y., Belin, P., and Roussel, N. (2019). Influence of non-adsorbing polymers on drying of fresh mortars. *Cement and Concrete Research*, 116, 38–44.
- Khelifi, H., Lecompte, T., Perrot, A., and Ausias, G. (2015). Mechanical enhancement of cement-stabilized soil by flax fibre reinforcement and extrusion processing. *Materials and Structures*, 48, 1–14.
- Khelifi, H. et al. (2013). Prediction of extrusion load and liquid phase filtration during ram extrusion of high solid volume fraction pastes. *Powder Technology*, 249, 258–268.
- Klinzing, G. E., Rizk, F., Marcus, R., and Leung, L. S. (2010). *Pneumatic conveying of solids*. 3 ed. s.l.: Springer.
- Kloft, H. et al. (2019). Additive Manufacturing of concrete elements by Shotcrete 3D Printing (SC3DP). Under submission. To be published in 2019
- Krauss, H. -W. et al. (2018). Concrete Additive Manufacturing—challenges and solutions illustrated by the SC3DP process. Weimar, s.n
- Kruger, P., van Zijl, G., Seung, C., and Zeranka, S. (2019). Ab initio approach for characterization of nanoparticle-infused 3D printable concrete. Submitted to *Construction and Building Materials*, p. under review.
- Kuder, K. G., and Shah, S. P. (2006). Rheology of Extruded Cement-Based Materials. *ACI Materials Journal*, 104(3), 479–484.
- Kusterle, W. et al. (2014). Sprayed concrete in tunnelling. *Betonkalender*, Ch. IX, 304–390.
- Kwon, S., Kyong, P., Kim, J., and Surendra, P. (2016). State of the Art on Prediction of Concrete Pumping. *International Journal of Concrete Structures and Materials*, 10, 75–85.
- Kwon, S. et al. (2013). Prediction of concrete pumping: Part II -analytical prediction and experimental verification. *ACI Materials Journal*, 110, 657–667.
- Lecompte, T., and Perrot, A. (2017). Non-Linear modelling of yield stress increase due to SCC structural build-up at rest. *Cement and Concrete Research*, 92, 92–97.
- Le, T. T. et al. (2012). Mix design and fresh properties for high-performance printing concrete. *Materials and Structures*, 45, 1221–1232.
- Lim, S. et al. (2012). Developments in construction-scale additive manufacturing processes. *Automation in Construction*, 21, 262–268.
- Li, Z., and Zhou, X. (2015). Manufacturing cement-based materials and building products via extrusion: From laboratory to factory. *Civil Engineering*, 168(6), 1–6.
- Lloret, E. et al. (2017). *Smart Dynamic Casting: Slipforming with Flexible Formwork—Inline Measurement and Control*. Tromsø, Norway, s.n.
- Lowke, D. et al. (2018). Particle-bed 3D printing in concrete construction—Possibilities and challenges. *Cement and Concrete Research*, 112, 50–65.
- Marchon, D. et al. (2018). Hydration and rheology control of concrete for digital fabrication: Potential admixtures and cement chemistry. *Cement and Concrete Research*, 112, 96–110.
- Martin, P., Wilson, I., and Bonnett, P. (2006). Paste extrusion through non-axisymmetric geometries: Insights gained by application of a liquid phase drainage criterion. *Powder Technology*, 168(2), 64–73.
- Mechtcherine, V. et al. (2020). Extrusion-based additive manufacturing with cement-based materials—Production steps, processes, and their underlying physics: A review. *Cement and Concrete Research*, 132, 106037.
- Mechtcherine, V., Nerella, V., and Kasten, K. (2014). Testing pumpability of concrete using Sliding Pipe Rheometer. *Construction and Building Materials*, 53, 312–323.
- Mechtcherine, V. et al. (2019). Large-scale digital concrete construction—CONPrint3D concept for on-site, monolithic 3D-printing. *Automation in Construction*, 107, 102933.
- Mettler, L. K., Wittel, F. K., Flatt, R. J., and Herrmann, H. J. (2016). Evolution of strength and failure of SCC during early hydration. *Cement and Concrete Research*, 89, 288–296.

- Mills, D. (2004). *Pneumatic Conveying Design Guide*. s.l.:Elsevier.
- Mu, B., Li, Z., Chui, S. N., and Peng, J. (1999). Cementitious composite manufactured by extrusion technique. *Cement and Concrete Research*, 29(2), 237–240.
- Nehdi, M., and Soliman, A. M. (2011). Early-age properties of concrete: overview of fundamental concepts and state-of-the-art research. *ICE Proceedings—Construction Materials*, 164(2), 57–77.
- Nerella, V., and Mechtcherine, V. (2018). Virtual Sliding Pipe Rheometer for estimating pumpability of concrete. *Construction and Building Materials*, 170, 366–377.
- Nerella, V. N. (2019). Development and characterization of cementitious materials for extrusion-based 3D-printing. s.l.:Doctoral Dissertation, TU Dresden
- Nerella, V. et al. (2019a). Inline quantification of extrudability of cementitious materials for digital construction. *Cement and Concrete Composites*, 95(1), 260–270.
- Nerella, V. N., Hempel, S., and Mechtcherine, V. (2019b). Effects of layer-interface properties on mechanical performance of concrete elements produced by extrusion-based 3D-printing. *Construction and Building Materials*, 205, 586–601.
- Neuner, M., Cordes, T., Drexel, M., and Hofstetter, G. (2017). Time-Dependent Material Properties of Shotcrete: Experimental and Numerical Study. *Materials*, 10.
- Neville, A. M. (2011). *Properties of Concrete*. 5 ed. s.l.: Pearson.
- Novelli, F., and Weyandt, M. (2018). A quick look at pneumatic conveying system basics. [Online] Available at: <https://www.nol-tec.com/wp-content/uploads/2018/11/A-Quick-Look-at-Pneumatic-Convey-Systems-Basics.pdf>.
- Ovarlez, G., and Roussel, N. (2006). A Physical Model for the Prediction of Lateral Stress Exerted by Self-Compacting Concrete on Formwork. *Materials and Structures*, 39(2), 269–279.
- Pane, I., and Hansen, W. (2008). Investigation on key properties controlling early-age stress development of blended cement concrete. *Cement and Concrete Research*, 38(11), 1325–1335.
- Perrot, A. (2006). *Conditions d'extrudabilité des matériaux à base cimentaire*. s.l.:PhD thesis, Rennes, INSA.
- Perrot, A., Lanos, C., Mélinge, Y., and Estellé, P. (2007). Mortar physical properties evolution in extrusion flow. *Rheologica Acta*, 46(8), 1065–1073.
- Perrot, A., Melinge, Y., Estelle, P., and Lanos, C. (2009). Vibro-extrusion: a new forming process for cement-based materials. *Advances in Cement Research*, 21(3), 125–133.
- Perrot, A. et al. (2012). Use of ram extruder as a combined rheo-tribometer to study the behaviour of high yield stress fluids at low strain rate. *Rheologica Acta* 51(8), 743–754.
- Perrot, A., Pierre, A., Vitaloni, S., and Picandet, V. (2014a). Prediction of lateral form pressure exerted by concrete at low casting rates. *Materials and Structures*, 48(7), 1–8.
- Perrot, A., Rangeard, D., and Mélinge, Y. (2014b). Prediction of the ram extrusion force of cement-based materials. *Applied Rheology*, 24(5), 53320.
- Perrot, A., Rangeard, d., and Pierre, A. (2016). Structural built-up of cement-based materials used for 3D-printing extrusion techniques. *Materials and Structures*, 49(4), 1213–1320.
- Pierre, A., Weger, D., Perrot, A., and Lowke, D. (2018). Penetration of cement pastes into sand packings during 3D. *Materials and Structures*, p. 51:22.
- Poiseuille, J. L. (1844). *Recherches expérimentales sur le mouvement des liquides dans les tubes de très-petits diamètres*. s.l.:Imprimerie Royale.
- Qian, Y., Lesage, K., El Cheikh, K., and De Schutter, G. (2018). Effect of polycarboxylate ether superplasticizer (PCE) on dynamic yield stress, thixotropy and flocculation state of fresh cement pastes in consideration of the Critical Micelle Concentration (CMC). *Cement and Concrete Research*, 107, 75–84.
- Rabideau, B. D. et al. (2010). The extrusion of a model yield stress fluid imaged by MRI velocimetry. *Journal of Non-Newtonian Fluid Mechanics*, 165, 394–408.
- Rabideau, B. D. et al. 2012. Internal flow characteristics of a plastic kaolin suspension during extrusion. *Journal of the American Ceramic Society*, 95(2), 494–501.

- Reinold, J., Nerella, V., Mechtcherine, V., & Meschke, G. (2019). Particle Finite Element Simulation of Extrusion Processes of Fresh Concrete during 3D-Concrete Printing. Univ Pavia, Pavia, Italy, s.n., pp. 428–439.
- Reinold, J., Nerella, V., Mechtcherine, V., & Meschke, G. (2020). Extrusion Process Simulation and Layer Shape Prediction during 3D-Concrete-Printing Using The Particle Finite Element Method. Preprint, p. 2020070715.
- Reiter, L., Wangler, T., Roussel, N., and Flatt, R. J. (2018). The role of early age structural build-up in digital fabrication with concrete. *Cement and Concrete Research*, 112, 86–95.
- Roosbahani, M., Borela, R., and Frost, J. (2017). Pore size distribution in granular material microstructure. *Materials* 10(11), 1237.
- Roussel, N. (2005). Steady and transient flow behaviour of fresh cement pastes. *Cement and Concrete Research*, 35(9), 1656–1664.
- Roussel, N. (2006a). A theoretical frame to study stability of fresh concrete. *Materials and Structures*, 39(1), 81–91.
- Roussel, N. (2006b). A thixotropy model for fresh fluid concretes: theory, validation and applications. *Cement and Concrete Research*, 36(10), 1797–1806.
- Roussel, N. (2018). Rheological requirements for printable concretes. *Cement and Concrete Research*, 112, 76–85.
- Roussel, N., and Coussot, P. (2005). “Fifty-cent rheometer” for yield stress measurements: From slump to spreading flow. *Journal of Rheology*, 49, 705–718.
- Roussel, N., and Cussigh, F. (2008). Distinct-layer casting of SCC: The mechanical consequences of thixotropy. *Cement and Concrete Research*, 38, 624–632.
- Roussel, N. et al. (2007). Computational model-ing of concrete flow: General overview. *Cem. Concr. Res.* 37(9), 1298–1307.
- Roussel, N., and Gram, A. (2014). *Simulation of fresh concrete flow*. s.l.:Springer, ISBN .978-94-017-8883-0.
- Roussel, N., Nguyen, T. L. H., and Coussot, P. (2007). General Probabilistic Approach to the Filtration Process. *Physical Review Letters*, 98(11), 114502.
- Roussel, N., Ovarlez, G., Garrault, S., and Brumaud, C. (2012). The origins of thixotropy of fresh cement pastes. *Cement and Concrete Research*, 42, 148–157.
- Salet, T., Ahmed, Z., Bos, F., and Laagland, H., 2018. Design of a 3D printed concrete bridge by testing. *Virtual and Physical Prototyping*, 13, 222–236.
- Schultheiss, M. et al. (2016). Feedback control of Smart Dynamic Casting through formwork friction measurements. Washington, DC, USA, s.n.
- Secrieru, E. (2018). Pumping behaviour of modern concretes—Characterisation and prediction. s.l.:Doctoral Dissertation, TU Dresden.
- Storch, F. et al. (2020). Development of a printhead for large-scale, extrusion-based additive manufacturing with coarse aggregate concrete. *Construction Printing Technology*, 4, 16–21.
- Subramaniam, K. V., and Wang, X. (2010). An investigation of microstructure evolution in cement paste through setting using ultrasonic and rheological measurements. *Cement and Concrete Research*, 40(1), 33–44.
- Suiker, A. S. J. (2018). Mechanical performance of wall structures in 3D printing processes: Theory, design tools and experiments. *International Journal of Mechanical Sciences*, 137, 145–170.
- Szabó, A. et al. (2018). Adapting Smart Dynamic Casting to Thin Folded Geometries. Zurich, Switzerland, s.n.
- Thomas, A. (2009). *Sprayed concrete lined tunnels*. s.l.: Taylor & Francis.
- Toutou, Z., Roussel, N., and Lanos, C. (2005). The squeezing test: a tool to identify firm cement-based material’s rheological behaviour and evaluate their extrusion ability. *Cement and Concrete Research*, 35, 1891–1899.
- Valencia, N. (2017). World’s first 3D printed bridge opens in Spain. [Online] Available at: <https://www.archdaily.com/804596/worlds-first-3d-printed-bridge-opens-in-spain> [Accessed 10 December 2017].

- Wang, J., Niu, D., and Zhang, Y. (2015). Mechanical properties, permeability and durability of accelerated shotcrete. *Construction and Building Materials*, 95, 312–328.
- Wangler, T. et al. (2016). Digital concrete: opportunities and challenges. *RILEM Technical Letter*, pp. 67–75.
- Warner, J. (1995). Understanding shotcrete—the fundamentals. *Concrete International*, 17(5), 59–64.
- Washburn, E. (1921). The dynamics of capillary flow. *Physical Review*, 17, 273.
- Weger, D. et al. (2018). Additive manufacturing of concrete elements using selective cement paste intrusion—Effect of layer orientation on strength and durability. Zurich, s.n.
- Wittmann, F. H. (1983). Creep and shrinkage mechanisms (Chapter 6). In: *Creep and shrinkage in concrete structures*. s.l.:Wiley, pp. 129–161.
- Wolfs, R., Bos, F., and Salet, T. (2019). Triaxial compression testing on early age concrete for numerical analysis of 3D concrete printing. Submitted to *Cement and Concrete Composites*, p. Under review.
- Wolfs, R. J. M., Bos, F. P., & Salet, T. A. M. (2018). Early age mechanical behaviour of 3D printed concrete: Numerical modelling and experimental testing. *Cement and Concrete Research*, 106, 103–116.
- Yammine, J. et al. (2008). From ordinary rheology concrete to self compacting concrete: A transition between frictional and hydrodynamic interactions. *Cement and Concrete Research*, 38, 890–896.
- Yun, K. -K., Choi, P., and Yeon, J. H. (2015). Correlating rheological properties to the pumpability and shootability of wet-mix shotcrete mixtures. *Construction and Building Materials*, 98, 884–891.
- Zhou, X., and Li, Z. (2005). Characterization of rheology of fresh fiber reinforced cementitious composites through ram extrusion. *Materials and Structures*, 38(1), 17–24.
- Zhou, X., Li, Z., Fan, M., & Chen, H. -P. (2013). Rheology of semi-solid fresh cement pastes and mortars in orifice extrusion. *Cement and Concrete Composites*, 37, 304–311.

# Chapter 4

## Printable Cement-Based Materials: Fresh Properties Measurements and Control



**Timothy Wangler, Robert J. Flatt, Nicolas Roussel, Arnaud Perrot, Mohammed Sonebi, Rob Wolfs, Freek Bos, Dirk Lowke, Niklas Freund, Dietmar Stephan, Ursula Pott, Lex Reiter, Steffen Grünewald, Wilson Ricardo Leal da Silva, and Geert De Schutter**

### 4.1 Introduction

Digital fabrication with cementitious materials is a fast-developing field, and advances have been particularly rapid within the past half decade. Cementitious materials are widely used in construction due to the wide availability of the raw materials, the relative ease of production, processing and handling, and especially the ability to transform from a fluid material that can fill a mould to a solid material that can bear a structural load. It is this last quality that makes cementitious materials so

---

T. Wangler (✉) · R. J. Flatt · L. Reiter  
Institute for Building Materials, ETH Zurich, Stefano-Francini-Platz 3, 8093 Zurich, Switzerland  
e-mail: [wangler@ifb.baug.ethz.ch](mailto:wangler@ifb.baug.ethz.ch)

N. Roussel  
Laboratoire NAVIER, Gustave Eiffel University, 5 Boulevard Descartes, 77420  
Champs-sur-Marne, France

A. Perrot  
University Bretagne-Sud, IRDL, UMR CNRS 6027, 56100 Lorient, France

M. Sonebi  
School of Natural and Built Environment, Queen's University Belfast, Belfast BT9 5AG, Northern  
Ireland, UK

R. Wolfs · F. Bos  
Department of the Built Environment, Eindhoven University of Technology, P.O. Box 513,  
NL-5600, MB Eindhoven, The Netherlands

D. Lowke · N. Freund  
Institute of Building Materials, Concrete Construction and Fire Safety, Technische Universität  
Braunschweig, Beethovenstr. 52, 38106 Braunschweig, Germany

D. Stephan · U. Pott  
Technische Universität Berlin, Department of Civil Engineering, Building Materials and  
Construction Chemistry, Gustav-Meyer-Allee 25, 13355 Berlin, Germany

© RILEM 2022

N. Roussel and D. Lowke (eds.), *Digital Fabrication with Cement-Based Materials*,  
RILEM State-of-the-Art Reports 36, [https://doi.org/10.1007/978-3-030-90535-4\\_4](https://doi.org/10.1007/978-3-030-90535-4_4)



attractive for a wide variety of digital fabrication processes for construction, including extrusion-based 3D printing. These processes have been defined and classified in Chap. 2.

All fabrication processes with cementitious materials are governed by certain physical properties. Cementitious materials are classified rheologically as yield stress fluids, thus properties such as the yield stress and plastic viscosity have traditionally played a major role in conventional construction processes; especially in the prediction of flow during pumping and casting of conventionally vibrated and self-compacting concretes. In Chap. 3, however, the basic physics behind digital fabrication processes with cementitious materials have been identified and well developed, and while yield stress and viscosity play their expected major roles, other properties now take on a larger significance in the prediction of processing performance and success. These properties include the evolution of yield stress (commonly called “structural build-up”, or sometimes “thixotropy”) and elastic modulus. The yield stress evolution, in particular, has had some study in the context of self-compacting concrete casting and flow loss, but until now remains ill-characterised in terms of how the evolving microstructure leads to particular rheological behaviour. Thus, characterisation techniques for this property are a major portion of this chapter.

The goal in this chapter is to shortly distil the key properties identified from the basic physics given in Chap. 3, giving a short focus to the structural build-up. The traditional measurements for properties of interest are then shortly described, followed by a more detailed description of the newest measurement techniques that have been developed so far.

## 4.2 Process Rheological Requirements

### 4.2.1 *Competing Stresses During Printing*

In most printing processes in industry or academia, gravity-induced stresses inside the element being printed often dominate all other external sources of stresses (e.g. capillary driven stresses, vibrations, temperature fluctuations, to mention a few). Obviously, these stresses increase proportionally with the density of the material and

---

S. Grünewald

Delft University of Technology, Faculty of Civil Engineering and Geosciences, Concrete Structures Group, Stevinweg 1, 2628 CN Delft, The Netherlands

W. R. L. da Silva

Danish Technological Institute, Taastrup, Denmark

S. Grünewald · G. De Schutter

Ghent University, Department of Structural Engineering and Building Materials, Magel-Vandepitte Laboratory, Technologiepark-Zwijnaarde 60, 9052 Ghent, Belgium

with length scale. This length scale may either be the thickness of the filament during the deposition stage or the height of the object already printed, which is therefore time-dependent (Roussel 2018; Mechtcherine et al. 2020). These stresses induce, in turn, some material deformation which can turn into flow if stress exceeds the material strength or cohesion (Roussel 2018; Mechtcherine et al. 2020). For some non-Newtonian-fluid-type printable materials, this strength or cohesion is called yield stress. It was, however, shown that, for some stiffer printable materials, this strength is very similar to the mechanical strength obtained and measured for brittle quasi-solid materials (Mettler et al. 2016).

Even if the conditions required for material flow onset and, therefore, printing instabilities are not reached, the “small” deformations induced by these gravity-driven stresses may be at the origin of non-acceptable deviations in the final object geometry. This is why, in addition to some strength requirements, there also exists requirements on the material rigidity or stiffness (Roussel 2018; Mechtcherine et al. 2020; Wolfs et al. 2018).

In other words, most printing processes success will be dictated by the result of a competition between gravity-induced stresses—that do scale with a local deposition thickness and/or object height—and some strength/cohesion/rigidity/stiffness material properties. If at any point through the entire printing process, gravity-driven stresses win the above competition, the process shall fail.

The exact terms used to describe the above strength/cohesion/rigidity/stiffness features of a given printable material vary among authors and printing processes but include e.g. **yield stress, cohesion, plasticity limit, friction angle, compressive strength, elastic modulus, critical strain, etc.** Most of these properties are expressed in Pa or kPa. Elasto-plastic models are often used to describe the material along with various plasticity criteria such as the Von Mises plasticity criterion and Tresca plasticity criterion, as well as the Mohr–Coulomb criterion in the case of frictional materials.

As these properties are often expected to change with time for cement-based materials for various chemical and physical reasons (see further in this chapter), material properties of interest also often include some kind of structuration/thixotropy rate (Roussel et al. 2019, 2012; Roussel 2005, 2006). These material properties, no matter their name or the way they are measured, capture the speed at which the strength/cohesion/rigidity/stiffness of the material being printed increases with time and are often expressed in Pa/s.

#### 4.2.1.1 Printing Head Feeding

Before the printing phase dominated by gravity-induced stresses as described above, most processes in industry or academia involve some kind of material transport through a pipe. This transport typically occurs over a distance of several meters between a mixing device and a mobile printing or deposition head. Depending on the material consistency, pipe diameter and flow rate, these transport phases are either referred to as pumping or extrusion (Schutter and Feys 2016; Perrot et al. 2019). In

both cases, they involve a competition between a pressure applied to the material and its resistance to flow. The result of this competition drives the material flow rate in the pipe.

In the case of high flow rates, fluid materials and/or small pipes, the resistance to flow typically involves the material bulk viscosity if the material is fully sheared in the pipe or, most often, the viscosity of a so-called lubrication layer at the vicinity of the pipe wall. This lubrication layer is induced by the so-called “shear-induced particle migration” (Spangenberg et al. 2012; Choi et al. 2013) that pushes particles away from high shear rate zones. Shear rate concentrates in this lubrication layer depleted of coarse particles while the bulk material is almost unsheared, depending on its yield stress. In this case, the bulk material rheological behaviour matters less than the ability of the material to form a lubrication layer along with the layer’s rheological properties.

In the case of low flow rates, stiff materials and/or large pipes, the above lubrication layer thickness possibly becomes of the order of the size of the smallest particles in the material. As a result, the concept of a lubrication layer displaying its own viscosity fails and the resistance to flow is often considered to find its origin into the frictional/tribological properties of the material (Perrot et al. 2019).

#### **4.2.1.2 Filament Stability and Geometry Control**

It is possible to go into more details when focusing on the deposition process. The length scale driving local gravity-induced stresses is obviously the thickness of the layers/filament/lace  $H_0$ . This thickness varying between 1.0 mm (for so-called “micro-printing”) to around 10.0 cm for some large-scale industrial application, the resulting gravity-driven stress ( $\rho \cdot g \cdot H_0$ ) shall be between around a couple of tens of Pa and a couple thousands of Pa. In order for the layer/filament/lace to be stable, the yield stress of the material,  $\tau_0$ , being printed shall be in the same order of magnitude or higher, i.e. from 100 Pa to 10 kPa. The reader should note that this range of yield stresses is the same as the one covered by modern concretes, i.e. from 50 Pa for Self-Compacting Concretes to a few thousand Pa for traditional vibrated concretes (Yammine et al. 2008). We can expect that, at the stage of the deposition process, deformations greater than a couple % cannot be accepted. As a consequence, the minimum value of the elastic modulus of the material expressed as the ratio between the applied gravity-driven stress and the tolerable strain shall be between around 1.0 and 100 kPa.

#### **4.2.2 Object Stability and Geometry Control**

Through the printing process, the gravity-induced stress in a given layer increases with the number of layers printed above the considered layer. The competition between this gravity-induced stress that increases with time and the

strength/cohesion/rigidity/stiffness of the material being printed requires that the strength/cohesion/rigidity/stiffness of the material always stays higher. This requires, in turn, that either that the strength/cohesion/rigidity/stiffness (a) are, from the start, higher than the highest gravity-driven stress reached at the end of the printing process or (b) increase fast enough to always dominate gravity.

From a stress point of view, we can expect in the case of a slender vertical element that, for every meter in the vertical direction element of height, the strength/cohesion should increase by 20 kPa. The reader should note that this value is around the highest cohesion acceptable for a material that has to be pumped or extruded (see above). As a consequence, the above listed option (a) can only be applied to the printing of objects where the vertical dimension of which stays lower than 1.0 m.

In most cases, however, either the printing time is long (i.e. long printing perimeter) or the material is chemically or physically accelerated (see section further in this chapter). Hence, the increase of the material strength/cohesion in time has to be taken into account in the evaluation of the printing process and allows for higher vertical printed dimensions.

However, it was shown in a milestone paper (Wolfs et al. 2018) that, for high vertical dimensions, object stability is not driven anymore by the competition between gravity-induced stress and strength or cohesion but by the risk of so-called self-buckling or gravity-driven buckling. Such instability was shown to scale with the vertical dimension of the object at the power three (Roussel 2018). This imposes requirements not on strength/cohesion but primarily on the material rigidity/stiffness. These can reach levels as high as a few MPa for a 3.0 m high printed element. The reader should note that such levels of rigidity can only be reached through some kind of chemical reactions and not by the natural flocculation/structuration of cement-based products (see Sect. 4.3 further in this paper).

### 4.3 Background Chemistry and Chemical Admixtures

What has been termed structural build-up or yield stress evolution in cementitious materials is related to, primarily, two processes: the flocculation of particles, and the formation of hydration products. After a fluid cementitious material undergoes a shearing event (such as pumping and extrusion in digital fabrication), it is then placed, where it undergoes a period of rest and builds strength due to these two processes, which, despite occurring simultaneously, do occur to varying degrees and at different time scales. The areas where these two processes are primarily dominant are depicted in Fig. 4.1, with flocculation processes being dominant in the early stages up to a maximum, and then hydration processes dominating when these processes are initiated at the onset of the acceleration period. These processes their implications for digital fabrication with cementitious materials as well as a brief description of methods used to control them are described as follows. It should be stated, though, that the general relationship between microstructure and rheology and its evolution

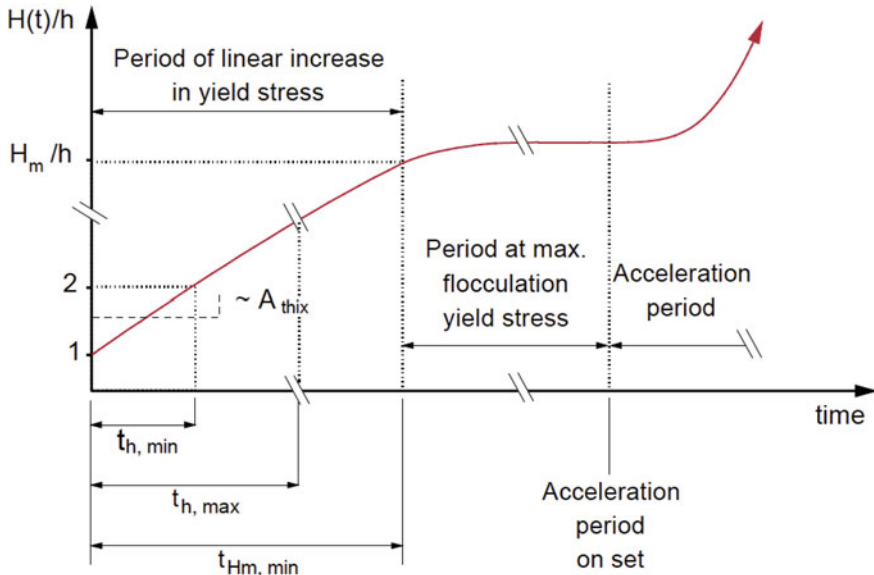


**Fig. 4.1** Strength build-up (given in terms of height) over time for a cementitious material, schematically showing the period of the first linear increase due to flocculation before reaching a maximum, and then the exponential increase that occurs just after onset of the acceleration period. Figure adapted from Wangler et al. (2016), with variables fully described therein

is still a topic of intense research for cementitious materials, and it will remain so for the foreseeable future.

### 4.3.1 Flocculation (Thixotropy)

The term “Flocculation” is usually applied to processes that occur on short time scales during the dormant period of cementitious binders. Often these processes (time scales of seconds to minutes) are termed “thixotropic” processes (Roussel 2006; Roussel et al. 2012; Wallevik 2009; Assaad et al. 2003a, b).

The processes that generally govern interparticle forces when a colloidal suspension such as a cementitious binder is put at rest after a shearing event include: (1) Brownian, (2) colloidal, and (3) hydrodynamic forces. The colloidal forces, in particular, dominate the yield stress behavior of dense particle suspensions such as cementitious systems, varying in magnitude with interparticle separation. These forces can be either attractive (van der Waals) or repulsive (electrostatic or steric), with modifications to these interactions possible through the use of adsorbent molecules such as superplasticizers (Yang et al. 1997; Gelardi and Flatt 2016). Besides these forces, suspension characteristics such as solid volume fraction (related

to the w/c ratio) along with particle size and distribution play a large role (Zhou et al. 1999; Flatt and Bowen 2006).

During the period dominated by flocculation processes, however, low-level hydration is also occurring, which contributes to structural build-up through the formation of solid bridges between particles (Roussel et al. 2012) or the formation of additional surface area for consumption of superplasticizer from solution (Mantellato et al. 2019).

### 4.3.2 Hydration

Cementitious systems are unique for colloidal suspensions in the sense that they are reactive. Hydration processes, related to the dissolution of aluminates ( $C_3A$ ) and silicates ( $C_3S$ ,  $C_2S$ ) clinker mineral phases and the subsequent nucleation and growth of new phases (hydrates), begin immediately upon the first contact with water. These processes vary over time and magnitude for the different mineral phases, with different consequences for the overall rheological behaviour of the suspension. This chemical activity evolves heat, which can be measured in a calorimetry experiment (Sect. 4.5) A typical heat evolution curve for a cementitious material is depicted in Fig. 4.2.

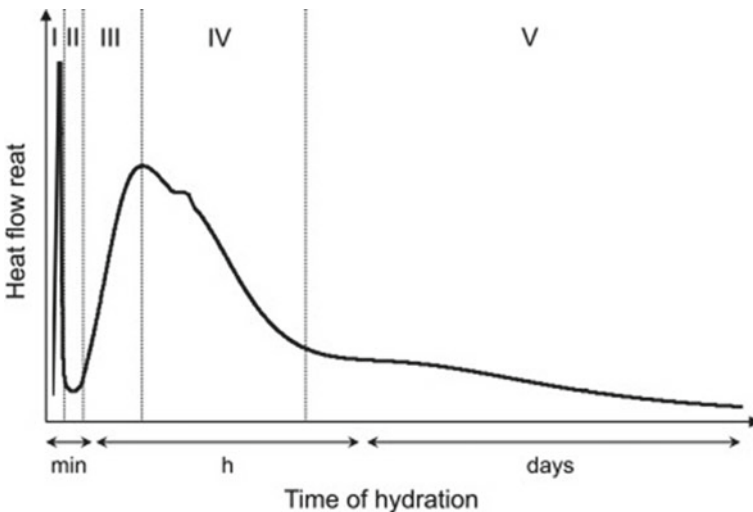


**Fig. 4.2** Typical hydration heat curve for a cementitious material, showing 5 distinct stages. Of greatest interest for digital fabrication processes are stages I and II, until the onset of the acceleration period, which occurs when stage II transitions to stage III. Figure from Marchon and Flatt (2016)

The hydration curve is characterised by stages noted in Fig. 4.2:

- Stage I: dissolution of sulfate and highly reactive  $C_3A$  phases, happening rapidly within the first minutes of water contact.
- Stage II: dormant period or induction period, with low chemical activity and characterised by having a workable paste, generally lasting on the order of one to two hours (also known as the “open time”).
- Stage III: acceleration period, where paste loses its workability (setting) and  $C_3S$  hydration dominates (formation of primary strength-giving phase, calcium silicate hydrate, C-S-H), generally lasting for some hours.
- Stages IV and V: deceleration period, where diffusion controlled growth dominates, lasting for days to months.

For the purposes of digital fabrication processes, Stage I and II are of primary interest, when concrete must remain fluid (and processable) up to placement. These correspond to the period of time where both flocculation and local hydration processes are dominant (Roussel 2012). The Stage II transitions to Stage III is termed the “onset” of acceleration. The massive generation of hydration products increases yield stress in cementitious materials because of the formation of new surface area, which consumes superplasticizer and increases contact points between cement grains, and ultimately the formation and strengthening of C-S-H bridges between cementitious particles.

### 4.3.3 Chemical Admixture Control—Set-On-Demand

As described in detail in Chap. 3 and reminded shortly in Sect. 4.3.1, the rheological requirements of cementitious materials within a given digital fabrication process can vary widely. Rheological changes from a more fluid, low yield stress and pumpable material, to a stiff, high yield stress material sometimes must occur within a matter of seconds. More critically, the buildability of the material requires that yield stress increases linearly over time to match the build rate, or depending on component geometry, that the elastic modulus of the material increases exponentially (Wolfs et al. 2018; Roussel 2018; Reiter et al. 2018). The maximum yield stress increase of cementitious materials in the dormant period is limited (Wangler et al. 2016), thus the use of chemical admixtures that are very strongly flocculating or that actually induce or enhance the formation of hydration products are strongly advised.

A review of the chemical admixtures used in digital fabrication processes has recently been published (Marchon et al. 2018), and the primary types are summarised as follows:

- **Superplasticizers:** these admixtures reduce yield stress and viscosity at constant solids content, which makes them natural choices for the initial rheological requirements of flowable concretes, helping mixes to reach a proper pumpability. In certain digitally controlled casting processes such as Smart Dynamic Casting,

they are essential not just in the pumping process but also the placement process. The most widespread type of these admixtures are the polycarboxylate ethers (PCEs), which are comb copolymers consisting of an anionic backbone which adsorb to the cement particles, and uncharged side chains that extend into the solution and prevent particle contact through steric hindrance.

- **Viscosity modifying agents (VMAs):** these admixtures are generally long-chain organic molecules that increase suspension viscosity by bridging and binding across particles. They also tend to increase the yield stress through this mechanism, and it is in this that they have found utility in digital fabrication processes, by imparting a sometimes rather high initial yield stress, as well as by increasing buildability through increasing thixotropy.
- **Retarders:** these admixtures generally consist of sugars and other carbohydrates, with sucrose being one of the most powerful. They control the open time of a given batch of cementitious material, allowing it to remain workable and processable for extended periods of time.
- **Accelerators:** accelerators are a class of admixture that accelerate the formation of hydration products, which as described earlier, is the most useful mechanism for building strength quickly in digital fabrication systems. Accelerators typically can act on the silicate phases, accelerating the formation of C-S-H (the primary strength-giving phase in cementitious materials) through either the addition of calcium ions (in calcium salt formulations) or the addition of C-S-H seeds to seed nucleation (Thomas et al. 2009; Myrdal 2007). Recent results have suggested that this pathway to strength build-up may be too slow for targeted vertical build speeds of some digital fabrication processes, and thus the accelerators that target the formation of aluminate phases, especially ettringite, have been the focus of research. These accelerators are already being used successfully for many years in shotcrete processes, and generally consist of aluminium salts which promote the fast precipitation of ettringite. More recently, the use of mineral substitutions of phases high in calcium, aluminium, and sometimes sulfate (in calcium aluminate cement or calcium aluminosulfate cement) has been explored and in some cases successfully implemented in digital fabrication processes (Khalil et al. 2017; Reiter et al. 2020), and further development of these chemical processing systems remains a major interest as the field develops.

The identification of the suitability of chemical admixtures for a digital fabrication process is simply the first step, however. Their successful implementation in a digital fabrication process involves precision in when and where to add them in the process. Reiter et al. (2018) pointed out that acceleration should take place as close as possible to the point of placement to avoid hardening in the processing lines, and with some of the fast-acting accelerators described above, this is absolutely essential. The development of inline or secondary mixing steps, in which an accelerator is added just before placement, has been described in Chap. 3 and is depicted in Fig. 4.3 below from Reiter et al. (2020). This concept shows a combination of retarded concrete to which an activator is added just before placement. Other systems have been developed



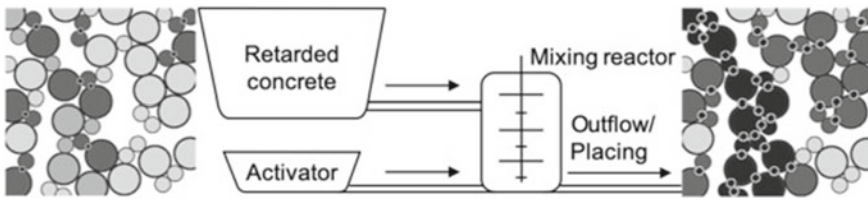


**Fig. 4.3** Concept for processing of concrete in a Set on Demand system. A retarded concrete batch is pumped to a mixing reactor, where an activator is mixed in just before outflow and placement. Such a system enables well-timed control of material rheology, enabling proper structural build-up for process success. Figure from Reiter et al. (2020)

in which material is continuously mixed upstream, giving adequate open time in the line to avoid retardation before the inline mixing step.

## 4.4 Measurement Methods

### 4.4.1 Existing Measurement Methods

#### 4.4.1.1 Free Flow

Free flow of cement-based materials is understood to be the flow of the material under its own weight. In most conventional construction site, rheology of fresh concrete is evaluated every day using gravity thanks to the Abrams cone (Roussel 2011). This standardised procedure is used as quality control test to ensure that the concrete has proper workability or so called “consistency” in order to fill formworks. However, the Abrams cone has been shown to be able to provide rheological parameters when using adequate assumption on the flow geometry (Bouvet et al. 2010; Pierre et al. 2013; Roussel and Coussot 2005; Ferraris and Larrard 1998). Such measurements have been considered to be fast and simple to carry out, and the Abrams cone has been called the “fifty-cent rheometer” (Roussel and Coussot 2005; Pashias et al. 1996). The slump test is used more often as a means of rapid and continuous checking to ensure uniformity of fresh concrete production or supply, rather than solely as a test for the assessment of workability. In all cases, the analysis is based on the description of the flow stoppage when the material yield stress balances the gravity-induced stresses.

For stiff concrete, when the slump is lower than the initial height of the cone, the flow can be considered as purely elongational, and the yield stress can be easily computed from the final height of the tested sample (Roussel and Coussot 2005; Pashias et al. 1996). On the other hand, for fluid concrete such as self-compacting mixtures, purely sheared flow is generated in a thin layer. In this case, the yield stress can be computed from the diameter of the spread flow (Bouvet et al. 2010; Roussel and Coussot 2005). Between those two extreme cases, a combination of these types

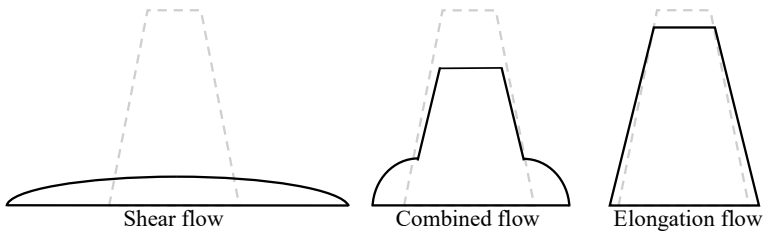


**Fig. 4.4** Different scenarios of gravity-induced flow of a cementitious material cone (Dotted line: initial shape—Black line: final shape)

of flow occurs, and several studies have provided a relationship between the material yield stress and slump (Bouvet et al. 2010; Pierre et al. 2013). These three cases are illustrated in Fig. 4.4.

It can be noted that the cone geometry can be downscaled to the mortar scale (Bouvet et al. 2010) and that viscosity can also be estimated when performing the spread flow. The relationship linking the time to reach a spread diameter to the material plastic velocity is reported by Drewniok et al. (2017). Recently, The Danish Technology Institute has developed a version of the slump flow with further rheological parameter estimation based on the image analysis recorded by a camera during testing (Thrane et al. 2007, 2009).

Other geometries have been used to evaluate the rheological behaviour using gravity as the motor of the flow, especially with fluid concrete. Among those geometries, the L-Box, the LCPC-box can be used to determine the material yield stress (Nguyen et al. 2006; Roussel 2007; Thrane et al. 2004; Nielsson and Wallevik 2003) from the free surface obtained at the low stoppage and the V-funnel and the Marsh cone can be used to determine the viscosity from the time when mortar or concrete flow out from Marsh cone or V-funnel (Utsi et al. 2003; Le Roy and Roussel 2005; Roussel and Le Roy 2005). Those geometries can be seen in Fig. 4.5.

#### 4.4.1.2 Rotational Flow

##### Generalities on Rotational Rheometry

Rotational rheometry can be considered as the conventional way to characterise the rheological behaviour of fluid materials and equipped commercially available rheometers. Conventional rheometers can be used for cement pastes and fine sand mortars and robust and specially dedicated rheometers have been designed for concrete (Koehler et al. 2005; koehler and Fowler 2004; Wallevik 2008, 2015; De Larrard et al. 1996; Hu et al. 1996).

Among others, three types of geometry have been used to measure the rheological properties of materials: coaxial cylinders, parallel plate geometry and cone plate geometry. Cone plate geometry is not often used in case of cementitious materials

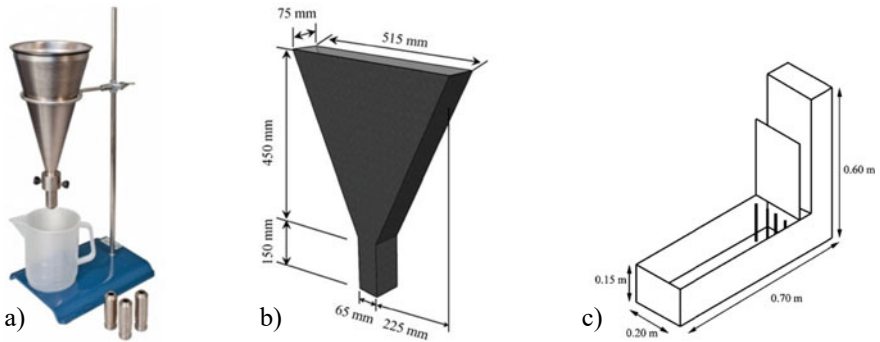


**Fig. 4.5** Different types of geometries for rheological characterisation of cementitious materials using gravity-induced flow: **a** Marsh cone; **b** V-funnel (Ma and Wang 2018); **c** L-Box (Nguyen et al. 2006). Note that the LCPC-box is just the straight horizontal canal of the L-box

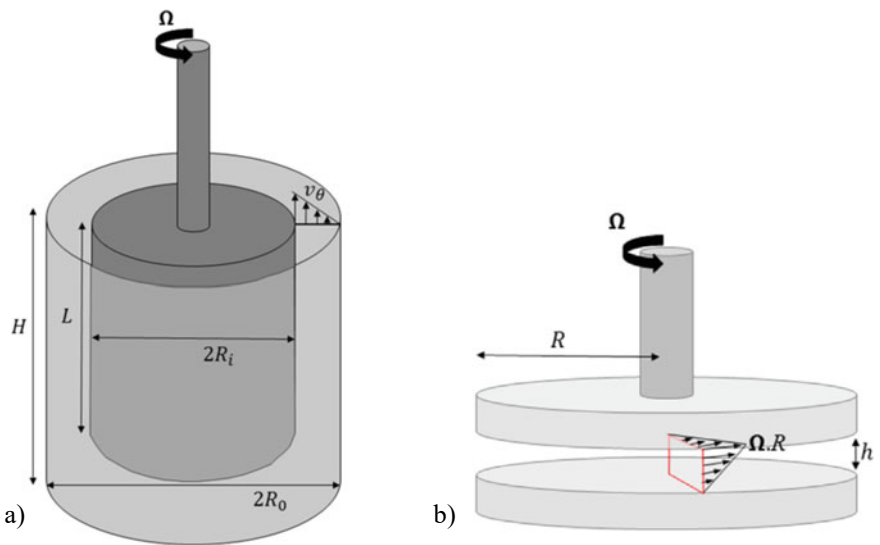


**Fig. 4.6** Schematic of conventional rotational geometries. **a** Coaxial cylinders; **b** Parallel plates. Reproduced from Feys et al. (2018)

because of the size of the particles that are not adapted to the gap size at the center of the sample. Parallel plates and coaxial cylinders are depicted in Fig. 4.6.

In comparison to other materials such as polymers, one major issue when testing cementitious materials is linked to slippage. In order to solve this problem, a rough surface can be used to prevent slippage, and special tool such as 4 or 6-bladed vane or helicoidal tool that describes a cylinder during their rotation can be used as the inner cylinder in the coaxial geometry (Wallevik 2003, 2008; Barnes and Nguyen 2001; Estelle and Lanos 2012).

In all geometries, the tested material is confined between two surfaces (gap), one surface being fixed and the other can be submitted to a rotational movement in order to induce a shear flow. The basic principles of the test consist in imposing a rotational velocity to the rotating tool and to measure the resisting torque (controlled shear rate—CSR—mode) or in imposing a torque and measuring the resulting rotational velocity (controlled shear stress—CSS—mode).

Depending on the imposed solicitation, it is possible to measure shear static yield stress (Mahaut et al. 2008; Perrot et al. 2012), structural build-up (Tchamba et al. 2008; Ma et al. 2018; Lecompte and Perrot 2017), the entire material flow-curve at steady state (Feys et al. 2012; Estelle et al. 2008) or the viscoelastic properties of the studied materials (Mostafa and Yahia 2016; Schultz and Struble 1993).

### Yield Stress Determination

For each geometry, the measurement of the static yield stress (i.e. the yield stress after a given resting time) can be measured using different test procedure including stress growth (CSR mode) (Mahaut et al. 2008; Perrot et al. 2012), stress ramp (CSS mode) (Banfill and Kitching 1990) or also creep recovery (CSS mode) (Feys et al. 2018; Qian and Kawashima 2016; Yuan et al. 2017). For the stress growth, plotting the recorded stress versus the strain can also help to describe the behaviour before the flow onset and can be used to compute a shear elastic modulus (Roussel et al. 2010). Repeating the test procedure after different resting time makes it also possible to compute the structural build-up rate  $A_{thix}$  of the tested cementitious material (Roussel 2006).

### Identifying the Parameters of the Rheological Behaviour

Using strain rate ramp (CSR mode), it is possible to describe the steady-state rheological behaviour over a range of several orders of magnitude of strain rates using coaxial geometry (Koehler et al. 2005; Estellé and Lanos 2012) or parallel plate geometry (Wallevik 2015, 2016). The aim of such procedure is to obtain the parameter of steady-state rheological behaviour such as dynamic yield stress and plastic viscosity for the Bingham model and also the flow index for the Herschel-Bulkley model (Feys et al. 2012; Estellé et al. 2008). Different methods of data processing can be found in the literature. In coaxial geometry, the most used method is based on the Reiner-Riwlin equation that takes into account the possibility of an unsheared zone within the gap due to the material yield stress (Feys et al. 2012, 2018).

It has been pointed out that the data should be carefully analysed using an adequate choice of the model; otherwise non-physical negative yield stress value can be found (Feys et al. 2018; Wallevik et al. 2015). Also, care must be taken to the material homogeneity during the measurement (Feys et al. 2018; Wallevik et al. 2015): the strain rate field within the gap is very heterogeneous for the parallel plates and the coaxial geometry promoting shear-induced particle migration (Spangenberg et al.

2012). Also, flow curves are difficult to obtain for dilatant high yield stress material, because of failure localisation at the rotating tool surface at the flow onset. In this case, once the sample is broken, space is remaining between the rotating tool and the sample because gravity is not sufficient to make the material flowing and filling this space (Pierre et al. 2016).

### Oscillatory Rheometry

Oscillatory rheometry has been used on cement pastes and mortars in order to follow the evolution of the viscoelastic properties of the cementitious material at rest (Feys et al. 2018; Ma et al. 2018; Schultz and Struble 1993). Such measurement can be used with coaxial, cone plate or parallel plate geometry. The basic principles of this kind of test called “Small Amplitude Oscillatory Shear” is to impose an oscillatory strain solicitation with an amplitude below the critical strain of the tested material (around  $10^{-4}$  for a cement paste at rest) at low frequency (around 1.0 Hz) (Feys et al. 2018; Ma et al. 2018; Mostafa and Yahia 2016; Yuan et al. 2017). The imposed oscillatory strain is sinusoidal and can be written as follows:

$$\gamma(t) = \gamma_0 \sin \omega t \quad (4.1)$$

With  $\gamma_0$  the strain amplitude and  $\omega$  the oscillatory frequency. The stress response of the material can be written in the following form (Schultz and Struble 1993):

$$\tau(t) = \gamma_0(G' \sin \omega t + G'' \cos \omega t) \quad (4.2)$$

With  $G'$  the shear storage modulus and  $G''$  the shear loss modulus. The storage modulus  $G'$  describes the in-phase elastic solid-like component of the material behaviour while  $G''$ , the loss modulus, represents the viscous out-of-phase component of the behaviour.

At low shear strain, the viscous effect can be neglected in comparison with elastic effect, which means that the stress response is almost in phase with the strain solicitation and, therefore, that the apparent elastic modulus can be approximated by the storage modulus (Roussel 2018; Roussel et al. 2010). Assuming a constant critical shear strain and a linear elastic behaviour, the yield stress,  $\tau_c$ , can be computed from the storage modulus  $\tau_c = G' \cdot \gamma_c$ . Consequently, the monitoring of the storage modulus can be used to study the material structural build-up as performed in several studies.

This continuous measurement of the structural build-up may stop when the torque capacity of the rheometer is exceeded or when the becoming rigid material starts to slip at the interface.

#### 4.4.1.3 Confined Flow

For high yield stress cement-based materials, free flows and rotational flows are not suitable for determining the viscous component (i.e. after the flow onset) of the material behavior because gravity forces are too low and because of shear localisation (Pierre et al. 2016).

In order to assess the viscosity and the steady-state flow curve of such firm mixtures, confined flows can be used and studied in order to both generate sufficient stresses to both make the material flowing and avoid the generation of some localised fractured shear surfaces. Different geometries can be used to generate confined flows: squeeze flow (Roussel and Lanos 2003; Engmann et al 2005; Toutou et al. 2005), back extrusion (Perrot et al. 2011) or ram extrusion (Zhou and Li 2005; Perrot et al. 2012; Zhou et al. 2013).

Squeeze flow is used to describe the rheological behaviour of firm concentrated suspensions such as molten polymers, food materials or ceramic pastes (Roussel and Lanos 2003; Engmann et al. 2005; Chan and Baird 2002). The test consists of a simple compression test on a cylindrical sample placed between two coaxial and circular plates. The compression of the sample of radius,  $R$ , height,  $h$ , and at a constant velocity,  $v$ , induces an elongational flow. The radii of the sample and the plates can be the same or not. In the first case, the volume of the sample remains the same during the test (sample diameter lower than plates diameter), and in the second, the surface between the sample and the test remains constant (sample diameter equal to the plate diameter). In any case, it is important to use a rough surface to avoid material slippage at the plates interface (Roussel and Lanos 2003). Analytical model of the squeeze flow of Bingham or Herschel-Bulkley fluids are available in the literature (Engmann et al. 2005).

Axisymmetric ram extrusion flows are used to estimate the flow properties of so-called “zero-slump” mortars for which rotational rheometers are not applicable (Zhou and Li 2005; Perrot et al. 2012; Zhou et al. 2013; Mimoune and Aouadja 2004; Alfani and Guerrini 2005; Alfani et al. 2007). The methods and techniques used for cement-based materials are inspired by the literature on ceramics, especially the works of Benbow and Bridgwater (Benbow and Bridgwater 1993; Händle 2007). The material located inside the extruder barrel is pushed by a ram towards a circular die that gives its final shape to the material. The required force that allows to overcome the shaping force required to give its final shape to the material in the shaping zone denoted  $F_{pl}$  and the wall friction force,  $F_{fr}$ , developed along the extruder barrel is linked to the interfacial stress.

The shaping force is used to study the bulk rheology of the material using the methodology proposed by Perrot et al. (2012) or Zhou et al. (2013). Contrary to rotational rheometry, several tests are needed to describe the whole flow curve of a cement-based material, because one extrusion test carried out at a constant ram speed is representative of a single average shear rate. This means that an extrusion test provides only one point of the flow curves. The friction force is used to measure the tribological behaviour (interfacial rheology) of the cement-based materials.

Axisymmetric back extrusion is used to generate an upward flow in the gap between the plunger and the container. The induced shear flow can be used to determine the rheological behaviour of firm cement-based material (Perrot et al. 2011).

For those confined geometries, a problem of water filtration may appear, leading to a heterogeneous mortar (Perrot et al. 2014, 2019). Such filtration is likely to appear for low-velocity test or for mortar or cementitious material which do not contain fine powder or viscosity modifying admixtures and, therefore, exhibit a high permeability (Perrot et al. 2014). When filtration appears, the recorded force increases, and the above described techniques cannot be used to reliably measure the rheological behavior of studied material.

#### **4.4.1.4 Limitations for 3D Printing Formulations**

From the above section on conventional rheological methods, it can be seen that there is no experimental method that is optimised for the online monitoring of the rheological behaviour of the cementitious material during printing.

Such an idealistic method should be simple, robust and be able to describe the full range of rheological behaviour from fresh fluid to early setting solid material. Free flow is not suitable for high yield stress material or high thixotropy material. For rotational rheometry, oscillatory shear is interesting but requires an expensive device and is limited by the torque capacity of the rheometer. Also, confined flows are destructive methods that cannot be used to follow the structural build-up of the materials.

Therefore, it is required to develop new types of rheological tests that are process-related and able to assess the evolution of the required parameter of the material behaviour.

#### ***4.4.2 Methods Utilised or Developed for Digital Fabrication with Concrete***

Test methods typically adopted to assess the properties of fresh concrete before setting target the material in a fluid state, as discussed in Sect. 4.4.1, with well-known and robust methods established to measure both yield stress and viscosity. While these properties are of great importance to control the processing phases in digital fabrication, (e.g. pumping and extruding), the properties in the subsequent static state of fresh concrete should be addressed as well, in particular, their evolution in time. Due to the absence of confinement by traditional formwork, which characterises the majority of digital fabrication processes, the mechanical properties of fresh concrete and their development in time, or structuration rate, are of vital importance to control the structural behaviour during the fabrication process and prevent collapse. As the

relatively high initial strength and stiffness, or rigidity, of material compositions often adopted prevent correct measurements by traditional rheological tests, or because the nature of these test simply does not provide the appropriate parameters, various mechanical tests have been adopted instead. These are outlined in the following sections.

In contrast to traditional construction practice, concrete is typically not compacted in a digital fabrication process. It was shown that an overestimation in material properties may occur when material is extracted and compacted before testing, for instance to remove the presence of layer interfaces in samples created by a 3D printing process (Wolfs et al. 2019), as this affects the presence of e.g. voids or (micro)-cracks after extrusion. As such, regardless the adopted test, it is essential that the fresh concrete is tested in a state and scale representable of the digital fabrication process. Besides, due to the sample state and size, it is generally not possible to apply physical measurement devices without initiating unintentional thixotropic breakdown. Such a device may, moreover, restrict and influence the (natural) deformation behaviour of the fresh material, which generally exhibits relatively large deformations. It was successfully shown that optic measurement techniques may be adopted instead (Wolfs et al. 2018). Finally, in comparison to mechanical testing of hardened concrete, tests on fresh material should be executed swiftly to eliminate the influence of ongoing hydration and flocculation within a single test and to be able to attribute the properties to a specific age (Mettler et al. 2016; Wolfs et al. 2018).

The result of these challenges has led to a number of researchers developing a variety of methods to measure these properties, with some measurements able to measure more than one property. These measurements are detailed in the following.

#### 4.4.2.1 Compression

Compression tests may be performed on fresh concrete to derive the compressive strength, Young's modulus, and Poisson's ratio, as well as their development as a function of concrete age. Based on ASTM D2166, these tests are typically performed on cylindrical samples with a height-to-diameter ratio between 2.0 and 2.5, whereby the largest particle size is smaller than one-sixth of the specimen diameter. The cylinders are vertically compressed by a loading plate, and the corresponding vertical and lateral deformation is recorded. The resulting load–displacement relation may be translated into stress–strain diagrams to derive the desired material properties. The unconfined compressive strength is defined for each test as the maximum occurring stress, and the Young's modulus and Poisson's ratio are derived within the linear range of the stress–strain relation. A compression test does not allow for testing of multi-axial stress states. In various studies, the compressive strength and stiffness were found to increase significantly as the material ages, and their evolution may follow both a linear (Roussel 2006) and non-linear trend (Lecompte and Perrot 2017).

In a time span of a typical digital fabrication process with concrete, i.e. several minutes to a couple of hours, a transition of plastic towards brittle failure may be observed. For instance, in Fig. 4.7, the failure modes of compressed specimens are



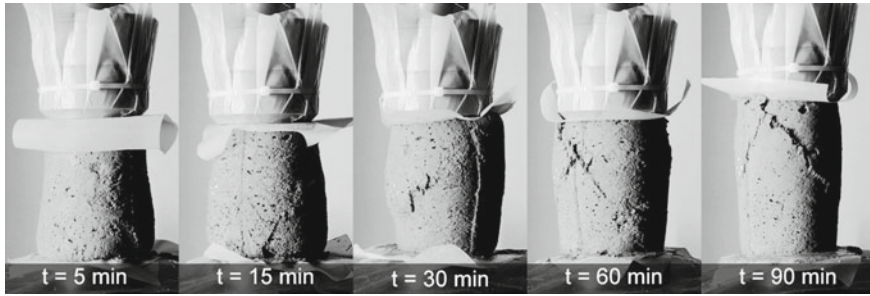
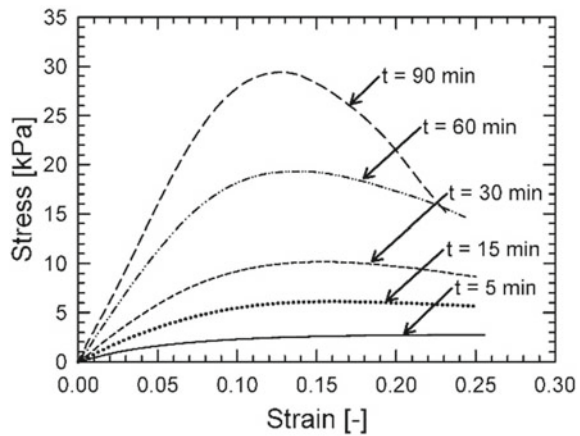


**Fig. 4.7** Failure modes as observed in the compression test on fresh 3D printed concrete. Reproduced from Wolfs et al. (2018)

**Fig. 4.8** Stress–strain relation of 3D printed concrete tested by compression at various ages, depicted in Fig. 4.7. Reproduced from Wolfs et al. (2018)

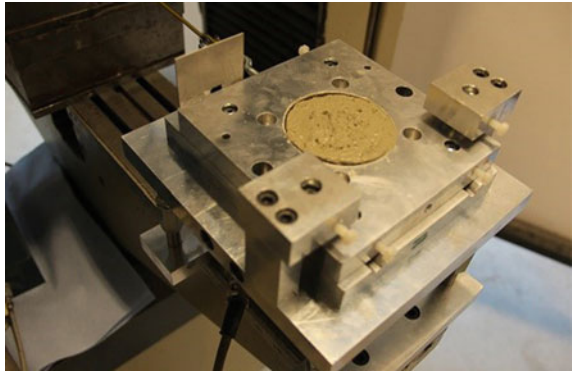


depicted for 3D printed concrete at various ages of 5 to 90 min after extrusion. Due to the relatively low stiffness, the early age specimens significantly expand in lateral direction as the vertical deformation increases, and fail by plastic ‘barrelling’ (bulging). In contrast, older specimens expand less in the lateral direction, and show a distinct and brittle failure plane formation. The intermediate samples show an intermediate failure behaviour. This transition of failure modes was likewise observed in similar studies targeting the material properties of fresh concrete in the context of digital fabrication (Mettler et al. 2016; Wolfs et al. 2019).

#### 4.4.2.2 Shear

Shear tests may be performed on fresh concrete to define a failure criterion and its evolution as the material ages. A variety of shear tests is available (see e.g. ASTM D2166, or D6128), but in essence, they are all based on the horizontal displacement of a two-part, often cylindrical, specimen, see Fig. 4.9. One part is kept stationary,

**Fig. 4.9** Close up of a direct shear test on 3D printed concrete, without a normal force applied. Reproduced from Wolfs et al. (2018)



while the other is horizontally displaced by an external load. In vertical direction, a constant normal force may be applied to the specimen prior to shearing. The resulting maximal shear force may be used to derive the specimen shear strength. Due to the non-uniform stress and strain distribution during shearing, this test is not suitable to derive stiffness properties.

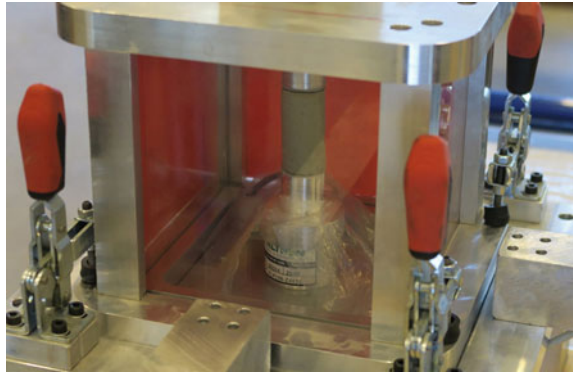
By deriving the shear strength for various vertical forces applied, a failure criterion can be constructed. It was shown that, for certain 3D printable mixture compositions, the Mohr–Coulomb theory may provide a satisfactory failure criterion (Wolfs et al. 2018; Jayathilakage et al. 2019), as the increment in normal force resulted in higher shear strength. This criterion is based on two material parameters, the cohesion and angle of internal friction, which are easily derived by performing a series of shear tests with various normal forces. Similar to the properties derived by the compression test, see Sect. 4.4.2.1, the cohesion and angle of internal friction were found to increase during the time span of a typical digital manufacturing process in recent studies (Mettler et al. 2016; Wolfs et al. 2018), indicating a transition from a fluid material towards a solid.

A well-known issue in shear tests is the friction between the two halves of the test setup, reported by e.g. Assaad et al. (2014, Liu et al. (2005)). In particular, for (very) early-age concrete, the resulting friction force may contribute significantly to the total shear force and compromise the accuracy of the test. This issue may be addressed by treating the setup prior to testing, for instance, by machine-milling grooves in the two halves of the setup and applying rollers in between (Wolfs et al. 2018).

#### 4.4.2.3 Triaxial Compression

A triaxial compression test may be adopted to derive both the stiffness properties and those needed to define a failure criterion for fresh concrete. As such, it can provide all required properties needed to assess both failure by elastic buckling and plastic collapse. Based on ASTM D2850, in a triaxial test a specimen is subjected

**Fig. 4.10** Close up of a triaxial compression test on 3D printed concrete. Reproduced from Wolfs et al. (2019)



to a constant confining pressure and is then compressed in vertical direction until failure. Similar to the compression test, triaxial tests are performed on cylindrical samples with a height-to-diameter ratio between 2.0 and 2.5, such that a shear failure plane may be induced. The confining pressure may be applied via e.g. water, oil or air, and as such, the specimens are tested in a closed chamber, see for instance Fig. 4.10. In contrast to triaxial tests on hardened matter (e.g. soil, rock, concrete), the specimen deformation cannot be measured directly on the sample, which may be overcome by designing the triaxial chamber in cubic shape, such that optic deformation measurements may be applied instead.

By recording the specimen deformation and vertical force for various confining pressures, a failure criterion may be derived, such as the Mohr–Coulomb criterion that was found to be suitable for fresh concrete in the time span of a typical 3D printing process (Wolfs et al. 2019). A triaxial test with no confining pressure applied may be considered as uniaxial compression test, and as such, provides the stiffness and deformation parameters of the fresh material.

The deformation measurements of the triaxial test may be additionally applied to derive the dilatancy behaviour of fresh concrete, which indicates the change in volume associated with (plastic) shear distortion of the material. However, since plastic deformation during a digital fabrication process may already be considered as failure, the dilation behaviour is of lesser importance for the majority of studies targeting fresh concrete in this context.

#### 4.4.2.4 Tension

A tensile test may be performed on fresh concrete to define the early age tensile strength and its development. The test may be performed using a mould of two separable parts, of which one part is horizontally separated from its fixed counterpart, see Fig. 4.11. The tensile force required to induce sample failure may be used to define the specimen tensile strength.

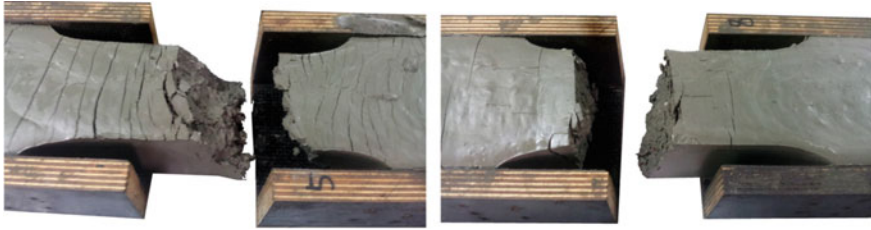


**Fig. 4.11** Close up specimens of fresh concrete in a tensile test. Reproduced from Mettler et al. (2016)

Contrary to the tensile test on hardened specimens, fresh concrete cannot be clamped. An internal pin structure may be attached to the box walls, to enhance shear force transmission from the mould to the sample (Mettler et al. 2016). By applying a round notch to the specimen, controlled failure at the specimen center may be induced without introducing peak stresses.

#### 4.4.2.5 Ultrasound

The measurement of ultrasonic pulse velocity in cementitious materials has been used by some groups for monitoring strength build-up of cementitious materials in digital fabrication technologies (Wolfs et al. 2018; Chen et al. 2019), and it has anyway been used historically to monitor setting times and strength build-up in cementitious material systems in general (Lee et al. 2004; Reinhardt et al. 2000; Trtnik et al. 2008). The physical principle is based on the measurement of the speed of sound in a sample; a transducer emits a signal which is received by another transducer or reflected back to the original transducer. The time delay and distance travelled between emission and reception gives a velocity. This velocity is proportional to the shear modulus of the material, which is then assumed to be proportional to the yield stress. It should be noted that because this method is nondestructive, a critical deformation must be assumed in order to estimate the yield stress, and this critical deformation is not necessarily constant with the material evolution. Therefore, as it was performed in the study of Wolfs et al. (2018), ultrasonic pulse velocity measurements to determine the strength evolution over time is only useful if empirically correlated with strength measurements.

#### 4.4.2.6 Penetration

The methods described until now for measuring yield stress, while having many advantages, often have disadvantages such as that of requiring extensive sample preparation, large sample sizes, or being pointwise measurements requiring multiple samples, as in the compressive, tensile, triaxial strength measurements, to mention

a few. Certain methods can also have the limitation of not being destructive, which requires then an estimation of the critical deformation, which is not necessarily constant over time. Even destructive measurements, which actually do deform the material until the onset of flow can have the limitation of having a shearing surface at the interface of the material with the instrument, rather than within the bulk of the material, such as in vane rheometry experiments. The ideal method thus would have the advantages of being a continuous measurement on a single sample, with the shear surface within the bulk of the sample. Penetration tests can offer such advantages, if designed appropriately.

Penetration tests have been used historically with cementitious materials to measure setting times of pastes and mortars (ASTM C191 and ASTM C403) and have also been used to measure the penetration resistance of soils (ASTM D3441 and D1558). The tests on cementitious materials can be called “fast” penetration tests, as they are performed pointwise, and the soil penetration resistance tests can be called “slow” penetration tests, as they measure penetration force with time at a slower displacement rate, and it can happen over a time interval of interest with a single measurement. A more recent European Norm (EN 14,488–2) describes the use of penetration tests to determine the compressive strength of young sprayed concretes by shooting or pressing a penetration tip into the material, another “fast” penetration test.

As the penetration force is primarily influenced by the yield stress of the material, one can consider the penetration test to be a rheological measurement. A 2009 paper by Lootens et al. (2009) examined the use of these penetration tests in the assessment of yield stress of setting cement pastes. The authors found a very strong correlation of these tests with the yield stress, and they developed analytical relations between the test type, needle and tip geometry, and the respective yield stress or compressive strength. Generally speaking, the test should be performed in a controlled manner in material undisturbed by previous testing. The penetration force is expected to scale with the shearing surface, which is expected to be proportional to the penetration tip surface in contact with the material, as depicted in Fig. 4.12.

As these tests are of great relevance in the region of interest for cementitious materials used in digital fabrication, some researchers have examined their use in the context of digital fabrication, which is detailed in the following.

### Fast Penetration

Within the Shotcrete 3D Printing process (SC3DP) (Kloft et al. 2020; Dressler et al. 2020) both process-related (e.g. pumping and spraying) and material-related factors (e.g. set-accelerator dosage) have a significant effect on the resulting yield stress evolution. In order to investigate these influencing factors systematically within the printing process, an in situ yield stress measurement on printed test specimens is indispensable. For this purpose, a shotcrete penetrometer (Mecmesin Shotcrete Penetrometer) with a defined needle geometry (diameter: 3.0 mm, cylindrical height: 12.5 mm, cone height: 2.5 mm) has been used (Dressler et al. 2020)—the

measurement has been performed manually. This penetrometer is designed and used based on EN 14,488–2. The penetration depth is set at 15.0 mm, Fig. 4.13 (left). A repetition of 5–10 measurements is recommended in order to obtain a statistical certainty. Depending on the research objective, measurements can be performed at any time interval. According to the study by Lootens et al. (2009), the penetration resistance can be calculated to a yield stress. Figure 4.13 (right) shows exemplary results obtained on the basis of fast penetration tests. It shows the effect of different set accelerator dosages on the yield stress evolution of Shotcrete 3D printed samples.

In the same fashion, Lloret et al. (2015) used fast penetration tests to assess the structural build-up of a self-compacting mortar in Smart Dynamic Casting, a digitally controlled slipforming process. They empirically correlated penetration force to slipping speed to determine a material processing window. The previously cited study of Mettler et al. (2016) went further with this method to correlate the penetration load to yield stress of the self-compacting mortar, as well as to detail its transition from the liquid to the solid state. They used a penetration tip of a disc with a diameter of approx. 19.0 mm mounted on a triaxial table and driven at a speed on the order of 1.0 or 2.0 mm/s. They calculated a force per unit area of the penetration tip and found a strong correlation of the penetration force to other methods of measuring strength, including compressive strength. This method has proven rather pragmatic and useful as a strength monitoring method for determining slipping speed (Lloret Fritschi 2016).

### Slow Penetration

Fast penetration tests are pointwise measurements, giving an indication of yield stress at a certain point in time and requiring multiple samples or sampling sites to form an adequate image of strength build-up for processing. Slow penetration tests, on the other hand, are distinguished by using a single sample and measurement to

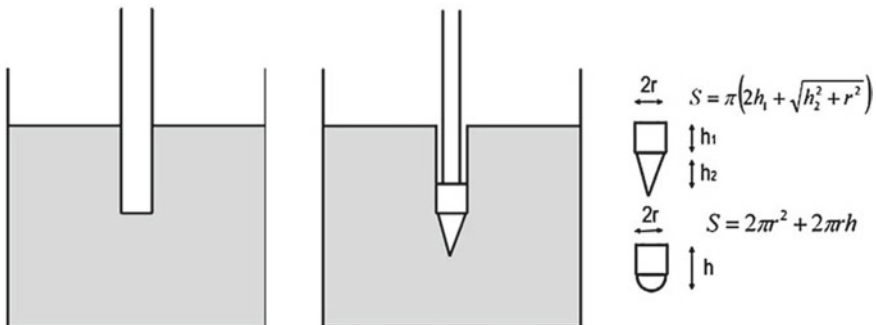


**Fig. 4.12** Schematic of some penetration test geometries: Vicat needle (left) and penetration test (right). The load-bearing surface of the test depicted on the right is constant over time and is the basis for most penetration tests, with varying tip geometries. Figure from Lootens et al. (2009)

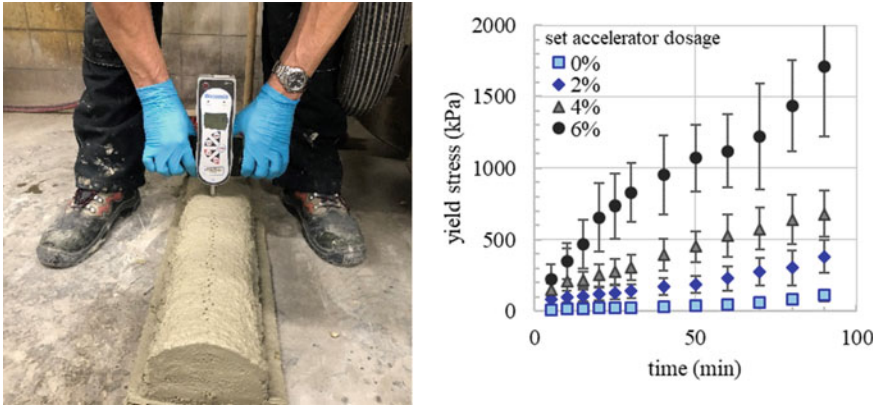


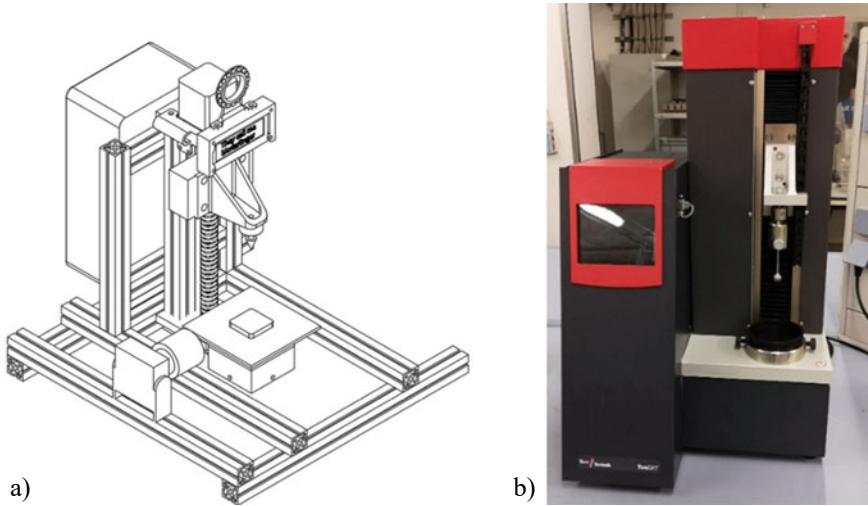
**Fig. 4.13** (left) Fast penetration test on a SC3DP sample using a shotcrete penetrometer, (right) results of fast penetration tests showing the effect of set accelerator dosage (0, 2, 4 and 6% bwoc—by weight of cement) on the yield stress evolution (Dressler et al. 2020)

monitor the structural build-up over an entire processing time window. These slow penetration tests are performed by having a needle penetrating the paste or mortar only once at a very slow speed. During the slow penetration test, a force is measured as a function of the penetration depth. Since the yield stress of the material mainly influences the force during penetration, the penetration resistance of a tool can be considered as a rheological measurement. Compared to the fast penetration test, the slow one has several advantages. Firstly, the material is measured under static and unshered conditions. In a fast penetration test, it must be ensured that the resulting cylindrical volume of the penetrated tool in the sample does not affect subsequent measurements. In addition, the material is affected by the permanent movement of the instrument before and after penetration due to vibrations. These problems do not occur with a slow penetration test.

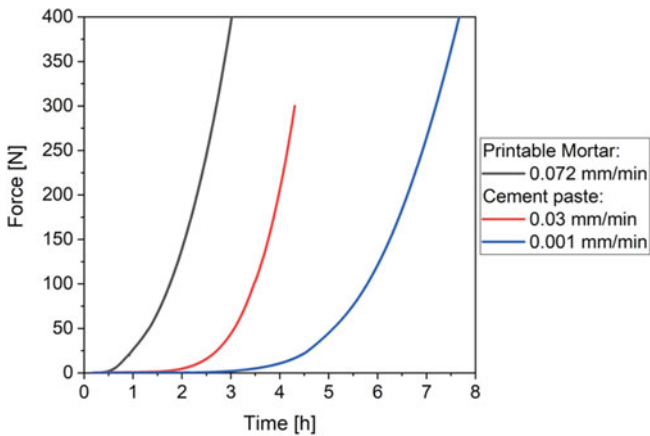
A slow penetration test cannot be performed with every device. Successful performance depends on how precisely a device can perform slow movements and simultaneously measure small changes in force. With some experience, such a penetrometer can be custom made (Pott et al. 2020) (Fig. 4.14a). Otherwise, commercially manufactured systems can be purchased (example in Fig. 4.14b).

Figure 4.15 shows the results of three penetration tests—one mortar and two cement pastes at different penetration speeds. For this investigation, a spherical tool was used as a penetration tip (Fig. 14b). It can be seen that with different speeds and different maximum forces, different durations of hydration can be stated and that different materials can be investigated. Moreover, the slow penetration test is a suitable method for testing paste-rich printable mortars.

The handling is straightforward and fast, and the results are well reproducible. The method is well suited for testing the hydration process of different mortars (Reiter et al. 2020; Lootens et al. 2009; Pott et al. 2020; Reiter 2019). The measured force can be used to calculate the yield stress of the material. Lootens et al. (2009) give



**Fig. 4.14** a Custom-made penitrometer at TU Berlin b Penitrometer of the company Toni Technik with a spherical tool



**Fig. 4.15** Results of a slow penetration test of a cement paste (CEM I) and a printable mortar with a w/b-ratio of 0.36 at penetration speeds of 0.072, 0.03 and 0.001 mm/min

formulas for different penetration tips/configurations. However, these formulae must be used with caution, as the calculated yield stress depends only on the measured yield force and the shear surface. The investigations of the authors have shown that bodies with the same shell surface, but different geometries do not show the same force and, therefore, the calculation would not give the same yield stress for the same material. Further optimisations for the yield stress calculation via the penetration test are therefore desirable.



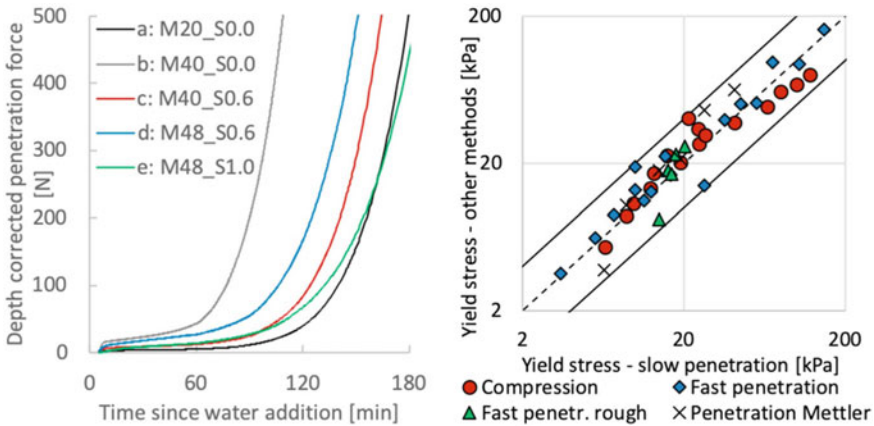
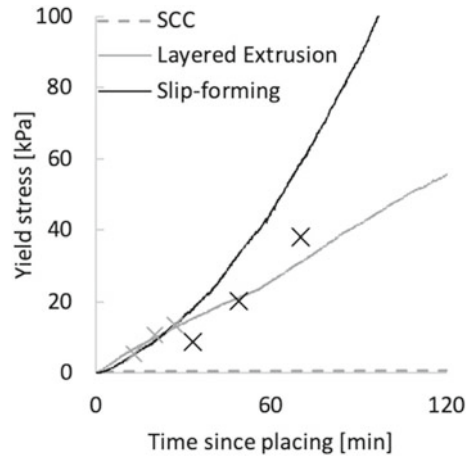


**Fig. 4.16** (left) penetration force over time for mortars. The nomenclature  $M_x_Sy$  refers to  $x$  = sand content and  $y$  = superplasticizer dosage. (right) Yield stress calculated from penetration force using best fit  $N_C$  and its correlation to other methods. Solid lines give the  $0.5\text{--}2 \times$  range of expected values. Figures from Reiter et al. (2020)

Recent work by Reiter (2019) and Reiter et al. (2020) detail a similar slow penetration test, but modelled as a geomechanical soil stability problem. More specifically, the penetration force can be related to the yield stress for plastic materials through the use of a bearing capacity factor  $N_C$ , which is an analytically or empirically derived value relating stress at the penetration tip  $\sigma_f$  to the cohesion  $c_0$ , which is then related to the yield stress. This relation, based on soil mechanical considerations, can also be adapted to take into account minor effects such as surcharge, soil weight, heave, and cone bluntness, which can be considered depending on the penetration test setup. They used a universal testing machine setup, which drove a needle at a speed of 20.0 mm/h while continuously measuring the penetration force. The penetration tip had a cone geometry with a height of 30 mm and a radius of 10 mm. Some results for mortars are shown in Fig. 4.16, showing the strong effect of volume content of solids (sand content) in yield stress increase, as well as the two regimes of yield stress increase: an initial, slow evolution in yield stress followed by an exponential increase associated with the onset of hydration and the growth of hydration products. In the same figure, one can also observe that this penetration force, through a best fit bearing capacity factor  $N_C$ , compares favorably with other yield stress measurement methods such as compression and fast penetration. The method has also been successfully adapted to both slipforming and layered extrusion digital fabrication processes, seen in Fig. 4.17.

As it has been stated before, this method offers numerous advantages, especially the advantage of a single measurement which, with a proper setup, can give accurate yield stress evolution over a time span of hours, thus covering the time period of relevance for most digital fabrication processes. The analysis of Reiter (2019) demonstrates that the penetration tip geometry is a crucial factor as well, as using this

**Fig. 4.17** Penetration (solid lines) and yield stress from compressive strength (crosses) for two different digital fabrication mortars, one for layered extrusion and one for slipforming. Also included is a retarded SCC, showing no increase in yield stress over time. Figure from Reiter et al. (2020)



soil mechanical approach demonstrates that the shearing surface does not occur on the penetration tip surface, but rather at a surface away from the tip, in homogeneous, previously unsheared material, and therefore can be considered a true static yield stress of the material.

The method is reliable for giving continuous, accurate yield stress measurements for mortars, but it does have certain limitations. The briefly described soil mechanical approach shows linearity between penetration force and the cohesion for plastic materials not dominated by frictional contacts between aggregate particles. When frictional contacts begin to dominate, then the friction angle must be considered, and this cannot be determined by the penetration test. Generally, however, digital fabrication mortars are paste-rich and can be considered as plastic materials over the ranges of relevance for processing, about 1–200 kPa. Reiter et al. (2020) cautions, however, that the method does not detect when this transition to a frictional material occurs, so materials of unknown compositions may require some cross-correlation between the slow penetration method with more established discrete methods such as compression. Reiter et al. (2020) also describes other issues with the method that must be dealt with carefully, such as the possibility of wall slip at the container edges leading to a lower penetration force, thus the container size must be selected appropriately to avoid this.

#### 4.4.2.7 Measurements for Slipforming

In the special case of slipforming, a formwork smaller than the element being produced slides upward and a cementitious material exits the formwork with enough strength to support itself and the material above it (Lloret et al. 2015; Lloret Fritschi 2016). The process success hinges on ensuring the concrete has enough strength at the exit, but not so much that the friction between the concrete and the formwork

causes the material to tear off. Friction measurements have been demonstrated by the use of force sensors mounted to the formwork that measure a global friction force (Schultheiss et al. 2016) and an upper bound of material strength (and lower bound on the slipping speed) established by ensuring that through measurement of the volume of concrete in the formwork, a force balance can be calculated to ensure that there is no tensile stress at the exit (Lloret et al. 2017) and the risk of fracture is minimised.

More difficult is the measurement of the structural build-up within the bulk of the material inside the formwork, which determines if the material has enough strength to avoid collapse. Generally, as pointed out earlier, this is done by taking some similar material aside and performing penetration tests over time. In Lloret et al. (2017), however, it was shown that a small deformable membrane near the exit of the formwork could be used to measure the formwork pressure dilatometrically. With this measurement, one can provide a reasonable estimate of the material yield stress at the exit point of the formwork, which would give a lower bound on the material strength (and upper bound on slipping speed) for process success.

Craipeau et al. (2019) introduced a novel measurement in which pore water pressure, measured via a special gauge attached to the formwork, was correlated to shear stress at the formwork/material interface. These results showed that the pore water transition from pressure to suction correlates well with the material's structuration and the transition from the liquid to the solid state. This method offers another possibility for process monitoring of digitally controlled slipforming processes.

## 4.5 Indirect Methods: Calorimetry

As discussed in this chapter, the mechanical strength of cementitious binders in the fresh and hardening state is related to a physical microstructure, generated via two processes: flocculation of particles and the formation of hydration products. The earlier sections in this chapter have been devoted to direct measures of mechanical properties, either destructive or non-destructive. However, other methods can be correlated to the measurement of strength and can also potentially prove simpler to measure, lending themselves better to in-situ monitoring, and they are briefly discussed in this section. These methods are chemical in nature as well, as opposed to direct destructive or non-destructive mechanical methods, which were detailed earlier. The most widely used of these methods is calorimetry.

Calorimetry is the measurement of heat and heat production, and it is a general way of studying processes, including cement hydration, being used as a standard technique now for decades (Bensted 1987). The processes that underly cement hydration generate heat, and the heat generated is proportional to the amount of hydration products formed, and thus to the strength. The most common calorimetric techniques are (1) (semi)-adiabatic calorimetry and (2) isothermal calorimetry (Wadsö et al. 2016). Adiabatic calorimetry methods involve the direct measurement of temperature

evolution of an insulated sample over time, while heat losses to the environment, which occur in reality, should be accounted for (thus the “semi-” prefix). Isothermal calorimetry methods directly measure the thermal power (heat production) in a sample. More detailed information is available from isothermal calorimetry, and thus it is the more widely used method for research purposes. However, (semi)-adiabatic calorimetry finds more utility in the field and on-site applications due to the fact that larger sample sizes, including coarse aggregates, can be used.

A typical heat evolution curve has been shown in Fig. 4.2, where the important time periods in the hydration of cement are shown and detailed in Sect. 4.3.2 of this chapter. While all zones should be of importance to any process with cementitious materials, the most critical zone for 3D printed materials is right at the boundary of Zones II and III, where the onset of the acceleration period begins, as this coincides with where setting occurs—the transformation of the material from a fluid, shapeable material, to a solid material. One can imagine that following a calorimetry curve and following when the curve begins to increase at the onset of the acceleration period would give a useful processing parameter. Nonetheless, initial developments of set-on-demand systems for Smart Dynamic Casting (Shahab et al. 2014) demonstrated little correlation between mechanical strength build-up for process success and isothermal calorimetry curves. The same study, however, did note that isothermal calorimetry was a useful tool for process development in terms of giving indications of accelerator and retarder effectiveness. Hence, at this point, it is not advised to use calorimetry methods for in situ process monitoring to make predictions of strength for digital concrete processing. However, more recent developments in accelerator systems that give a very strong initial heat signal, in particular ettringite based systems (Sect. 4.3.3), may allow this to be revisited.

## 4.6 Robustness and Quality Control

RILEM TC 228-MPS (Khayat and Schutter 2014) defines robustness of SCC as ‘The characteristic of a mixture that encompasses its tolerance to variations in constituent characteristics and quantities, variations during concrete mixing, transport, and placement, as well as environmental conditions.’ Although rheological characteristics of SCC are also very relevant for 3D-printed concrete, other characteristics such as elasticity in the fresh state or structuration rate also have to be considered. A general definition of robustness of 3D-printed concrete can be derived from the definition of robustness of SCC from Van Der Vurst et al. (2017): The robustness of 3D-printed concrete is the capacity to retain its required rheological parameters despite small variations in mix proportioning, material properties and production method. This definition focuses on the robustness of a material against internal and external influences in order to achieve and maintain the required properties in fresh state. Besides the material robustness, a process robustness can also be assessed and/or improved. More generally spoken, the variation in relevant

**Table 4.1** Sources of variation for concrete strength and rheological characteristics

Source of variation	Source specification
Material	Variations in characteristics of cement, supplementary materials, fine aggregates (silt, grading), coarse aggregates (dust, bond), admixtures
Manufacturing	Variation in ingredient weights (water, cementitious materials, admixture), mixing, transporting, delivery time, temperature, air content, workability

production aspects has to be sufficiently low or to be compensated for to achieve the ambitious quality of a printed object.

Obla (2015) listed sources of concrete strength variation. The same parameters are expected to affect the characteristics of 3D-printed concrete in the fresh state (Table 4.1).

For Ready-mix concretes produced in traditional concrete plants, it is now accepted that the most sensitive parameter is the final water content of the mixture (Bonen et al. 2007). This parameter sensitivity finds its origin in the high flocculation of the aggregates' humidity, which is delicate to assess precisely in large stockpiles. As a result, the accuracy in both water and sand content dosage is weaker than the ones of any other components as shown in Fig. 4.18.

However, printable materials seem today to be often used under the form of pre-mixed bags (dry mortars). All components are then fully dried, and the main robustness issue of ready-mix concrete might be expected to vanish.

Moreover, the production tools for printing facilities are expected to involve lower capacities mixers as the required material consumption per hour is extremely low compared to a standard concrete casting phase. With lower volume batches, all weighting equipment are still to be invented or at least chosen. It is therefore, at

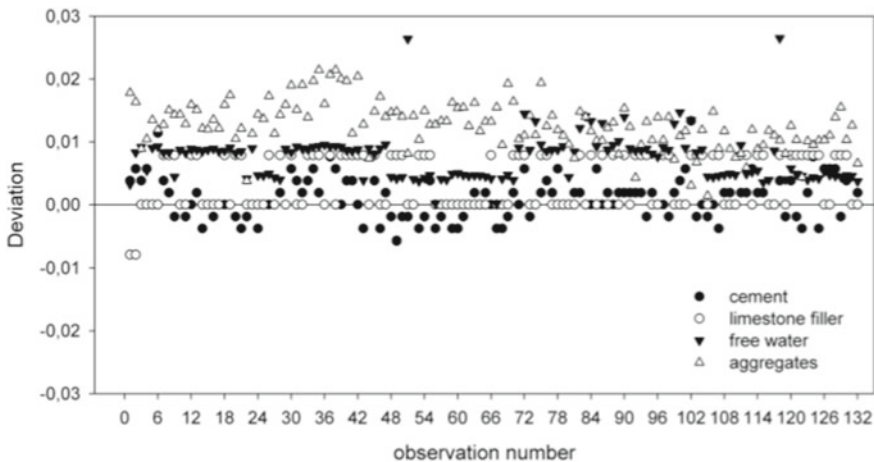


**Fig. 4.18** Observed deviations of constituent materials during one week of concrete production in a precast factory. Figure from Nunes (2008)

this stage, extremely tricky to anticipate if the most sensitive component will be water (like standard concrete), the pre-mix powder or the accelerating additive.

As printable materials are mostly defined by their ability to build up a structure and increase their cohesion/yield stress with time, it means that they are expected to be extremely sensitive to the silicate/aluminate balance and to the admixture/cement interactions. Both are, in turn, expected to be sensitive to dissolution and precipitation processes at extremely early stage along with sulfate availability. However, binders used in the design of printable mixtures (cement, fillers and additives) may more or less vary in their size distribution, shape, porosity, mineral composition and content of secondary chemical components such as sulfates. Availability and delivery capacity of cement factories are major reasons for changes in raw materials or product characteristics.

Cement (i.e. clinker and sulfate carriers) variation is, therefore, expected, at this stage of 3D printing technological development, to have the most important effect on the robustness fresh properties of printable concrete in fresh and hardened states.

## 4.7 Summary

This chapter focuses on the measurement of fresh properties for cementitious materials in digital fabrication processes. The determination of these properties, and especially their monitoring over time, is critical for processing success. The strength/yield stress/cohesion and the elastic modulus, as well as how they evolve with time (often called structural build-up) are primary among fresh state properties. The importance of these has been briefly discussed in this chapter, as well as the background chemistry and the methods of using chemical admixtures to control these properties for digital fabrication processes.

Up until now, simple and robust techniques, such as the slump/spread flow test, as well as sensitive techniques, such as rheometry, exist for the measurement of these properties. However, recently, some have been specially developed or applied to printable cementitious materials for digital fabrication processes. These include techniques that can generate all important material parameters for processing, but require high investments in labour and material (such as triaxial compression) as well as techniques that require a single sample to monitor the yield stress over the entire process relevant time window (slow penetration).

It is important to emphasise that in the case of yield stress/strength/cohesion measurements, destructive tests are necessary, and other types of non-destructive tests require some assumptions and correlations to be made. This chapter is intended to give a spectrum of current possibilities for these measurements that can serve as starting points for further development as the field of digital fabrication with cementitious materials grows further.

Finally, it is important for the printing process to control the materials and to assess and understand the variation. It is not possible to provide robustness in all kind of scenarios and the worst conditions with regard to variation. Tailor-made concrete

requires experienced production personnel and adequate quality control, to a greater extent than existing ready mix plants. The selection of components and production process with low variation are key for the robust production with 3D-printed concrete.

## References

- Alfani, R., and Guerrini, G. L. (2005). Rheological test methods for the characterization of extrudable cement-based materials—a review. *Materials and Structures*, 38, 239–247.
- Alfani, R., Grizzuti, N., Guerrini, G. L., Lezzi, G. (2007). The use of the capillary rheometer for the rheological evaluation of extrudable cement-based materials. *Rheologica acta*, 46, 703–709.
- Assaad, J. J., Harb, J., Maalouf, Y. (2014). Measurement of yield stress of cement pastes using the direct shear test. *Journal of Non-Newtonian Fluid Mechanics*, 214, 18–27. <https://doi.org/10.1016/j.jnnfm.2014.10.009>.
- Assaad, J., Khayat, K. H., and Mesbah, H. (2003a). Assessment of Thixotropy of Flowable and Self-Consolidating Concrete. *MJ*, 100, 99–107. <https://doi.org/10.14359/12548>.
- Assaad, J., Khayat, K. H., and Mesbah, H. (2003b). Variation of Formwork Pressure with Thixotropy of Self-Consolidating Concrete. *MJ*, 100, 29–37. <https://doi.org/10.14359/12460>.
- Barnes, H. A., and Nguyen, Q. D. (2001). Rotating vane rheometry—a review. *Journal of Non-Newtonian Fluid Mechanics*, 98, 1–14.
- Banfill, P. F. G., and Kitching, D. R. (1990). 14 USE OF A CONTROLLED STRESS RHEOMETER TO STUDY THE YIELD STRESS OF OILWELL CEMENT SLURRIES. In: *Rheology of Fresh Cement and Concrete: Proceedings of an International Conference*, Liverpool, 1990. CRC Press, p. 125.
- Benbow, J., and Bridgwater, J. (1993). *Paste flow and extrusion*. Oxford Series on Advanced Manufacturing, No. 10, Clarendon Press, Oxford.
- Bensted, J. (1987). Some applications of conduction calorimetry to cement hydration. *Advances in Cement Research*, 1, 35–44. <https://doi.org/10.1680/adcr.1987.1.1.35>.
- Bonen, Deshpande, Olek, Shen, L., Struble, L., Lange, D., and Khayat, K. (2007). Robustness of Self-Consolidating Concrete. In: *Proceedings of the Fifth International RILEM Symposium on Self-compacting Concrete*. Ghent, Belgium, pp 33–42.
- Bouvet, A., Ghorbel, E., and Bennacer, R. (2010). The mini-conical slump flow test: Analysis and numerical study. *Cement and Concrete Research*, 40, 1517–1523.
- C01 Committee Test Methods for Time of Setting of Hydraulic Cement by Vicat Needle. ASTM International.
- C09 Committee Test Method for Time of Setting of Concrete Mixtures by Penetration Resistance. ASTM International.
- Chan, T. W., and Baird, D. G. (2002). An evaluation of a squeeze flow rheometer for the rheological characterization of a filled polymer with a yield stress. *Rheologica Acta*, 41, 245–256.
- Chen, Y., Li, Z., Chaves Figueiredo, S., Copuroglu, O., Veer, F., Schlangen, E. (2019). Limestone and Calcined Clay-Based Sustainable Cementitious Materials for 3D Concrete Printing: A Fundamental Study of Extrudability and Early-Age Strength Development. *Applied Sciences*, 9, 1809. <https://doi.org/10.3390/app9091809>.
- Craipeau, T., Lecompte, T., Toussaint, F., and Perrot, A. (2019). Evolution of Concrete/Formwork Interface in Slipforming Process. In: Wangler, T., Flatt, R. J. (eds) *First RILEM International Conference on Concrete and Digital Fabrication—Digital Concrete 2018*. Springer International Publishing, pp. 12–23.
- Choi, M., Roussel, N., Kim, Y., and Kim, J. (2013). Lubrication layer properties during concrete pumping. *Cement and Concrete Research*, 45, 69–78. <https://doi.org/10.1016/j.cemconres.2012.11.001>.

- D18 Committee Test Method for Mechanical Cone Penetration Testing of Soils. ASTM International.
- D18 Committee Test Method for Moisture Content Penetration Resistance Relationships of Fine-Grained Soils. ASTM International.
- D18 Committee Test Method for Unconsolidated-Undrained Triaxial Compression Test on Cohesive Soils. ASTM International.
- D18 Committee Test Method for Shear Testing of Bulk Solids Using the Jenike Shear Cell. ASTM International.
- D18 Committee Test Method for Unconfined Compressive Strength of Cohesive Soil. ASTM International.
- Dressler, I., Freund, N., and Lowke, D. (2020). The Effect of Accelerator Dosage on Fresh Concrete Properties and on Interlayer Strength in Shotcrete 3D Printing. *Materials*, 13, 374. <https://doi.org/10.3390/ma13020374>.
- Drewniok, M., Cygan, G., and Gołaszewski, J. (2017). Influence of the Rheological Properties of SCC on the Formwork Pressure. *Procedia Engineering*, 192, 124–129.
- De Larrard, F., Sedran, T., Hu, C., et al. (1996). Evolution of the workability of superplasticised concretes: assessment with the BTRHEOM rheometer. In: *RILEM PROCEEDINGS*, pp. 377–388.
- EN 14488–2: Testing sprayed concrete—Part 2: Compressive strength of young sprayed concrete.
- Engmann, J., Servais, C., and Burbidge, A. S. (2005). Squeeze flow theory and applications to rheometry: a review. *Journal of Non-Newtonian Fluid Mechanics*, 132, 1–27.
- Estellé, P., Lanos, C., Perrot, A., and Amziane, S. (2008). Processing the vane shear flow data from Couette analogy. *Applied Rheology*, 18, 34037.
- Estellé, P., Lanos, C., and Perrot, A. (2008). Processing the Couette viscometry data using a Bingham approximation in shear rate calculation. *Journal of Non-Newtonian Fluid Mechanics*, 154, 31–38.
- Estellé, P., and Lanos, C. (2012). High torque vane rheometer for concrete: principle and validation from rheological measurements. *Applied Rheology*, 22, 12881.
- EN 206–1. Concrete - Part 1: Specification, performance, production and conformity.
- Flatt, R. J., and Bowen, P. (2006). Yodel: A Yield Stress Model for Suspensions. *Journal of the American Ceramic Society*, 89, 1244–1256. <https://doi.org/10.1111/j.1551-2916.2005.00888.x>.
- Ferraris, C. F., and de Larrard, F. (1998). Modified slump test to measure rheological parameters of fresh concrete. *Cement, Concrete and Aggregates*, 20, 241–247.
- Feys, D., Cepuritis, R., Jacobsen, S., Lesage, K., Secrieru, E., and Yahia, A. (2018). Measuring rheological properties of cement pastes: most common techniques, procedures and challenges. *RILEM Technical Letters*, 2, 129–135.
- Feys, D., Wallevik, J. E., Yahia, A., Khayat, K., and Wallevik, O. H. (2012). Extension of the Reiner–Riwlin equation to determine modified Bingham parameters measured in coaxial cylinders rheometers. *Materials and Structures*, 46, 289–311. <https://doi.org/10.1617/s11527-012-9902-6>.
- Gelardi, G., and Flatt, R. J. (2016). 11 - Working mechanisms of water reducers and superplasticizers. In: *Science and Technology of Concrete Admixtures*. Woodhead Publishing, pp. 257–278.
- Händle, F. (2007). *Extrusion in ceramics*. Springer Science & Business Media.
- Hu, C., de Larrard, F., Sedran, T., Boulay, C., Bosc, F., and Deflorenne, F. (1996). Validation of BTRHEOM, the new rheometer for soft-to-fluid concrete. *Materials and Structures*, 29, 620–631.
- Jayathilakage, R., Sanjayan, J., and Rajeev, P. (2019). Direct shear test for the assessment of rheological parameters of concrete for 3D printing applications. *Mater Struct*, 52, 12. <https://doi.org/10.1617/s11527-019-1322-4>.
- Khalil, N., Aouad, G., El Cheikh, K., and Rémond, S. (2017). Use of calcium sulfoaluminate cements for setting control of 3D-printing mortars. *Construction and Building Materials*, 157, 382–391. <https://doi.org/10.1016/j.conbuildmat.2017.09.109>.
- Khayat, K., Schutter, G. D. (2014). *Mechanical Properties of Self-Compacting Concrete: State-of-the-Art Report of the RILEM Technical Committee 228-MPS on Mechanical Properties of Self-Compacting Concrete*. Springer International Publishing.



- Kloft, H., Krauss, H. –W., Hack, N., Herrmann, E., Neudecker, S., Varady, P. A., and Lowke, D. (2020). Influence of process parameters on the interlayer bond strength of concrete elements additive manufactured by Shotcrete 3D Printing (SC3DP). *Cement and Concrete Research*, 134, 106078. <https://doi.org/10.1016/j.cemconres.2020.106078>.
- Koehler, E. P., Fowler, D. W., Ferraris, C. F., and Amziane, S. (2005). A new, portable rheometer for fresh self-consolidating concrete. *ACI SPECIAL PUBLICATIONS*, 233, 97.
- Koehler, E. P., and Fowler, D. W. (2004). Development of a portable rheometer for fresh portland cement concrete. ICAR Research Report-105–3F, University of Texas at Austin.
- Le Roy, R., and Roussel, N. (2005). The Marsh Cone as a viscometer: theoretical analysis and practical limits. *Materials and Structures*, 38, 25–30.
- Lecompte, T., and Perrot, A. (2017). Non-linear modeling of yield stress increase due to SCC structural build-up at rest. *Cement and Concrete Research*, 92, 92–97. <https://doi.org/10.1016/j.cemconres.2016.11.020>.
- Lee, H. K., Lee, K. M., Kim, Y. H., Yim, H., and Bae, D. B. (2004). Ultrasonic in-situ monitoring of setting process of high-performance concrete. *Cement and Concrete Research*, 34, 631–640. <https://doi.org/10.1016/j.cemconres.2003.10.012>.
- Lloret Fritschi, E. (2016). Smart Dynamic Casting—A digital fabrication method for non-standard concrete structures. ETH Zurich.
- Lloret, E., Shahab, A. R., Linus, M., Flatt, R. J., Gramazio, F., Kohler, M., and Langenberg, S. (2015). Complex concrete structures: Merging existing casting techniques with digital fabrication. *Computer-Aided Design*, 60, 40–49. <https://doi.org/10.1016/j.cad.2014.02.011>.
- Lloret Fritschi, E., Reiter, L., Wangler, T., Gramazio, F., Kohler, M., and Flatt, R. J. (2017). Smart Dynamic Casting: Slipforming with Flexible Formwork—Inline Measurement and Control. In: *Proceedings HPC/CIC Tromsø 2017*. Norwegian Concrete Association, paper no. 27.
- Lootens, D., Jousset, P., Martinie, L., Roussel, N., and Flatt, R. J. (2009). Yield stress during setting of cement pastes from penetration tests. *Cement and Concrete Research*, 39, 401–408. <https://doi.org/10.1016/j.cemconres.2009.01.012>.
- Liu, S. H., Sun, D., and Matsuoka, H. (2005). On the interface friction in direct shear test. *Computers and Geotechnics*, 32, 317–325. <https://doi.org/10.1016/j.compgeo.2005.05.002>.
- Mantellato, S., Palacios, M., and Flatt, R. J. (2019) Relating early hydration, specific surface and flow loss of cement pastes. *Mater Struct*, 52, 5. <https://doi.org/10.1617/s11527-018-1304-y>.
- Marchon, D., and Flatt, R. J. (2016). 8 - Mechanisms of cement hydration. In: Aïtcin, P. –C., Flatt, R. J. (eds.) *Science and Technology of Concrete Admixtures*. Woodhead Publishing, pp. 129–145.
- Marchon, D., Kawashima, S., Bessaies-Bey, H., Mantellato, S., and Ng, S. (2018). Hydration and rheology control of concrete for digital fabrication: Potential admixtures and cement chemistry. *Cement and Concrete Research*, 112, 96–110. <https://doi.org/10.1016/j.cemconres.2018.05.014>.
- Ma, G., and Wang, L. (2018). A critical review of preparation design and workability measurement of concrete material for largescale 3D printing. *Frontiers of Structural and Civil Engineering*, 12, 382–400.
- Mahaut, F., Mokéddem, S., Chateau, X., Roussel, N., and Ovarlez, G. (2008). Effect of coarse particle volume fraction on the yield stress and thixotropy of cementitious materials. *Cement and Concrete Research*, 38, 1276–1285. <https://doi.org/10.1016/j.cemconres.2008.06.001>.
- Ma, S., Qian, Y., and Kawashima, S. (2018). Experimental and modeling study on the non-linear structural build-up of fresh cement pastes incorporating viscosity modifying admixtures. *Cement and Concrete Research*, 108, 1–9.
- Mostafa, A. M., and Yahia, A. (2016). New approach to assess build-up of cement-based suspensions. *Cement and Concrete Research*, 85, 174–182. <https://doi.org/10.1016/j.cemconres.2016.03.005>.
- Mimoune, M., and Aouadja F. Z. (2004). Rheometrical exploitation of experimental results obtained from new simulation device for extrusion on clay pastes. *Materials and Structures*, 37, 193–201.

- Mechtcherine, V., Bos, F. P., Perrot, A., da Silva, W. R. L., Nerella, V. N., Fataei, S., Wolfs, R. J. M., Sonebi, M., and Roussel, N. (2020). Extrusion-based additive manufacturing with cement-based materials—Production steps, processes, and their underlying physics: A review. *Cement and Concrete Research*, 132, 106037. <https://doi.org/10.1016/j.cemconres.2020.106037>.
- Mettler, L. K., Wittel, F. K., Flatt, R. J., and Herrmann, H. J. (2016). Evolution of strength and failure of SCC during early hydration. *Cement and Concrete Research*, 89, 288–296. <https://doi.org/10.1016/j.cemconres.2016.09.004>.
- Myrdal, R. (2007). Accelerating admixtures for concrete. State of the art. SINTEF Building and Infrastructure; COIN - Concrete innovation Centre.
- Nguyen, T. L. H., Roussel, N., and Coussot, P. (2006). Correlation between L-box test and rheological parameters of a homogeneous yield stress fluid. *Cement and Concrete Research*, 36, 1789–1796.
- Nielsson, I., and Wallevik, O. H. (2003). Rheological evaluation of some empirical test methods—preliminary results. In: Third international RILEM symposium, RILEM Pub. PRO, pp. 59–68.
- Nunes S. da C. B. (2008). Performance-based design of self-compacting concrete (SCC): A contribution to enhance SCC mixtures robustness. Ph.D., Universidade do Porto (Portugal).
- Obla, K., Lobo, C. (2015). Prescriptive Specifications: A reality check. *Concrete International*, pp. 29–31.
- Pashias, N., Boger, D. V., Summers, J., and Glenister, D. J. (1996). A fifty cent rheometer for yield stress measurement. *Journal of Rheology*, 40, 1179–1189.
- Perrot, A., Rangeard, D., and Mélinge, Y. (2014). Prediction of the ram extrusion force of cement-based materials. *Applied Rheology*, 24, 53320.
- Perrot, A., Mélinge, Y., Estellé, P., Rangeard, D., and Lanos, C. (2011). The back extrusion test as a technique for determining the rheological and tribological behaviour of yield stress fluids at low shear rates. *Applied Rheology*, 21, 53642.
- Perrot, A., Mélinge, Y., Rangeard, D., Micaelli, F., Estelle, P., and Lanos, C. (2012). Use of ram extruder as a combined rheo-tribometer to study the behaviour of high yield stress fluids at low strain rate. *Rheologica acta*, 51, 743–754.
- Perrot, A., Lecompte, T., Khelifi, H., Brumaud, C., Hot, J., and Roussel, N. (2012). Yield stress and bleeding of fresh cement pastes. *Cement and Concrete Research*, 42, 937–944. <http://dx.doi.org/https://doi.org/10.1016/j.cemconres.2012.03.015>.
- Pierre, A., Perrot, A., Histace, A., Gharsalli, S., and Kadri, E. H. (2016). A study on the limitations of a vane rheometer for mineral suspensions using image processing. *Rheologica Acta*.
- Pott, U., Ehm, C., Jakob, C., and Stephan, D. (2020). Investigation of the Early Cement Hydration with a New Penetration Test, Rheometry and In-Situ XRD. In: Mechtcherine, V., Khayat, K., and Secieru, E. (eds.) *Rheology and Processing of Construction Materials*. Springer International Publishing, Cham, pp. 246–255.
- Perrot, A., Rangeard, D., Nerella, V., and Mechtcherine, V. (2019). Extrusion of cement-based materials—an overview. *RILEMTechLett* 3. <https://doi.org/10.21809/rilemtechlett.2018.75>.
- Pierre, A., Lanos, C., and Estellé, P. (2013). Extension of spread-slump formulae for yield stress evaluation. *Applied Rheology*, 23, 63849.
- Qian, Y., and Kawashima, S. (2016). Use of creep recovery protocol to measure static yield stress and structural rebuilding of fresh cement pastes. *Cement and Concrete Research*, 90, 73–79.
- Reiter, L., Wangler, T., Roussel, N., and Flatt, R. J. (2018). The role of early age structural build-up in digital fabrication with concrete. *Cement and Concrete Research*, 112, 86–95. <https://doi.org/10.1016/j.cemconres.2018.05.011>.
- Reiter, L., Wangler, T., Anton, A., and Flatt, R. J. (2020). Setting on demand for digital concrete—Principles, measurements, chemistry, validation. *Cement and Concrete Research*, 132, 106047. <https://doi.org/10.1016/j.cemconres.2020.106047>.
- Reiter, L. (2019). *Structural Build-up for Digital Fabrication with Concrete—Materials, Methods, and Processes*. ETH Zurich.

- Reinhardt, H. W., Große, C. U., and Herb, A. T. (2000). Ultrasonic monitoring of setting and hardening of cement mortar—A new device. *Mat Struct*, 33, 581–583. <https://doi.org/10.1007/BF02480539>.
- Roussel, N. (2006). A thixotropy model for fresh fluid concretes: Theory, validation and applications. *Cement and Concrete Research*, 36, 1797–1806. <https://doi.org/10.1016/j.cemconres.2006.05.025>.
- Roussel, N., and Lanos, C. (2003). Plastic fluid flow parameters identification using a simple squeezing test. *Applied Rheology*, 13, 132–139.
- Roussel, N., Lemaître, A., Flatt, R. J., and Coussot, P. (2010). Steady state flow of cement suspensions: A micromechanical state of the art. *Cement and Concrete Research*, 40, 77–84. <https://doi.org/10.1016/j.cemconres.2009.08.026>.
- Roussel, N. (2007). The LCPC BOX: a cheap and simple technique for yield stress measurements of SCC. *Materials and Structures*, 40, 889–896.
- Roussel, N. (2005). Steady and transient flow behaviour of fresh cement pastes. *Cement and Concrete Research*, 35, 1656–1664. <https://doi.org/10.1016/j.cemconres.2004.08.001>.
- Roussel, N. (2006). A thixotropy model for fresh fluid concretes: Theory, validation and applications. *Cement and Concrete Research*, 36, 1797–1806. <http://dx.doi.org/https://doi.org/10.1016/j.cemconres.2006.05.025>.
- Roussel, N. (2011). *Understanding the rheology of concrete*. Elsevier.
- Roussel, N. (2018). Rheological requirements for printable concretes. *Cement and Concrete Research*, 112, 76–85. <https://doi.org/10.1016/j.cemconres.2018.04.005>.
- Roussel, N., Bessaies-Bey, H., Kawashima, S., Vasilic, K., and Wolfs, R. J. M. (2019). Recent advances on yield stress and elasticity of fresh cement-based materials. *Cement and Concrete Research*, 124, 105798. <https://doi.org/10.1016/j.cemconres.2019.105798>.
- Roussel, N., and Coussot, P. (2005). “Fifty-cent rheometer” for yield stress measurements: From slump to spreading flow. *Journal of Rheology*, 49, 705–718. <http://dx.doi.org/https://doi.org/10.1122/1.1879041>.
- Roussel, N., Ovarlez, G., Garrault, S., and Brumaud, C. (2012). The origins of thixotropy of fresh cement pastes. *Cement and Concrete Research*, 42, 148–157. <https://doi.org/10.1016/j.cemconres.2011.09.004>.
- Roussel, N., and Le Roy, R. (2005). The Marsh cone: a test or a rheological apparatus? *Cement and Concrete Research*, 35, 823–830.
- Schultz, M. A., and Struble, L. J. (1993). Use of oscillatory shear to study flow behavior of fresh cement paste. *Cement and Concrete Research*, 23, 273–282.
- Schutter, G. D., and Feys, D. (2016). Pumping of Fresh Concrete: Insights and Challenges. *RILEM Technical Letters*, 1, 76–80. <https://doi.org/10.21809/rilemtechlett.2016.15>.
- Schultheiss, M., Wangler, T., Reiter, L., Roussel, N., and Flatt, R. J. (2016). Feedback control of Smart Dynamic Casting through formwork friction measurements. In: *SCC 2016 - 8th International Rilem Symposium on Self-Compacting Concrete, Flowing toward Sustainability*. RILEM Publications, pp. 637–644.
- Shahab, A., Lloret, E., Fischer, P., Gramazio, F., Kohler, M., and Flatt, R. J. (2014). Smart dynamic casting or how to exploit the liquid to solid transition in cementitious materials. In: *Proceedings CD of the 1st International Conference on Rheology and Processing of Construction Materials and of the 7th International Conference on Self-Compacting Concrete*. Paris, France.
- Spangenberg, J., Roussel, N., Hattel, J. H., Stang, H., Skocek, J., and Geiker, M.R. (2012). Flow induced particle migration in fresh concrete: theoretical frame, numerical simulations and experimental results on model fluids. *Cement and Concrete Research*, 42, 633–641.
- Thomas, J. J., Jennings, H. M., and Chen, J. J. (2009). Influence of Nucleation Seeding on the Hydration Mechanisms of Tricalcium Silicate and Cement. *J Phys Chem C*, 113, 4327–4334. <https://doi.org/10.1021/jp809811w>.
- Thrane, L. N., Pade, C., and Svensson, T. (2007). Estimation of Bingham rheological parameters of SCC from slump flow measurement. In: *5th International RILEM Symposium on Self-Compacting Concrete*. RILEM Publications SARL, pp. 353–358.

- Thrane, L. N., Pade, C., and Nielsen, C. V. (2009). Determination of rheology of self-consolidating concrete using the 4C-Rheometer and how to make use of the results. *Journal of ASTM International*, 7, 1–10.
- Tchamba, J. C., Amziane, S., Ovarlez, G., and Roussel, N. (2008). Lateral stress exerted by fresh cement paste on formwork: Laboratory experiments. *Cement and Concrete Research*, 38, 459–466. <http://dx.doi.org/https://doi.org/10.1016/j.cemconres.2007.11.013>.
- Toutou, Z., Roussel, N., and Lanos, C. (2005). The squeezing test: a tool to identify firm cement-based material's rheological behaviour and evaluate their extrusion ability. *Cement and Concrete Research*, 35, 1891–1899.
- Trtnik, G., Turk, G., Kavčič, F., and Bosiljkov, V. B. (2008). Possibilities of using the ultrasonic wave transmission method to estimate initial setting time of cement paste. *Cement and Concrete Research*, 38, 1336–1342. <https://doi.org/10.1016/j.cemconres.2008.08.003>.
- Thrane, L. N., Szabo, P., Geiker, M., Glavind, M., and Stang, H. (2004). Simulation of the test method “L-Box” for self-compacting concrete. *Annual Transactions of the NORDIC rheology society*, 12, 47–54.
- Utsi, S., Emborg, M., and Carlsward, J. (2003). Relation between workability and rheological parameters. In: *Third international RILEM symposium, RILEM Pub. PRO*, pp. 154–164.
- Van Der Vurst, F., Grünewald, S., Feys, D., Lesage, K., Vandewalle, L., Vantomme, J., De Schutter, G. (2017). Effect of the mix design on the robustness of fresh self-compacting concrete. *Cement and Concrete Composites* 82:190–201. <https://doi.org/10.1016/j.cemconcomp.2017.06.005>.
- Wallevik, J. E. (2009). Rheological properties of cement paste: Thixotropic behavior and structural breakdown. *Cement and Concrete Research*, 39, 14–29. <https://doi.org/10.1016/j.cemconres.2008.10.001>.
- Wallevik, J. E. (2006). Relationship between the Bingham parameters and slump. *Cement and Concrete Research*, 36, 1214–1221.
- Wangler, T., Lloret, E., Reiter, L., Hack, N., Kohler, M., Bernhard, M., Dillenburger, B., Buchli, J., Roussel, N., and Flatt, R. J. (2016). Digital Concrete: Opportunities and Challenges. *RILEM Technical Letters*, 1, 67–75. <https://doi.org/10.21809/rilemtechlett.2016.16>.
- Wolfs, R. J. M., Bos, F. P., and Salet, T. A. M. (2018). Early age mechanical behaviour of 3D printed concrete: Numerical modelling and experimental testing. *Cement and Concrete Research*, 106, 103–116. <https://doi.org/10.1016/j.cemconres.2018.02.001>.
- Wallevik, J. E. (2008). Minimizing end-effects in the coaxial cylinders viscometer: Viscoplastic flow inside the ConTec BML Viscometer 3. *Journal of Non-Newtonian Fluid Mechanics*, 155, 116–123.
- Wallevik, J. E. (2015). Parallel Plate Based Measuring System for the ConTec Viscometer–Rheological Measurement of Concrete with Dmax 32 mm. *Nordic Concrete* 50.
- Wallevik, J. E. (2003). Rheology of particle suspensions: fresh concrete, mortar and cement paste with various types of lignosulfonates. *Fakultet for ingeniørvitenskap og teknologi*.
- Wallevik, J. E. (2016). Development of parallel plate-based measuring system for the ConTec viscometer. *Newsletter*.
- Wallevik, O. H., Feys, D., Wallevik, J. E., and Khayat, K. H. (2015). Avoiding inaccurate interpretations of rheological measurements for cement-based materials. *Cement and Concrete Research*, 78, 100–109.
- Wolfs, R. J. M., Bos, F. P., and Salet, T. A. M. (2019). Triaxial compression testing on early age concrete for numerical analysis of 3D concrete printing. *Cement and Concrete Composites*, 104, 103344. <https://doi.org/10.1016/j.cemconcomp.2019.103344>.
- Wolfs, R. J. M., Bos, F. P., and Salet, T. A. M. (2018). Correlation between destructive compression tests and non-destructive ultrasonic measurements on early age 3D printed concrete. *Construction and Building Materials*, 181, 447–454. <https://doi.org/10.1016/j.conbuildmat.2018.06.060>.
- Wadsö, L., Winnefeld, F., Riding, K., Sandberg, P. (2016). Calorimetry. In: *A Practical Guide to Microstructural Analysis of Cementitious Materials*. CRC Press, pp. 56–93.
- Yammine, J., Chaouche, M., Guerinet, M., Moranville, M., and Roussel, N. (2008). From ordinary rheology concrete to self compacting concrete: A transition between frictional and hydrodynamic

- interactions. *Cement and Concrete Research*, 38, 890–896. <https://doi.org/10.1016/j.cemconres.2008.03.011>.
- Yang, M., Neubauer, C. M., and Jennings, H. M. (1997). Interparticle potential and sedimentation behavior of cement suspensions: Review and results from paste. *Advanced Cement Based Materials*, 5, 1–7. [https://doi.org/10.1016/S1065-7355\(97\)90009-2](https://doi.org/10.1016/S1065-7355(97)90009-2).
- Yuan, Q., Zhou, D., Khayat, K. H., Feys, D., and Shi, C. (2017). On the measurement of evolution of structural build-up of cement paste with time by static yield stress test vs. small amplitude oscillatory shear test. *Cement and Concrete Research*, 99, 183–189.
- Zhou, X., and Li, Z. (2005). Characterization of rheology of fresh fiber reinforced cementitious composites through ram extrusion. *Materials and structures*, 38, 17–24.
- Zhou, X., Li, Z., Fan, M., and Chen, H. (2013). Rheology of semi-solid fresh cement pastes and mortars in orifice extrusion. *Cement and Concrete Composites*, 37, 304–311.
- Zhou, Z., Solomon, M. J., Scales, P. J., and Boger, D. V. (1999). The yield stress of concentrated flocculated suspensions of size distributed particles. *Journal of Rheology*, 43, 651–671. <https://doi.org/10.1122/1.551029>.

# Chapter 5

## Properties and Testing of Printed Cement-Based Materials in Hardened State



**Jolien Van Der Putten, Venkatesh Naidu Nerella, Viktor Mechtcherine, Mélody D'Hondt, Mohammed Sonebi, Daniel Weger, Zhendi Wang, Constantino Menna, Nicolas Roussel, Dirk Lowke, Kim Van Tittelboom, and Geert De Schutter**

**Abstract** 3D printing is offering a totally new construction method, but an in-depth understanding of the consequences of the different production conditions compared to traditional formwork-based casting operations is required. Bulk material properties (intrinsic strength and durability) will follow the same fundamental material laws. However, in printed structures, the role of the interfaces will become increasingly important as they affect the mechanical performance, transport properties and durability behaviour. Additionally, the anisotropic nature of 3D printed structures

---

J. Van Der Putten (✉) · K. Van Tittelboom · G. De Schutter  
Department of Structural Engineering and Building Materials, Ghent University,  
Magnet-Vandepitte Laboratory, Technologiepark-Zwijnaarde 60, 9052 Ghent, Belgium  
e-mail: [Jolien.vanderputten@ugent.be](mailto:Jolien.vanderputten@ugent.be)

V. N. Nerella · V. Mechtcherine  
Technische Universität Dresden, Dresden, Germany

M. D'Hondt  
Centre Scientifique Et Technique du Bâtiment (CSTB), Division Structure, Maçonnerie et  
Partition, Champs-sur-Marne, France

M. Sonebi  
School of Natural and Built Environment, Queen's University Belfast, Belfast BT9, UK

D. Weger  
Ingenieurbüro Schiessl—Gehlen—Sodeikat GmbH, München, Germany

Z. Wang  
Institute of Concrete Science and Engineering, China Building Materials Academy, Beijing, China

C. Menna  
Università Degli Studi Di Napoli Federico II, Naples, Italy

N. Roussel  
Laboratoire NAVIER, Gustave Eiffel University, 5 Boulevard Descartes, 77420  
Champs-sur-Marne, France

D. Lowke  
Institute of Building Materials, Concrete Construction and Fire Safety, Technische Universität  
Braunschweig, Beethovenstr. 52, 38106 Braunschweig, Germany

implies that there are new opportunities to develop new methods of analysis. The aim of this chapter is to focus on the current practices for performance testing and to give an overview of the parameters which affect the hardened properties of a printed cementitious material.

**Keywords** Anisotropic behaviour · Mechanical properties · Durability · Microstructure

## 5.1 Introduction

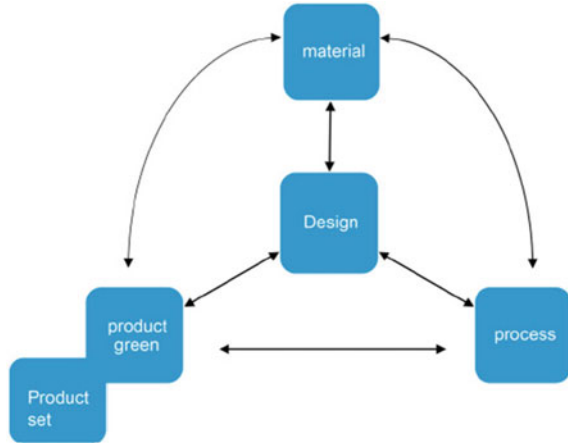
In recent years, 3D printing of concrete has become one of the emerging technologies that can minimize the supply chain in the construction (2017) process by automatically producing building components with complex geometries layer by layer, directly from a digital model without human intervention (Zareiyan and Khoshnevis 2017; Panda et al. 2018). Hence, to some extent, it could save material wastage, construction time and manpower on construction sites.

In general, 3D printing is already successfully applied in different sectors and with the use of different materials, for example, polymers. These materials are extruded in a liquid state and subsequently harden. The transfer to concrete, a material that undergoes a similar phase transition, seems obvious. However, in spite of a similar behaviour, there are some limitations and challenges concerning material properties and print processes that have to be faced in case of concrete printing (Wangler et al. 2016; Panda et al. 2017). Not only the complex characteristics of the material, such as shrinkage, creep, age-dependency, etc. will create many challenges and conflicting requirements, also the different production technique and the additional influence of print process and nozzle geometry will affect the mechanical performance of concrete compared with traditionally cast material.

Regardless of the application of this technique, there is always an interdependency between material, process and product (Fig. 5.1). This is even more pronounced in case of concrete, because of two reasons. First, the slow setting reaction in the printed concrete results in a strong interaction with the applied print parameters such as print speed and pump pressure. Secondly, concrete itself is not a single fixed material, but can have a wide range of compositions that may be more or less suitable in relation to the printing process and the required properties of the final product. Consequently, the print strategy cannot be chosen independently from the design, material or final product considerations (Bos et al. 2016).

In the following sections of this chapter, these specific challenges and pitfalls compared with the traditional way of casting concrete will be discussed.

**Fig. 5.1** Interdependency of design, material, process and product (Bos et al. 2016)



## 5.2 Additive Manufacturing: Challenges and Pitfalls

### 5.2.1 Anisotropy: Occurrence and Influencing Factors

In traditional casting, concrete is generally placed in one continuous pour in a form-work and subsequently vibrated afterwards to obtain a homogenous and isotropic structural element, having similar properties in different directions. However, in case of 3D printed concrete, the elements are build-up from different filaments and anisotropy will occur in the material due to the applied print process and as a consequence of interface properties between the different layers. However, there are currently no studies indicating that the anisotropy exists in the deposited bulk material, but the number of layers can be so dense that effectively anisotropic behaviour should be assumed, rather than that the reduced strength of the discrete layers should be considered.

The anisotropic behaviour of printed materials, fabricated with both extrusion-based techniques and binder jetting technologies, has already been investigated intensively (Panda et al. 2017; Nerella et al. 2019; Le et al. 2012a; Paul et al. 2018; Wolfs et al. 2019; Weger et al. 2016a). Focusing on the material properties in the hardened state, the directional dependency of the printed layers was taken into account by determining the mechanical properties in three different directions, as depicted in Fig. 5.2. First observations (Le et al. 2012a, b; Van et al. 2016; Feng et al. 2015) showed that in general, the material strengths are superior in horizontal direction (Orientation I, Fig. 5.2) and that the tensile strength in vertical direction (Orientation II, Fig. 5.2) is related to the bonding strength among the successive layers. Secondly, it was also noted that anisotropy primarily exists with regard to strength and that the interfaces become increasingly important as these interfaces govern the overall structural performance of the components, with the bulk material properties as the upper limit of the performance that could theoretically be achieved (Bos et al. 2016).



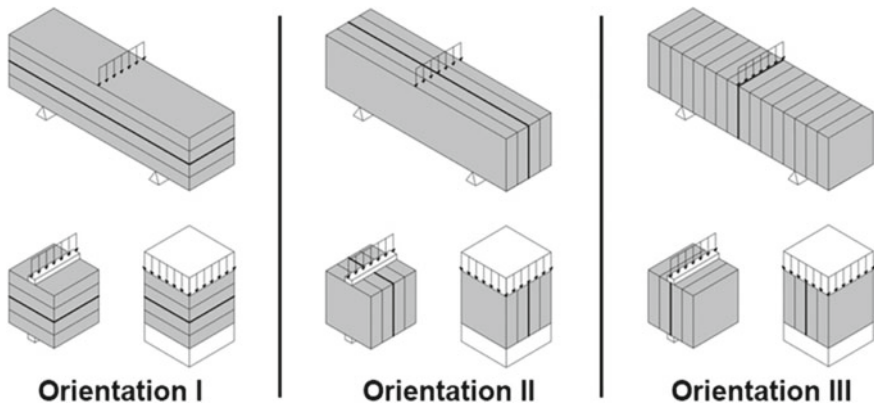


**Fig. 5.2** Directionally dependent mechanical testing respective to layer orientation of extrusion-printed concrete (Wolfs et al. 2019)

Another consequence of the anisotropic behaviour is the limited application of current structural design codes as these codes consider concrete as homogenous and do not take into account the effects of print process parameters. The classical concept of cube or cylinder testing as the basis for compliance testing will no longer hold, as moulded cube specimens cannot be obtained in the traditional way and would be not representative for 3D printed concrete. Durability indicator test methods (e.g. air permeability tests) will also need reassessments. Due to the porous interlayer zone, the air flow while performing an air permeability test will follow a preferential path, impairing the basic assumptions for the interpretation of the obtained pressure. Similar, in capillary suction tests, the results can be considerably affected by porous interlayer joints (Schröfl et al. 2019).

## 5.2.2 *Interlayer Time Interval*

As mentioned before, the interlayer is extremely important and the strength of this layer is expected to relate to a number of process parameters. A crucial print parameter is the interlayer time interval as it should be high enough to ensure enough strength during the print process. Moreover, a limitation of this delay time is required to ensure an adequate bonding between different layers. Several studies showed that an increased time interval results in a reduction of the interface strength and the compressive strength. Most investigations showed this strength reduction through simple macroscopically mechanical tests, but the findings are also supported by microscopical investigations by Van Der Putten et al. (2019) and Nerella et al. (2019), Venkatesh et al. (2017).

### 5.2.3 Print Process Parameters

Other influencing parameters related to the overall strength of the printed specimen have been investigated including printing path, print head speed and print nozzle height. Curing conditions also have a predominant influence on the anisotropy of the printed structure as discussed further in Sect. 5.2.6.2. Feng et al. (2015) investigated the mechanical properties of a layered structure, whereby a different print path was used in comparison to other investigations. In this research, every layer was a combination of different strips, printed next to each other as shown in Fig. 5.3. Preliminary results showed that the compressive strength is the highest in when testing Orientation I (Fig. 5.2). According to the printing process, the specimens can be seen as a lot of thin overlaying strips. The printing speed in this orientation is high, and the time of printing adjacent strips in Orientation II is much shorter than the time of printing adjacent layers in Orientation III.

The bond between two parts of the material appears to be higher when they are printed within a shorter time period, resulting in a higher strength inside a continuous strip than the one between strips, which is in turn higher than the strength between two layers. In these investigations, also the crack formation was observed during the compression tests. Feng et al. (2015) concluded that, when the specimens were loaded according to Orientation I, the cracks pass through inter-layer interfaces and strips. This observation is in contrast to specimens loaded in the second orientation, where the cracks pass through the inter-layer interfaces and inter-strip interfaces. Conducting the compression test according to Orientation III, the cracks pass through the inter-strip interfaces and inter-layer interfaces. As shown in Fig. 5.4, the crack surfaces have an angle of  $45^\circ$  (to the horizontal plane). The vertical path is slightly longer than the horizontal path, giving a higher strength in Orientation III because the inter-strip strength is higher than the inter-layer strength (Feng et al. 2015).

Feng et al. (2015) also investigated the influence on specimens fabricated on a structure where the different layers were printed in different strips (Fig. 5.3), and concluded that the deformation was not obvious until the maximum load was attained. Once this value was reached, the bottom of the specimen was cracked and this consequently led to a sharp drop in load. The observed failure modes could be

**Fig. 5.3** Structure of a 3D printed cubic specimen (Feng et al. 2015)

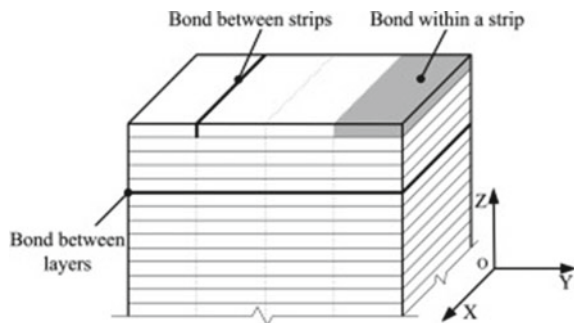
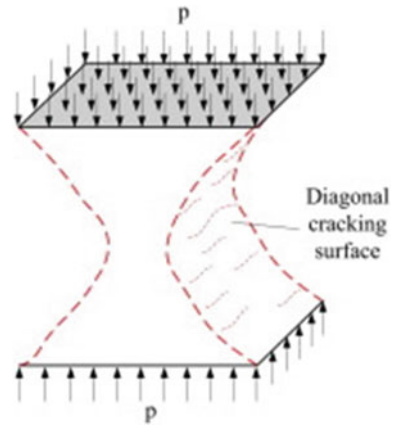


**Fig. 5.4** Failure mode of cubic specimens under compression (Feng et al. 2015)



divided into two main groups: First of all, when loading according to Orientation I, the cracks propagated suddenly through almost the whole section after cracking. However, in case of Orientation III, the crack developed slower compared with the ones in Orientation I, but the crack lengths were less than half of the cross-section depth correspondingly. Secondly, when loading occurs according to Orientation III, the position of the cracks was different and cracks appeared at the mid-section of the specimen. This in contrast with Orientation I, where the cracks deviated slightly from the middle to the part of the specimen printed late due to non-uniformity caused by the printing process.

The variation in results due to the influence of nozzle shape was observed by Bos et al. (2016) and Paul et al. (2018). Circular nozzles, as expected, create voids in the printed object and lower the strength. In the case of a rectangular or square nozzle, this problem may not be significant.

The differences in strength when applying a 3D printing technology can also be attributed to the direction-dependent compaction. Panda et al. (2017) and Sanjayan et al. (2018) postulated during their research that printed layers go through varying degrees of compression in various directions, resulting in corresponding compressive strength variation. On closer observations, two different types of compaction can be identified: (a) compaction in the extruder in the direction of the concrete extrusion and (b) compaction in deposited concrete by weight of the concrete layers deposited on top of it. These different compaction degrees result in different densities and consequently different mechanical properties.

The direction of deposition (i.e. vertically or horizontally), combined with nozzle-to-layer separation distance has a strong influence on the interlayer bond (Panda et al. 2018). While the horizontal deposition enables extrusion of layers with right-angled corners and smooth surfaces, as in the case of CONPrint3D (Mechtcherine et al. 2019), vertical deposition where new layers are “pressure-extruded” on to a substrate layer leads to better interlayer bonds and thus less anisotropy. It must be emphasized that the enhancement of bond most likely takes place only if the

concrete is extruded with flowrate higher than the required flowrate calculated as nozzle opening multiplied with nozzle-to-layer-height and print head velocity.

Lowke et al. (2015, 2018) showed that, by using binder activation methods, the application of the activator (water) influences the material properties. By spraying the water on the particle-bed surface (mixture of aggregates and binder, e.g. cement), the water will penetrate mainly driven by capillary forces. After spreading the next particle layer, the water also penetrates in the dry layer above. NMR measurements showed that there exists a water deviation between the layers, which leads to weak zones between the layers supposed due to a lower hydration. Experiments with a higher amount of water decreased this effect resulting in higher compressive and flexural strength of the material. Therefore, an application of the water with higher pressure or optimizing the packing density of the particle-bed to achieve an equal water distribution could lead to a better material performance.

#### 5.2.4 Mix Composition

The anisotropy in printed structures is affected by the mix composition. More specifically, the water to cement ratio, binder volume, cement type (setting time), cementitious materials (silica fume, fly ash, etc.) particle size and shape, type of superplasticizer, viscosity modifying agent, etc. will affect the degree of anisotropy in case of printed specimens. One means by which the mix composition influences anisotropy is through rheological properties, which have a vital influence on the specimen geometry, deposition time interval and layer surface properties. Nerella et al. (2016) studied two different compositions, one with Portland cement as the sole binder, another with a binder consisting of Portland cement, fly ash and micro silica and the compressive strength was tested in different directions. They reported that the mixture containing high amounts of supplementary cementitious materials, showed superior performance in terms of both homogeneities of microstructure and low dependency of mechanical properties on the direction of loading when compared to mixture made with Portland cement as its sole binder. It is here noteworthy that the concrete composition determines its early age shrinkage. Early plastic and drying shrinkage values manifested as volumetric changes, especially in case of long time intervals, can lead to weak interface strengths and therefore to anisotropy in printed structures (Beushausen et al. 2007).

Another influencing component is the aggregate size and cement-to-aggregate ratio. The average compressive strength as a function of the before mentioned parameters are investigated by Zareiyan and Khoshnevis (2017) and are shown in Fig. 5.5. These results indicate that smaller sized aggregates, with consequently higher cement-to-aggregate ratio, yield to higher compressive strengths. The increase in compressive strength can be due to a decrease in aggregate volume relative to the total composite. The aggregate size also has an influence on the fracture surface. In general, failure under uniaxial compression occurs by debonding of the cementitious

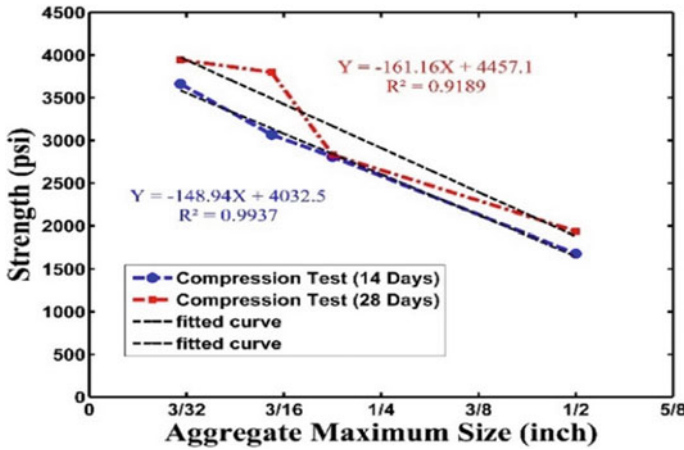


**Fig. 5.5** Compressive strength after 14 and 28 days for different maximum aggregate sizes (Zareiyan and Khoshnevis 2017)

mixture from aggregate particles. These micro-cracks form at the interface of aggregate. Therefore, cracks propagate around the aggregate rather than through it. This phenomenon is shown in Fig. 5.6. Composites containing large aggregates reveal a large number of cracks that propagates parallel to the loading axis. This is in contrast with smaller aggregates where gradual softening of the specimens resulted in the smoothest fracture surface and smaller (width, depth and length) cracks (Zareiyan and Khoshnevis 2017).

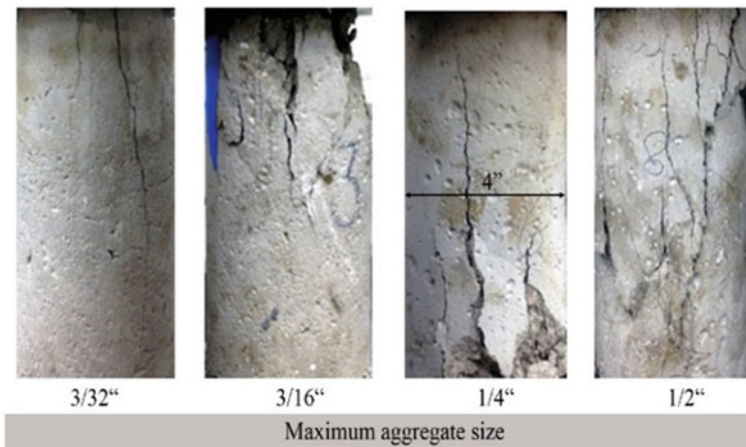


**Fig. 5.6** Surface fracture comparison of different maximum aggregate sizes (Zareiyan and Khoshnevis 2017)

Not only the compressive strength, also the flexural strength can be affected by the mix composition. In case of a high amount of supplementary cementitious materials, Nerella et al. (2019) reported a moderate strength reduction compared with a reference mixture with only Portland cement. These results stand for the most crucial test direction (Orientation III, Fig. 5.2), which means that the flexural strength values yield information on the tensile strength of the interlayer bond.

Weger et al. (2016a, b, 2018a, b) presented that, by using the particle-bed technology of the binder (cement paste) in combination with the flow resistance of the particle-bed (aggregate) determines the penetration behaviour of the binder. To provide sufficient strength and durability, the cement paste has to penetrate the particle layer completely, which needs at least a very low yield stress and viscosity. However, if the binder is too fluid with respect to the flow resistance of the particle-bed, the shape accuracy of the printed object will impair and the void content between the aggregates will increase again. Therefore, an optimum between the particle-bed flow resistance and the binder rheology has to be found (Weger et al. 2016a, b, 2018a, b; Lowke et al. 2018; Pierre et al. 2018).

### 5.2.5 Addition of Fibre

Reinforcement of the structure through fibre addition will try to tackle the inadequate tensile strength of the printed mortars. However, these fibres will affect the anisotropic behaviour of the material. Moreover, there are different fibre types with different properties and different behaviour available.

Rahul et al. (2019) investigated the mechanical behaviour of a 3D printed mortar including polypropylene (PP) fibres and compared the results with traditionally cast concrete. He observed that the bulk phase of the 3D printed mortar is denser than the corresponding mould cast specimen, due to the higher energy applied during the manufacturing process. The effect of his fibre addition on the anisotropic behaviour of the specimen was most pronounced in case of the bond shear strength, where in horizontal and vertical layers a strength reduction of about 24–25% and 22–30% was found compared with the traditionally cast specimen, respectively.

The compressive strength was not influenced by the fibre addition and similar results could be observed in all three testing directions. The results with respect to the flexural strength were inconsistent and highly dependent on the region where the samples were taken.

These results are inconsistent with the observations of Marchment et al. (2017), where the addition of PP fibres influenced the compressive strength positively when loading was applied perpendicular to the interface. He attributed this phenomenon to the preferential fibre alignment parallel to the direction of extrusion. The addition of fibres significantly enhanced the flexural performance of the printed samples. The use of fibre dosages equal to 0.75 and 1.00 vol% caused deflection-hardening behaviour of the 3D printed geopolymers as well as a higher fracture energy. However, an increase in fibre volume caused a minor reduction in interlayer bonding strength.

In the case of glass fibres, a slight reduction in compressive strength could be observed. This can be explained by the fact that glass fibres, located parallel to the loading direction, act like voids depending on the cement matrix ability to accommodate it in one of the three loading directions. Hambach and Volkmer (2017) on the other hand added three different types of fibres to his cementitious mixture: carbon, glass and basalt fibres. The diameter of the included fibres was equal to 7, 20 and 13  $\mu\text{m}$ , respectively. Two different print patterns, a parallel shaped and a crosshatch shaped pattern (Fig. 5.8), and two different test directions (Orientation I and III, Fig. 5.2) were employed in order to investigate the influence of different fibre types and changing fibre orientations along predetermined print paths. Preliminary results showed that, in case of a parallel print path, fibre type has no influence on the compressive strength when testing the specimens according to Orientation I. Testing the elements along Orientation II decreased the compressive strength from 80 to 30 MPa. In the case of a crosshatched shaped path, the same conclusions can be made (Hambach and Volkmer 2017) (Fig. 5.7).

Rubio et al. (2019) studied the effect of natural fibres (sisal) on the mechanical properties of a 3D printing mortar. They reported that triplicating the amount of sisal fibres did not affect the compressive strength and this conclusion could be drawn for both traditional cast cubes and layered specimens (Fig. 5.8). However, the

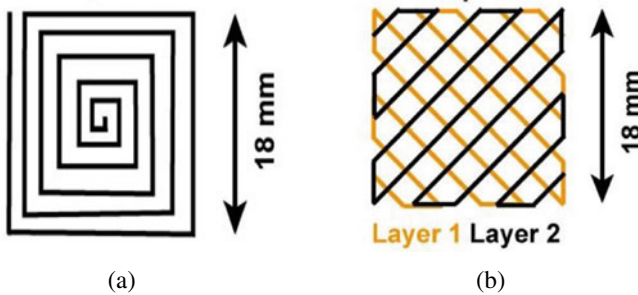
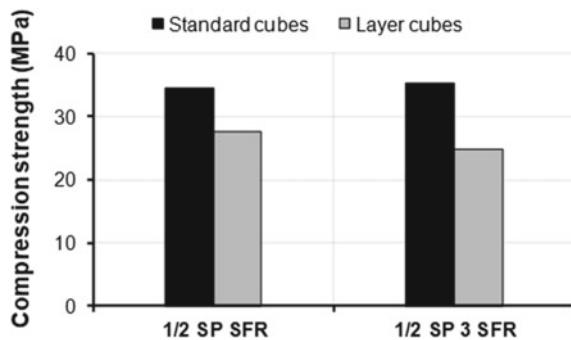


**Fig. 5.7** Top view of the printed paths for specimens used for uniaxial compressive strength: **a** parallel printing path and **b** crosshatch shaped path (Marchment et al. 2017)

**Fig. 5.8** Effect of adding different dosages of natural fibres (SFR) on the compressive strength at 7 days (Hambach and Volkmer 2017)



compressive strength of the layered cubes was approximately 25% lower compared to the standard cubes due to the inhomogeneity of the layered samples and the higher amount of entrapped air.

Based on the investigations of Hambach and Volkmer (2017), a decrease of approximately 25% in compressive strength is observed when comparing layered and standard cubes. This phenomenon can be explained by the heterogeneity of the layered cubes due to the lack of compaction and the higher amount of entrapped air.

## 5.2.6 Distinct Casting of Layers

### 5.2.6.1 Formation

As mentioned before, the interlayer time interval between two subsequent layers is a critical parameter and confronts the researchers with a paradox concerning the production rate of this particular process. On the one hand, the time gap between two deposited layers must be sufficiently long to provide adequate mechanical strength capable of sustaining the weight of the subsequently deposited layer. On the other hand, the time gap has to be short enough to ensure optimized bonding strength as well as building rate. Consequently, the optimum time gap should be the shortest that allows the stability of the layers during construction (Perrot et al. 2016).

Roussel and Cussigh (2008) reported a specific distinct-layer prevention methodology that may be relevant to the digital fabrication of concrete in fresh state: (1) the interface between two layers of fresh concrete must be rough; the roughness at the interface creates a (frictional) bond between two layers even if they do not mix and (2)  $A_{thix}$  of the first layer has to be low enough to allow the stresses generated at the interface between the two layers to re-initiate flow in the first layer. This research also showed that small amounts of accelerator can be used to achieve an increase in structuration which was mostly thixotropic (Roussel and Cussigh 2008; Di Carlo 2012).

High thixotropy may lead to an increase in the entrapment of air and the formation of lift lines in multilayer casting, which could reduce the bond strength. This reduced bond strength between two layers can create cold joints. These joints arise between successively cast layers of concrete that have limited intermixing. This can occur if a critical resting time is exceeded. The critical resting time depends on the density of the material, the gravitational force, the layer height, the structural build-up rate and the construction rate, as shown in Eq. (5.1) (Wangler et al. 2016; Roussel and Cussigh 2008).

$$t_c = \frac{\sqrt{\frac{(\rho gh)^2}{12} + \left(\frac{2\mu_p V}{h}\right)^2}}{A_{thix}} \quad (5.1)$$



With:

$t_c$	Critical value for the interlayer time interval	[s]
$\rho$	Density of the cementitious material	[kg/m <sup>3</sup> ]
$g$	Gravitational acceleration	[m/s <sup>2</sup> ]
$H$	Layer height	[m]
$\mu_p$	Plastic viscosity	[Pa.s]
$V$	Printing velocity	[m/s]
$A_{thix}$	Structuration rate	[Pa/s]

The properties of the interlayer in fresh state affect the mechanical behaviour of the element in the hardened state. To determine the interlayer bonding strength, test methods performed in the field of repair mortars serve as inspiration source. These different test methods are discussed more in-depth in section ‘Tensile strength’ but not all of them are applicable due to the different manufacturing process.

As the properties of the interlayer are extremely important, many researchers are investigating solutions to improve the interlayer quality and the solutions are mostly found in the field of repair mortars. However, as in the case of 3D printed mortars the bonding should be foreseen between two relatively fresh mortars, the behaviour is not completely the same and the number of influencing parameters will increase drastically.

Parameters that could have an influence on the interlayer bonding are:

- Surface preparation (and the possible use of bonding agents);
- Compressive strength of the weakest concrete layer;
- Moisture content of the substrate;
- Curing conditions;
- Additional voids;
- Stress state at the interface and the presence of cracking;
- Amount of steel reinforcement crossing the interface, among others.

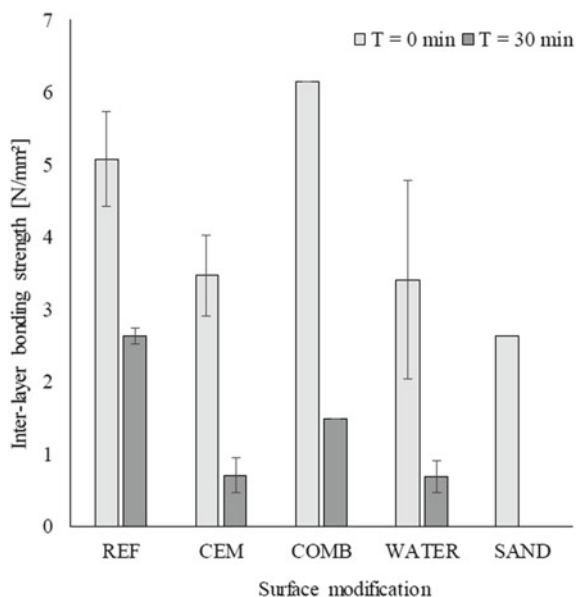
Considering the interface between two relatively fresh layers in 3D printing applications, the amount of influencing parameters will be extended when taking into account the print process itself. More specifically, the occurrence of chemical bonding as well as the effect of restrained shrinkage and a changing stiffness over time are phenomena that cannot be neglected. In the following sections, different surface preparation techniques are listed as a possible improvement of the interlayer quality.

### 5.2.6.2 Enhancement Methods

#### Surface Preparation

Previous research (Le et al. 2012a; Zareiyan and Khoshnevis 2017; Júlio et al. 2004; Santos et al. 2012) states that a higher surface roughness will lead to an increased

**Fig. 5.9** Interlayer bonding strength after different surface modification techniques (Van Der Putten et al. 2019)



bonding strength between the different concrete parts. However, as some researchers using nozzles equipped with trowels to flatten the substrate layer and to ensure a similar roughness over the entire length of the printed specimen, enhancement methods are required. A first possibility to increase the surface roughness is by adding sand particles in between two printed layers or by using nozzles with grooves. These techniques increase the surface roughness with 17 and 68%, respectively. Unfortunately, a similar trend could not be observed when comparing the interlayer bonding strength (Fig. 5.9) as only a nozzle with grooves (COMB, Fig. 5.9) improves the bonding when the time gap between the layers is equal to zero. The non-automated addition of sand particles deteriorates the bonding as it creates large cavities between the printed layers due to an inadequate attachment. The latter weakens the interface zone and results in a lower interlayer bonding strength. In the case of a 30 min time gap, complete de-bonding was observed.

Another enhancement method is performing topological interlocking, which is a design principle that holds the element together purely by geometrical constraints without using any binder or connector. Fabricating printed elements with interlocked parts will increase the bonding strength due to an increased contact surface between the layers until a certain depth of the particular interlock (Figs. 5.10 and 5.11).

The addition of fibres and the construction process (cast or extruded) can also influence the surface roughness of a printed element. Peled and Shah (2003) described the surface roughness of extruded composites with and without the addition of fly ash and after adding PVA fibres with different lengths. She detected that in case of extruded composites without fly ash and 2 mm fibres, a large number of long fibrils were lying on top of the fracture surface. These long fibrils will increase the roughness

**Fig. 5.10** Interlocking systems (Di Carlo 2012)

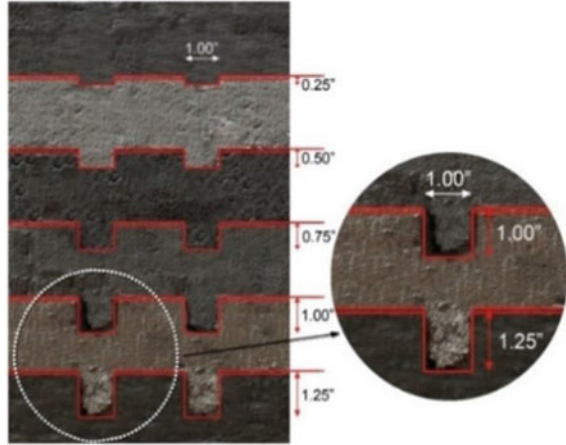
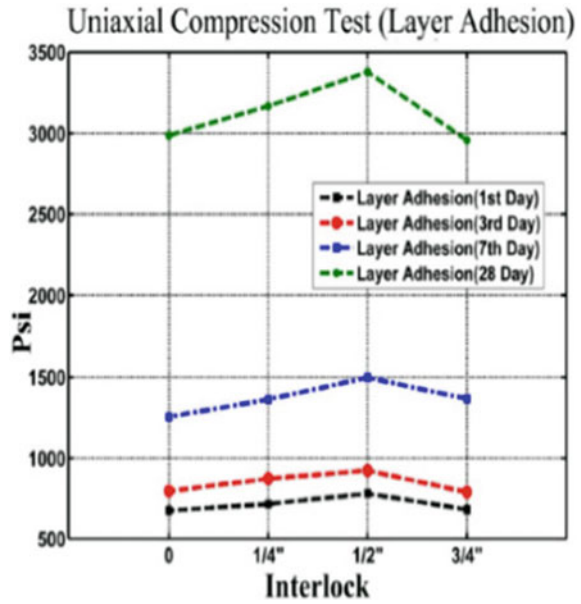


**Fig. 5.11** Bond interface of four types of interlock (Di Carlo 2012)



of the surface and indicate an aggressive pull-out process with high friction between the fibre and the cement matrix, suggesting a strong bond between the layers. In the extruded composite, also a layer of cementitious matrix is seen on the fibre surface, indicating that the de-bonding process is taken place not only at the fibre-matrix interface, but also in the matrix near the fibre.

## Moisture Content and Curing Conditions

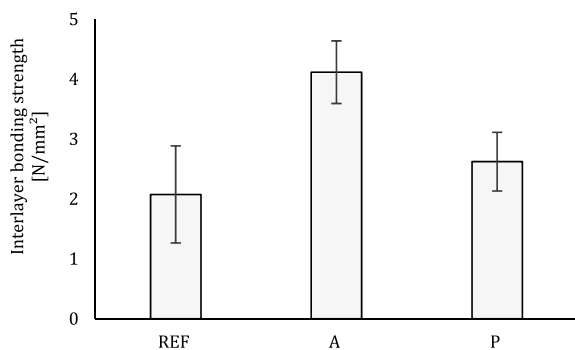
Moisture content of the substrate layer is a very specific issue and literature shows very contradictory results. In the first instance, Emmons and Emmons (1993) mentioned that an excessively dry substrate may absorb too much water from the overlay while excessive moisture in the substrate may clog the pores and prevent absorption of the overlay. Therefore, a saturated substrate with a dry surface will be considered as the best.

However, in case of printed elements, the moisture content of the substrate layer depends on the time gap between the printed layers and also in this case, the results are inconsistent. Sanjayan et al. (2018) observed that a layer interval of 20 min creates the lowest surface moisture content and consequently results in the lowest bonding between two subsequent layers compared to other time intervals (i.e. 10 and 30 min). On the other hand, Van Der Putten et al. (2019) reported a continuing decrease in moisture content for an increasing time gap and a similar trend could be observed for the interlayer bonding strength of the specimens. To overcome the problem of a drying interface, researchers moisturized the substrate layer just before printing the second layer after a predefined time gap. Unfortunately, the results were not as good as expected and the bonding between the layers could not be improved.

The addition of superabsorbent polymers (SAPs) is not only effective for a reduction in autogenous (Wyrzykowski et al. 2018) or plastic (Serpukhov and Mechtcherine 2015) shrinkage, it also has a positive effect on the interlayer bonding strength as reported by Van Der Putten et al. (2019). Due to the creation of a lower tensile stress and a prolonged moisture state of the interface, an increase in bonding strength could be observed for both smaller (SAP A) and bigger (SAP P) sized polymers (Fig. 5.12).

Curing conditions can also affect the bonding between the different layers. Storage of the specimens in laboratory environment will lead to a higher interlayer adhesion compared to specimens stored in outside conditions due to the changing relative humidity. Also curing immediately after the addition of the top layer and this for at least 3–7 days will improve the bonding strength (Santos and Eduardo Nuno Brito Santos 2011).

**Fig. 5.12** Interlayer bonding strength of a 3D printed cementitious material with two different sized SAPs (error bars represent the standard deviation) (Van Der Putten et al. 2019)



## Compressive Strength

Developing higher strength concrete is important because of its effect on bond strength. Beushausen and Alexander (2008) investigated the influence of the new concrete compressive strength on the shear bond between old and new concrete and they found a constant correlation between the two parameters. Neville (1995) also mentioned the increase in tensile strength was the result of an increase in compressive strength, but at a slower rate than shear. Thus, developing higher strength concrete resulted in better adhesion.

## Print Parameters

As mentioned in section ‘Cold joints’, the interval time between layer depositions has a great influence on the structural properties of the printed element. Poorly controlled time gaps result in cold joints at the interface and reduce the overall strength of the structure. To avoid a plane of discontinuity and eliminate long delays, the optimum time lags between the layers should be carefully determined. New layers must be added after the previous layer is sufficiently hardened and before it’s over cured. Therefore, the fabrication speed must be designed to allow layers to bond in a proper way.

In general, different researchers (Panda et al. 2018; Nerella et al. 2019; Le et al. 2012a; Van Der Putten et al. 2019; Tay et al. 2018) reported a decreasing adhesion between the layers with an increasing time gap. The same conclusions were made by Panda et al. (2018). Figure 5.13a shows the effect of an increasing time gap on the interlayer bonding strength of specimens made out of the same batch material. When the applied time gap exceeds the open time of the material, it becomes necessary to print elements with different batch material. The results are shown in Fig. 5.13b. In both cases, an increasing time gap will induce a lower strength.

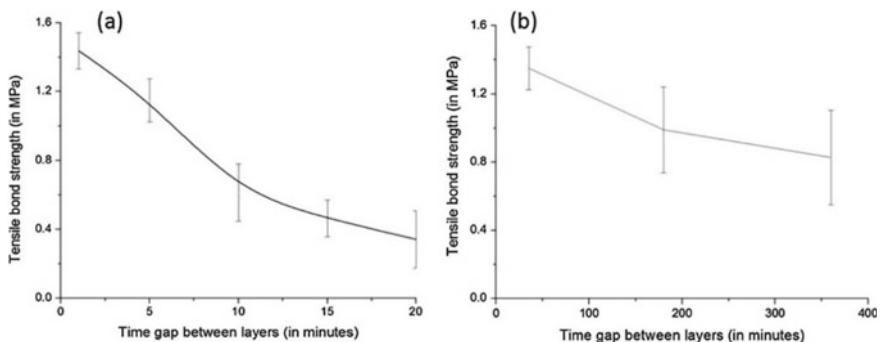


**Fig. 5.13** Effect of an increasing time gap on the interlayer bonding strength of specimens made out of **a** the same and **b** different batch of material (Panda et al. 2018)

Besides the time gap, also the mix composition and the number of layers will have an influence on the bonding strength. Zareiyan and Khoshnevis (2017) stated that mixtures with small aggregates lead to a higher split cylinder test (approximately 80%). The bonding of a four layer element compared with a monolithic part is in general 19% lower.

On the other hand, Sonebi et al. (2001) investigated the effect of the water-to-binder ratio in case of underwater concrete cast on old concrete used for underwater repair. Within this research, two types of binders were used. The first type was a combination of cement with silica fume (10%), while in the second type cement was combined with silica fume (6%) and fly ash (20%). Preliminary results showed that an increased water-to-binder ratio reduces the interlayer bonding and adhesion in slant shear strengths. More specifically, by increasing the water-to-binder ratio from 0.41 to 0.47, the adhesion values were reduced by approximately 40%. It was also reported that the combination of silica fume and fly ash exhibited the greatest adhesion in slant-shear in air and water compared to 100% cement mixture (Mohammed Sonebibond water-to-binder 2001).

### 5.2.6.3 Early Age Shrinkage

In general, shrinkage is one of the major issues for concrete elements as it will lead to unwanted deformations that affect the geometry, durability as well as the mechanical properties. Especially, when the deformations are restrained, shrinkage may lead to (tensile) stresses and cracking that degrade the quality of the printed specimen and increases the amount of preferential ingress paths for chemical substances. Shrinkage can be categorized according to two characteristics: time/duration and chemical and/or physical cause and different types of shrinkage can be distinguished. First of all, after placement and before final setting, a cementitious material subject to desiccation undergoes in fresh state volumetric deformations, referred to as plastic shrinkage. In this phase, the paste is still fresh and can be considered as solid particles suspended in cement–water. The printing environment (e.g. wind, high temperature, low humidity,...) might cause a rapid loss of water to the surroundings by evaporation. As 3D printed elements are manufactured without formwork, their surface area exposed to the environment is larger resulting in an acceleration of the plastic and drying shrinkage behaviour and an increased cracking risk (Fig. 5.14).

A possible solution to reduce plastic and/or drying shrinkage is curing. Both external and internal curing methods are adequate. Le et al. (2012a) showed the effect of the different external curing mechanisms on the early age drying shrinkage of printed specimens and compared them with shrinkage in sprayed concrete (Fig. 5.15).

It was shown that curing in water or damp hessian (burlap) can reduce shrinkage. When comparing the different curing methods, curing in water is the best technique to avoid shrinkage. These conclusions are not surprising, but it leaves the challenging question on how to practically cure 3D printed elements in an efficient and economical way. Manual curing was provided by constantly wetting the printed elements during the first day, which does not seem to be an optimal or efficient solution.



Fig. 5.14 Early age shrinkage cracking in 3D printed walls (Schröfl et al. 2019)

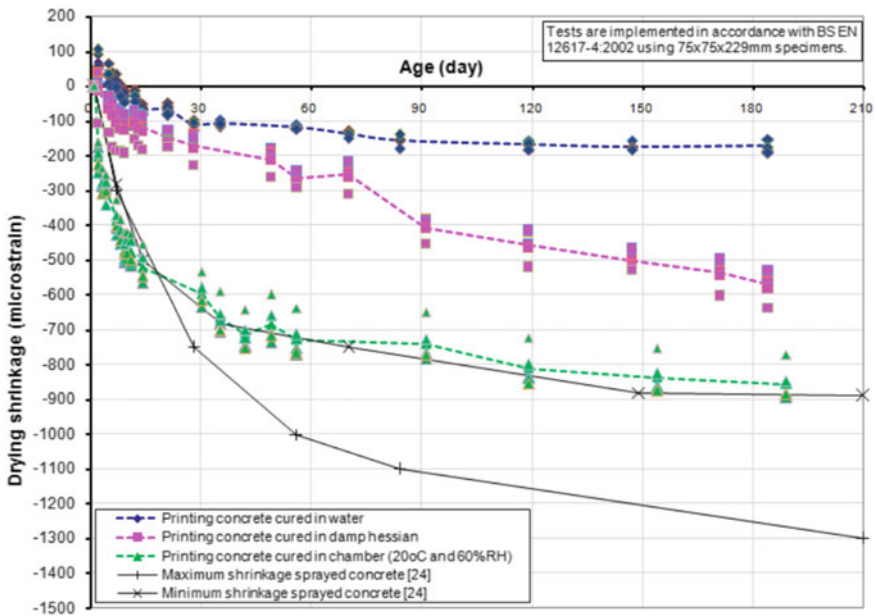


Fig. 5.15 Dry shrinkage in three curing conditions compared with sprayed concretes (Le et al. 2012a)

Internal curing can be obtained by including superabsorbent polymers (SAPs) in the mix design. Different researchers already demonstrated the positive effect of this addition on the shrinkage behaviour. First of all, Serpukov and Mechtcherine (2015) showed that the incorporation of superabsorbent polymers can mitigate plastic shrinkage cracking of both ordinary concrete and strain-hardening cement-based

composites (SHCC). These results were also confirmed during a RILEM inter-laboratory study (2019). Secondly, the addition of SAPs to reduce shrinkage is an ongoing research at Ghent University (Van Der Putten et al. 2019), where different types of polymers (i.e. different sizes but similar chemical composition) are mixed in a 3D printed mortar. After measuring both autogenous and unrestrained (free) shrinkage, preliminary results showed for both shrinkage types that smaller SAPs have the best prospective as they release the entrained water in a more gradual way. They also decrease the nanoporosity in the range of 100 to 500 nm, which is ascribed to a better hydration rate around the SAPs, closing up the smaller pores as well as to their autogenous shrinkage mitigation that reduces the amount of micro-cracking.

Another reason that induces a higher shrinkage risk is the mix composition of the printable mixture. In most 3D printable cementitious materials, the cement content is high to ensure rapid early age strength. This, combined with the lack of coarse aggregates, will induce a higher shrinkage risk. In order to obtain a more durable cementitious mixture, Zareiyan and Khoshnevis (2017) replaced ordinary Portland cement (OPC) partly by Calcium Sulphoaluminate Cement (CSA) and described this replacement as a possible solution to decrease shrinkage. Although CSA increases the concrete strength more rapidly than the concrete shrinkage stress, it also requires about 50% more water than OPC for hydration. As most of the water in the mixture is used for hydration, this replacement can negatively affect the autogenous shrinkage of the material. Further research on this is necessary.

Other researchers (Le et al. 2012a; Serpukhov and Mechtcherine 2015; Zingg et al. 2009; Mechtcherine et al. 2014) used fibres (steel fibres and polymeric microfibers respectively) to exploit their potential and their effect on shrinkage and deformation in plastic state. As their addition reduces the formation of fine cracks, they decrease plastic shrinkage cracking, resulting in a more durable material.

#### 5.2.6.4 Reinforcement

Printed cement-based materials are quasi-brittle like casted materials, but as they are often fine-grained they tend to be more brittle and their failure behaviour is mostly characterized by a low ratio of tensile to compressive strength and a low ultimate tensile strain compared to their fracture strain. Although this implies that fundamental structural behaviour of digitally fabricated reinforced elements will not differ from conventionally build reinforced elements, the fabrication of novel reinforced concrete structures using digital technologies necessarily requires the definition of suitable strategies for reinforcement implementation. The successful integration of existing reinforcement systems (steel rebar, rods, wires, fibres or filaments) will indeed allow for printed concrete structures to be designed using standard structural codes as the same type of reinforcement is used (material, reinforcement degree, position). However, as the integration of reinforcement has to be compatible with either the specific printing technique adopted for the structural element production as with the shape, more specific properties related to the print process (e.g. anisotropy, weak interfaces and reduced inter-layer bonding) also have to be considered (Asprone et al.



**Table 5.1** Grouping of possible approaches to address reinforcement integration in DFC (Asprone et al. 2018)

<u>By structural principle</u>	
Ductile printing material <i>e.g. fibre reinforced materials</i>	Rebar reinforcement is not required and fibres are able to provide the tensile strength and the ductility that are required by the application
DFC composite: <i>e.g. passive reinforcement</i>	Rebar reinforcement is needed and it can also be installed with automated/robotized processes
Compression load structures <i>e.g. due to shape or pre-stress</i>	Additional tensile reinforcement is not required
Hybrid solutions <i>e.g. combining any of the previous cases</i>	
<u>By stage of the manufacturing process</u>	
Before manufacturing	Reinforcement is arranged and placed in the final configuration before concrete deposition through a digital fabrication method
During manufacturing	Reinforcement is added during concrete manufacturing or belongs to the material itself (e.g. fibres)
After manufacturing	Reinforcement is installed once the concrete element has been manufactured through a digital fabrication method

2018). The different ways of implementation can be classified by structural principle or by place in the manufacturing process, as listed in Table 5.1 (Asprone et al. 2018).

The most basic approach is to use the printed concrete not as the primary structural material, but rather as a formwork into which conventional steel reinforcement bars are positioned and which is subsequently filled with cast concrete. An alternative construction way is to place the reinforcement first and subsequently deposit the concrete around it. This approach is applied in the Smart Dynamic Casting (SDC) (Lloret et al. 2017) project, in which a dynamic formwork slip-forms the geometry around a pre-placed reinforcement mesh. An updated version of this technique is the application of Mesh Moulding (MM), a digital fabrication technique in which the reinforcement and formwork are unified in a robotically controlled system (Hack et al. 2017; Hack and Lauer 2014). With this technique, conventional deformed bars in grid form (40 × 40 mm) with diameters equal to 4.5 or 6 mm are used and the concrete is continuously cast in the core of the structure, reducing the potential layering issues.

Other developments aim to create reinforcement methods that are integrated during the printing process and the most advanced technique is currently under development at the TU/e, where a reinforcement cable is directly entrained during printing. This wired reinforcement type is not only strong and ductile, but also very flexible to produce concrete elements with complex geometries. Several experiments have already been conducted, using three different galvanized cables with ultimate tensile loads and diameters ranging from 420 to 1925 N and 0.63 to 1.20 mm respectively, having a significant ductility. However, due to the layered print process, cable slippage was a dominant failure mechanism when higher strength cables were applied.

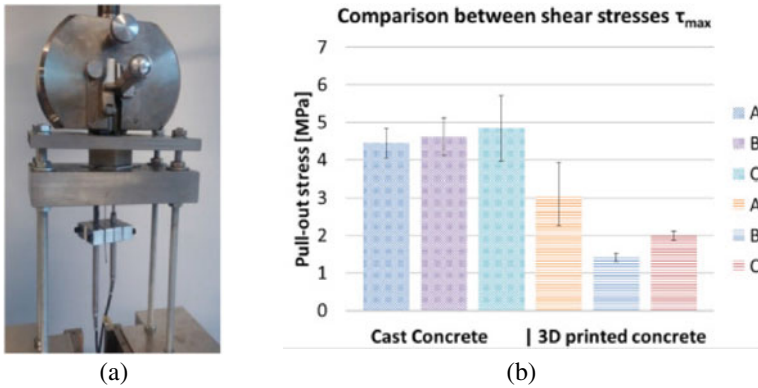


**Fig. 5.16** Pull-out test on concrete with embedded reinforcement cable: **a** experimental set-up with printed specimen, **b** comparison of average bond strengths in cast and printed concrete for 3 different cables (Bos et al. 2017)

This could be attributed to the poorer concrete compaction around the cables and the induction of peak stresses at the loaded side of the cables, inducing gradual debonding before the cable strength was fully reached. As can be seen in Fig. 5.16, the shear stress of printed specimens, based on pull-out tests, is only one third of the shear stress measured in case of cast concrete and is also lower than the calculated values.

The differences between the calculated values, based on model codes, and the experimental results can be attributed to the design model and the fact that these basic models are primarily based on the concrete quality, with some additional parameters accounting for various conditions. For instance, Eurocode2 (EC2) defines the design bond strength based on Eq. (5.2):

$$f_{bd} = 2,25 \cdot \eta_1 \cdot \eta_2 \cdot f_{ctd} \tag{5.2}$$

where  $\eta_1$  depends on the embedment quality,  $\eta_2$  on the reinforcement diameter, while  $f_{ctd}$  is the design tensile strength of the concrete. However, as listed below, the conditions for reinforced printed concrete are rather different for normal cast concrete and different parameters related to the printing process are not taken into account.

- The strength class and maximum grain size of printed mortars is significantly lower than the ones applied in case of ordinary structural concrete buildings;
- The stress–strain behaviour of the cables differs from the normal reinforcement steel bars, indicating a higher linear elastic strength limit and a lower stiffness;
- A smooth cable surface and lower dilatancy resistance, which influences the proportion between adhesive and dilatancy resistance;
- In normal calculation models, concrete is considered as homogeneous while printed mortars behave in an anisotropic way. The print process will also induce

a higher amount of voids and air bubbles, resulting in a poorer bonding strength and adhesion between both components;

- The required limitations (e.g. minimal diameter and minimal embedment length) can often not be achieved due to the geometrical limitations of the printed element.

In spite of the many advantages of this technique, the main drawback remains the orientation of the reinforcement that is necessarily in the direction of the printed filament. A possible way to cope with the geometrical freedom is the combination of printed concrete and steel by using gas-metal arc welding (Mechtcherine et al. 2018). Although this technique shows high potential, preliminary results showed that the printed steel bars exhibit a yield stress and tensile strength of approximately 20% less, but they also received a higher strain capacity compared with conventional reinforcement bars. The bonding between the printed steel bars and the concrete was comparable with the bonding performance of conventional steel bars. Microstructural investigations of the fracture surfaces showed less ductile regions in case of printed elements, probably caused by the rapid cooling of the melted metal during the welding process (Mechtcherine et al. 2018).

A third possibility to introduce passive reinforcement is to integrate it with the concrete after the fabrication process. The external reinforcement makes it possible to incorporate a higher amount of steel reinforcement. The preliminary outcomes of the experimental activities carried out so far have demonstrated that the initial flexural stiffness of the printed RC beam is comparable with an equivalent RC beam, whereas the overall nonlinear flexural behaviour is influenced by local failure mechanism, i.e. shear damage at the interfaces and steel–concrete anchoring failure. For a limited number of structural applications there are other possibilities to overcome the necessity of tensile capacity and ductility by designing structures loaded in compression only or by the application of a certain pre-stress. The latter has a broader application range due to its capacity to counteract tensile stresses. However, the application of a certain pre-stress limits the form of freedom and introduces an additional step in the manufacturing process.

Another possibility is mixing a certain amount of short fibres into the cementitious material before deposition. This is well known as a straight forward and efficient way to considerably enhance the mechanical performance of concrete. Researchers investigated different types of fibres (e.g. carbon fibres, glass fibres, basalt fibres) with different lengths and volume%. In fresh state, a strong alignment of these fibres in the direction of the flow due to extrusion process could be observed. In the hardened state, a higher flexural strength and tensile strength could be obtained (Le et al. 2012a; Nematollahi et al. 2018; Christ et al. 2015).

Nematollahi et al. (2018) investigated the effect of polypropylene (PP) fibres (0.25 and 1.00 vol%) on the properties of a 3D printed fibre reinforced geopolymer mortar. Fibre addition influenced the compressive strengths positively only when loading was applied perpendicular to the interface. This phenomenon can be traced back to the preferential fibre alignment parallel to the direction of extrusion. The addition of fibres significantly enhanced the flexural performance of the printed samples. The use of fibre dosages equal to 0.75 and 1.00 vol% caused deflection-hardening behaviour

of the 3D printed geopolymers and higher fracture energy. However, an increase in fibre volume caused a minor reduction in interlayer bonding strength.

With respect to the structural performances, the use of strain-hardening cement-based composites (SHCC) is particularly promising (Curosu et al. 2017). Under uniaxial tensile loading, SHCC exhibit quasi-ductile behaviour with a strain capacity up to several percent, resulting from the formation of multiple fine cracks prior to reaching the tensile strength of the composite. Ogura et al. (2018) developed and characterized a series of printable SHCC containing 1.00% to 1.50 vol% of high-density polyethylene (HDPE) microfibers. The specimens extracted from the printed walls exhibited multiple fine cracks and pronounced strain-hardening characteristics under uniaxial tensile loading, even for fibre volume fractions as low as 1.00 vol%. In fact, the strain-hardening characteristics of the printed elements were superior to those of mould-cast SHCC specimens (Fig. 5.17). However, the mechanical performance of printed SHCC in the direction perpendicular to layer-to-layer interfaces is expected to be much less convincing. The anisotropic behaviour and possible mitigating measures should be investigated in detail both for SHCC and other FRC in the context of digital concrete (Fig. 5.18).

A new technique, developed at China Building Materials Academy and the university of Catalonia, uses staplers as reinforcement. As the printer head includes both a printing nozzle and a stapler, the reinforcement and printing process occurs simultaneously and in a periodical manner. The stapler pushes a wire profile into the printed clay for a half a layer deep and these staples profiles form an over mesh structure (Wang et al. 2018). The big advantage of this technique is that the staples profiles form an overall mesh structure that fuses the printed layers together and compliments the overall structural soundness of the print. Integration of this process in large scale 3D concrete printing industry could push the geometrical limits of what could be realized (i.e. increased printing height and inclination maximum, better support for openings,..) as different geometries of staplers can be used (kumarji and Geneidy 2019).

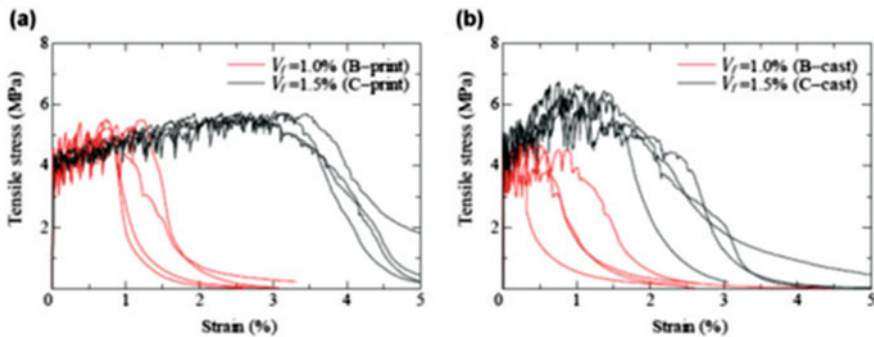


**Fig. 5.17** Stress–strain curves obtained from uniaxial tension tests on **a** printed specimens and **b** mould-cast specimens (Ogura et al. 2018)

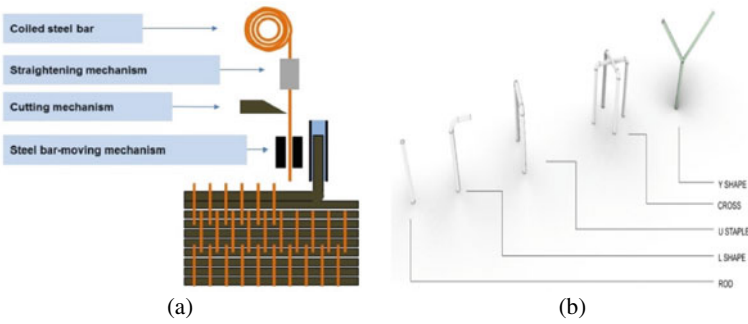


**Fig. 5.18** Simultaneous reinforcement of concrete while 3D printing: **a** Schematic diagram of reinforcement (Wang et al. 2018), **b** Different sized stapler geometries (Kumarji and Geneidy 2019)

### 5.3 Sampling and Quality Control

To measure the mechanical properties and to control the quality of printed elements, different specimens were saw cut from an original printed element and mostly compared with traditionally cast concrete elements, as shown in Fig. 5.19. In Le et al. (2012a), cubes, cylinders and prisms with different dimensions were taken from a 3D printed structure and tested in three loading directions (parallel to the side surface, parallel to the printing surface and parallel to the cut surface) to investigate the anisotropic behaviour (Bos et al. 2016).

Depending on the type of printing processes, voids of various magnitudes can form between the filaments, affecting the hardened properties and decreasing the overall structural stability. The shape of the filament has a significant influence on the voids at the layer-interfaces, with circular filaments leading to intrinsic voids

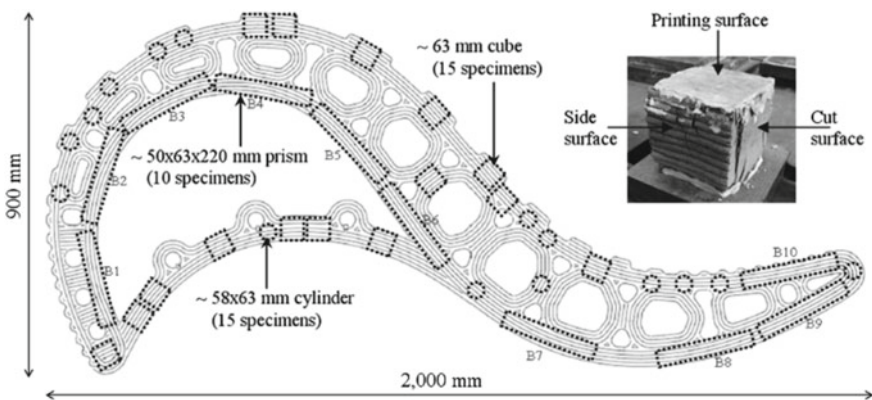


**Fig. 5.19** Diagram showing positions of extracted printed specimens (Le et al. 2012a)

between the layers (Fig. 5.20). Voids can also form due to feeding irregularities, deposition inaccuracies (e.g. nozzle oscillations) and inadequate rheology. Therefore, void measurements based on image analysis can be used to control the quality of the extracted concrete and to classify them in different categories as shown in Fig. 5.20. In mould-cast concrete, the amount of voids ranging from 0.2–4.0 mm size was 3.8%. In poorly printed concrete, the amount of voids was higher (4.8%) and in case of well printed specimens, only 1% voids were measured (Fig. 5.21).

Weger et al. (2018a, b) showed that the density (or porosity) of objects manufactured with the particle-bed based 3D printing method selective paste intrusion (SPI) depends on the penetration behaviour of the cement paste into the particle-bed. That penetration behaviour is affected by the mutual interaction of the rheological and thus the flow properties of the binder (cement paste) and the flow resistance of the particle-bed (aggregates). As the binder penetrates the layers of the aggregate sufficiently, the density of the material achieves values between  $2200 \text{ kg/m}^3$  and  $2400 \text{ kg/m}^3$ , comparable to normal mould-cast concrete specimen. However, as the binder shows insufficient penetration, the density decreases (porosity increases) which results in decreased strength and durability performance. Furthermore, Weger et al. (2018a, b) showed that the density of the specimens is a proper value to control the production quality (penetration ratio) of SPI objects, see Fig. 5.20.

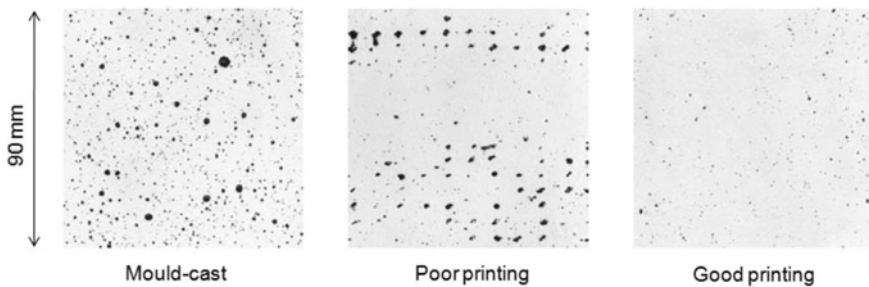


**Fig. 5.20** Quality control based on voids measurements (Le et al. 2012a)

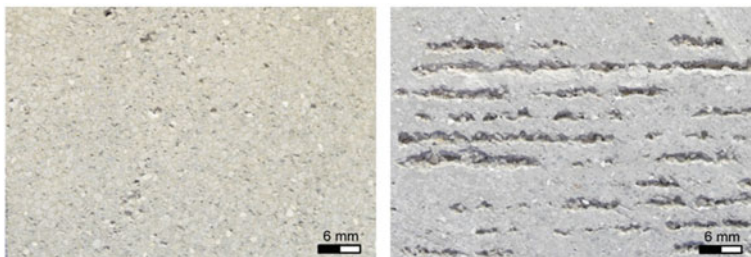


**Fig. 5.21** The particle-bed based 3D printing method selective paste intrusion. Cut through a cross section, left: with sufficient penetration of the layers of the particle-bed by the cement paste, right: with a non-sufficient penetration resulting in a decreased density and increased porosity (Weger et al. 2016a, b, 2018b)

**Table 5.2** Dimensions and binder type of the samples used for mechanical testing of 3D printed structures (Le et al. 2012a; Wolfs et al. 2019; Van Der Putten 2019; Rahul et al. 2019)

Filament [mm]	Compression (Cube size) [mm]	Tensile bond [mm]	Beam (Flexural) [mm]	Beam (Shrinkage) [mm]	Bindertype
Ø 9	100	Ø 58	100 × 100x400	75 × 75x229	CEM I, FA, SF
Ø 25	50		40 × 40x160		GP
20 × 20 30 × 15		~ 30 x ~ 90			FA/GP
			6 × 12x60		OPC, SF
			300 × 50x80		
			25 × 25x120		OPC

## 5.4 Mechanical Performance of 3D Printed Specimens

### 5.4.1 Measurements

Printed materials can be as good and as strong as cast material and it is possible to achieve materials with a higher density than cast equivalents, however the reproduction of ‘as good as cast’ properties on a commercial manufacturing scale has yet to be demonstrated. Creating solid objects from a conglomeration of extruded filaments predisposes printed objects to anisotropy, which influences end use performance.

Table 5.2 provides details of the papers that have investigated hardened properties as they are affected by filament bonding. Samples tended to be saw cut, or cored from printed materials.

There is no consistent format for describing the printing process parameters such as nozzle size, layer height, filament dimensions, print speed, component size from which the layers are taken or layer cycle times but all of them will have an influence on the mechanical properties and require to be taken into account when measuring and analysing the mechanical properties. The discrepancy in reporting process parameters and the variability in test geometry reported in Table 5.2, demonstrate the need for standardized testing methods as they exist in case of normal cast concrete. In the sections below, an overview of the test methods used for characterization of the mechanical performance of printed material can be found.

### 5.4.2 Compressive Strength

Most research groups (Panda et al. 2017; Le et al. 2012a; Paul et al. 2018; Le et al. 2012b; Van Zijl et al. 2016; Feng et al. 2015; Shakor et al. 2017) determine the compressive strength of printable concretes by means of a uniaxial compression test

on cubic or cylindrical specimens, similar to traditionally cast concrete. To examine the effect of the layered structure and the anisotropic behaviour, different testing directions are taken into account as mentioned in Section ‘Anisotropy’.

Many researchers reported anisotropy in compressive strengths (Panda et al. 2017; Nerella et al. 2019; Marchment et al. 2017). In addition to the mixture composition, compressive strength of printed elements depends on deposition time interval, process parameters and testing setup. Panda et al. (2019) and Sanjayam et al. (Wyrzykowski et al. 2018) explained the anisotropic behaviour of printed elements under compression loading using a hypothesis based on direction-dependent compaction. Nerella et al. tested printed specimens under compression in three loading cases (Fig. 5.22). A consistent conclusion based on these measurements could not be drawn, but the highest compressive strength was obtained in direction Par2 (Fig. 5.22, Orientation III Fig. 5.2). Although the differences in measured strengths were not very pronounced, they could be explained based on two phenomena:

- Differential water evaporation;
- Different failure criteria;

In addition to the uniaxial compression tests, Nerella et al. (2019), Venkatesh et al. (2017) hypothesized that the extent of the (weak) interface area lying outside the tri-axial compressive core and the size of individual defects (weak) interfaces lying in the crossing of shear planes are factors decisive for the observed load level at failure. In the specimens they investigated, the weak interface area outside the tri-axial compressive zone is the largest in case of a perpendicular loading (Orientation I, Fig. 5.2), which may explain why the strength values measured in these directions are the lowest. Another cause for the anisotropic behaviour of printed elements under compression loading is the varying degrees of compression that printed layers

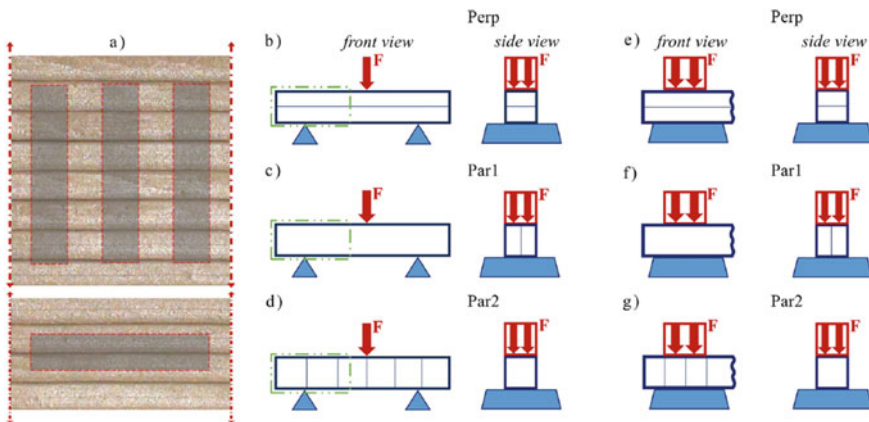


**Fig. 5.22** Representation of specimen extraction from a printed concrete wall as reported by Nerella et al. (2019)



go through in various directions, resulting in corresponding compressive strength variation (Sanjayan et al. 2018).

### 5.4.3 Flexural Strength

Another parameter in defining the mechanical behaviour of a specimen is measuring the flexural strength. Most researchers (Panda et al. 2017; Le et al. 2012a; Paul et al. 2018; Van Zijl et al. 2016; Feng et al. 2015) determine this parameter by means of a 3-point bending test on prismatic specimens, again very similar to traditionally cast concrete. To examine the effect of the layered structure and the anisotropic behaviour, different testing directions are taken into account (Fig. 5.2).

Rahul et al. (2019) proved the dependency of the flexural strength on the region subjected to the maximum bending moment in the three-point bending test. When tested along Orientation I, the maximum bending moment and corresponding maximum flexural stress occurs at the interface and showed values that were 32% lower. However, in case of parallel testing (Orientation II/III), a flexural strength increase of 20% could be observed as the maximum flexural stress.

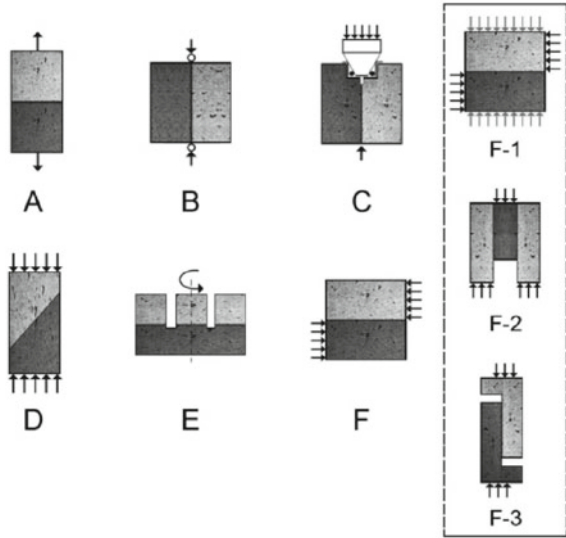
Lowke et al. (2015) showed flexural strength up to 5.3 MPa (Orientation I, Fig. 5.2) using the particle-bed based 3D printing method selective binder (cement) activation. The achieved flexural strength values were strongly connected to the water distribution between the layers.

### 5.4.4 Tensile Strength (Inter-Layer Bonding Strength)

To produce homogeneous structures and to ensure the structural stability, bonding between the different layers is considered as one of the key parameters. In case of a weak interface, cold joints can appear which can induce mechanical strength loss of more than 40% and a local increase of the porosity (Roussel and Cussigh 2008).

To understand bond mechanisms, it is essential to measure bond strength at the interface between new and old layers. A lot of test methods are developed for measuring the bond strength of old and new concrete. These test results vary substantially based on loading rate, specimen size, experimental set-up, etc. The existing methods can be divided into several categories. The first category measures the bond under tensile stress. The most common test set-up in this category is the pull-off test (ASTM D7234-05, Fig. 5.23A). This test evaluates the bond strength in tension of the interface and is highly dependent on the eccentricity of the applied load. Consequently, the results of this test method can be very scattered. When the tensile strength is lower than the bonding strength, the specimen will break at the layers and quantifying interlayer adhesion is not possible. Another test method in this category is the splitting test (ASTM C496, Fig. 5.23B). This test has a higher efficiency compared with the pull-off test because only a very small part of the bonded plate is

**Fig. 5.23** Interface bond strength test methods (Di Carlo 2017)



subjected to the maximum stress. An extension of the latter is the wedge splitting test (Fig. 5.23C). In this case, the interface strength is measured by fracture mechanics parameters (tensile interface strength and fracture energy).

The second category measures the bond under shear stress and is called direct shear bond methods. An example of this is the direct shear test (Fig. 5.23F). The bond surface is subjected to shear stress and small bending stress. The smaller stress concentration leads to a smaller scatter in test results. The third category is the one that combines shear and compression. An example of this one is the slant shear test according to ASTM C882/C882M (Fig. 5.23D). This test set-up uses a square prism or a cylindrical sample made of two identical halves bonded at 30° or 45° and tested under axial compression. During loading, the interface surface is under compression.

The choice of a proper bond strength test method is crucial, and different test methods cause distinct interface stress conditions in specimens. Consequently, the test results will differ when comparing different test methods. Literature shows that the measured bond strength decreases with the test method in the following order: slant shear, direct shear, splitting and pull-off (Aysha et al. 2014). The appropriate test for a particular case is the one for which the nature of loading is the most similar to that of stress conditions of the actual structure.

In case of 3D printing of concrete, the interlayer adhesion between the layers can be measured by applying pull-off tests (Zareiyan and Khoshnevis 2017; Panda et al. 2018; Le et al. 2012a; Zareiyan and Khoshnevis 2017) equipped with cubic or cylindrical specimens, saw cut or drilled from an original printed element. During these measurements, researchers reported the importance of failure in the interlayer and a very specific specimen preparation is required. First of all, high deviations on specimen dimensions should be avoided as they result in a high scatter due to the rather small specimen size. The alignment of the specimens in the test equipment is

also an important factor in order to avoid bending moments and measure only the bonding between the layers.

An updated version of the pull-off tests is developed and reported by Rahul et al. (2019) as depicted in Fig. 5.24. The interface of the specimen is placed horizontally in the grooves of upper and lower jaws of fixture. The jaws were then pulled apart at a constant displacement rate (i.e. 0.1 mm/min). The failure is divided by the cross-sectional area of the cylinder to obtain the bond shear strength. To induce only tensile stresses at the bonding area, Liu et al. (2019) developed a new method called cross-bonding (Fig. 5.25). This method enables the evaluation of both tensile strength and interfacial shear strength. In addition with this method, a decreasing trend in interlayer bonding strength could be observed in case of an increased interlayer time interval.

When comparing different test methods for measuring the bond strength, two distinctive failure modes (in cast specimens) can be observed: adhesive and cohesive failure. Adhesive failure or interface de-bonding occurs at the interface whenever the bond strength is reached. Due to mechanical interlocking, small particles were observed at the interface of these failed specimens. On the other side, cohesive failure occurs in the bulk by concrete crushing. Figure 5.26 gives an example of

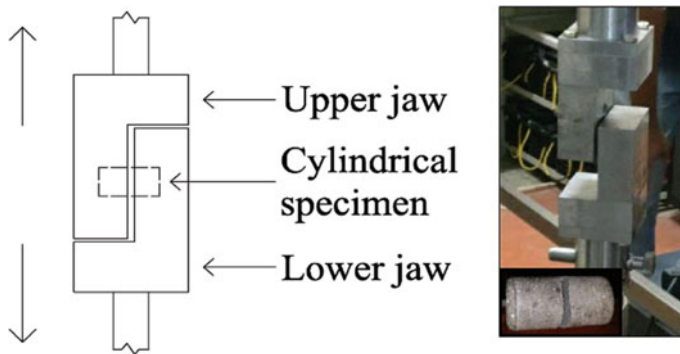


Fig. 5.24 Fixture for bond shear test (Rahul et al. 2019)

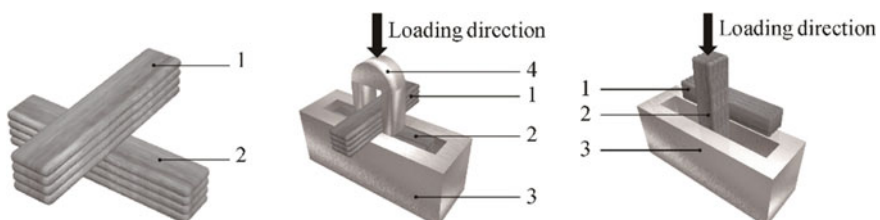
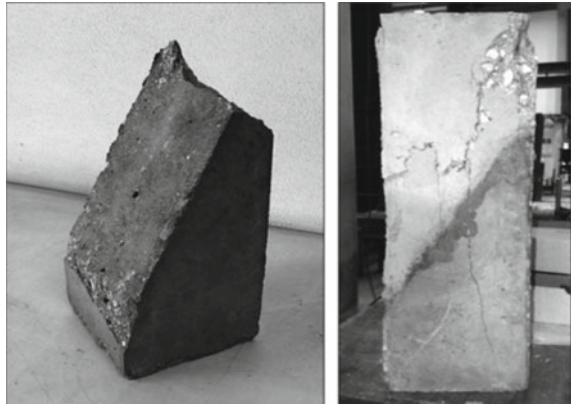


Fig. 5.25 Cross-bonding method (1. Upper printed block, 2. Bottom printed block, 3. Bed frame, 4. U-type loading head) (Liu et al. 2019)

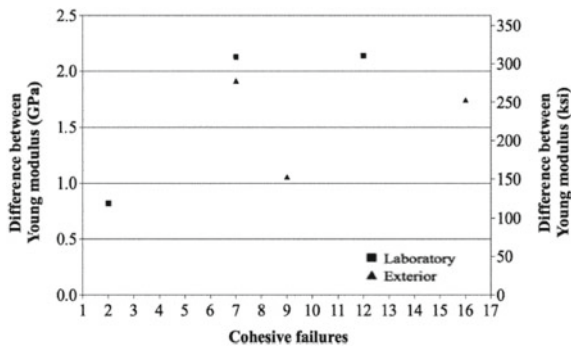
**Fig. 5.26** Failure mode for slant shear test: adhesive (left) and cohesive (right) (Santos and Eduardo Nuno Brito Santos 2011)



these failure modes. Splitting test specimens all presented adhesive failures, while slant shear specimens presented both (Santos and Eduardo Nuno Brito Santos 2011).

The failure mode of a specific element can be influenced by the surface roughness and the compressive strength. First of all, the number of cohesive failures increases when increasing the surface roughness of the interface and this for two curing conditions (lab environment and in-situ environment). Secondly, the failure mode will also be influenced by the compressive strength of the material. The compressive strength of two layers, elaborated on a different time, will be correlated with different Young’s modulus of each layer. Consequently, this varying modulus will induce differential stiffness of the composite concrete member and will change the stress distribution at the interface. Literature showed that the number of cohesive failures increases with the increase of the difference between the Young’s modulus of each concrete layer, as shown in Fig. 5.27. The existence of a correlation between the cohesive failure and the differential stiffness is extremely important because it means that it is possible to change the failure mode of a composite concrete member by designing the differential stiffness between both concrete layers.

**Fig. 5.27** Differential stiffness versus cohesive failures (Santos and Eduardo Nuno Brito Santos 2011)



## 5.5 Durability and Transport Mechanisms in 3D Printed Materials

### 5.5.1 Fire Resistance

Besides the above mentioned mechanical properties of the cementitious material, also the fire resistance plays an important role when implementing 3DP materials in real buildings. Within the Civil and Environmental Engineering Department of IMT Lille, some preliminary fire resistance tests have already been performed on concrete slabs, fabricated with a combination of crushed limestone sand, ordinary Portland cement CEM I 52.5 and superplasticizer to cement ratio equal to 1.5%.

During these tests, two slabs have been extracted from a square test specimen and were placed on top of each other in a concrete frame, covering one side of the gas oven used to apply the thermal stress and soliciting them on one side with a conventional ISO 834–1 time–temperature curve. No mechanical restriction was applied to the edges of the slabs, which could expand freely. The slabs were exposed to fire for more than 120 min and temperature measurements on the unexposed face of the slabs as well as on the plate thermometers in the oven have been performed. The position of the concrete slabs was aligned with the external face of the support wall and thermocouples were fixed on the edges of the slabs (Fig. 5.28) (D’Hondt et al. 2019).

Preliminary test results showed a fire resistance of the material without marked scaling or cracking. The temperature measurements in the oven and on the unexposed side reveal a high thermal gradient (higher than 100 °C/cm) over the thickness of the slab (about 5 cm). This thermal gradient induces a thermal curvature of the slabs with a maximum distortion close to 3 mm (directed towards the oven). Nevertheless, as can be seen on Fig. 5.29, the two slabs seem to be working together while they

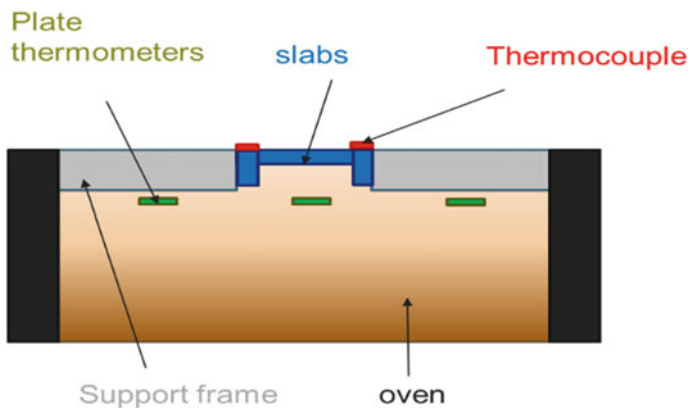
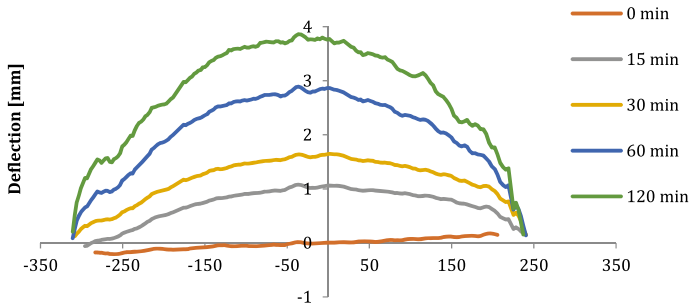


Fig. 5.28 Slab alignment in the oven (D’Hondt et al. 2019)



**Fig. 5.29** Measured concrete slab deflection after different times of fire exposure (D'Hondt et al. 2019)

should be mechanically independent of each other. The material also exhibits a structural integrity and airtightness after 120 min of heating and cooling. The post-cooling observations reveal micro cracks over the height of the slabs, next to the horizontal interfaces. Progressive crumbling characterized by the loss of powdered material on the exposed face has been noticed over time after cooling and storage. All these phenomena occurred on both slabs, suggesting an uniformity of the properties governing the fire behaviour.

Recent research performed at Centre Scientifique et Technique du Bâtiment (CSTB) showed the influence on the compressive strength of printed specimens after fire exposure. The compression tests on these samples were performed perpendicularly and alongside the axis of the cord. According to the test results, the cold material performed a quasi-isotropic behaviour. After fire exposure, a reduction of 73% was obtained when testing the samples alongside the axis of the cord. Due to the high damage level after fire exposure, a compression test perpendicularly to the axis of the cord could not be performed (D'Hondt et al. 2019).

### 5.5.2 Transport Mechanisms

Schröfl et al. (2019) studied water uptake into two formulations of 3D-printed concrete via capillary suction using neutron radiography. The samples varied in their layer-to-layer deposition time intervals and the use of different binders. Time intervals of 2 and 13 min were short enough to avoid preferential capillary suction at interlayer bonding areas in the fine-grained printable concretes containing supplementary cementitious materials. An increase in time interval to 24 h gave rise to quick capillary suction through the layer-to-layer interfaces (Fig. 5.30). However, moisture did not redistribute into the matrix regions from the interfaces. For mixtures with ordinary Portland cement as sole binder combined with an additional superabsorbent polymer (SAP), the short layer-to-layer deposition interval of two minutes resulted in tight interlayer bonds with quasi-null capillary suction. Intervals of 13 and 36 min,

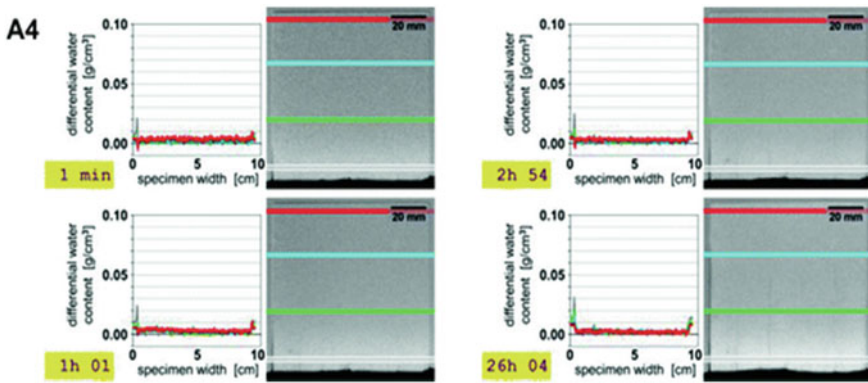


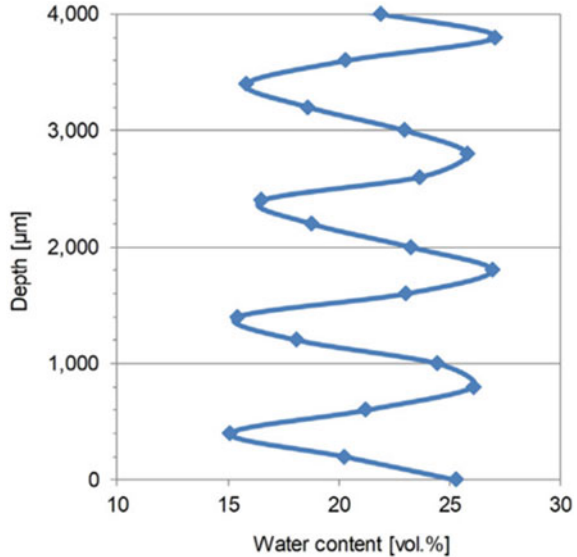
**Fig. 5.30** Differential water content of specimens with one 24 h and three two minute layer-to-layer deposition interval (A19) at four heights indicated in the images and neutron radiography referenced differential images (Schröfl et al. 2019)

however, resulted in partially quick and intense absorption of water and immediate absorption by adjacent SAP particles.

Van Der Putten et al. investigated the effect of different print parameters on the capillary water uptake of multi-layered printed specimens by means of neutron radiography. Within these investigations, two till four layered specimens, fabricated with different printing speeds and/or different mix compositions (with and without the addition of superabsorbent polymers) were exposed to a water basis with different surfaces (bottom and front surface). Preliminary results showed that, when the bottom surface of the samples was exposed to water, no uniform water ingress front could be observed in case of higher printing speeds due to the non-uniform distribution of the sand particles within the bulk material, as proven in other research (Van Der Putten et al. 2019). When the front layer was exposed to the water, all series showed a uniform water ingress front with no preferential water ingress at the interfaces due to a zero minute time gap. The water uptake in the upper layer was always higher due to the lower compaction of this layer during the printing process. For every printing speed and every water exposure surface, compositions with SAPs showed a higher water uptake ability due to the increased porosity of the samples.

Lowke et al. (2015, 2018) showed that using the particle-bed based 3D printing method selective binder (cement) activation, the strength of the material is depending on the water distribution between the layers driven by the surface tension of the water, the adsorption behaviour (Lowke et al. 2018) onto the particle surfaces as well as by capillary force (Boyce et al. 2016). If the amount of water is insufficient, it does not homogeneously penetrate the height of the particle layer. Hence, unhydrated areas remain in deeper parts of the particle layer resulting in a weak layer bonding. In particular at low water-to-cement ratios, insufficient hydrated areas were clearly visible in the cross-section of the printed specimens. To validate this hypothesis, the water distribution over four 1.0 mm layers of an additively printed specimen was determined by one-sided  $^1\text{H}$  NMR (Fig. 5.31). The water content significantly

**Fig. 5.31** Water distribution in the layers determined by one-sided  $^1\text{H}$  NMR spectroscopy (Lowke et al. 2015)



oscillates in accordance with high water content at the top region of the layer and a significantly lower water content at the bottom region (Fig. 5.29). To enhance inter-layer bonding and thus strength, the interlayer water gradient should be minimized by modification of either the particle packing or the water application technique. One method is to increase the water pressure in by jetting the water into particle-bed instead of spraying it onto the surface of the particle-bed.

### 5.5.3 Pore Structure and Porosity

One of the main disadvantages of concrete printing is the fact that voids can form easily between the filaments. This might not only affect the hardened properties significantly, but also the durability of the material as these voids are ideal ingress paths for chemical substances. Only a few researches (Le et al. 2012a; Hambach and Volkmer 2017; Peled and Shah 2003; Shakor et al. 2017) investigated already the creation of voids and the porosity of the printed elements.

Le et al. (2012a) concluded that the pore size distribution is significantly affected by the way elements are produced. The void measurements, showed in Fig. 5.32, were performed by image analyses. The surfaces of different concrete elements (mould cast, poor and good printed specimens) were polished and sprayed with black paint. Once dry, a white paint was rolled on to reveal the voids that retained the black colour. Afterwards, the surface was scanned and the image was transferred to a void measuring software which counted the number of voids in a specific area. As can be seen in Fig. 5.32, the area of small voids (ranging from 0.2–1.6 mm) in



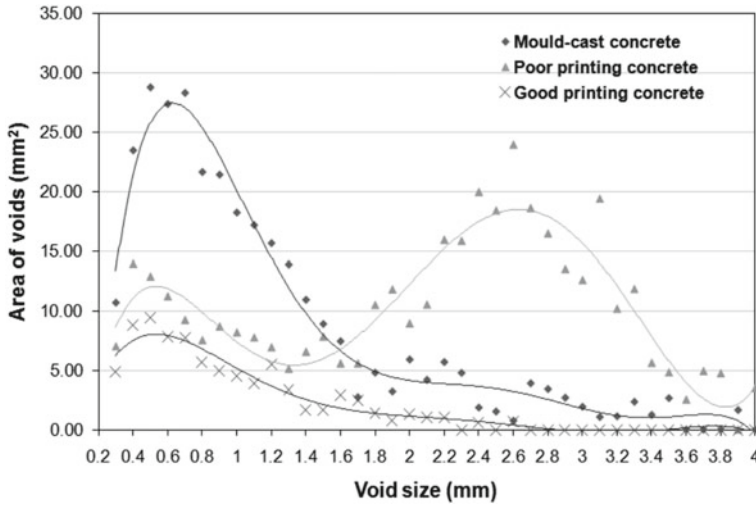


**Fig. 5.32** Distribution of voids in three concrete groups (Le et al. 2012a)

mould-cast concrete is much higher compared to 3D printed elements. The amount of larger voids in poorly printed concrete was significantly higher compared with mould casted concrete and is mostly located between the printed filaments. This is also indicated in Fig. 5.20 (Section ‘Sampling and quality control’). Once these voids can be eliminated, for example by correctly controlling the printing path and concrete rheology, a denser structure can be formed with a smaller amount of voids. The distribution of voids in good printed concrete agreed well with this as the area of 0.2–4 mm voids was significantly lower than both mould-cast and poor printed concrete.

Van Der Putten et al. (2019) investigated intensively the pore structure of printed specimens, manufactured with different time gaps, by means of Mercury Intrusion Porosity measurements (MIP) measurements. For these investigations, drilled specimens were sawn in different pieces to measure the pore distribution of the upper, lower and interlayer separately. First results showed that in case of no time gap, the pore size distribution is comparable for every region. Higher interlayer time intervals not only increased the smaller pores in the centre and lower part of the specimen but also the amount of pores in the upper part. In this research, BSE-SEM analyses were also used for the determination of the pores formed during the hydration process. First observations confirm the above mentioned conclusions. More specifically, in case of a higher time gap, the capillary pores increase due to the moisture exchange between two printed layers with a different moisture content of the layers.

Other researchers (Peled and Shah 2003) investigated not only the effect of the construction process but also the addition of fly ash and fibres by measuring the pore size distribution while conducting Mercury Intrusion Porosimetry (MIP) tests. During these tests, a specific pressure corresponds to an aperture of a pore, and the amount of mercury intrusion approximates to the pores volume. Based on this, the

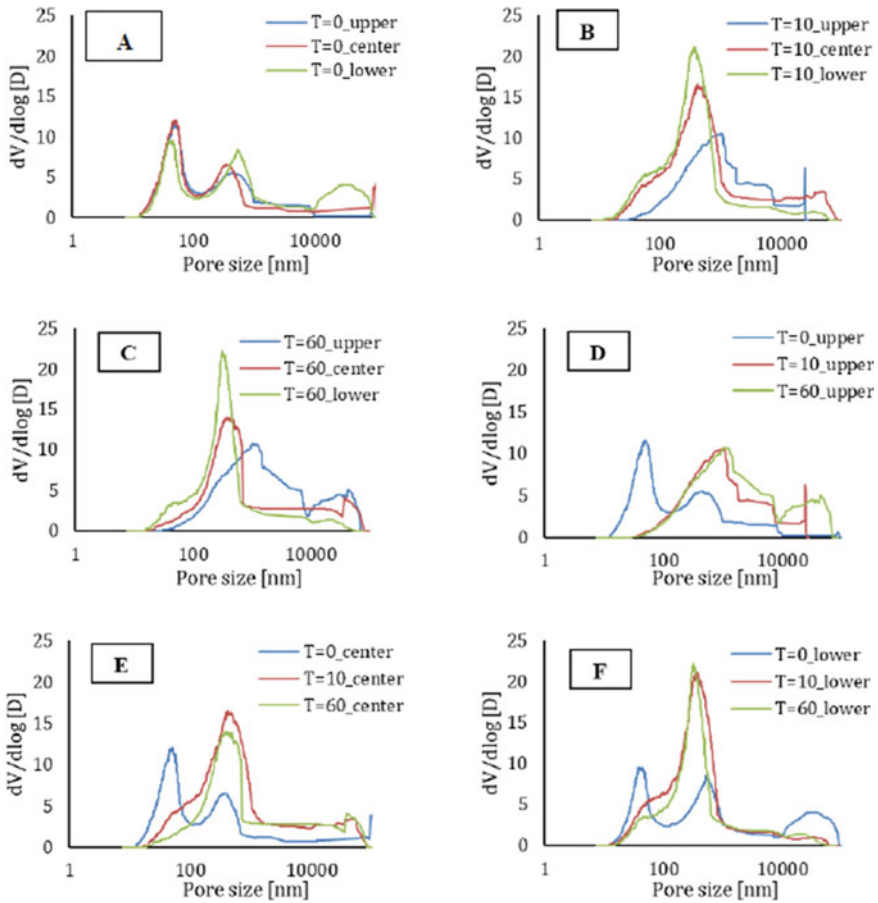


**Fig. 5.33** Pore distribution in different regions of printed specimens, manufactured with increasing time gaps (Van Der Putten et al. 2019)

amount and size of the pores can be determined. Peled and Shah (2003) revealed that the addition of fly ash increases the porosity in all pore ranges (Fig. 5.34a and b). Composites without fly ash are denser and have a lower porosity. This is the case for every fibre type (PVA or acrylic ones).

A similar trend was observed for the cast specimens with and without fly ash. On the other hand, Fig. 5.35 compares the pore size distribution of PVA fibre composites in case of cast and extruded specimens. The extrusion process results in a denser and more compacted composite. The before mentioned differences in porosity between the different construction systems can lead to a stronger matrix and may affect the strength of the fibre-matrix bond. However, it should be kept in mind that MIP measurements determine the pore size distribution of the whole testes specimens, while the porosity and properties at the fibre-matrix interface can differ.

**Fig. 5.34** Pore distribution of extruded and composites with and without fly ash: **a** PVA fibres, **b** Acrylic fibres (Mohammed Sonebibond water-to-binder 2001)

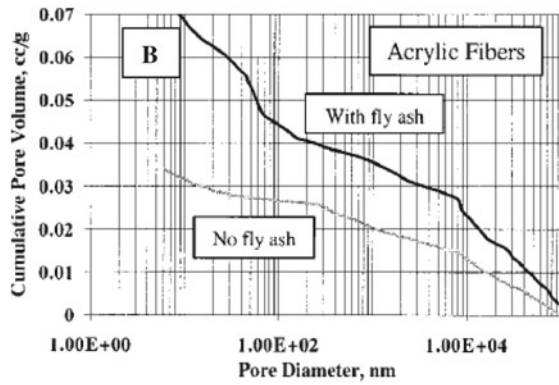
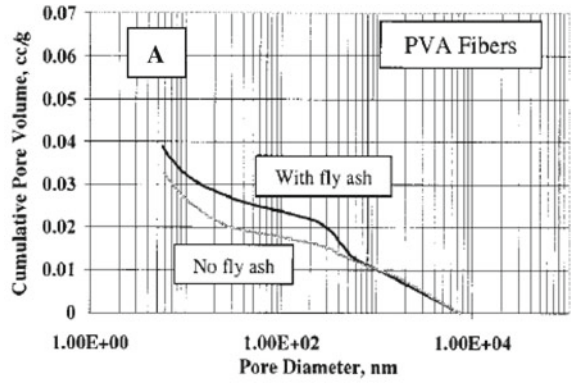
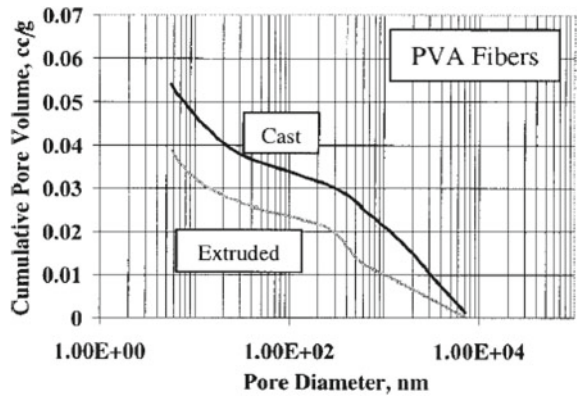


**Fig. 5.35** Pore distribution of extruded and casted composites with PVA fibres (with fly ash) (Mohammed Sonebibond water-to-binder 2001)



Shakor et al. (2017) on the other hand, determined the porosity of the samples using Eq. (5.3). The concrete samples were cast using a specific mix of ordinary Portland cement and calcium aluminate cement. Lithium carbonate was added to some samples in order to reduce the setting time. The porosity measurements were combined with Scanning Electron Microscopy (SEM) analyses to profile the surfaces of the specimens.

$$P_a = \frac{m_3 - m_1}{m_3 - m_2} \bullet 100 \tag{5.3}$$

With:

$P_a$	Porosity	[%]
$m_1$	Weight of the samples after drying for 2 h at 105 °C	[g]
$m_2$	Weight of the samples in soaked water	[g]
$m_3$	Weight of the samples after rolling 4 sides on a damp cloth	[g]

The porosity of the specimens with and without lithium carbonate showed a decreasing trend when increasing the saturation level of the specimens. SEM analyses showed the occurrence of a plate-like large crystal growth which has some other unreacted particles on the surface of the element. Moreover, as shown in Fig. 5.36, there are deep holes and incohesive particles on the SEM figures, which indicate an incomplete hydration between the cement particles. This will consequently have an effect on the mechanical properties of the structure (Fig. 5.37).

Shakor et al. (2017) shows the effect of curing and different saturation degrees on the compressive strength of printed elements composed of a cement mix where ordinary Portland cement was combined with calcium aluminate cement. Increasing the saturation level increases the compressive strength gradually. By increasing the saturation level, total porosity decreases for 3D printed specimens. Maier et al. (2011)

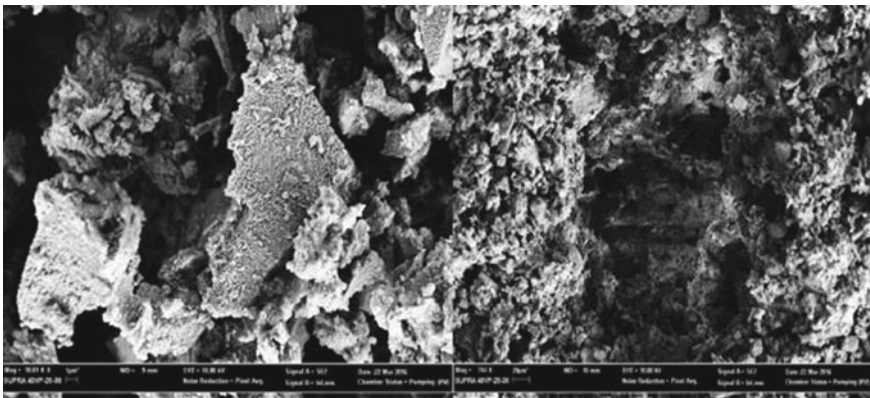
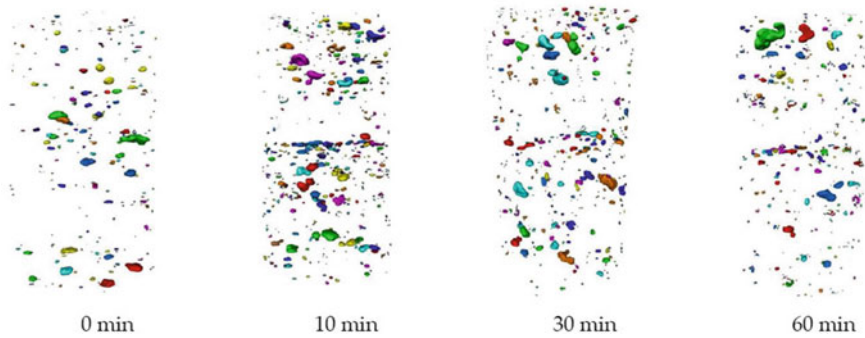


Fig. 5.36 SEM image of 3D printed samples: left (1 μm), right (20 μm) (Shakor et al. 2017)



**Fig. 5.37** 3D rendering of the air voids in 3D printed elements with different time gaps (Van Der Putten et al. 2019)

stated that capillary pores and other large holes are mainly responsible for the reduction in elasticity and strength. They also found that after curing for 72 h, an intermixed crystal network developed and this filled up the pore spaces and minimized the total porosity.

#### 5.5.4 Air Voids

Based on the observations of Van Der Putten et al. (2019), one can conclude that the decreasing strength can be attributed to the lower moisture content of the substrate layer and the higher amount of voids that were induced, resulting in lower adhesion between the printed layers. In case of higher time gaps,  $\mu$ CT-scanning revealed the gathering of air voids at the interface in case, decreasing the overall strength of the printed specimen. These results were also confirmed by Tay et al. (2018), where microscopically investigations of the interlayer showed larger cavities in case of higher time gaps (Fig. 5.38).

Nerella et al. (2017) investigated the effect by Scanning Electron Microscopy (SEM analyses) and classified the interface between the layers into four categories: weakly bonded (a), weakly bonded due to shrinkage or carbonation (b), temporary weakly bonded (c) and strongly bonded (d). Case (a) is when the observed interface between the layers is weakly bonded and is unlikely to be self-healed or bridged by hydration products between the age of 28 days. Case (b) occurs when the observed interface' weak bond can be traced back to plastic, drying shrinkage and/or carbonation rather than to the material rheological properties or time gap. Case (c) represents temporarily weakly bonded interfaces, which are narrow and clearly indicate a self-healing tendency over time due to the build-up of hydration products and in Case (d), the interface between the layers look very similar to reference regions in the core. As expected, the performed time gap between the layers and the applied curing conditions showed a significant influence on the interface quality. Time gaps of 1 day

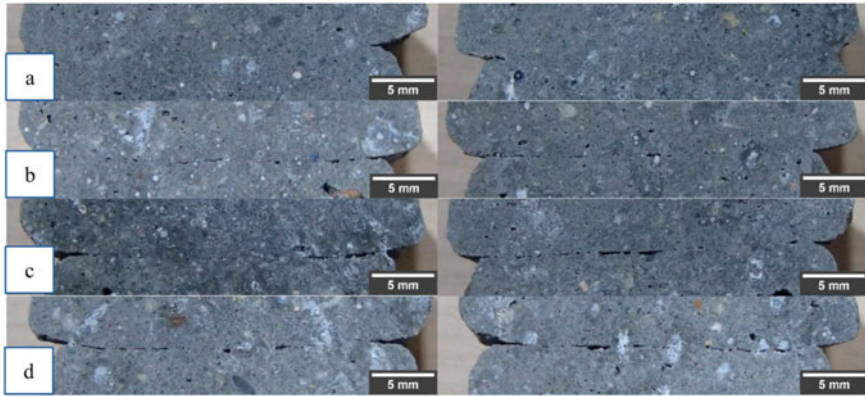


**Fig. 5.38** Samples printed at different time gaps (1, 5, 10 and 20 min) as reported by Tay et al. (2018)

showed the occurrence of cavities and the formation of calcite layers, preventing the development of a proper bonding.

The amount of air voids, entrapped in the cementitious material, not only depend on the interlayer time interval, also the print technique plays an important role as concluded by Nolte (2018) based on CT-scanning. He stated that elements, fabricated by means of a shotcrete principle (i.e. vertical filaments instead of horizontal ones) showed a decreased amount of voids (Fig. 5.40).

### 5.5.5 Carbonation and Corrosion

Dedicated studies on this subject are not yet reported, however, carbonation of printed layers within one day after printing was reported (Nerella et al. 2019) which could have prevented strong interlayer bonding. The concrete composition, surrounding conditions and measured curing influence the carbonation in a significant way. When printed specimens were protected by covering with wet cloths and polythene sheets from the surrounding atmosphere, 3D printed specimens consisting out of a combination of Portland cement, fly ash and micro silica, underwent remarkable carbonation when the applied time interval equals one day. Especially when the top surface of the previous layer (produced one day earlier) showed clear formation of calcites, which prevented it from developing a complete bond with the subsequent layer (Fig. 5.41).

High carbonated specimens were also observed during investigations performed at the university of Ghent and a high dependency on the printing speed and time interval was observed. Within this research, 12 days old four-layered specimens were stored for one week under an increased CO<sub>2</sub> volume of 1%. Visual inspections based on phenolphthalein spray showed that in case of a zero time gap, an uniform carbonation front could be observed for both printing speed. An increased interlayer

time interval increased the carbonation depth in the interlayer between the printed specimens. The dependency of the printed specimens on the applied time gap and printing speed are similar to the capillary water uptake capacity of these specimens as mentioned in Sect. 5.2.

Weger et al. (2018a, b) investigated the carbonation resistance of specimens produced with the particle-bed based 3D printing method selective paste intrusion. For the testing, prisms were printed in Orientation I and II/III and reference specimens were mould-casted. The specimens were stored for one day at 20 °C in the particle bed and the mould, respectively. Afterwards, the specimens were stored at 20 °C under water for seven days. Then, the specimens were stored in standardized conditions (20 °C, 65% R.H.) until the day of testing. One series of specimens was tested in accordance with DIN CEN/TS 12,390–10:2007 under atmospheric conditions after 182 days, another series after 28 days under an increased CO<sub>2</sub> volume of 2%. For the visual identification of the carbonation, phenolphthalein was applied to a freshly broken surface of the specimens. Neither the printed nor the cast specimens showed any carbonation which can be explained by the low water to cement ratio of 0.3.

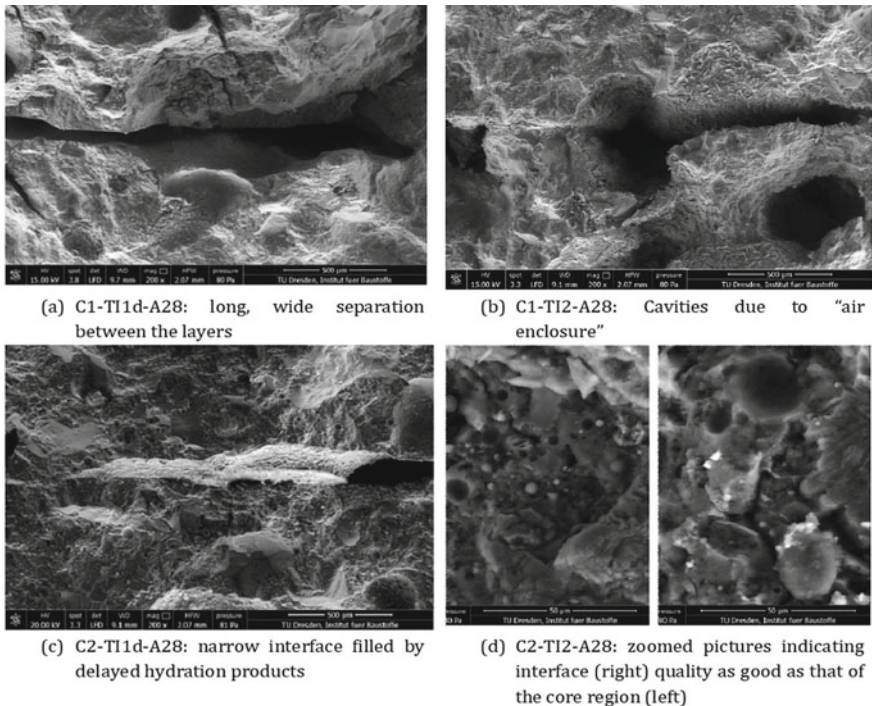
For testing the chloride migration coefficient  $D_{RCM}$ , specimens were produced with the particle-bed based 3D printing method selective paste intrusion. Weger et al. (2018a, b) printed specimens in orientation I and II/III and casted cubes in moulds. The specimens were stored for one day in the particle bed and the mould, respectively. Afterwards, the specimens were stored at 20 °C under water until the 28th day. Within one week before starting of the test procedure, cylinders with a diameter of 100 mm and a height of 50 mm were drilled and sawn from the specimens. At a concrete age of 28 days, the circumference surface of the cylinders was sealed before starting the chloride impact according to (BAW 2017, 2012a, b). The printed as well as the mould-casted reference cylinders showed similar results after 28 days and a resistance to exposure class XF2 and XD2 according to EN 206:2013 + A1:2016 after an age of 56 d and even after 28 days (age of 56 days was only tested with casted specimens). The specimens exhibited no anisotropic behaviour. The results of the casted specimens even almost achieved the limit for exposure class XF3 and XD3 according to EN 206:2013 + A1:2016. The limits for the classification can be found in (BAW 2017, 2012a, b).

### 5.5.6 Freeze–Thaw Resistance

Tian and Han (2018) investigated the effect of different freeze–thaw cycles on the non-air entrained concrete by digital image process (DIP) analysis and mechanical tests. First of all, the porosity of the specimens increased with the increase of freeze–thaw cycles. This implied that the specimens were formed with initial defects, such as pores and micro cracks, and the repeated freeze–thaw actions caused an expansion in volume and movement of the non-frozen water due to hydraulic pressure. These forces induced pore propagation and connection and decreased the durability of the

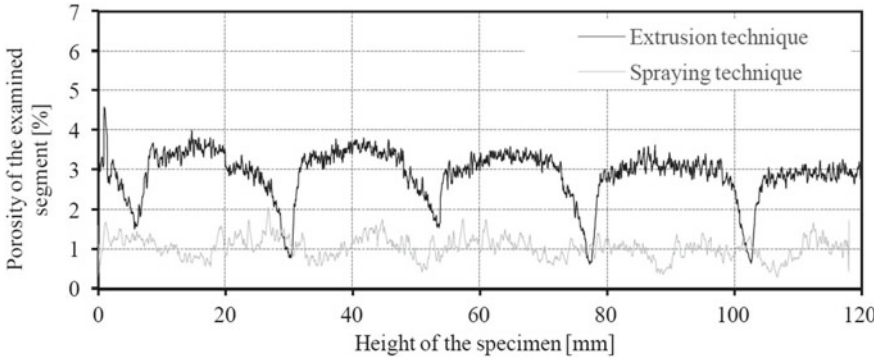
printed specimen. The pores distribution characteristics showed an increase in bigger pores. The larger pores in the material ruptured were cut through by cracks, forming smaller pores. The higher amount of pores also negatively affected the compressive strength (Fig. 5.38) and created printed specimens with different failure mechanisms (Fig. 5.39). In the first type, the main crack went through the specimen along the diagonal, while in the second type two sets of diagonal cracks appeared on the specimens' centre of height, and cracks propagated quickly (Figs. 5.40, 5.41, 5.42 and 5.43).

Weger et al. (2018a, b) tested the freeze–thaw-resistance without (CIF) and with (CDF) de-icing salts of specimens produced with the particle-bed based 3D printing method selective paste intrusion. Therefore, specimens were printed in orientation I and II/III and additionally casted as reference test specimens. The specimens were stored respectively one day in the particle-bed and in the mould and afterwards at 20 °C under water until day 7. Thereafter, the specimens were stored until 28 days at a temperature of 20 °C and a relative humidity of 65%. Then, the freeze–thaw resistance was tested according to DIN CEN/TS 12,390–9:2017–05 and was analysed according to (BAW 2018). The printed specimens were tested perpendicular (Orientation I,

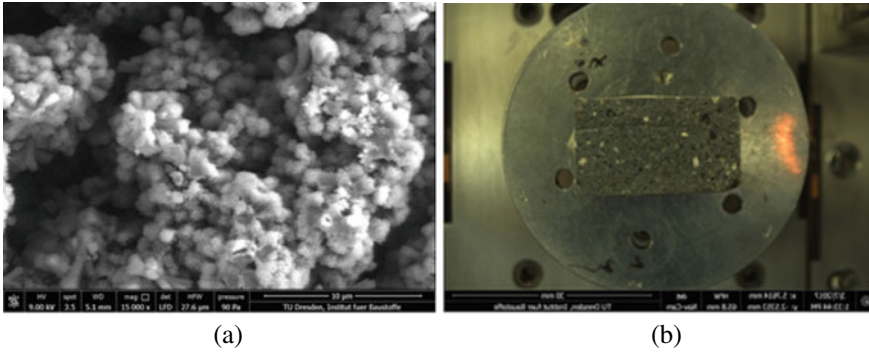


**Fig. 5.39** SEM images captured at 28 days concrete age showing the four observed types of layer-interface microstructure of mixtures C1 and C2. TI indicates the time interval (Venkatesh et al. 2017)



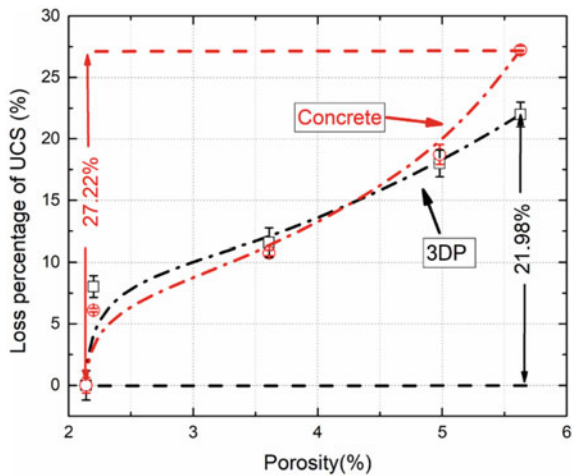


**Fig. 5.40** Pore size distribution of specimens created by spraying or extrusion technique (Nolte et al. 2018)



**Fig. 5.41** **a** Calcite formation at the layer interface and **b** general view of the corresponding specimen (Nerella et al. 2019)

**Fig. 5.42** Relationship between porosity >0.1 mm and loss percentage of uniaxial compressive strengths as reported by Tian and Han (2018)



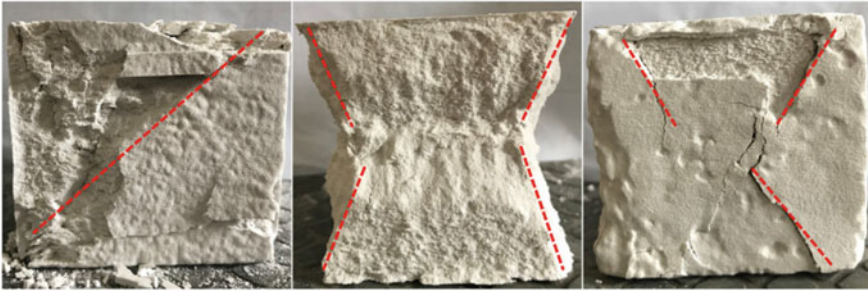


**Fig. 5.43** Failure pattern of 3DP specimens under uniaxial compression

Fig. 5.2) and parallel (Orientation II/III, Fig. 5.2) to the printed layers. The attacked side was not treated and hence the original printed surface. All tested specimens showed high resistance against freeze–thaw attacks without (CIF) and with (CDF) de-icing salts passing even the hardest failure criteria for XF3 and XF4. Additionally, based on the fact that there is no clear tendency in scaling or inner damage depending on the orientation, an isotropic freeze–thaw resistance could be expected.

## 5.6 Recommendations

In order to provide useful support for knowledge development in the engineering community involved in concrete 3D printing activities, technical committees have been recently established among the different international associations, authorities and institutions operating the field of concrete technology or, in general, of construction materials. The research outcomes concerning properties and testing of printed materials/structures in the fresh/hardened state are commonly discussed in these international working group and technical documentation for supporting testing and design are expected to be released in the coming years.

Among these and in addition to the 276-DFC committee (Digital fabrication with cement-based materials) established by RILEM in 2016, the FIB (Fédération Internationale du Béton) has recently opened the activities of Task Group 2.11: Structures made by Digital Fabrication which mainly focus on the mechanical behaviour of manufactured structures rather than on the aspects related to the technological processes; following this, the primary objective consists in identifying and overcoming the limitations of the current design practice for the implementation of novel, digitally-fabricated concrete structures. Preliminary activities deal with the following topics: mechanical behaviour of printed elements in the hardened state; reinforcement strategies; structural design approaches for digitally fabricated elements. The American Concrete Institute (ACI), a leading authority involved in concrete design, construction, and materials, has also launched the committee ACI

564: 3D Printing with Cementitious Materials with the objective of developing technical documentation on the ways additive manufacturing may be integrated into the concrete community. This technical group is currently working on the collection of available/applicable reinforcing and anchoring systems for Additively Constructed Concrete (ACC), including passive reinforcement (e.g. reinforcing bars, fibre reinforcement, interface reinforcement, print ties/stabilizers); active reinforcement (e.g. internal prestressing, external prestressing); alternative reinforcing (e.g. cables, FRP etc.).

## References

- al., B.e. (2019). The effect of Superabsorbent polymers on the Mitigation of Plastic Shrinkage Cracking of Conventional Concrete, Results of a RILEM inter-laboratory test by TC 260-RC. Under submission, Materials and Structures.
- Asprone, D., et al. (2018). Rethinking reinforcement for digital fabrication with concrete. *Cement and Concrete Research*, 112, 111-121.
- Aysha, H., et al. (2014). An overview of interface behaviour between concrete to concrete. *International Journal of Advanced Structures and Geotechnical Engineering*, 03(02), 110-114.
- (BAW), B.f.W. (2017). BAW Merkblatt Dauerhaftigkeitsbemessung und -bewertung von Stahlbetonbau-werken bei Carbonatisierung und Chlorideinwirkung (MDCC).
- (BAW), B.f.W. (2012a). BAW Code of Practice - Resistance of Concrete to Chloride Penetration (MCL).
- (BAW), B.f.W. (2012b). BAW Merkblatt Dauerhaftigkeitsbemessung und -bewertung von Stahlbetonbau-werken bei Carbonatisierung und Chlorideinwirkung (MDCC).
- (BAW), B.f.W. (2018). BAW Merkblatt: Frostprüfung von Beton (MFB): Ausgabe 2012.
- Bos, F., et al. (2016). Additive manufacturing of concrete in construction: potentials and challenges of 3D concrete printing. *Virtual and Physical Prototyping*, 11(3), 209–225.
- Boyce, C., Ozel, A., and Sundaresan, S. (2016). Intrusion of a Liquid Droplet into a Powder under Gravity. *Langmuir*, 32.
- Beushausen, H., and Alexander, M. G. (2007). Localised strain and stress in bonded concrete overlays subjected to differential shrinkage. *Materials and Structures*, 40(2), 189-199.
- Beushausen, H., and Alexander, M. G. (2008). Bond strength development between concretes of different ages. *Magazine of Concrete Research*, 60(1), 65–74.
- Bos, F. P., et al. (2017). Experimental Exploration of Metal Cable as Reinforcement in 3D Printed Concrete. *Materials (Basel, Switzerland)*, 10(11), 1314.
- Christ, S., et al. (2015). Fiber reinforcement during 3D printing. *Materials Letters*, 139, 165-168.
- Curosu, I., et al. (2017). Tensile behavior of high-strength strain-hardening cement-based composites (HS-SHCC) made with high-performance polyethylene, aramid and PBO fibers. *Cement and Concrete Research*, 98, 71-81.
- D'Hondt, M., et al. (2019). Fire behavior of a printed sample for building. in *Dixite 3D Print*. 2019. Champs-sur-Narme.
- Di Carlo, T. (2012). Experimental and numerical techniques to characterize structural properties of fresh concrete relevant to contour crafting. University of Southern California California, p. 196.
- Emmons, P. H., and Emmons, B.H. (1993). Concrete Repair and Maintenance Illustrated: Problem Analysis; Repair Strategy; Techniques, in *Concrete Repair and Maintenance Illustrated: Problem Analysis; Repair Strategy; Techniques*, p. 314.
- Feng, P., et al. (2015). Mechanical properties of structures 3D printed with cementitious powders. *Construction and Building Materials*, 93, 486-497.

- Hambach, M., and Volkmer, D. (2017). Properties of 3D-printed fiber reinforced Portland cement paste. *Cement and Concrete Composites*, 79, 62-70.
- Hack, N., et al. (2017). MESH MOULD: AN ON SITE, ROBOTICALLY FABRICATED, FUNCTIONAL FORMWORK.
- Hack, N., and Lauer, w. v. (2014). Mesh-Mould: Robotically Fabricated Spatial Meshes as Reinforced Concrete Formwork. *Architectural Design*, 84.
- Júlio, E. N. B. S., Branco, F. A. B., and Silva, V. T. D. (2004). Concrete-to-concrete bond strength. Influence of the roughness of the substrate surface. *Construction and Building Materials*, 18(9), 675-681.
- Kumarji, S., and Geneidy, O. (2019). <http://www.iaacblog.com/tag/concrete-3d-printing/>.
- Le, T. T., et al. (2012a). Hardened properties of high-performance printing concrete. *Cement and Concrete Research*, 42(3), 558-566.
- Le, T. T., et al. (2012b). Mix design and fresh properties for high-performance printing concrete. *Materials and Structures*, 45(8), 1221-1232.
- Lloret, E., et al. (2017). SMART DYNAMIC CASTING SLIPFORMING WITH FLEXIBLE FORMWORK -INLINE MEASUREMENT AND CONTROL
- Liu, Z., et al. (2019). Interlayer Bond Strength of 3D Printing Cement Paste by Cross-Bonded Method. *Journal of the Chinese Ceramic Society*, 47(5), 648-652.
- Lowke, D., et al. (2015). 3D-Drucken von Betonbauteilen durch selektives Binden mit calciumsilikatbasierten Zementen – Erste Ergebnisse zu betontechnologischen und verfahrenstechnischen Einflüssen.
- Lowke, D., et al. (2018). Particle-bed 3D printing in concrete construction – Possibilities and challenges. *Cement and Concrete Research*, 112, 50-65.
- Marchment, T., et al. (2017). Effect of delay time on the mechanical properties of extrusion-based 3D printed concrete, in 34th International Symposium on Automation and Robotics in Construction. Taiwan.
- Mechtcherine, V., et al. (2019). Large-scale digital concrete construction – CONPrint3D concept for on-site, monolithic 3D-printing. *Automation in Construction*, 107, 102933.
- Maier, A. -K., et al. (2011). Three-dimensional printing of flash-setting calcium aluminate cement. *Journal of Materials Science*, 46(9), 2947-2954.
- Mechtcherine, V., et al. (2014). Effect of internal curing by using superabsorbent polymers (SAP) on autogenous shrinkage and other properties of a high-performance fine-grained concrete: results of a RILEM round-robin test. *Materials and Structures*, 47(3), 541-562.
- Mohammed Sonebibond water-to-binder. (2001). r., Effect of Silica Fume, Fly Ash and Water-to-Binder Ratio on Bond Strength of Underwater, Self-Consolidating Concrete. *ACI Symposium Publication*, 199.
- Mechtcherine, V., et al. (2018). 3D-printed steel reinforcement for digital concrete construction – Manufacture, mechanical properties and bond behaviour. *Construction and Building Materials*, 179, 125-137.
- Nerella, V. N., Hempel, S., and Mechtcherine, V. (2019). Effects of layer-interface properties on mechanical performance of concrete elements produced by extrusion-based 3D-printing. *Construction and Building Materials*, 205, 586-601.
- Nerella, V. N., et al. (2016). Studying printability of fresh concrete for formwork free Concrete on-site 3D Printing technology technology (CONPrint3D), in *Rheol. Messungen an Baustoffen 2016 - Tagungsband Zum 25. Workshop und Kolloquium*, pp. 236-246.
- Neville, A. M. (1995). *Properties of concrete*. Vol. 4. 1995: Longman London.
- Nematollahi, B., et al. (2018). Effect of Type of Fiber on Inter-Layer Bond and Flexural Strengths of Extrusion-Based 3D Printed Geopolymer. *Materials Science Forum*, 939, 155-162.
- Nolte, N., et al. (2018). Schichtenverbund bei der additiven Fertigung-Einflussgrößen und Verfahrensvergleich.
- Ogura, H., Nerella, V. N., and Mechtcherine, V. (2018). Developing and Testing of Strain-Hardening Cement-Based Composites (SHCC) in the Context of 3D-Printing. *Materials (Basel)*, 11(8).

- Paul, S. C., et al. (2018). Fresh and hardened properties of 3D printable cementitious materials for building and construction. *Archives of Civil and Mechanical Engineering*, 18(1), 311–319.
- Panda, B., Chandra Paul, S., and Jen Tan, M. (2017). Anisotropic mechanical performance of 3D printed fiber reinforced sustainable construction material. *Materials Letters*, 209, 146–149.
- Panda, B., et al. (2018). Measurement of tensile bond strength of 3D printed geopolymers mortar. *Measurement*, 113, 108–116.
- Perrot, A., Rängeard, D., and Pierre, A. (2016). Structural built-up of cement-based materials used for 3D-printing extrusion techniques. *Materials and Structures*, 49(4), 1213–1220.
- Pierre, A., et al. (2018). Penetration of cement pastes into sand packings during 3D printing: analytical and experimental study. *Materials and Structures*, 51(1), 22.
- Peled, A., and Shah, S. P. (2003). Processing Effects in Cementitious Composites: Extrusion and Casting. *Journal of Materials in Civil Engineering*, 15(2), 192–199.
- Rahul, A. V., et al. (2019). Mechanical characterization of 3D printable concrete. *Construction and Building Materials*, 227, 116710.
- Rubio, M., et al. (2019). Mechanical properties of 3D bio-printing cement-based materials. in *Third International Conference on “Bio-Based Building Materials (ICBBM)*. Belfast.
- Roussel, N., and Cussigh, F. (2008). Distinct-layer casting of SCC: The mechanical consequences of thixotropy. *Cement and Concrete Research*, 38, 624–632.
- Sanjayan, J. G., et al. (2018). Effect of surface moisture on inter-layer strength of 3D printed concrete. *Construction and Building Materials*, 172, 468–475.
- Santos, D. S., Santos, P. M. D., and Dias-da-Costa, D. (2012). Effect of surface preparation and bonding agent on the concrete-to-concrete interface strength. *Construction and Building Materials*, 37, 102–110.
- Santos, P. M. D., and Eduardo Nuno Brito Santos, J. (2011). Factors Affecting Bond between New and Old Concrete. *Materials Journal*, 108(4).
- Serpukhov, I., and Mechtcherine, V. (2015). Early-Age Shrinkage of Ordinary Concrete and a Strain-Hardening Cement-Based Composite (SHCC) in the Conditions of Hot Weather Casting, pp. 1504–1513.
- Schröfl, C., Nerella, V. N., and Mechtcherine, V. (2019). *Capillary Water Intake by 3D-Printed Concrete Visualised and Quantified by Neutron Radiography*. 2019. Cham: Springer International Publishing.
- Shakor, P., et al. (2017). Modified 3D printed powder to cement-based material and mechanical properties of cement scaffold used in 3D printing. *Construction and Building Materials*, 138, 398–409.
- Tay, Y. W. D., et al. (2018). Time gap effect on bond strength of 3D-printed concrete. *Virtual and Physical Prototyping*, 14, 104–113.
- Tian, W., and Han, N. (2018). Pore characteristics (>0.1 mm) of non-air entrained concrete destroyed by freeze-thaw cycles based on CT scanning and 3D printing. *Cold Regions Science and Technology*, 151, 314–322.
- Van Zijl, G.P.A.G., S.C. Paul, and M.J. Tan. (2016). Properties of 3D Printable Concrete, in *2nd International Conference on Progress in Additive Manufacturing*, Singapore.
- Van Der Putten, J., et al. (2019a). Microstructural Characterization of 3D Printed Cementitious Materials. *Materials*, 12(18).
- Van Der Putten, J., et al. (2019b). 3D Printing of cementitious materials with superabsorbent polymers, in *Durable Concrete for Infrastructure under Severe Conditions - Smart Admixtures, Self-responsiveness and Nano-additions*. Ghent, pp. 86–89.
- Van Der Putten, J., De Schutter, G., and Van Tittelboom, K. (2019). Surface modification as a technique to improve inter-layer bonding strength in 3D printed cementitious materials. *RILEM Technical Letters*, 4(0).
- Venkatesh, N., Hempel, S., and Mechtcherine, V. (2017). Micro- and macroscopic investigations on the interface between layers of 3D printed cementitious elements, in *International Conference on Advances in Construction Materials and Systems*. Chennai.

- Wang, Z. W. L., and Zhao, X. (2018). Apparatus and method for preparing a building structure with 3d printing, C.C.N.I.P.A.R.f. <https://patents.google.com/patent/US20200391409A1/en?inventor=zhendi+wang&oq=zhendi+wang>, Editor.
- Wangler, T., et al. (2016). Digital Concrete: Opportunities and Challenges RILEM Technical Letters, 1, 67–75.
- Weger, D., Lowke, D., and Gehlen, C. (2016a). 3D printing of concrete structures using the selective binding method – Effect of concrete technology on contour precision and compressive strength, in 11th fib International PhD Symposium in Civil Engineering, A.K.a.J.Y. K. Maekawa, Editor. Tokyo, pp. 403–410.
- Weger, D., Lowke, D., and Gehlen, C. (2016b). 3D Printing of Concrete Structures with Calcium Silicate based Cements using the Selective Binding Method - Effects of Concrete Technology on Penetration Depth of Cement Paste, in 4th International Symposium on Ultra-High Performance Concrete and High Performance Construction Materials 2016, Kassel University Press: Kassel
- Weger, D., Gehlen, C., and Lowke, D. (2018a). Additive Fertigung von Betonbauteilen durch selektive Zementleim-Intrusion.
- Weger, D., et al. (2018b). Additive manufacturing of concrete elements using selective cement paste intrusion-effect of layer orientation on strength and durability in RILEM 1st International Conference on Concrete and Digital Fabrication. Zürich.
- Wolfs, R. J. M., Bos, F. P., and Salet, T. A. M. (2019). Hardened properties of 3D printed concrete: The influence of process parameters on interlayer adhesion. Cement and Concrete Research, 119, 132–140.
- Wyrzykowski, M., et al. (2018). Recommendation of RILEM TC 260-RSC: using superabsorbent polymers (SAP) to mitigate autogenous shrinkage. Materials and Structures, 51(5), 135.
- Zareiyan, B., and Khoshnevis, B. (2017). Interlayer adhesion and strength of structures in Contour Crafting - Effects of aggregate size, extrusion rate, and layer thickness. Automation in Construction, 81, 112–121.
- Zareiyan, B., and Khoshnevis, B. (2017). Effects of interlocking on interlayer adhesion and strength of structures in 3D printing of concrete. Automation in Construction, 83, 212–221.
- Zingg, A., et al. (2009). Interaction of polycarboxylate-based superplasticizers with cements containing different C3A amounts. Cement and Concrete Composites, 31(3), 153–162.

# Chapter 6

## Structural Design and Testing of Digitally Manufactured Concrete Structures



**Domenico Asprone, Costantino Menna, Freek Bos, Jaime Mata-Falcón, Liberato Ferrara, Ferdinando Auricchio, Ezio Cadoni, Vítor M. C. F. Cunha, Laura Esposito, Asko Fromm, Steffen Grünewald, Harald Kloft, Viktor Mechtcherine, Venkatesh Naidu Nerella, and Roel Schipper**

**Abstract** The form freedom enabled by digital fabrication with concrete technologies provides advantages for a wide range of concrete based objects, from architectural to structural elements. The current chapter focuses on the specifics of structural design and engineering of DFC with emphasis on those technologies based on Additive Manufacturing with extrusion. Since it is a new and innovative way to build, a clear common approach to structural engineering has not yet been developed. As a result, this chapter aims to introduce the specific challenges of structural design and engineering with the additive manufacturing technology, providing an overview of

---

D. Asprone (✉) · C. Menna · L. Esposito  
Università Degli Studi Di Napoli Federico II, Naples, Italy  
e-mail: [d.asprone@unina.it](mailto:d.asprone@unina.it)

F. Bos  
Technische Universiteit Eindhoven, Eindhoven, The Netherlands

J. Mata-Falcón  
ETH Zürich, Zurich, Switzerland

L. Ferrara  
Politecnico Di Milano, Milan, Italy

F. Auricchio  
Università Degli Studi Di Pavia, Pavia, Italy

E. Cadoni  
Scuola Universitaria Professionale Della Svizzera Italiana, Manno, Switzerland

V. M. C. F. Cunha  
ISISE / IB-S, University of Minho, Guimarães, Portugal

A. Fromm · H. Kloft  
Technische Universität Braunschweig, Braunschweig, Germany

S. Grünewald  
Ghent University, Ghent, Belgium

S. Grünewald · R. Schipper  
Delft University of Technology, Delft, The Netherlands

V. Mechtcherine · V. N. Nerella  
Technische Universität Dresden, Dresden, Germany

structural typologies that have been developed (especially concerning the reinforcement strategies, including fibre reinforcement). Furthermore, the structural principles adopted in DFC and the codified approaches used in conventional reinforced concrete is compared, and putative structural testing procedures and validation methods for DFC are reported.

**Keywords** Additive Manufacturing · Structural design · Reinforcement strategies · Testing

## 6.1 Introduction

The form freedom enabled by digital fabrication with concrete (indicated as DFC below), technologies provides advantages for a wide range of concrete based objects, varying from “sculptural” urban furniture to artificial reefs, and from sewage pits to art objects. For load-bearing elements in building structures, DFC has high potential too, particularly by introducing the possibility to materialise a topological optimisation by straightforwardly bridging the design process with the manufacture, i.e. to adjust the geometry in order to optimise structural performance for minimal material use (if necessary, customised optimisation for each individual element), without prohibitive cost increases. Indeed, a variety of construction projects for which DFC or DFC parts structurally are applied, have been presented in recent years (Labonette et al. 2016; Bos et al. 2016; Buswell et al. 2018)—and the number of examples is growing rapidly.

The current chapter focuses on the specifics of structural design and engineering of DFC with emphasis on those technologies based on Additive Manufacturing process that use extrusion.

A clear common approach to the structural engineering of DFC technologies has not yet been developed and thus bespoke procedures have been applied to obtain the required approvals, following, for instance, the indications enclosed in Annex D of the Eurocode 0, which allow individual approvals based on experimental testing. To nevertheless facilitate the development of a common understanding of structural engineering for DFC and related issues, thus moving actual applications towards achieving the full potential offered by DFC technologies, this chapter aims to:

- Introduce the specific challenges of structural design and engineering with DFC, especially for the additive manufacturing technology.
- Provide an overview of structural typologies that have been developed or are under development, particularly with regard to reinforcement strategies.
- Compare the structural principles and modelling approaches of structural DFC to codified approaches used in conventional reinforced concrete.
- Discuss discrete fibre reinforcement for DFC, as one of the main strategies to obtain toughness, ductility and post-cracking tensile strength in DFC elements.
- Finally, discuss putative structural testing procedures and validation methods for DFC.



The projects that have been carried out until now are generally small in scale, use a range of different DFC processes and materials, are based on a variety of structural principles, and in terms of the consequences of an eventual structural failure are mostly minor. Due to the challenges further elaborated in this chapter, the geometrical freedom offered by DFC has hardly been capitalised upon in actual in-use projects.

As a result, the discourse in the field of structural engineering of DFC has been relatively limited. DFC projects have received plenty of popular and professional attention, but in-depth publications on the applied structural approaches have been scarce. Theo et al. (2018) has presented the design, testing and construction of a bicycle bridge. Based on the same as well as another project, (Bos et al. 2019) discussed large scale structural testing for 3D concrete printing. However, neither provided generalised discussions with regard to the structural engineering of such projects. The first endeavour to provide a holistic view on this issue, which can be found in (Salet and Nijmegen 2019), established a safety protocol for the design and testing of a 30 m multi-span pedestrian and bicycle bridge (see case study, Chap. 2 Sect. 3.1). Nonetheless, it starts from comprehensive observations regarding the structural particularities of 3D concrete printing, and thus provides a dedicated elaboration of the very generally stated requirements in Annex D of Eurocode 0.

The challenges associated with the structural engineering of DFC can be categorised into three groups (see Fig. 6.1):

- The materials and processes effects on printed products.
- Input structural design calculation.
- Aspects of design.

**Structural engineering challenges of DFC**

Material & Process		Calculation Input		Design	
1	Anisotropy	4	Material properties data	7	Geometrical 'freedom'
2	Creep & shrinkage	5	Structural behavior data	8	Reinforcement
3	Durability	6	Geometrical data	9	Detailing / connections

**Approach:** How to engineer efficiently?

**Fig. 6.1** Structural engineering challenges associated with DFC

These will be briefly elaborated below. Jointly, they summon the question of how a DFC structure can be efficiently designed and calculated—a topic for further research. Since existing codes have limited applicability to DFC as argued above, the validation of the structural design developed for a project is a further challenge to be addressed and which is more extensively discussed in Sect. 6.5.

### 6.1.1 *Material & Process*

The materials and processes used in DFC result in an intrinsic behaviour and properties that can be distinctively different from those commonly found on conventional cast concrete. With most DFC processes material is positioned in layers that results in anisotropic (tensile) strength (anisotropic stiffness has not been shown). Generally, the tensile strength perpendicular to the interface is lower than in the other directions. However, quantitatively this effect can vary from negligible to dramatic (<5% to >90% strength reductions) depending on material and process input parameters. This can be due to well-known or yet unrecognised influencing factors. The directional dependency of strength properties was recognised at an early stage by (Le et al. 2012), and has been the topic of a considerable number of studies (Feng et al. 2015; Nerella et al. 2016; Zareiyan and Khoshnevis 2017; Panda et al. 2017, 2018; Paul et al.; Nerella et al. 2018; Wolfs et al.; Van Der Putten et al. 2019; Panda et al. 2019; Marchment et al. 2017; Keita et al. (2019); Zahabizadeh et al. 2019), a summary of which is provided by (Timothy et al. 2018). However, because these studies have tended to be phenomenological in nature, rather than theoretical and explanatory, this has not yet resulted in a full understanding of the impact of layering and time between consecutive layers. Furthermore, with the exception of (Le et al. 2012), the focus has entirely been on the vertically stacked layers. Nevertheless, considering the scale of existing printing nozzles as well as often presented zig-zag infill structures, (local) interfaces between horizontally joining layers are also likely to occur in actual DFC projects.

The effects of creep and shrinkage are much less studied. Since printing mortars generally lack aggregates above approximately 2–3 mm grain size and the cement content is high when compared to conventional concretes, shrinkage and creep should be expected to be relatively high. The often thin-walled DFC geometries and lack of formwork increase the magnitude and rate of drying shrinkage compared to conventional concrete. In combination with restrained deformations (that may already occur due to friction of the print bed during initial stages of curing, or from uneven curing and shrinkage), this may have a significant influence on the structural integrity of the printed object, due to resulting cracking.

Several studies have pointed out that the layered structure in DFC may also result in reduced durability of the printed component. It was shown that increased interlayer interval times result in an increase in porosity (Van Der Putten et al. 2019), capillary water ingress (Schröfl et al. 2019), and chloride penetration (Bran Anleu et al. 2018).

However, it is yet unknown to what extent this impacts structural engineering considerations (e.g. with regard to strength development over the reference life span). In addition, some authors have argued that the chemicals used in some DFC processes, such as retarders and accelerators, may have a harmful on the long-term effect on the reinforcement (Lloret-Fritschi et al. 2019; Stefanoni et al. 2019).

### 6.1.2 Calculation Input

A structural calculation requires several types of input. Generally, a structural checking is executed by comparing a calculated structural response due to certain predetermined combination(s) of action(s), which are statistically determined, to limit values for that response. To calculate the response, geometrical and material properties data are used as an input. Material property data are also required to determine the limit values, such as the structural behaviour data. Partially due to the particularities discussed in the previous subsection, and partially due to the sheer novelty of the technology, there is a quantitative lack of data in all these three categories (i.e. material, structural, geometrical).

First of all, although some suppliers provide product data of their printable mortars obtained by mechanical behaviour studies (see previous subsection), such data are usually incomplete (i.e. do not provide values for all relevant parameters required for designing). Moreover, they are quantitatively limited (thus their statistical validity is unknown), and they are based on experimental procedures that are both not fully detailed and have not been universally agreed upon. Because the relations of material properties with manufacturing process parameters are still largely unknown, it is also unclear to what extent the provided values could be generally used. Strength classes, as the ones for concretes, fibre reinforced concretes, cements, and mortars, have not yet been developed, which makes interchangeability between materials (and suppliers) and between manufacturing systems impossible without a full reconsideration of the structural performance.

Secondly, it should be noted that a significant number of limit values provided by codes is based on empirically obtained relations (for instance for the shear resistance of reinforced concrete beams) based on testing of structural elements (rather than on materials testing). Such empirical data is practically non-existent for DFC. An important factor regarding the latter technology is that although the manufacturing method of conventional (reinforced) concrete is basically the same everywhere, the processes in DFC can vary considerably from one installation to another (see (Buswell et al. 2020) and Chap. 2). This makes it much difficult to obtain generally validated empirical relations. Nonetheless, theoretical solutions should be pursued, and/or more detailed modelling and checking should be applied (e.g. through Finite Element Modelling; FEM), as discussed further in Sect. 6.3.

Finally, a structural analysis of DFC may also be encumbered by a lack of geometrical data. For instance, in most filament-extrusion-based DFC processes, the filament height, width and density can be adjusted through adaptations to the pump pressure,

nozzle speed, nozzle geometry, and layer off-set. However, more often than not, it is not exactly known which settings result in which geometrical dimensions. This issue is further complicated when stacking layers of fresh material, that may deform previously deposited layers, or by changes in nozzle speed due to the followed print paths (e.g. at corners).

### **6.1.3 Design Aspects**

The geometrical freedom offered by DFC is enriching to the realm of structural concrete, but also introduces many challenges. Most codes are based on relatively simple, 1D (beams, columns) or 2D (flat shells, plates) mechanical schemes. In complex geometries, such the ones enabled through DFC, these approaches are no longer suitable. Thus, sophisticated modelling approaches based on FEM should be required.

Nevertheless, DFC also dictates some geometrical restrictions. In filament-extrusion technologies, this generally includes, among others, a fixed filament section dimension (i.e. a sort of print resolution), a continuous print path per layer in the object, and preferably a print path that per layer connects start to end, to achieve efficient printing of subsequent layers. In a stacked-layer process, cantilevering is often limited and 2.5D objects are obtained. Finally, it should be noted that the print path design of a globally identical shape may have a significant impact on the resistance of an object, due to the location of (vertical) interfaces and orientation of fillets—and magnitude of associated peak stresses.

A rather different, but at least equally important aspect of DFC structural design is that of reinforcement, which is required due to the fact that printable cementitious mortars, like conventional concretes, are quasi-brittle. In conventional concrete, the use of (ribbed) steel bars has long been the dominant method of reinforcement, the design of which belongs to the basic toolbox of practically any structural engineer. Besides that, reinforcement based on the application of a variety of discrete fibres, separately or in combination with steel bars, has been developed for several decades and is now entering “code-type” guidelines for structural engineering (e.g. FIB (2010)). Other reinforcement solutions include various types of meshes or bars from other materials.

Contrary to conventional concrete, no standardised reinforcement method is yet available for DFC (Asprone et al.). Instead, a solution strategy has to be designed, calculated, and tested for each case—a considerable burden on any project. The application of steel bars is incompatible or undesirable for DFC, amongst others because of geometrical difficulties, uncertainties regarding the reinforcement-to-matrix bond, and the integration of the application of reinforcement bars in the printing process. The fact that it is nevertheless sometimes applied is due to a lack of sufficiently matured alternatives, which are, however, under development as discussed in Sect. 6.2. Fibre reinforced DFC is probably the most obvious option,

as well as one of the most promising, strategies and is extensively discussed in Sect. 6.3.

For detailing and connections, finally, a similar situation as for reinforcement can be discerned: there are no standardised solutions available. Including connection provisions in the casting of an element (such as starter bars), as is often done in conventional reinforced concrete, is not obvious in DFC processes. A project-specific post-processing step will generally be required. Special attention is needed for the introduction of stresses into the respective DFC elements, as here too; no standardised analysis methods are available.

Considering the shortage of data on a considerable number of relevant aspects, the question is justified whether responsible structural design with DFC is currently possible. Even though the material behaviour is not fundamentally different from conventional concrete, the answer is nevertheless affirmative—as underlined by the realised projects. On a basic level, the structural behaviour of DFC is very similar to conventional concrete. Therefore, the structural use of DFC requires specific attention throughout an integrated project approach, i.e. from the design, to the analysis, (experimental) validation, production (printing path and techniques), assembly, and demolition. The extent to which this is required is highly dependent on both the specific project requirements and the employed DFC process.

## 6.2 Catalogue of Digital Fabrication Processes to Manufacture Concrete Structures

### 6.2.1 *Structural Systems*

Based on their topology, structural systems might be divided in (i) framed structures, made up of linear elements (defined by either a straight or curved axis); (ii) surface structures, made up of planar (plates, slabs) or curved elements (shells); and (iii) solid structures (Buswell et al. 2018). It should be noted that most structures combine elements with different structural topologies. Given the fact that concrete is suitable to resist compressive forces, but requires reinforcement to cope with tensile forces (Asprone et al.), a relevant distinction between structural elements in the context of DFC is the load-carrying mechanism, depending on whether acting loads are carried (i) by normal forces (in the case of linear elements) and membrane forces (in the case of surface elements), or (ii) developing significant bending moments, tensile and/or shear forces. The most common standard structural elements are briefly discussed in the following paragraphs concerning this classification.

Linear elements in framed structures with general stress resultants (i.e. developing bending and shear actions as well as normal forces) are typically known as beams, which can be either straight or curved. Straight elements with external compressive loads exclusively in the axis direction are frequently referred to as columns. For a certain load state, the axis of a beam can be selected in such a way that the bending

and shear actions disappear, and only compression forces occur; this element is an arch. A truss structure (i.e. straight elements connected via hinges with loads applied at the joints only) is another framed structure with elements subjected only to normal forces (compression or tension).

A shell is the most general surface structure, as it can be single or double curved and includes all general stress resultants (membrane and shear forces plus bending and out-plane twisting moments). Similarly, as for the arch, the shape of a shell can be defined to have primarily membrane forces for a certain load case; these particular shells are known as membrane shells, membranes or funicular shells. Plane structures can basically be divided in slabs, when loads are acting perpendicular to its plane (subjected to bending and twisting moments plus shear forces) and plates, when carrying in-plane loads (subjected only to membrane forces). Concrete plates can also be analysed by means of a truss analogy (Marti 1985; Schlaich et al. 1987), i.e. some areas are subjected to compression stress while others areas are in tension and, therefore, require reinforcement.

From the previous overview of structural systems, it is clear that only a very limited range of structural elements (i.e. columns, arches, compressed bars of trusses and funicular shells) might be designed (in terms of failure resistance/ultimate strength) to work as compression-only structures for permanent actions. However, tensile forces will still arise in these structures for variable loads and long-term actions, except for massive structures (as is the case of ancient structures still standing nowadays), which are out of the scope of DFC that mainly aims to minimise the material use and exploit form freedom. Consequently, modern load-bearing concrete structures unavoidably require reinforcement for resisting tensile forces in order to ensure structural code compliance (as only for very particular verifications, e.g. shear and punching shear in slabs, it is allowed to rely on the tensile strength of concrete). Moreover, besides reinforcement not been needed for strength, modern design codes for structural concrete still require providing a minimum reinforcement amount to ensure other performances such as good durability, serviceability, sufficiently ductile behaviour and robustness.

The implementation of reinforcing solutions into digital manufacturing technologies is a key aspect when fabricating load-bearing concrete structures, as reinforcement is required regardless of the structural system. The following Sect. 6.2.2 gives an overview and classification of different reinforcing strategies suitable for DFC, while Sect. 6.2.3 discusses the feasibility and potential to adopt these reinforcement strategies for the main digital concrete manufacturing processes (especially for additive manufacturing).

### ***6.2.2 Classification of Reinforcing Strategies***

Reinforcement used in concrete structures can be categorised in distinct ways, such as internal or external, metallic or non-metallic, and passive or pre-stressed (active). Metallic reinforcement products are typically used as bars, wires, welded fabric or

discrete fibres for passive reinforcement, while wires, wire-strands and bars are the most frequent option for active reinforcement ones. Non-metallic reinforcement (e.g. carbon, glass, aramid or polyvinyl) is available in a very wide range of products, as bars, laminates, strips, sheets, grids, fibres or knit textiles. In conventionally built structures, passive internal reinforcement consisting of deformed steel bars with a characteristic yield strength around 450–500 MPa is by far the most used combination. This type of reinforcement is inexpensive, ductile, robust and easy to place on-site, but the use of non-conventional manufacturing technologies affects the way this reinforcement can be installed/incorporated. Therefore, other types of reinforcement, such as textile reinforcements and fibrous reinforcements, which have not yet been widely accepted and applied in current for a wide range of concrete structures, might be reinforcing solutions more suitable or compatible for DFC. Asprone and coauthors (Asprone et al.) proposed a classification (Table 6.1) of reinforcement strategies for DFC taking into account the structural principle of the reinforcing solution, as well as the digital manufacturing stage when the reinforcement is placed. It should be noted that, according this classification, hybrid solutions composed of several reinforcing strategies are possible as well. Reinforcing solutions consisting of the application of a ductile printing material will typically be applied during concrete manufacturing. In structures submitted to pure compressive loads due to the application of active reinforcement, the reinforcement can either be manufactured before (pre-tensioned reinforcement) or after concrete manufacturing (post-tensioned reinforcement). In the composite alternative, the reinforcement might be placed before, during or even after manufacturing (providing some gluing/connection system). Avoiding the use of reinforcement (compressed-only structures due to shape) has been extensively explored especially in the context of DFC (Akbarzadeh et al. 2015) because the difficulty of implementing reinforcement. However, this strategy is only applicable to a very limited range of applications, as discussed in Sect. 6.2.1.

Nerella et al. (2018) provided an alternative classification of reinforcement manufacturing processes for DFC, distinguishing between continuous and discontinuous reinforcing processes, clearly linked to the classification provided in Table 6.1. Discontinuous processes correspond to the installation of reinforcement before or after the concrete manufacturing, while continuous processes require adding reinforcement during concrete manufacturing.

### ***6.2.3 Strategies to Fabricate Concrete Structures***

Digital processes to manufacture concrete structures include a digital process for forming of concrete (discussed in Chap. 2) as well as a suitable reinforcement strategy (see classification in Sect. 6.2.2). While the reinforcement should ideally be placed automatically to allow for digital manufacturing of the entire structural elements, most reinforcing strategies suitable for DFC are not mature enough and still require a high amount of hand-labour. This is admissible at the current early age of digital fabrication of concrete structures (e.g., digital processes for forming

**Table 6.1** Classification of reinforcement strategies for DFC

By structural principle	By stage of the reinforcement manufacturing
Reinforced printing material (e.g. fibre reinforced materials):	Before concrete manufacturing:
This is the case where rebar reinforcement is not needed and only the fibres are able to provide the tensile strength and the deformation capacity required for the application	Reinforcement is arranged and placed in the final configuration before concrete deposition through a digital fabrication method
DFC composite (e.g. with placement of passive reinforcement):	During concrete manufacturing:
This is the case where rebar/continuous reinforcement is needed, and it can be also installed with automated/robotised processes	Reinforcement is added during concrete manufacturing or belongs to the material itself (e.g. fibres)
Compression loaded structures (e.g. due to shape or pre-stressing):	After concrete manufacturing:
This is the case where no reinforcement or only pre-stressed reinforcement is required	Reinforcement is installed once concrete element has been manufactured through a digital fabrication method

of concrete still require considerably manual intervention in spite of being much more mature). Even the difficulty to integrate and automate reinforcing solutions for DFC, researchers should avoid facing exclusively concrete manufacturing without reinforcement, unless aiming to produce non-structural elements.

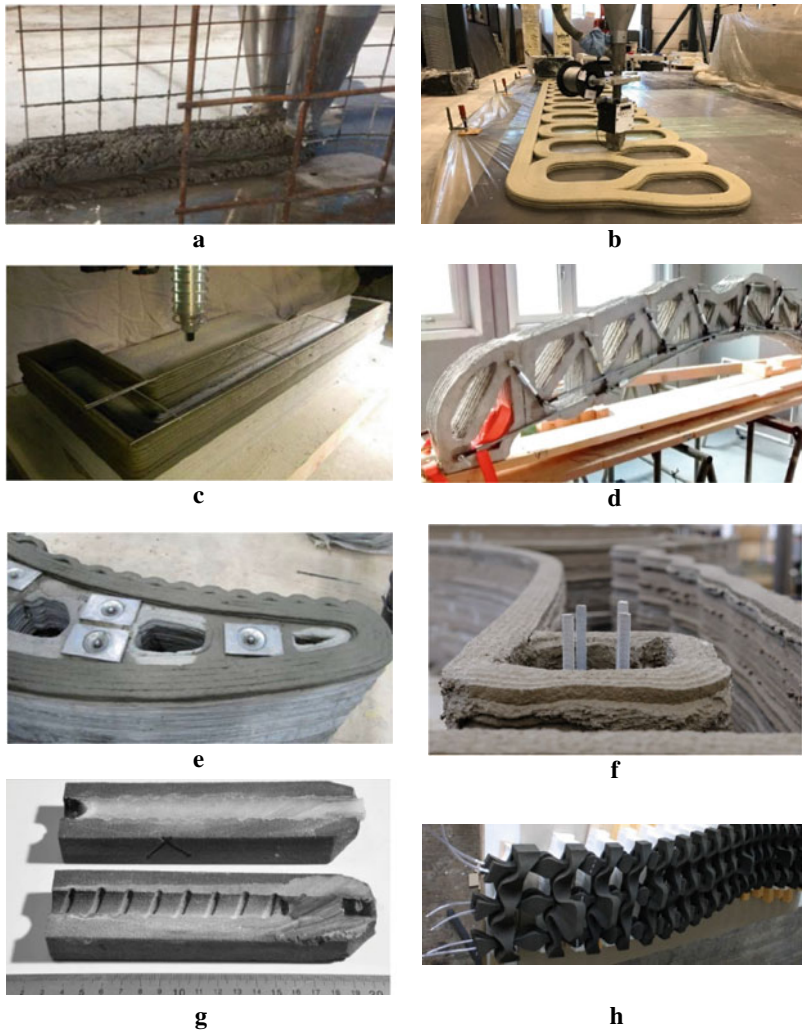
The feasibility and potential of the reinforcement strategies presented in Table 6.1 depend on the digital process used for forming concrete. Partially based on the work of Asprone et al. (2018) and Nerella et al. (2018), reinforcement strategies suitable for some of the main digital concrete manufacturing processes are discussed in the following:

- Additive manufacturing—extrusion:
  - *Enveloping reinforcement with concrete* (reinforced before concrete manufacturing; composite (concrete / steel) structure): a forked nozzle lays concrete on both sides of the reinforcement (Fig. 6.2a). This strategy allows reinforcing perpendicularly and within the printing direction, but currently, this method is limited to single curved elements with only one layer of reinforcement (see case study of the Sect. 3.8 in Chap. 2).
  - *Printable fibre reinforced concrete* (reinforced during concrete manufacturing; reinforced printing material): short fibres suitable to be pumped are added to the concrete matrix providing post-cracking tensile and stress-bridging capacity across the cracks. This solution provides strong fibrealignment in the printing direction, which could increase the fibre reinforcement effectiveness. Given the potential of this solution, it will be further discussed in Sect. 6.3.
  - *Entraining cable into the concrete filament* (reinforced during concrete manufacturing; composite structure): a flexible reinforcement cable is directly



entrained into the extruded layer during printing (Fig. 6.2b). This concept allows reinforcing the elements in the printing direction even for complex shapes but is difficult to ensure a proper anchorage of the cables when working with smooth high strength cables (see case study of the Sect. 3.1 in Chap. 2).

- *Placing reinforcement between 3D-printed concrete layers* (reinforced during concrete manufacturing; composite structure): reinforcement such as steel bars or textile reinforcement can be placed in between two layers, providing reinforcement in the printing direction (Fig. 6.2c). When using stiff reinforcement bars, a pre-bent in usually complex shapes is required.
  - *External reinforcement arrangement* (reinforced after concrete manufacturing; composite structure): two separate external steel reinforcing layers are post-installed on both sides of the hardened concrete element and connected through orthogonal threaded rods (Fig. 6.2d). This approach allows to reinforce complex shapes, but it is hand-labour intensive, and its durability/fire resistance should be addressed.
  - *Pre-stressed external reinforcement* (reinforced after concrete manufacturing; compression loaded structure): pre-stressing with post-placing of reinforcement in 3d-printed conduits (Fig. 6.2e). While this solution might limit the form freedom, known strategies and detail solutions from conventional externally pre-stressed structures can be directly applied.
  - *Reinforcement inside 3D-printed concrete formwork* (reinforced after concrete manufacturing; composite structure): here a 3D-printed element is used as a lost-formwork and a conventional reinforced concrete structure is produced inside the lost formwork (Fig. 6.2f and case study of the Sect. 3.3 in Chap. 2). In this approach, complex reinforced structures can be produced with the injection reinforcement technique (Fig. 6.2h). Digital manufacturing generally refers to the formwork and not to the entire manufacture of the component. The Injection reinforcement technology, on the other hand, also allows complete automation of the process.
- Additive manufacturing—spraying:
    - *Spraying around or on top of reinforcement* (reinforced before concrete manufacturing; composite structure): in this process, concrete is sprayed around (or even just on top) a pre-built mesh or textile reinforcement (Fig. 6.3a). This alternative is more promising than the equivalent extrusion process (enveloping reinforcement with concrete), as in this case the form freedom is not restricted, due to the flexibility of the spraying process. A specific implementation of such a process is the case study of Sect. 3.2 in Chap. 2, in which there are two spraying processes, i.e. before and after the reinforcement placement.
    - *Sprayed fibre reinforced concrete* (reinforced during concrete manufacturing; reinforced printing material): either short pumpable fibres can be added to the matrix or longer ones can be added sprayed together with the concrete. While fibre alignment is less controllable than when applied with extrusion production, by spraying is possible to provide fibre reinforcement in any direction of the structural element.

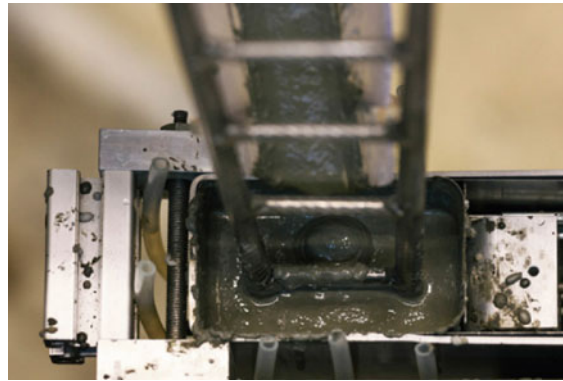


**Fig. 6.2** Reinforcing strategies for extrusion based additive manufacturing: **a** enveloping reinforcement with concrete (Schlaich et al. 1987), **b** entrained cable into the concrete filament (Bos et al. 2017), **c** reinforcement placed between 3D-printed concrete layers (TotalKustom 2015), **d** external reinforcement arrangement (Asprone et al. 2018), **e** prestressed external reinforcement (Lim et al. 2012), **f** reinforcement inside 3D-printed concrete formwork (Apis-cor 2017), **g-h** injection reinforcement inside 3D-printed concrete formwork (Kreiger et al. 2019)

- The external reinforcement arrangement and the pre-stressed external reinforcement, already presented for extrusion processes, might be applicable very similarly to sprayed concrete elements.
- Formative manufacturing:

- *Forming around existing reinforcement* (reinforced before concrete manufacturing; composite structure): in forming methods, the reinforcement integrated can be fabricated before concrete manufacturing and then the concrete is shaped around it (see the case study of Sect. 3.6 in Chap. 2, Fig. 6.3b). The complex

**Fig. 6.3** Reinforcing strategies for spraying based additive manufacturing and for formative manufacturing: **a** spraying on top of knit textile membrane (Knitcrete et al. 2018), **b** forming around existing reinforcement (Smart Dynamic Casting 2019), **c** robotically fabricated reinforcement as permeable formwork (Mesh Mould 2019)

**a****b****c**

geometry of the vertical structural element is thus the main source of difficulty when using internal deformed steel bars, which could be solved using robotic reinforcement assemblies.

- *Reinforcement as permeable formwork* (reinforced before concrete manufacturing; composite structure): this strategy corresponds to the Mesh Mould technology in which a double side fine reinforcement mesh is robotically fabricated to serve at the same time as structural reinforcement and permeable formwork. In the first implementation of this strategy the meshes are produced by welding short reinforcement bars in one direction, therefore the mechanical capacity of the reinforcement is limited to this direction.
- The use of fibre reinforced concrete or external pre-stressing might be applied as well for formative manufacturing, but the suitability of these reinforcing strategies should be studied for each specific application.

### 6.3 Fibre Reinforcement in Digitally Fabricated Concrete

As highlighted in previous sections of this chapter, fibres do represent one of the key alternatives to face the need of providing adequate reinforcement in digitally fabricated concrete materials and structural components. As a matter of fact, the possibility of extruding/3D printing a fibre reinforced composite represents a straightforward solution encompassing the structural requisites highlighted above with the peculiarities of the extrusion-based digital fabrication technologies.

Fibre Reinforced Concrete (FRC) and Fibre Reinforced Cementitious Composites (FRCCs), after more than fifty-year intensive scientific investigation and structural applications pushed it from a pioneer solution to a more and more widespread solution. Nonetheless, just recently, it has been internationally recognised the full status/dignity of a structural material in the last edition of the *fib* Model Code 2010 (2010) (see also recommendations by RILEM TC 162-TDF (2003, 2002)). Structural design approaches for FRC-only and hybrid reinforced (fibres + conventional reinforcement) concrete structures are therein provided in a framework fully consistent with the one for ordinary reinforced concrete structures and complemented with guidelines and recommendations for the identification of post-cracking residual strength classes based on design material parameters from standardised material classification tests (EN 14651 2005). Similar conceptual approaches can also be found in documents recently published by TC 544-Fibre Reinforced Concrete of the American Concrete Institute (ACI).

Extrusion techniques in the manufacturing of (also fibre reinforced) cement-based composite products have been studied and applied, also at the commercial scale, since quite long before digitally fabricated concrete materials and components even came onto stage (Burke and Shah 1999; Peled et al. 2000; Peled and Shah 2003; Kuder and Shah 2003, 2010). Requisites for “extrudability” of a cement-based mix were quantified in terms of fundamental rheological properties in the domain of capillary rheology (Srinivasan et al. 1999; Zhou and Li 2005).

Like in several other cases of fibre reinforced cementitious composites with adapted rheology (including, *e.g.*, Fibre Reinforced Self-Compacting Concrete FRSCC—(Ferrara 2014)), in the case of digitally fabricated—extrusion-based fibre reinforced cement-based materials two issues of paramount importance have to be considered.

First of all, in the concept and design of the composition of the fibre reinforced composite, not only the compatibility of the fibres, in terms of size and stiffness, with the printing equipment has to be considered but also the influence of the fibres on the rheology of the composite has to be considered, through suitable models (Ferrara et al. 2007; Martinie et al. 2010), as a function of their type and dosage, geometrical and physical–mechanical characteristics. This means that producing a successfully 3D printable FRCC does not mean to merely add fibres to a successfully 3D printable plain matrix and check the maximum amount of fibres that can be added without losing the “processability” features.

Secondly, once again like in all other categories of fibre reinforced cementitious composites with adapted rheology, processing can substantially influence the fibre dispersion and orientation (Martinie and Roussel 2011; Ferrara 2015), which affect the performance of the composite both in the fresh and hardened state, with resulting outcomes on the quality and on the structural performance of the application as well as on the total cost of the production (not only due to the cost of the constituent materials, whose use can be optimized through enhanced structural efficiency of the composite but also related to the ease with which the material can be handled).

In this framework, it is henceforth evident that the relationship between processing and performance of the material represents a crucial aspect in establishing a “holistic approach” which tailors the design of the material and of the extrusion process to the anticipated structural performance and structural use and efficiency of the material under the intended service load scenarios.

Studies on the influence of flow-driven fibre alignment on the mechanical properties of fibre reinforced cementitious composites with adapted rheology have been quite abundant in the last decade or so (Ferrara et al. 2011; di Prisco et al. 2013; Abrishambaf et al. 2013), highlighting the resulting strong material anisotropy whose implications on the performance of structural applications have been also interestingly addressed (Baril et al. 2016; Ferrara et al. 2017; Abrishambaf et al. 2015a, b).

Hamback and Volkmer (2017) were among the earliest to investigate the effects of 3D-printing path on the flexural and compressive behavior of Portland cement pastes reinforced with 1% by volume of carbon fibres. The authors, confirming that an effective fibre alignment was enforced along the print path direction highlighted how the build path itself could be used to spatially control the fibre orientation within the printed structures so to optimize the structural efficiency of the material (Figs. 6.4 and 6.5). Such a “fine-tuning” the mechanical performance of a fibre reinforced cementitious composite, also through the possibility of printing “hierarchical” / functionally graded structures, which could further benefit from such an enhanced structural efficiency. The latter intrinsically calls for the development of 3D printable FRCCs featuring a strain-hardening tensile behavior (Figueredo et al. 2019)

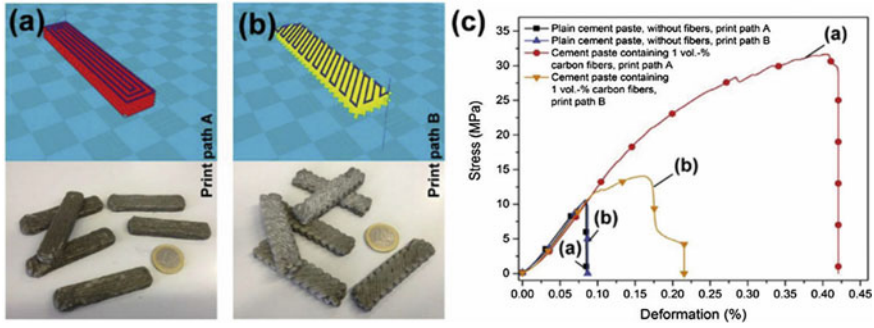


**Fig. 6.4** 3D-print path models in 3D-printing software and photographs of specimens fabricated via **a** print path A and **b** print path B for 3-point bending test, **c** stress-deformation plots for plain cement samples (without fibers) and carbon fiber-reinforced samples in 3-point bending test proving high flexural strength of print path A samples being reinforced with carbon fibers (Hambach and Volkmer 2017)

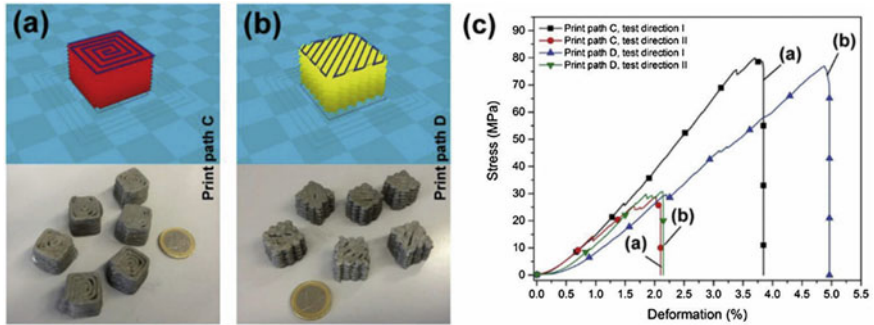


**Fig. 6.5** 3D-print path models in 3D-printing software and photographs of specimens printed via **a** print path C and **b** print path D for uniaxial compressive strength test, **c** Stress-deformation plots for plain cement samples (without fibers) in uniaxial compressive strength test showing high strength for test direction I and low strength for test direction II (Hambach and Volkmer 2017)

with adequate strain capacity, able to resist effectively, without the need for conventional reinforcement the tensile actions where needed, (including, e.g. tie elements in truss structures and tensile chords/meridians in two-dimensional planar or curved structural elements).

First results on the development of printable strain-hardening cementitious composite (the authors used the denomination Engineered Cementitious Composite) have been published by Soltan and Li (2018). Based on considerations of extrudability (indicating the ability of the mixture to pass through a printing system) and buildability (indicating the ability of a mixture to remain stable after deposition and during printing), that together define the printability, they developed several mixtures with 2% by volume polyvinyl alcohol (PVA) 12 mm length fibres. While investigating the influence of several ingredients on fresh state workability and processing

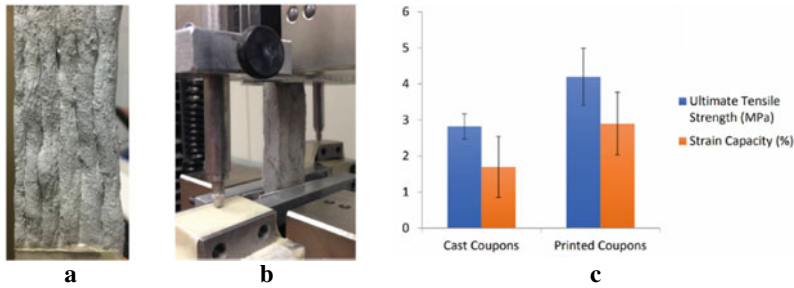


**Fig. 6.6** A 3D-printed coupon specimens, **b** direct tension tests and **c** effect of the printed structure on the tensile strength and strain capacity (Soltan and Li 2018)

parameters, the authors ended up with a 3D printable mix showing strain-hardening tensile behaviour, though the assessment of fresh state properties was only based on the flow tests and not on the measurement of a fundamental rheological property. In addition, the real printability was not truly yet established as only several layers were deposited with a manual piston. Nonetheless, by 3D printing coupon specimens for direct tension tests (see Fig. 6.6) and testing them in comparison with “conventionally” fabricated ones, the authors found that the former, with highly aligned fibre orientation, outperform the latter both in terms of ultimate tensile strength and strain capacity (see Fig. 6.6c). No significant difference was detected in terms of compressive strength.

Similar results were obtained by Ogura et al. (2018), who printed 1 m long walls, 120 and 30 mm thick, employing strain-hardening cementitious composites reinforced with up to 1.5% by volume short (6 mm long) high density polyethylene fibres (Fig. 6.7). From these walls, they obtained “layered” 250 mm long, 40 mm wide and 25 mm thick coupon specimen that were tested in direct tension, also in comparison with dog-bone conventionally mould-cast ones (Fig. 6.6). A better performance of the printed specimens was confirmed preliminary in terms of strain capacity, the higher the fibre dosage the higher the performance, the extrusion-induced fibre orientation also resulting in a well-distributed multiple fine crack patterns as compared to the less regular and less “saturated” one, in terms of crack spacing, featured by mould-cast specimens. Though, the authors remarked that up to a strain of 0.3%, which largely includes the widest possible service range scenarios (it is worth here remarking that the yielding strain of conventional steel reinforcement bars is around 0.2%); the differences among the printed and mould-cast specimens and even between fibre volume ratios equal to either 1 or 1.5% were negligible. Such a consideration may play a relevant role when deciding about the most suitable mix-composition with reference to the identified values of its design parameters to be used in serviceability and ultimate limit state checks of the intended application.

While consistent structural design approaches are being developed for this category of cement-based materials, the pioneer studies reviewed above have highlighted peculiar issues related to digital fabrication technologies, which have to be addressed

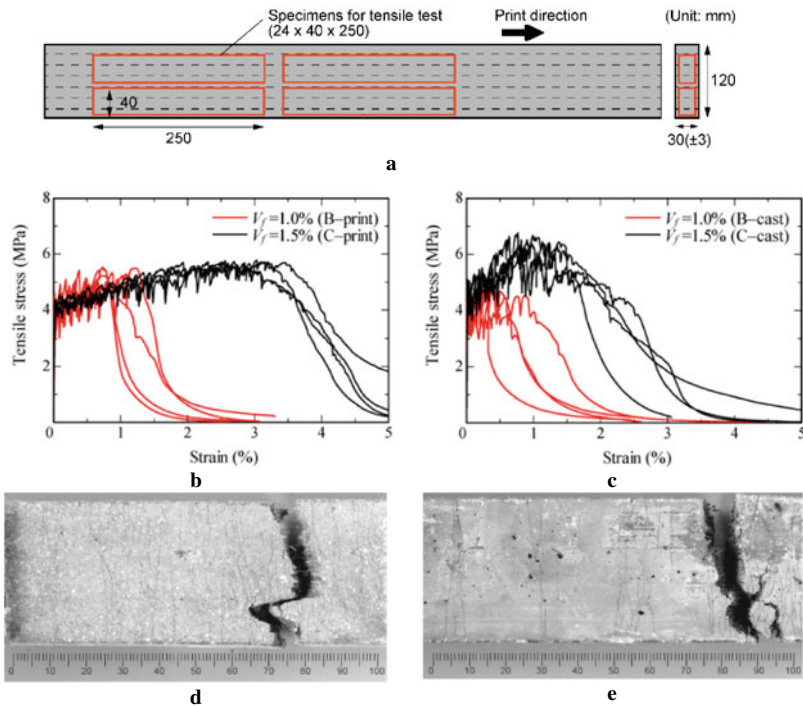


**Fig. 6.7** a Position of the specimens for direct tension tests in the printed wall; stress–strain curves obtained from uniaxial tension tests on **b** printed and **c** mould-cast specimens and representative crack patterns of specimens after failure in uniaxial tension tests on print specimen **d** and **e** mould-cast specimen (Ogura and Mechtcherine 2018)

in order to customize the same approaches to the specific one-of-a-kind features of digitally fabricated elements and structures, including:

- The development of the tensile strain-hardening behaviour in the very early ages (fluid to solid state transition), i.e. in temporary design situations reflecting and affecting the ongoing fabrication.
- The influence of the interlayer bond on the effectiveness of the aforementioned behaviour.
- The need to develop tailored specimen fabrication and testing procedures for the identification of tensile design parameters in such a way to adequately take into account all the aforementioned issues, i.e. suitably representing the influence not only of the “extrusion”-induced orientation of the fibres (which is by now a fully design-wise acquired concept) but also, if not primarily, of the fabrication process characteristic parameters, including, e.g. layer thickness, speed of extrusion, fabrication path.



## 6.4 Design Principles and Modelling

The fundamental structural principles on which digitally fabricated elements (reinforced or not) are based do not differ from those of conventional cast or pre-cast RC structures; in these terms, proper design methods based on consistent mechanical models should be applied to DFC manufactured elements as well. However, available mechanical models need to be re-tuned at the material/component scale in order to account for particularities and/or specific effects induced by the novel fabrication method. Focusing on the scale of concrete material, some of these “new” effects include:

- Reduced bond strength between layers.
- Anisotropy.
- Shape-related mechanical effects.
- Printing path and sequence.
- Concrete interaction with a specific reinforcement strategy.

The thorough knowledge and understanding of the above-mentioned aspects represent a fundamental step for the design of DFC structures because they affect the macroscopic response of the fabricated elements.

### 6.4.1 Approach to Anisotropy

Concrete layer interfaces might represent a source of weakness for printed elements due to the formation of cold joints, which originate from the time gap between two consecutive layers. In this regard, Wolfs et al. (2019) and Le et al. (2012) investigated the bond strength of layered elements through properly designed experimental tests and found that printed element strength and stiffness are affected by the loading direction relative to layer orientation (Fig. 6.8).

However, a very limited influence of layer orientation was found for a sufficiently short interlayer time interval and when the load acted along the normal direction to the layers (Orientation I in Fig. 6.8).

In terms of structural design, this situation is different from conventional concrete for which the “bulk” properties of the element are isotropic. Therefore, a possible “new feature” for such a material design (to consider the layer configuration) might entail the evaluation of printed element compressive strength,  $f_{c,d}^*$ , as shown in Eq. 6.1:

$$f_{c,d}^* = \alpha_{dir} \cdot f_{c,d} \quad \text{with } \alpha_{dir} \leq 1 \quad (6.1)$$

where  $f_{c,d}$  is the compressive strength of the equivalent cast concrete and  $\alpha_{dir}$  is a reduction factor depending on the loading direction relative to the layer orientation (to be calibrated through specific tests).

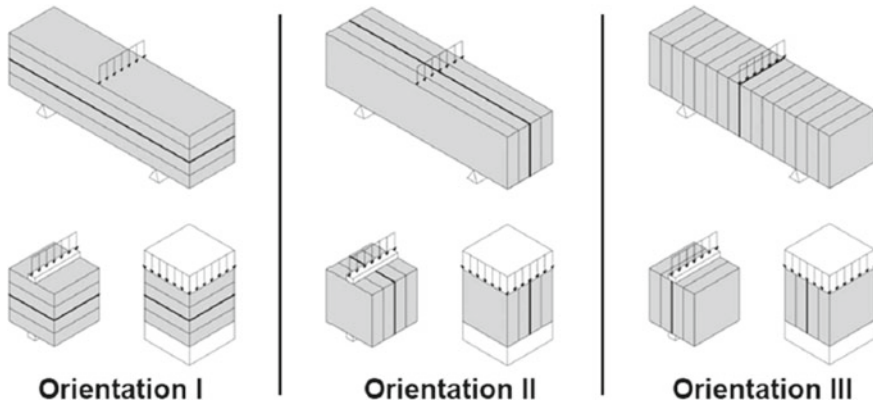


**Fig. 6.8** 3D Printed layer orientations in flexural tension, tensile splitting, and compression tests (Wolfs et al.)

Regarding the structural design of printed fibre reinforced composites similar challenges arise as the previous ones, since as overviewed in Sect. 6.3 the printing process will lead to a preferential fibre alignment along the printing path. The latter will be influenced by a panoply of variables, such by e.g. rheological properties of the matrix, fibre's aspect ratio, layer height, printing speed, among others. The expected anisotropy of the fibre distribution / orientation within a printed element subsequently will lead to anisotropic material properties, in particular for the tensile behaviour, since it is acknowledge that the fibre reinforcement has a relatively low influence on the compressive strength (and low to moderate effect on the compressive post-peak behavior).

Approaching the anisotropic tensile behaviour of printed fibre reinforced composites will pose a bigger challenge than the one presented under compression, since the benefits of fibres mainly arise after cracking and the material behaviour is usually translated by a tensile stress—crack opening or—strain. The shape of these material laws will depend on multiple variables, by e.g. fibre type, geometry and content, fibre/ matrix bond strength and fibre distribution / orientation, in particular the fibre's orientation regarding an active crack plane (i.e. towards the principal tensile stresses). Therefore, a mere reduction factor employed to the tensile strength and/or to the residual tensile strengths may not be suffice to correctly take into account this anisotropic behavior, consequently tensile stress—crack opening or—strain relationships should be obtained for distinct layer orientations through adequate test methodologies.

Another possibility is the use of a “virtual laboratory” supported on numerical analysis through the FEM to obtain the material tensile relationship for a certain direction regarding printing direction. Fibre reinforced composites can be regarded in a simplified way as two-phase materials. Hence, FRC can be modelled in a realistic fashion by bi-phase models, respectively, by the discrete and explicit representation of fibres and plain concrete contribution, i.e. unreinforced matrix (Soetens

and Matthys 2014; Radtke et al. 2010, 2011; Cunha et al. 2011, 2012; Abrishambaf et al. 2016; Zhan and Meschke 2016). In general, these models have into account the fracture process of the unreinforced matrix and the fibre reinforcement mechanisms of the discrete fibres bridging an active numerical crack. The fracture process of plain concrete, i.e. unreinforced matrix, or mortar can be modelled by smeared crack approaches, fracture-based energy interface models or damage mechanics constitutive models. On the other hand, reinforcement mechanisms of fibres being pulled out can be modelled using micro-mechanical behaviour laws (obtained through experimental, analytical or numerical techniques). These approaches rely on both the accurate knowledge of the fibre's micro-mechanical behaviour and the realistic representation of the fibres' structure, through an appropriate distribution and orientation of fibres.

Finally, another challenge regarding the structural design of printed fibre reinforced structures would be related to the modelling approaches that could be employed, since code-alike cross-sectional analysis for design would not take full advantage of the fibre reinforced composite capabilities in stress redistribution after the formation of an active crack. Hence, fully non-linear material analysis under the FEM framework would be necessary. Even though FEM methodologies have been used for a longtime to model conventional reinforced concrete as well as FRC, still nowadays they lack a consistent predictability under serviceability, namely in predicting crack patterns, crack openings and spacing. Moreover, the utilization of complex numerical models is intricate, usually not accessible to the common designer, and reliability of a certain numerical analysis is strongly dependent of the user's experience.

#### **6.4.2 Models and Load-Bearing Capacity**

From a practical point of view, it could be interesting to understand if the pre-existing models, developed for the calculation of the bearing capacity (moment, shear, torsion, etc.) of traditional RC elements, would be able to give reliable responses also for elements manufactured with DFC techniques. In this regard, to determine the capacity of a structural element (depending on the different limit states), it is first necessary to verify if the hypotheses of available models (i.e. developed so far for ordinary and pre-stressed concrete elements), are valid also in the case of digitally fabricated elements. For instance, for the evaluation of the ultimate moment capacity of reinforced or pre-stressed concrete cross-sections, the following assumptions are considered (EN 1992-1-1: 2004 par. 6.1):

- Plane sections remain plane.
- Strain in bonded reinforcement or bonded pre-stressing tendons is the same as that in the surrounding concrete.
- Tensile strength of the concrete is ignored.

- Stresses in the concrete in compression are derived from the design stress/strain relationship given in EC2.
- Stresses in the reinforcing or pre-stressing steel are derived from the design curves in EC2.
- Initial strain in pre-stressing tendons is considered when assessing the stresses in the tendons.

To put this discussion in the context of digitally fabricated concrete elements, these hypotheses could be still valid depending on the adopted printing and reinforcing technique. For example, in the case of the 3D printed RC beam (Asprone et al. 2018) in Fig. 6.21 with an external reinforcement system, the second hypothesis will not be applicable. Similarly, additional studies are needed to assess the validity of the first hypothesis, i.e. on how the planar cross-section can be guaranteed depending on the specific fabrication technique and shape of the element.

A further structural principle often applied to digitally fabricated elements, is the post-tension. There are several applications consisting of fabricating concrete segments subsequently connected by post-tensioned cables aligned with the deposition direction. Initially, this principle was applied at Loughborough University (UK) for the design and digital manufacturing of a free-shaped wall-like concrete bench using the ‘Concrete Printing’ approach (Lim et al. 2012), an automated extrusion-based process for concrete (see Fig. 6.9). The printed structure included a certain



**Fig. 6.9** Digital manufacturing of a free-shaped wall-like concrete bench (Buswell et al. 2018)



**Fig. 6.10** Printed showcase segment for the pedestrian and bicycle bridge (Bos et al. 2019)

number of conduits passing through the height of the bench. These were used for the post-printing placement of reinforcing bars that were post-tensioned and grouted to achieve a predetermined compressive stress state into the structure. A large-scale application of this principle is the pedestrian and bicycle bridge developed at the Eindhoven University of Technology (TU/e) (Fig. 6.10) (Theo et al. 2018), which was placed in Gemert, Netherlands (see the case study of the Sect. 3.1 in Chap. 2).

Thus, the application of the post-tension to the fabricated 3D printed concrete blocks could represent a valid solution to overcome the critical issues related to the assembly of several concrete segments but, at the same time, this would require particular attention to the effects produced by creep and shrinkage.

The use of totally different digital fabrication technologies impacts the way the reinforcement can be installed/incorporated and, consequently, calculated. It is well-known that the concrete tensile strength is small and so it is necessary to design an adequate reinforcement or develop suitable strategies to absorb tensile stresses. In traditional design of RC structural elements, reinforcement requirements ensure that the reinforcement is yielded in the ultimate limit state. This rule should be adapted to the available DFC technique in order to provide ductility for DFC elements. However, this aspect has not been adequately investigated so far or, for instance, has been found not to be applicable as in the case of the straight RC beam proposed by Asprone et al. (2018) in which the element failure (due to local mechanisms) preceded the yielding of the reinforcement. Quite the opposite, the compliance with reinforcement quantities provisions could be effortlessly achieved for some DFC technologies. An example is the 3D Concrete Formwork Technique through which the placement of horizontal and vertical reinforcement creates a regular reinforcing scheme in structural elements with a standard geometry. Using this technique, the US Army 3D printed complete barracks, also known as a B-Hut, within a three-year program called Automated Construction of Expeditionary Structures (ACES). The walls of the B-Hut acted as permanent formworks with a hollow core that was reinforced and backfilled with concrete after completion of the fabrication (see Fig. 6.11) (Kreiger et al. 2019).

In general, such a technique allows for the fabrication of RC structural panels or wall-like elements. To be considered a structural element it has to fulfill some code prescriptions about thickness, reinforcement percentage, ductility, seismic details



**Fig. 6.11** Rendering of B Hut A

and other specifications. For instance, two major issues need to be addressed in reference to code compliance for the Mesh Mould technique; these are the use of only a certain range of reinforcement rebar diameters and the use of different stirrups spans in element height.

An even different design scenario arises when the reinforcement is placed during concrete fabrication. One of the most advanced concepts, currently under development at TU Eindhoven, is the direct entrainment of reinforcement cable into concrete layer during printing. In this case, the conventional hypothesis on concrete-reinforcement bond (nr. 2) has to be verified in relation to the strain in the bonded cable reinforcement. Indeed, in conventional RC structure, cast in-place or pre-cast technology allow for a robust bond between reinforcement and the surrounding concrete which is modeled by means of semi-empirical bond-slip models (2010), available in current regulations.

From the design point of view, connections between digitally fabricated concrete elements represent a further source of uncertainty. In several practical cases, reinforcement is used not only to absorb the tensile stresses that develop in the structural element, but also to make the connection between concrete segments effective, providing (possibly) ductility. This latter function is of uttermost importance if rotational capacity and/or dissipative capacity must be conferred to the final structural element. In some digitally fabricated RC structures (Asprone et al.), local failure mechanisms were observed in concrete-reinforcement connection, thus requiring greater attention for the purposes of design and calculation.

In general, testing and detailed modelling of concrete-reinforcement interaction still represent an issue for the effective design and implementation of DFC structures. Fundamental aspects of capacity design (e.g. avoiding premature brittle failures, ductility etc.) are strongly reliant on the DFC technique adopted and, for this reason, deserve much attention in order to create reliable predictive models. Finite Element (FE) analyses and numerical modelling certainly can help to predict the

mechanical/structural behaviour of DFC structures (Wolfs et al. 2018); however, at this stage of development, there is not enough full-scale experimental evidence to support FE reliability.

From the above discussion it clearly appears that further experimental/numerical studies need to be carried out in the context of DFC structures. The common goal is to update/integrate current capacity models (developed for existing structural typologies such as steel–concrete composite elements, post-tensioned members etc.) available in national and international codes, with the final aim of creating the appropriate framework of calculation for DFC structures.

### 6.4.3 *Structural Optimization*

The geometrical freedom introduced by digital manufacturing technologies theoretically, is often expected to allow the application of structural design through optimization strategies. However, for the time being, a discrepancy remains between the underlying assumptions in existing optimization methods on the one hand, and the constraints of manufacturing on the other hand. Rippmann et al. (2018), presented the design, fabrication, and testing of a floor consisting of multiple elements, printed in sand using a powder-bed selective binding method. By using Thrust Network Analysis, the authors were able to create a purely compression-loaded floor, with a weight reduction of 70% compared to a solid floor. As the floor itself is tension-free, no reinforcement is required for the considered load case. Thus, the optimization strategy addresses an important manufacturing constraint. The applied method also allowed consideration of minimum wall thickness and maximum element size. On the other hand, directional variations in material rigidity were not incorporated in the approach. In comparison to powder-bed based selective binding methods, selective material deposition by extrusion features additional constraints, amongst which is the requirement of a continuous filament (and thus print path—although some suppliers have now presented stop-start technologies that could remove this constraint), and the fact that filament needs to be supported by previously deposited layers (or the print base plate). This further complicates the application of optimization strategies. Vantghem et al. (2019), designed, manufactured and tested a pre-stressed beam assembled from parts made by selective material deposition by extrusion. The design was based on a 2D topology optimized beam, taken from literature, as the authors recognized the match between the particular optimization case and the manufacturing possibilities. First results of a more general topology optimization approach for extrusion-based DFC, were published by Martens et al. (2017), and Martens (2018). The model included a selection of yield failure criteria (Drucker-Prager or von Mises), the variation of stiffness in different directions, a support angle constraint (i.e. to require a layer is supported by another), and the base plate orientation. Some challenges remain, nevertheless, particularly with regard to print path determination. Thus, optimization methods need further development to better include manufacturing constraints, and/or vice versa.

## 6.5 Structural Testing and Validation

At increasing level of development of DFC technologies, there is a strong need to investigate the mechanical performance / response of the fabricated structural elements, focusing on different scales (at the scale of the material or element). The structures made with DFC elements are innovative to the point that there are no codes and guidelines for the testing methods and assessment of the structural performance. For this reason, the design of these structures is always followed by tests that validate their performance.

At the scale of the printed element, several authors developed proper testing procedures to investigate the mechanical particularities of DFC products. As for the study of anisotropy, recent studies conducted by Wolfs et al. (2019) have shown how flexural tensile, tensile splitting and compressive strengths change with the printing direction (Fig. 6.8). Similarly, a proper test set-up (see Fig. 6.12) was proposed by Asprone et al. [89] in order to characterize the fracture energy during shear testing of concrete layers interfaces (cold joints). The set-up was inspired by the punch-through shear test, although some modifications on the original set-up and the specimen's geometry was made due to constraints related to the printing process.

In contrast to material scale testing, the full-scale experimental behaviour of DFC structures has been rarely investigated. A complete experimental characterization was carried out for a 3D concrete printing pedestrian and bicycle bridge in Eindhoven. The structure was fabricated following the concept of 'Design by Testing' (Theo et al. 2018) and certified safe for public use. In particular, the bridge design was the result of a vast experimental campaign aimed to prove the structural integrity of the printed element. A 1:2 bridge sample was tested in a load-controlled four-point bending test, as shown in Fig. 6.13. A final full-scale flexural test (see Fig. 6.14) was

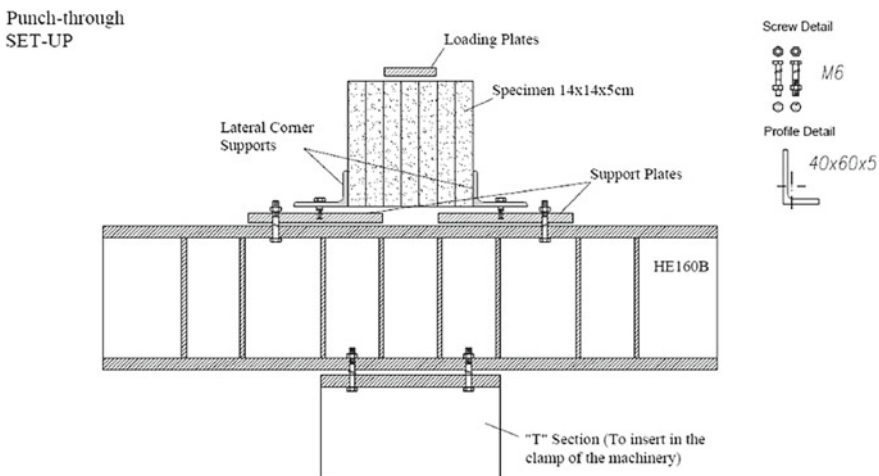


Fig. 6.12 Punch-through set-up (Asprone et al.)





**Fig. 6.13** Scale model in test 4-point bending test set-up (Theo et al. 2018)



**Fig. 6.14** In situ test (Theo et al. 2018)

performed in situ to guarantee that the bridge behaves as expected and be structurally safe. In situ full-scale testing is an example of a non-destructive assessment and it is used on a regular basis to verify the load-bearing capacity of older and existing infrastructures. A test phase with large-scale elements was conducted for the design of Nyborg Pavilion by (Bos et al. 2019). The Fig. 6.16 shows the cross-section of the perimeter wall of the pavilion (Fig. 6.15).

Approximately 750 mm wide straight segments of the wall section design were tested in different loading conditions.

**Fig. 6.15** Wall during printing process (Theo et al. 2018)

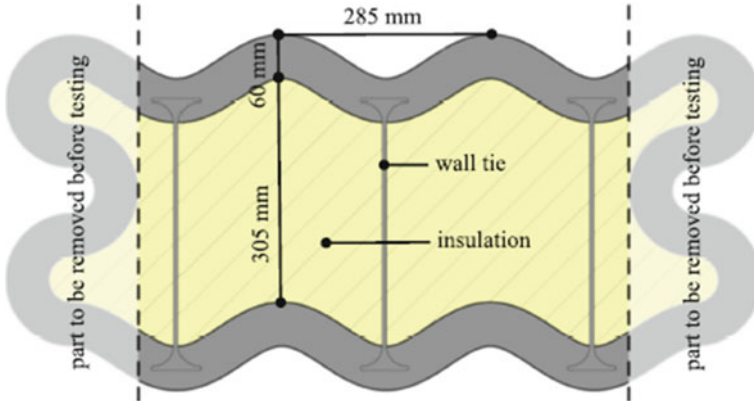


**Fig. 6.16** Cross-section of the wall (Bos et al. 2019)

Compression test with the load that was applied once on each face of the tested element (see Fig. 6.17).

Vertical flexural test, as a 3-point bending test on ‘standing’ elements, with the load acting horizontally (see Fig. 6.18).

Impact test during which the element was subjected to pendulum impact loading in a set-up derived from EN 12,600 (see Fig. 6.19)

With the aim to evaluate the flexural behaviour and failure mechanisms, another example of large-scale test was carried out with a straight beam, manufactured by means of technology solution, mentioned in the previous chapters, developed at the University of Naples “Federico II” (Asprone et al. 2018). In detail, a three-point bending test was conducted on the RC straight beam. The test scheme and set-up are shown in Figs. 6.20 and 6.21.

**Fig. 6.17** Compression test  
(Bos et al. 2019)



**Fig. 6.18** Vertical flexural test  
(Bos et al. 2019)



The test was carried out by means of a universal servo-hydraulic testing machine. The assumed load scheme ensures that the primary failure comes from tensile or compression stress. The test was conducted under displacement control, with a velocity of 0.5 mm/min.

Strain measurements on the steel components of the beam were achieved through strain gages placed at half-length of each stainless threaded rod, as shown by Fig. 6.20. For the strain measurements of compressed concrete, always strain gages were used only at the backside of the beam. Instead, in order to measure the displacement at the mid-span of the beam, two linear variable differential transducers (LVDTs) were placed at the bottom edge in correspondence of the half of the beam.

Successively numerical simplified analyses (2D models) were to compare experimental and numerical data were carried out and presented in order to validate



Fig. 6.19 Impact test (Bos et al. 2019)

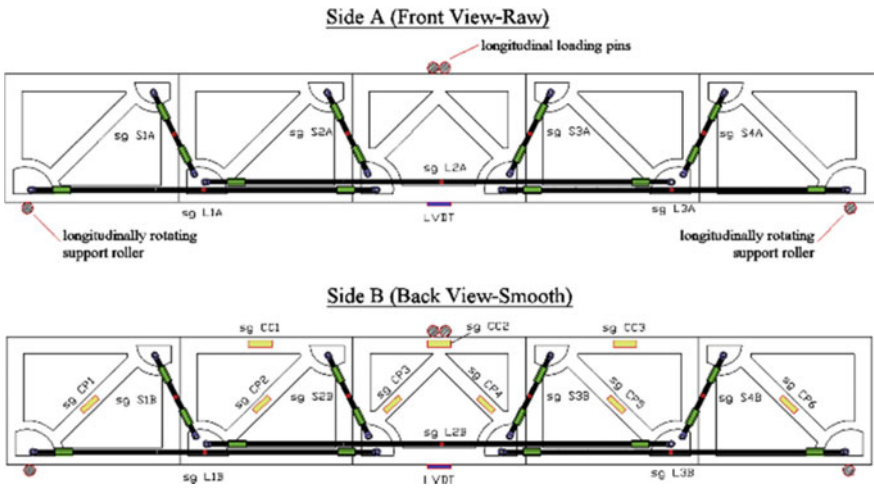
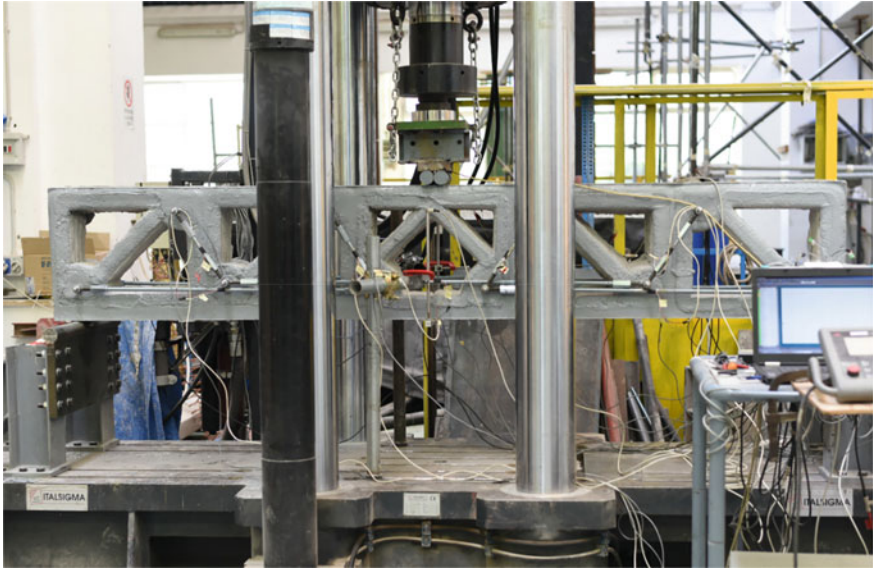


Fig. 6.20 Front view and back view of the straight beam with strain measurement devices (Asprone et al. 2018)



**Fig. 6.21** Equipped specimen for the three points bending test (Beam UniNa) (Asprone et al. 2018)

numerical simulations as well as to obtain a better interpretation of the experimental test.

This has led to outcomes that have demonstrated that the initial flexural stiffness of the printed RC beam is comparable with an equivalent solid RC beam whereas the overall nonlinear flexural behaviour is influenced by local failure mechanisms, i.e. shear damage at the interfaces between adjacent concrete segments and steel–concrete anchoring failure. Even though several issues need to be addressed, this DFC technique can introduce a novel rational use of additive manufacturing technologies in structural engineering as it enables the fabrication of complex shapes (e.g. curved beams of variable height). The topological optimization of shapes enables harvesting innumerable advantages such the reduction of concrete volume and mass (and consequently mitigation of self-weight loadings), the elimination of complex formwork systems, and easy transportability and installation.

## 6.6 Conclusions

Principally, laws and codes, as well as common sense, require structures to be safe for use. To safeguard this, elaborated quality control procedures have been implemented for traditionally produced concrete structures in the construction industry, which are generally founded on regulations regarding three different target pillars:

- Construction products and materials.

- Construction processes (execution).
- Design (e.g. structural and durability).

The implementation of DFC impacts on each of these pillars. Therefore, current quality assurance systems and design codes do not adequately address DFC applications in practical cases. Considering the current state of progress of DFC as well as the time involved in design code development and subsequently its legal binding implementation, it should be expected that this situation is likely to continue for some time. Meanwhile, with ever more and more ambitious projects being proposed, the need to understand the structural engineering specifics and subsequently to develop unified approaches, is rapidly increasing; it is evident that the scientific and technical communities are aware of this need and a number of research and development projects are being developed to fill this gap.

## References

- (2002) RILEM TC 162-TDF Design of steel fibre reinforced concrete using the  $\sigma$ -w method: principles and applications. *Materials and Structures*, 35(5), 262–278.
- (2003) Final recommendation of RILEM TC 162-TDF: Test and design methods for steel fibre reinforced concrete: sigma-epsilon-design method. *Materials and Structures*, 36(8), 560–567.
- (2005) EN 14651:2005, Test method for metallic fibre concrete - Measuring the flexural tensile strength (limit of proportionality (LOP), residual).
- Abrishambaf, A., Barros, J. A. O., and Cunha, V. M. C. F. (2013). Relation between fibre distribution and post-cracking behaviour in steel fibre reinforced self-compacting concrete panels. *Cement and Concrete Research*, 51, 57–66.
- Abrishambaf, A., Barros, J. A. O., and Cunha, V. M. C. F. (2015a). Tensile stress-crack width law for steel fibre reinforced self-compacting concrete obtained from indirect (splitting) tensile tests. *Cement and Concrete Composites*, 57, 153–165.
- Abrishambaf, A., Barros, J. A. O., and Cunha, V. M. C. F. (2015b). Time-dependent flexural behaviour of cracked steel fibre reinforced self-compacting concrete panels. *Cement and Concrete Research*, 72, 21–36.
- Akbarzadeh, Masoud, Tom Van Mele, and Philippe Block. (2015). On the equilibrium of funicular polyhedral frames and convex polyhedral force diagrams. *Computer-Aided Design*, 63, 118–128.
- Abrishambaf, A., Cunha, V. M., and Barros, J. A. (2016). A two-phase material approach to model steel fibre reinforced self-compacting concrete in panels. *Engineering Fracture Mechanics*, 162, 1–20.
- Apis-cor. (2017). Apis Cor - construction technology. Available: <http://apiscor.com/en/faq/tecnologia-stroitelstva/>. [Accessed: 29-Dec-2017].
- Asprone, D., Menna, C., Bos, F. P., Salet, T. A. M., Mata-Falcón, J., and Kaufmann, W. (2018). Rethinking reinforcement for digital fabrication with concrete. *Cement and Concrete Research*, 112, 111–121. ISSN 0008-8846. <https://doi.org/10.1016/j.cemconres.2018.05.020>. <https://www.sciencedirect.com/science/article/pii/S0008884618300309>
- Asprone, D., Auricchio, F., Menna, C., and Mercuri, V. (2018). 3D printing of reinforced concrete elements: Technology and design approach. *Constr. Build. Mater.* 165. doi:<https://doi.org/10.1016/j.conbuildmat.2018.01.018>.
- Baril, M. A., Sorelli, L., Rethore, J., Baby, F., Toutlemonde, F., Ferrara, L., Bernardi, S., and Fafard, M. (2016). Effect of Casting Flow Defects on the Crack Propagation in UHPFRC Thin Slabs by Means of Stereovision Digital Image Correlation. *Construction and Building Materials*, 129, 182–192.

- Bos, R. Wolfs, Z. Ahmed, and T. Salet. (2019). Large Scale Testing of Digitally Fabricated Concrete (DFC) Elements. In: T. Wangler, and R. J. Flatt (Eds.), *First RILEM Int. Conf. Concr. Digit. Fabr. – Digit. Concr.* 2018, Springer International Publishing, pp. 129–147.
- Bos, F. P., Ahmed, Z. Y., Jutinov, E. R., et al. (2017). Experimental Exploration of Metal Cable as Reinforcement in 3D Printed Concrete. *Materials (Basel, Switzerland)*, 10(11).
- Bos, F. P., Wolfs, R. J. M., Ahmed, Z. Y., and Salet, T. A. M. (2016). Additive manufacturing of concrete in construction: potentials and challenges. *Virtual and Physical Prototyping*, 11(3), 209–225.
- Bran Anleu, P. C., Wangler, T., and Flatt, R. J. (2018). Chloride Ingress Through Cold Joints in Digitally Fabricated Concrete by micro-XRF Mapping.
- Burke, P. L., and Shah, S. P. (1999). Durability of extruded thin sheet PVA fiber-reinforced cement composites. In: *ACI SP-190 high performance fiber-reinforced concrete thin sheet products*, pp. 133–64.
- Bridge Nijmegen (<https://www.rijkswaterstaat.nl/nieuws/2019/03/nijmegen-krijgt-langste-betonnen-3d-geprinte-voetgangersbrug-ter-wereld.aspx>).
- Buswell, R. A., Leal de Silva, W. R., Jones, S. Z., and Dirrenberger, J. (2018). 3D printing using concrete extrusion: A roadmap for research. *Cement and Concrete Research*, 112, 37–49. <https://doi.org/10.1016/j.cemconres.2018.05.006>.
- Buswell, R. A., da Silva, W. R., Bos, F. P., Schipper, R., Lowke, D., Hack, N., Kloft, H., Mechtcherine, V., Wangler, T., and Roussel, N. (2020). A process classification framework for defining and describing Digital Fabrication with Concrete. *Cement and Concrete Research, Special Issue for Digital Concrete*.
- Cunha V. M. C. F., Barros, J. A. O., and Sena-Cruz, J. M. (2012). A finite element model with discrete embedded elements for fibre reinforced composites. *Comput Struct J*, 94–95, 22–33.
- Cunha, V. M. C. F., Barros, J. A. O., Sena-Cruz, J. M. (2011). An integrated approach for modelling the tensile behaviour of steel fibre reinforced self-compacting concrete. *Cem Concr Res J*, 41, 64–76.
- di Prisco, M., Ferrara, L., and Lamperti, M. G. L. (2013). Double Edge Wedge Splitting (DEWS): an indirect tension test to identify post-cracking behaviour of fibre reinforced cementitious composites. *Materials and Structures*, 46(11), 1893–1918.
- DFAB House. <http://www.dfab.ch/tag/dfab-house/>.
- EN 1990:2002 Basis of Structural Design.
- Feng, P., Meng, X., Chen, J. F., and Ye, L. (2015). Mechanical properties of structures 3D printed with cementitious powders. *Construction and Building Materials* 93, 486–497.
- Ferrara, L. (2015). Tailoring the orientation of fibres in High Performance Fibre Reinforced Cementitious Composites: part 1 - experimental evidence, monitoring and prediction. *Journal of Materials and Structures Integrity*, 9, 1/2/3, 72–91.
- Ferrara, L., Ozyurt, N., and di Prisco, M. (2011). High mechanical performance of fibre reinforced cementitious composites: the role of “casting-flow” induced fibre orientation. *Materials and Structures*, 44(1), 109–128.
- Ferrara, L., Cremonesi, M., Faifer, M., Toscani, S., Sorelli, L., Baril, M. A., Réthoré, J., Baby, F., Toutlemonde, F., and Bernardi, S. (2017). Structural elements made with highly flowable UHPFRC: correlating Computational Fluid Dynamics (CFD) predictions and non-destructive survey of fibre dispersion with failure modes. *Engineering Structures*, 133, 151–171.
- Ferrara, L. (2014). Fibre reinforced SCC. In *Mechanical Properties of Self-Compacting Concrete. State of the Art Report of the RILEM Technical Committee 228-MPS on Mechanical Properties of SCC*, K.H. Khayat and Geert de Schutter, eds. (Chapter 6), pp. 161–220, Springer, 2014, ISBN 978-3-319-03244-3.
- Ferrara, L., Park, Y. D., Shah, S. P. (2007). A method for mix-design of fibre reinforced self compacting concrete. *Cement and Concrete Research*, 37, 957–971.
- Figuereido, S. C., Romero Rodriguez, C., Ahmed, Z. Y., Bos, D. H., Xu, Y., Salet, T. M., Copuroglu, O., Schlangen, E., and Bos, F. P. (2019). 2An approach to develop printable strain hardening cementitious composites. *Materials and Design*, 169, 107651.

- fib Model Code 2010 – 2 vol. Bulletin 55 and 56.
- FIB. (2010). fib Model Code for Concrete Structures. Ernst & Sohn, October 2013. ISBN: 978–3–433–03061–5.
- Fromm, Asko, Schein, Markus, Grohmann. (2017). Manfred: Reinforcement of Additive Manufactured Concrete Elements. In: Bögle, A., Grohmann, M., (Eds.), Proceedings of the IASS Annual Symposium 2017 September, 2017, Hamburg, Germany Annette Bögle, Manfred Grohmann (eds.). Interfaces: architecture. Engineering. Science 25 - 28th; 2017.
- Hambach, M., and Volkmer, D. (2017). Properties of 3D-printed fiber-reinforced Portland cement paste. *Cement and Concrete Composites*, 79, 62–70.  
<https://www.enr.com/articles/45002-army-researchers-refine-3d-printed-concrete-barracks>.  
<http://www.xtreee.eu/projects-yrys-concept-house/>.  
[http://www.winsun3d.com/En/News/news\\_inner/id/461](http://www.winsun3d.com/En/News/news_inner/id/461).  
[https://cybe.eu/portfolio-item/rdrone\\_laboratory\\_3dprinting\\_on-site\\_in\\_the\\_desert\\_of\\_dubai/](https://cybe.eu/portfolio-item/rdrone_laboratory_3dprinting_on-site_in_the_desert_of_dubai/).  
<https://all3dp.com/worlds-first-3d-printed-bicycle-bridge-opens-in-netherlands/>.
- Kreiger, E., Kreiger, M., and Case, M. (2019). Development of the Construction Processes for Reinforced Additively Constructed Concrete. *Additive Manufacturing*. <https://doi.org/10.1016/j.addma.2019.02.015>
- Knitcrete, E. T. H. Zurich: Knitcandela project. (2018). [Online]. Available at: <https://www.ethz.ch/en/news-and-events/eth-news/news/2018/10/knitted-concrete.html>. [Accessed on: 24.04.2019]. Image credits: Mariana Popescu.
- Kuder, K. G., and Shah, S. P. (2003). Effects of pressure on resistance to freezing and thawing of fiber-reinforced cement board. *ACI Mater J*, 100(6), 463–468.
- Kuder, K. G., and Shah, S. P. (2010). Processing of high-performance fiber-reinforced cement-based composites. *Construction and Building Materials*, 24, 181–186.
- Keita, E., Bessaies-Bey, H., Zuo, W., Belin, P., and Roussel, N. (2019). Weak bond strength between successive layers in extrusion-based additive manufacturing: measurement and physical origin. *Cement and Concrete Research*, 123, 105787. ISSN 0008-8846. <https://doi.org/10.1016/j.conres.2019.105787>. <https://www.sciencedirect.com/science/article/pii/S0008884618313760>
- Le, T. T., Austin, S. A., Lim, S., Buswell, R. A., Law, R., Gibb, A. G. F., and Thorpe, T. (2012). Hardened properties of high-performance printing concrete. *Cement and Concrete Research*, 42, 558–566.
- Labonette, N., Rønquist, A., Manum, B., and Rütther, P. (2016). Additive construction: State-of-the-art, challenges and opportunities. *Automation in Construction*, 72(3), 347–366.
- Lim, S., Buswell, R. A., Le, T. T., Austin, S. A., Gibb, A. G. F., and Thorpe, T. (2012). Developments in construction-scale additive manufacturing processes. *Autom. Constr.*, 21, 262–268. doi:<https://doi.org/10.1016/J.AUTCON.2011.06.010>.
- Lloret-Fritschi, E., Scotto, F., Gramazio, F., Kohler, M., Graser, K., Wangler, T., Reiter, L., Flatt, R. J., and Mata-Falcón, J. (2019). Challenges of Real-Scale Production with Smart Dynamic Casting. In: T. Wangler, and R. J. Flatt (Eds.), *First RILEM Int. Conf. Concr. Digit. Fabr. – Digit. Concr. 2018*, Springer International Publishing, pp. 299–310.
- Martinie, L., Rossi, P., and Roussel, N. (2010). Rheology of fibre reinforced cementitious materials: classifications and prediction. *Cement and Concrete Research*, 40, 226–240.
- Martinie, L., and Roussel, N. (2011). Simple tools for fibre orientation prediction in industrial practice. *Cement and Concrete Research*, 41, 993–1000.
- Marti, P. (1985). Truss models in detailing. *Concrete International*, 7(12), 66–73.
- Martens, P., Mathot, M., Bos, F. P., and Coenders, J. (2017). Optimising 3D printed concrete structures using topology optimisation. *High Tech Concrete: where technology and engineering meet: Proceedings of the 2017 fib Symposium, held in Maastricht, The Netherlands, June 12–14, 2017*. Hordijk, D. A., and Luković, M. (eds.). Cham: Springer, pp. 301–309 9.
- Martens, P. (2018). Optimising 3D Printed Concrete Structures: Concrete additive manufacturing and topology optimisation, MSc graduation thesis, TU Delft, the Netherlands.



- Mesh Mould. (2019). ETH Zurich: DFAB HOUSE project [Online]. Available at: [https://dfabhouse.ch/mesh\\_mould/](https://dfabhouse.ch/mesh_mould/). [Accessed on: 24.04.2019]. Image credits: Gramazio Kohler Research, ETH Zurich.
- Model Code 2010 - Final draft, Vol 1. (350 pp, ISBN 978-2-88394-105-2, March 2012).
- Marchment, T., Xia, M., Dodd, E., Sanjayan, J., and Nematollahi, B. (2017). Effect of delay time on the mechanical properties of extrusion-based 3D printed concrete. In 34th International Symposium on Automation and Robotics in Construction.
- Nerella, V. N., Ogura, H., and Mechtcherine, V. (2018 July). Incorporating reinforcement into digital concrete construction. Proceeding of the annual Symposium of the IASS—International Association for Shell and Spatial Structures: Creativity in Structural Design, July 2018, MIT, Boston.
- Nerella, V. M., Krause, M., Näther, M., and Mechtcherine, V. (2016). Studying printability of fresh concrete for formwork free Concrete onsite 3D Printing technology (CONPrint3D). In Proceeding for the 25th Conference on Rheology of Building Materials, Regensburg, Germany.
- Nerella, V. N., Hempel, S., and Mechtcherine, V. (2018). Effects of Layer-Interface Properties on Mechanical Performance of Concrete Elements Produced by Extrusion-Based 3D-Printing. doi:<https://doi.org/10.20944/preprints201810.0067.v1>.
- Ogura, Nerella, V., and Mechtcherine, V. (2018). Developing and Testing of Strain-Hardening Cement-Based Composites (SHCC) in the Context of 3D printing. *Materials*, 11, 1375. doi:<https://doi.org/10.3390/ma11081375>. 18 pp.
- Panda, B., Noor Mohamed, N. A., Tay, Y. W. D., and Tan, M. J. (2019). Bond Strength in 3D Printed Geopolymer Mortar. In: T. Wangler, and R. J. Flatt (Eds.), *First RILEM Int. Conf. Concr. Digit. Fabr. – Digit. Concr. 2018*. Springer International Publishing, pp. 200–206.
- Panda, B., Paul, S. V., and Tan, M. J. (2017). Anisotropic mechanical performance of 3D printed fibre reinforced sustainable construction material. *Materials Letters*, 2019, 146–149.
- Panda, B., Paul, S. C., Mohamed, N. A. N., Tay, Y. W. D., and Tan, M. J. (2018). Measurement of tensile bond strength of 3D printed geopolymer mortar. *Measurement*, 113, 108–116.
- Paul, S. C., Y. W. D. Tay, P. B., and Tan, M. J. Fresh and hardened properties of 3D printable cementitious materials for building and construction. *Archives of Civil and Mechanical Engineering*, 18, 311–319.
- Pavilion uibk (to be published shortly).
- Peled, A., Cyr, M., and Shah, S. P. (2000). High content of fly ash (Class F) in extruded cementitious composites. *ACI Mater J*, 97(5), 509–517.
- Peled, A., and Shah, S. P. (2003). Processing effects in cementitious composites: extrusion and casting. *J Mater Civil Eng*, 15(2), 192–199.
- Rippmann, M., Liew, A., Van Mele, T., Block, P. (2018). Design, fabrication and testing of discrete 3D sand-printed floor prototypes. *Materials Today Communications*, 15, 254–259. Doi: <https://doi.org/10.1016/j.mtcomm.2018.03.005>
- Rosanna Napolitano, Costantino Menna, Domenico Asprone, Lorenzo del Giudice. Experimental and numerical assessment of the interface behaviour of 3D Printed concrete elements w/wo interlaminar reinforcement. *Cement and concrete composites* (submitted).
- Radtke, F. K. F., Simone, A., Sluys, L. J. (2010). A computational model for failure analysis of fibre reinforced concrete with discrete treatment of fibres. *Engineering Fracture Mechanics*, 77(4), 597–620.
- Radtke, F. K. F., Simone, A., and Sluys, L. J. (2011). A partition of unity finite element method for simulating non-linear debonding and matrix failure in thin fibre composites. *International Journal for Numerical Methods in Engineering*, 86(4-5), 453–476.
- Salet, T. A. M., and Fietsbrug Nijmegen. (2019). Protocol voor de veiligheid van een voorgespannen geprinte betonnen fiets- en voetgangersbrug. [rapport ref number to be added], for Rijkswaterstaat. Eindhoven University of Technology, Netherlands.
- Soltan, D. G., and Li, V. C. (2018). A self-reinforced cementitious composite for building-scale 3D printing. *Cement and Concrete Composites*, 90, 1–13.

- Soetens, T., and Matthys, S. (2014). Different methods to model the post-cracking behaviour of hooked-end steel fibre reinforced concrete. *Construction and Building Materials*, 73, 458–471.
- Schlaich, J., Schäfer, K., and Jennewein, M. (1987). Toward a consistent design of structural concrete. *PCI Journal*, 32(3), 74–150.
- Stefanoni, M., Angst, U., and Elsener, B. (2019). Corrosion Challenges and Opportunities in Digital Fabrication of Reinforced Concrete. In: T. Wangler, and R. J. Flatt (Eds.), *First RILEM Int. Conf. Concr. Digit. Fabr. – Digit. Concr. 2018*, Springer International Publishing, pp. 225–233.
- Schröfl, C., Nerella, V. N., and Mechtcherine, V. (2019). Capillary Water Intake by 3D-Printed Concrete Visualised and Quantified by Neutron Radiography. In: T. Wangler, and R. J. Flatt (Eds.), *First RILEM Int. Conf. Concr. Digit. Fabr. – Digit. Concr. 2018*, Springer International Publishing, pp. 217–224.
- Smart Dynamic Casting. (2019). ETH Zurich: DFAB HOUSE project [Online]. Available at: <https://dfabhouse.ch/smart-dynamic-casting/>. [Accessed on: 24.04.2019].
- Srinivasan, S., Deford, D., and Shah, P. (1999). The use of extrusion rheometry in the development of extrudate fibre-reinforced cement composites. *Concrete Science and Engineering*, 1(11), 26–36.
- Theo A. M. Salet, Zeeshan Y. Ahmed, Freek P. Bos, and Hans L. M. Laagland. (2018). Design of a 3D printed concrete bridge by testing. *Virtual and Physical Prototyping*, 13(3), 222–236. DOI: <https://doi.org/10.1080/17452759.2018.1476064>.
- Timothy Wangler, Nicolas Roussel, Freek P. Bos, Theo A. M. Salet, and Robert J. Flatt. (2018). Digital Concrete: A Review. *Cement and Concrete Research*, 123(17), 105780. Doi: <https://doi.org/10.1016/j.cemconres.2019.105780>.
- TotalKustom: 3D-Printed Hotel. (2015). [Online]. Available at: <http://www.totalkustom.com/3d-printed-hotel-suite.html>. [Accessed on: 24.04.2019].
- Vantyghe, G., De Corte, W., Shakour, E., and Amir, O. (2019). Topology optimization and 3D printing of a post-tensioned concrete girder, submitted (under review).
- Van Der Putten, J., De Schutter, G., and Van Tittelboom, K. (2019). The Effect of Print Parameters on the (Micro) structure of 3D Printed Cementitious Materials. In: T. Wangler, and R. J. Flatt (Eds.), *First RILEM Int. Conf. Concr. Digit. Fabr.—Digit. Concr. 2018*, Springer International Publishing, pp. 234–244.
- Wolfs, R., Bos, F., and Salet, T. (2018). Early age mechanical behaviour of 3D printed concrete: Numerical modelling and experimental testing. *Cement and Concrete Research*, 106, 103–116. <https://doi.org/10.1016/j.cemconres.2018.02.001>.
- Wolfs, R., Bos, F., and Salet, T. (2019). Hardened properties of 3D printed concrete: The influence of process parameters on interlayer adhesion. *Cement and Concrete Research*, 119. <https://doi.org/10.1016/j.cemconres.2019.02.017>.
- Zhou, X., and Li, Z. (2005). Characterization of rheology of fresh fiber reinforced cementitious composites through ram extrusion. *Materials and Structures*, 38, 17–24.
- Zhan, Y., and Meschke, G. (2016). Multilevel computational model for failure analysis of steel-fibre-reinforced concrete structures. *J. Eng. Mech. ASCE*, 142(11), 1–14.
- Zareiyani, B., and Khoshnevis, B. (2017). Interlayer adhesion and strength of structures in Contour Crafting—Effects of aggregate size, extrusion rate, and layer thickness. *Automation in Construction*, 81, 112–121.
- Zahabizadeh, B., Cunha, V. M. C. F., Pereira, J., and Gonçalves, C (2019). The effect of loading direction on the compressive behaviour of a 3D printed cement-based material. In *IABSE Symposium, Guimaraes 2019: Towards a Resilient Built Environment Risk and Asset Management*, pp. 1658–1665.